

論文 / 著書情報
Article / Book Information

題目(和文)	流動鉛ビスマス条件下の鋼材及びセラミックスの組織変化と液体内化学制御に関する研究
Title(English)	Study on metallurgical change of steels and ceramics in flowing lead-bismuth and chemical control of liquid alloy
著者(和文)	近藤正聡
Author(English)	
出典(和文)	学位:博士(工学), 学位授与機関:東京工業大学, 報告番号:甲第6465号, 授与年月日:2006年3月26日, 学位の種別:課程博士, 審査員:高橋実
Citation(English)	Degree:Doctor of Engineering, Conferring organization: Tokyo Institute of Technology, Report number:甲第6465号, Conferred date:2006/3/26, Degree Type:Course doctor, Examiner:
学位種別(和文)	博士論文
Type(English)	Doctoral Thesis

G2005
Ko

**Study on Metallurgical Change of Steels and Ceramics
in Flowing Lead-Bismuth
and Chemical Control of Liquid Alloy**

**Dissertation Submitted to Tokyo Institute of Technology
for the Degree of Doctor of Engineering**

**by
Masatoshi KONDO**

**Supervised by
Associate Professor Minoru TAKAHASHI**

**Department of Nuclear Energy
Graduate School of Science and Engineering,
Tokyo Institute of Technology**

March 2006

Table of Contents

Abstract	v
Nomenclature	ix
List of Equations	x
List of Tables	xi
List of Figures	xii
1. Introduction	1
<hr/>	
1.1 Background	2
1.2 Lead-Bismuth Cooled Fast Reactor	2
1.3 Merit of Lead-Bismuth as FR or FBR coolant	3
1.4 Weak Point of Liquid Lead-Bismuth as FR or FBR Coolant	4
1.5 Review of Previous Studies on Lead-Bismuth Corrosion and Coolant Technology	6
1.5.1 Control of Oxygen Concentration in Liquid Lead-Bismuth	6
1.5.2 Corrosion in Static Condition	7
1.5.3 Corrosion in Flowing Condition	8
1.6 Unknown Factors on Lead-Bismuth Corrosion	9
1.7 Purpose	10
1.8 Outline of The Thesis	12
2. Chemical Control of Liquid Alloy	25
<hr/>	
2.1 Performance of Solid Electrolyte Type Oxygen Sensor in Flowing Lead-Bismuth	26
2.1.1 Introduction	26
2.1.2 Experimental Apparatus and Procedure	26
2.1.3 Performance of Oxygen Sensor in Flowing Lead-Bismuth	30
2.1.4 Corrosion of Sensor Materials in Flowing Lead Bismuth	32
2.1.5 Summary	33
2.2 Performance of Mass Exchanger Type Oxygen Control System in Flowing Lead-Bismuth	34
2.2.1 Introduction	34
2.2.2 Experimental Apparatus and Procedure	34
2.2.3 Performance of Mass Exchanger Type Oxygen Control System in Flowing Lead-Bismuth	36
2.2.4 Experimental Equation of Oxygen Solubility in Liquid Lead-Bismuth	37
2.2.5 Summary	39

2.3	Conclusions	39
3.	Liquid Metal Corrosion and Erosion Behaviors of Steels in Flowing Lead-Bismuth	53
<hr/>		
3.1	Introduction	54
3.2	Experimental Apparatus and Procedure	54
3.3	Test Materials	57
3.4	Liquid Metal Corrosion and Erosion of Steels	57
3.5	Weight Changes of Steels on Liquid Metal Corrosion and Erosion	59
3.6	Erosion Mechanism in Flowing Lead Bismuth	60
3.7	Conclusions	61
4.	Oxidation Corrosion Behaviors of Steels in Flowing Lead-Bismuth	75
<hr/>		
4.1	Introduction	76
4.2	Experimental Apparatus and Procedure	76
4.3	Test Materials	78
4.4	Oxide Layers on Steels	79
4.5	Weight Changes of Steels in Flowing Pb-Bi at High Oxygen Concentration	81
4.6	Effect of Oxide Layer Formation on Corrosion Resistance in Flowing Pb-Bi	81
4.7	Oxidation Corrosion in Flowing Pb-Bi	82
4.8	Pilling Bedworth Ratio (PB ratio) of Oxide Layers Formed in Steels in Flowing Pb-Bi	82
4.9	Conclusions	84
5.	Effect of Surface Treatment of Steels on Corrosion Resistance in Flowing Lead-Bismuth	100
<hr/>		
5.1.	Effect of Pre-Oxidation of Steels on Corrosion Resistance of Steels in Flowing Lead-Bismuth	101
5.1.1	Introduction	101
5.1.2	Experimental Apparatus and Procedure	101
5.1.3	Test Materials	102
5.1.4	Pre-Oxidation Process	103
5.1.5	Corrosion Characteristics of Pre-Oxidized Steels	103
5.1.6	Summary	105
5.2.	Effect of Surface Roughness of Steels on Corrosion Resistance of Steels in Flowing Lead-Bismuth	106

5.2.1	Introduction	106
5.2.2	Experimental Apparatus and Procedure	107
5.2.3	Test Materials	108
5.2.4	Surface Polishing Process	108
5.2.5	Effect of Surface Roughness of Steels on Corrosion Resistance of Steels	108
5.2.6	Summary	111
5.3	Conclusions	111
6.	Effect of Alloying Elements in Steels on Corrosion Resistance in Flowing Lead-Bismuth	127
6.1	Effect of Cr Contents in Steels on Corrosion Resistance in Flowing Lead-Bismuth	128
6.1.1	Introduction	128
6.1.2	Experimental Apparatus and Procedure	129
6.1.3	Test Materials	130
6.1.4	Effect of Cr Contents in Steels on Corrosion Characteristics	130
6.1.5	Summary	133
6.2	Effect of Alloying Elements, Silicon (Si) and Aluminum (Al) in Steels on Corrosion Resistance in Flowing Lead-Bismuth	134
6.2.1	Introduction	134
6.2.2	Experimental Apparatus and Procedure	134
6.2.3	Test Materials	135
6.2.4	Effect of Si and Al contents in Steels on Corrosion Characteristics	136
6.2.5	Formation Process of Si- and Al- Rich Oxide Layers on Steels in Flowing Pb-Bi	138
6.2.6	Summary	138
6.3	Corrosion Rates of Corrosion Resistant Steels in Flowing Lead-Bismuth	139
6.4	Conclusion	139
7.	Corrosion Characteristics of Ceramic Materials, SiC and Si₃N₄ in Flowing Lead-Bismuth	158
7.1	Introduction	159
7.2	Experimental Apparatus and Procedure	159
7.3	Test Materials	160
7.4	Corrosion Characteristics of SiC and Si ₃ N ₄	161

7.5	Conclusions	162
8.	Effect of Corrosion on Tube Rupture Behavior and Liquid Contamination	169
<hr/>		
8.1	Effect of Corrosion on Tube Rupture Behavior in Liquid Lead-Bismuth	170
8.1.1	Introduction	170
8.1.2	Experimental Procedure	170
8.1.3	Effect of Corrosion on Tube Rupture Behavior	171
8.1.4	Phenomenon of Liquid Metal Embrittlement	172
8.1.5	Summary	174
8.2	Effect of Corrosion on Performance of Electro Magnetic Pump and Flow Meter in Flowing Lead-Bismuth	175
8.2.1	Introduction	175
8.2.2	Experimental Apparatus and Procedure	175
8.2.3	Effect of Corrosion on Performance of Electro Magnetic Flow Meter	177
8.2.4	Effect of Corrosion and Precipitation on Performance of Electro Magnetic Pump	177
8.2.5	Precipitation of Corrosion Products	178
8.2.6	Summary	180
8.3	Conclusions	180
9.	Conclusion	190
<hr/>		
	List of publications	194
	Acknowledgments	199

Abstract

Application of lead-bismuth eutectic (Pb-Bi) to a coolant of fast breeder reactors (FBRs) is proposed due to the favorable neutronic characteristic, thermal hydraulic property and inactive with air and water. The corrosion of structural and cladding materials is one of the critical issues for the development of Pb-Bi cooled FBR (LFRs). The purpose of the thesis work is to outline the corrosion inhibition by using corrosion resistant materials and chemical control method in the flowing Pb-Bi. The various studies, which involve the corrosion phenomena in the flowing Pb-Bi, were done with the experimental approach. The results of the research are reported in nine chapters, and each chapter is summarized as follows;

In *Chapter 1 – Introduction*, the background and the corrosion study for the use of Pb-Bi as LFR coolant were introduced. Journals and literatures were reviewed in detail to illustrate the study on Pb-Bi corrosion. The purpose and outline of this thesis work were described.

In *Chapter 2 – Chemical Control of Liquid Alloy*, the performances of the solid electrolyte type oxygen sensor and mass exchanger (MX) type oxygen control system (OCS) were investigated.

It was found that the solid electrolyte type oxygen sensor had reliability for the long-term use in the flowing Pb-Bi. The performances of the sensor cells made of yttria stabilized zirconia and magnesia stabilized zirconia were the same, even though the former one caused the erosion.

In the study on the MX type OCS, it was found that the oxygen exchange between the flowing Pb-Bi and PbO was depended on the solubility of the oxygen in the Pb-Bi, that is, the oxygen concentration depended on the reaction temperature of the PbO sinter with Pb-Bi. According to a calculation applying the Nernst equation to the EMF signals, the oxygen concentration was controlled between 1×10^{-5} wt% (temperature of PbO sinter: 315°C) and 3×10^{-6} wt% (temperature of PbO sinter: 280°C), where is the corrosion-inhibition region. Finally, it was concluded that the oxygen concentration in the Pb-Bi flow can be controlled by using the oxygen sensor and MX type OCS.

In *Chapter 3– Liquid Metal Corrosion and Erosion Behaviors of Steels in Flowing Lead Bismuth*, the mechanism of erosion and corrosion of steels in the Pb-Bi flow was investigated. Nine steels were simultaneously exposed to the Pb-Bi flow at the temperature of 550°C, the loop temperature difference of 150°C, the flow velocity of 2m/s for 1,000 hours. The liquid metal corrosion (LMC), or Pb-Bi penetration into steels occurred in all the steels, and severe erosion took place in some of the steels under low oxygen concentration of 1.57×10^{-10} wt% in the Pb-Bi. The corrosion layer penetrated by Pb-Bi were deeper in the steels containing lower content of Cr. The erosion was caused by hydrodynamic carrying away of weakened surface materials due

to Pb-Bi penetration. Finally, it was explained that the large-scale erosion could be caused by the detachment of lumps of corroded materials that had defects formed by dissolution of alloying elements.

In *Chapter 4- Oxidation Corrosion Behaviors of Steels in Flowing Lead-Bismuth*, an oxidation corrosion characteristics of various steels in the flowing Pb-Bi were investigated by means of steel corrosion test performed in the flowing Pb-Bi for 1,000 hours. It was found that the LMC was inhibited by single or multiple oxide layers formed on the steel surfaces. The oxide layers can be classified to an inner layer and an outer one. The existence of the inner oxide layer might be more important for the corrosion resistance since the inner one was compact and stuck to the steel surface while the outer one was easily broken into small pieces with cracks and peeled from the substrate. Finally, it was discussed that an oxidation corrosion could be caused by the detachment of the unstable oxide layers in the flowing Pb-Bi. The stability of the formed oxide layers was discussed with Pilling-Bedworth ratio of the layers.

In *Chapter 5- Effect of Surface Treatment of Steels on Corrosion Resistance*, the effects of pre-oxidation and surface roughness of steels on corrosion in the flowing Pb-Bi were studied experimentally.

The corrosion characteristics of pre-oxidized steels were investigated by means of short term corrosion test with the specimens of SS430 SS405, SUH3, STBA26, SS316 and SCM420, which are pre-oxidized in moist air at the temperature of 500°C, partial pressure of water vapor of 92.5mmHg and oxidation time of 12, 24 and 72 hours. The weight losses of the pre-oxidized steels were lower than those of the test pieces without pre-oxidation, which means that the initial corrosion was inhibited by the existence of the preformed layers. However, the pre-formed oxide layer could not be observed after the exposure because they were flowed out by the heavy density fluid flow. The layer different from the pre-formed one was observed. Then, it was concluded that the preformed oxide layer was effective only for initially. And, the self-healed oxide layer was formed and the layer inhibited the corrosion after the flowed out of the preformed oxide layers.

The effect of surface roughness of the steels on the corrosion behaviors was investigated by the exposure of the specimens, which had the surface of smooth, rough and their middle roughness, in the flowing Pb-Bi at the temperature of 550°C. As the test steels, 12Cr- and 9Cr- steels were selected. In the surface-smoothened specimens, compact oxide layers were formed on the surfaces. In the surface-roughened specimens, oxide layers with cracks were detected on their surfaces, and the cracks mainly existed around the convex part of the substrate. This implies that frictional and shear stress by the heavy density Pb-Bi flow concentrated in the layer at the convex part of the substrate. It was found that the rough surfaces of steels promote the oxidation corrosion in the flowing Pb-Bi, while the steels with smooth surfaces form compact oxide layers.

In *Chapter 6- Effect of Alloying Elements in Steels on Corrosion Resistance*, the effect of steel alloying elements, Cr, Si, and Al in steels on the corrosion resistance of the steels in the flowing Pb-Bi was described.

The corrosion characteristics of high Cr steels were investigated by means of corrosion tests with steels, which have various Cr contents of steels in the flowing Pb-Bi. SS430 (18-Cr steel) showed excellent corrosion resistance after the exposure in the flowing Pb-Bi at 550°C up to 2,000 hours. The weight loss of the SS430 specimen in the Pb-Bi flow was negligibly small and much lower than the other steels. This is because the SS430 steel formed the Cr rich single layer, and the Cr-rich layer had resistance not only for the LMC but also for the oxidation corrosion in the flowing Pb-Bi.

The corrosion resistance of Si- and Al-rich steels in the flowing Pb-Bi was studied experimentally. The specimens of SUH3 (10Cr-1Mo-2Si), NTK04L (18Cr-3Al) and Recloy10 (18Cr-1Al-1Si) were exposed to the Pb-Bi flow at the temperature of 550°C up to 2,000 hours. The oxygen concentration in the flowing Pb-Bi was higher than that for the formation of the oxide of Al, Si, Cr and Fe. After the exposure, the surface of the Si-rich steel, SUH3, was kept smooth with no liquid metal corrosion (LMC). On the surface, thin oxide layer was formed. The layer had a double layer structure that consisted of an unstable outer layer and a compact inner one. The inner layer worked as barrier for the LMC, while detachment of the outer layer could cause oxidation corrosion. As for the Al-rich steel, NTK04L, an Al-rich single layer was formed and stuck on the surface. This layer protected the matrix from the LMC. Oxidation corrosion did not occur on the steel since this layer was oxidation resistant even at the condition of high oxygen potential. The weight loss of the NTK04L steel in 500-hour and 2000 hour-exposure was negligibly small. As for Al- and Si-rich steel, Recloy10, an Al- and Si-enriched single layer was formed on the surfaces. The weight loss of the Recloy10 steel was also negligibly small.

In *Chapter 7- Corrosion Characteristics of Ceramics, SiC and Si₃N₄ in Flowing Lead-Bismuth*, corrosion characteristics of SiC and Si₃N₄ ceramic materials in a flowing lead-bismuth were investigated. It was found that the specimens of SiC and Si₃N₄ kept smooth surface without a corrosion and an oxidation in the Pb-Bi. Although the surface showed several cracks, the Pb-Bi was not diffused in the cracks. These cracks might be caused by a shear and/or normal stress of the heavy density Pb-Bi flow. The weight loss of the SiC and Si₃N₄ specimens in the flowing Pb-Bi was negligibly small. Thus, the ceramic materials, such as SiC and Si₃N₄, can be used in the flowing Pb-Bi, even though the improvement of mechanical properties of them was necessary to avoid the occurrence of the cracks on the surfaces.

In *Chapter 8- Effect of Liquid Metal Corrosion on Steel Tube Rupture Behavior and Liquid Contamination*, metallurgical analysis for the ruptured tube and precipitated material in the flowing Pb-Bi was carried out. The rupture occurred while the loop temperature was being increased from room temperature to 250°C. The rupture occurred for a tube which had been used with Pb-Bi at 400°C for 3,500 hours and 23 increasing

temperature cycles. The tube expanded locally around the ruptured part, which indicated that the rupture was caused by the thermal expansion of the Pb-Bi in the tube. More severe liquid metal corrosion was observed at the inner tube surface around the ruptured part than elsewhere in the tube. The fracture mechanism in the rupture face could be classified into two types, *i.e.* brittle fracture without any sign of dimple marks in the inner region of the tube wall and ductile fracture in the outer region of the tube wall. By the analysis of the precipitated materials on the immersion part of the electro magnetic pump, it was found that the Fe precipitated in the flowing Pb-Bi in the low temperature region of the loop. The countermeasures for these problems were discussed finally.

In *Chapter 9- Conclusions*, the feature results were summed up, and conclusions were drawn.

Nomenclature

A	Constant A in general equation of oxygen solubility in liquid Pb-Bi	-
B	Constant B in general equation of oxygen solubility in liquid Pb-Bi	-
C	Oxygen concentration in liquid Pb-Bi (wt%)	-
C_s	Saturated concentration or the solubility of oxygen (wt%)	-
C_{Na}	Oxygen concentration in liquid Na (ppm)	-
D	Density of metal oxide (g/m^3)	-
d	Density of metal (g/m^3)	-
E	Electro motive force of oxygen sensor (V)	-
F	Faraday coefficient(C/mol)	=96485
ΔG^0_{PbO}	Oxygen potential of lead oxide formation	-
$\Delta G^0_{\text{Bi}_2\text{O}_3}$	Oxygen potential of bismuth oxide formation	-
$\Delta G^0_{\text{H}_2\text{O}}$	Oxygen potential of steam	-
M	Molecular weight of metal oxide (g)	-
m	Weight of metal	-
N	Period for operation at steady state condition (year)	-
N_i	Period for operation at irregular condition (year)	-
R	Gas constant (J/mol)	=8.3147
R_a	Arithmetical mean surface roughness (μm)	-
Φ_{ref}	Chemical potential in reference fluid	-
$\Phi_{\text{Pb-Bi}}$	Chemical potential in liquid Pb-Bi	-
T	Absolute temperature of Pb-Bi (K)	-
T_{sensor}	Temperature of liquid Pb-Bi at oxygen sensor (K)	-
T_{PbO}	Temperature of liquid Pb-Bi which contacts with PbO particle in reaction vessel (K)	-

List of Equations

Eq. (2-1)	Electro chemical system of oxygen sensor for liquid Pb-Bi	27
Eq. (2-2)	Nernst Equation	27
Eq. (2-3)	Reduction reaction of Bi oxide in reference fluid	28
Eq. (2-4)	Oxidation reaction of Pb in liquid Pb-Bi	28
Eq. (2-5)	Oxygen potential in reference fluid	28
Eq. (2-6)	Oxygen potential in liquid Pb-Bi	28
Eq. (2-7)	Nernst equation for oxygen sensor with Bi-oxide reference in liquid Pb-Bi controlled by Pb oxidation reaction	28
Eq. (2-8)	Nernst equation for oxygen sensor with Bi-oxide reference in liquid Pb-Bi controlled by Pb-Bi oxidation reaction	28
Eq. (2-9)	Oxygen solubility in liquid Pb-Bi provided by Gromov et al	28
Eq. (2-10)	Oxygen solubility in liquid Pb-Bi provided by Muller et al	29
Eq. (2-11)	Relation between sensor output and temperature of liquid Pb-Bi which contacts with PbO particles	37
Eq. (2-12)	Relation between sensor output and temperature of liquid Pb-Bi which contacts with PbO particles in case of Bi oxide is partly generated	37
Eq. (2-13)	General expression of oxygen solubility in liquid Pb-Bi at sensor	37
Eq. (2-14)	General expression of oxygen solubility in liquid Pb-Bi in PbO reaction vessel	38
Eq. (2-15)	Experimental equation for sensor output with PbO temperature and constant B	38
Eq. (2-16)	The arrangement of measured sensor output between theoretical equations	38
Eq. (2-17)	The arrangement of measured oxygen solubility between theoretical equations	38
Eq. (3-1)	The oxygen potential in liquid Pb-Bi with injection of gas mixture of argon, hydrogen and vapour	56
Eq. (3-2)	Oxygen solubility in liquid Pb-Bi provided by Gromov et al	56
Eq. (4-1)	Pilling Bedworth ratio of oxide layer	82
Eq. (5-1)	Equation for arithmetical mean surface roughness	107

List of Tables

Table 1-1	Comparison of properties of liquid metals	21
Table 1-2	Pb-Bi test apparatus (Static system)	22
Table 1-3	Pb-Bi test apparatus (Dynamic system)	23
Table 2-1	Mechanical characteristics of solid electrolyte conductors MSZ and YSZ	41
Table 2-2	Conditions of sensor performance tests	41
Table 2-3	Specifications of PbO particle	41
Table 2-4	Experimental conditions of oxygen control test	41
Table 3-1	Test conditions	63
Table 3-2	Chemical components of test steels	63
Table 3-3	Appearance of test piece surfaces in molybdenum holder	63
Table 4-1	Specifications of forced convective Pb-Bi corrosion test loop	86
Table 4-2	Experimental conditions	86
Table 4-3	Chemical components of test steels	86
Table 4-4	Size of specimens	87
Table 4-5	Thickness of oxide layers and Pb-Bi penetration obtained from SEM analysis	87
Table 4-6	Pilling Bedworth ration of oxide layer formed on steel in liquid Pb-Bi	88
Table 4-7	Self-diffusion coefficient of metal in metal oxide	88
Table 5-1	Chemical components of test steels	113
Table 5-2	Corrosion test conditions	113
Table 5-3	Corrosion test conditions	113
Table 5-4	Hydrodynamic conditions of test piece	113
Table 5-5	Chemical components of test materials	113
Table 6-1	Corrosion test conditions	141
Table 6-2	Chemical components of specimens (wt%)	141
Table 6-3	Chemical components of test steels (wt%)	141
Table 6-4	Test conditions	142
Table 6-5	Corrosion rates of steels in flowing Pb-Bi	142
Table 7-1	Corrosion test conditions	164
Table 7-2	Corrosion rates of SiC and Si ₃ N ₄ in flowing Pb-Bi	164
Table 8-1	Temperature change of Pb-Bi sampling line	182
Table 8-2	Total exposure time of Pb-Bi sampling line	182
Table 8-3	EMP operating conditions	182

List of Figures

Fig. 1-1	Corrosion rates of steels in flowing Na calculated using equation of corrosion rate for Joyo type reactor	24
Fig. 1-2	Diagram showing corrosion behavior of steels in flowing oxygen containing Pb for 3000 hours at 550°C [16]	24
Fig. 2-1	Schematic of Pb-Bi forced convection loop	42
Fig. 2-2	Schematic of oxygen sensor	42
Fig. 2-3	Schematic of sensor cell	43
Fig. 2-4	Initial EMF output of sensors with MSZ cell in T-1 operation	43
Fig. 2-5	Initial EMF output of sensors with MSZ and YSZ cells in T-2 operation	44
Fig. 2-6	Initial EMF output of sensor with YSZ cell in T-4 operation	44
Fig. 2-7	Metallurgical conditions of MSZ sensor (a) used in Pb-Bi for 4 hours; (b) for 1000 hours	45
Fig. 2-8	Surfaces of MSZ and YSZ sensor cells after 3500-hour use in flowing Pb-Bi	45
Fig. 2-9	Cross sections of MSZ sensor cells used in flowing Pb-Bi for 3500 hours	46
Fig. 2-10	FE-SEM image and EDX analysis results for the surface of MSZ sell surface after use in flowing Pb-Bi for 3500 hours	46
Fig. 2-11	FE-SEM image and EDX analysis results for adherent Pb-Bi on surface of MSZ sell after use in flowing Pb-Bi for 3500 hours	46
Fig. 2-12	Cross sections of YSZ sensor cells used in flowing Pb-Bi for 3500 hours	47
Fig. 2-13	FE-SEM image and EDX analysis results for surface of YSZ sell after use in flowing Pb-Bi for 3500 hours	47
Fig. 2-14	Schematic of MX with PbO particles	48
Fig. 2-15(a)	EMF transient due the change of reaction temperature between 275°C and 330°C	49
Fig. 2-15 (b)	Stable EMF transient according to the change of reaction temperature between 275°C and 320°C	49
Fig. 2-15 (c)	EMF signals of oxygen sensor at low temperature of PbO	50
Fig. 2-16	Comparison of calculated and measured EMF	50
Fig. 2-17	Const B	51
Fig. 2-18	Const A	51
Fig. 2-19	Comparison between oxygen solubility obtained from experiment and preliminary reported Eqs. (2-9) and (2-10) [2, 6]	52
Fig. 3-1	Lead-bismuth forced convection test loop	64
Fig. 3-2	Schematic of test piece holder	65

Fig. 3-3	Schematic of test section	65
Fig. 3-4	Preparation of test pieces for SEM/EDX observation and analysis	66
Fig. 3-5	Diagram of oxygen potential	66
Fig. 3-6	SEM/EDX observation and analysis for cross-section of eroded region in SCM420	67
Fig. 3-7	SEM/EDX observation and analysis for cross-section of corroded region in (a) ODS and (b) F82H	68
Fig. 3-8	SEM observation for cross section of eroded region in F82H (a) Pb-Bi penetration along narrow erosion, (b) Wide erosion, (c) Pb-Bi penetration in widely eroded region	68
Fig. 3-9	SEM/EDX observation and analysis for cross-section of corroded region in (a) STBA26 and (b) STBA28	69
Fig. 3-10	SEM/EDX observation for cross section of eroded region in STBA26: (a) erosion, (b) end of eroded region, (c) end of eroded region, (d) Pb-Bi penetration and EDX analysis	70
Fig. 3-11	SEM/EDX observation and analysis in NF616: (a) erosion, (b) Pb-Bi penetration in eroded region and EDX analysis, (c) Pb-Bi penetration in corroded region	71
Fig. 3-12	SEM/EDX observation and analysis for cross section of HCM12 and HCM12A :(a) corrosion and EDX analysis in HCM12, (b) Pb-Bi penetration in HCM12, (c) erosion in HCM12, (d) corrosion and EDX analysis in HCM12A	72
Fig. 3-13	SEM/EDX observation and analysis for cross section of eroded region in SS316: (a) erosion, (2) EDX analysis of Pb content in penetrated region (3) EDX analysis of Bi content in penetrated region	72
Fig. 3-14	Weight change of test pieces during 1000-hour exposure to Pb-Bi flow	73
Fig. 3-15	Depth of Pb-Bi penetration layers in steels	73
Fig. 3-16	Schematic of erosion mechanism	74
Fig. 4-1	Schematic diagram of corrosion test loop	89
Fig. 4-2	Specimen holder	89
Fig. 4-3	Test section	90
Fig. 4-4	Diagram of oxygen potential; symbol of black triangle: ΔG^0 is estimated from oxygen potential of $\text{Pb}_{0.45}\text{Bi}_{0.55}\text{O}_{1.275}$, symbol of black square: that is estimated from oxygen potential of PbO	90
Fig. 4-5	Appearance of specimen surfaces in Mo holder after 1,000 hr-exposure to Pb-Bi flow	91

Fig. 4-6	Oxide layers and metal elements in following material after 1,000 hr-exposure to Pb-Bi flow	92-98
	(a) HCM12A,	
	(b) HCM12,	
	(c) NF616,	
	(d) STBA26,	
	(e) SUS430,	
	(f) SUS405,	
	(g) ODS,	
	(h) F82H,	
	(i) SUS316 (Content of Fe),	
	(j) SUS316 (Content of Cr),	
	(k) SUH3,	
	(l) SCM420	
Fig. 4-7	Weight loss of steels in flowing Pb-Bi	98
Fig. 4-8	Place of oxidation corrosion of steels in liquid Pb-Bi in diagram of general corrosion pattern	99
Fig. 4-9	Effect of PB ratio in oxidation process in liquid Pb-Bi	99
Fig. 5-1	Pb-Bi forced convection loop	114
Fig. 5-2	Surface conditions of pre-oxidized specimens (a) before exposure to Pb-Bi flow, (b) after exposure to Pb-Bi flow	114
Fig. 5-3	Pre-formed oxide layers on test steels	115
Fig. 5-4	Weight gains of test steels in pre-oxidation process	116
Fig. 5-5	Weight loss of pre-oxidized specimens and bared specimens	116
Fig. 5-6	Surface cross section of SS430 with Cr content after exposure into Pb-Bi for 500 hours	117
Fig. 5-7	Surface cross section of SUH3 with Cr and Si contents after exposure into Pb-Bi for 500 hours	117
Fig. 5-8	Surface cross section of STBA26 with Cr content after exposure into Pb-Bi for 500 hours	118
Fig. 5-9	Surface cross section of pre-oxidized SS405 with Cr content after exposure into Pb-Bi for 500 hours	118
Fig. 5-10	Surface cross section of SS316 after exposure into Pb-Bi for 500 hours	118
Fig. 5-11	Pb-Bi forced convection test loop	119
Fig. 5-12	Diagram of oxygen potential; symbol of vacant triangle indicates oxygen concentration in the 500-hour and 1000-hour corrosion tests. symbol of black triangle indicate oxygen concentration in 2000-hour corrosion test.	119
Fig. 5-13	Analysis way of arithmetical mean surface roughness (Ra)	120
Fig. 5-14	Schematic of oxidized surface and laminar sub layer	120
Fig. 5-15	Test pieces with smooth, middle and rough surfaces	120

Fig. 5-16	Microscope images for specimen surfaces in HCM12A, HCM12, STBA28 and STBA26 after exposure to Pb-Bi flow for 500, 1000 and 2000 hours.	121
Fig. 5-17	Change of surface roughness during 500-, 1000- and 2000-hour exposure to Pb-Bi flow	122
Fig. 5-18	Surface cross section and Cr content profile of surface-smoothened STBA26 after exposure into Pb-Bi for 500 hours	122
Fig. 5-19	Oxide layers on the roughened, smoothened and medium rough surfaces of STBA28 exposed to Pb-Bi flow for 1,000 hours	123
Fig. 5-20	Oxide layers on the roughened and smoothened surfaces of STBA26 exposed to Pb-Bi flow for 2,000 hours	124
Fig. 5-21	Surface cross section and Cr content profile of surface-smoothened HCM12A after exposure into Pb-Bi for 500 hours	124
Fig. 5-22	Oxide layers formed on the roughened, smoothened and middle rough surfaces of HCM12 exposed to Pb-Bi flow for 1,000 hours	125
Fig. 5-23	Oxide layers on the roughened and smoothened surfaces of STBA26 exposed to Pb-Bi flow for 2,000 hours	126
Fig. 5-24	Crack behavior of oxide layer at convex part	126
Fig. 6-1	Schematic of Pb-Bi forced convection loop	143
Fig. 6-2	Surface observation of specimens after corrosion test	143
Fig. 6-3	Weight loss of steels and ceramic materials in 500 hour-test	144
Fig. 6-4	Weight loss of steels and ceramic materials in 1000hour-test	144
Fig. 6-5	Weight loss of steels and ceramic materials in 2,000 hour-test	145
Fig. 6-6	Weight loss of SS430 (18-Cr), HCM12A (12-Cr) and STBA26 (9-Cr) specimens in Pb-Bi flow	145
Fig. 6-7	Surface cross section of SS430, HCM12A, STBA26 after 500, 1,000, 2,000 hour-tests	146
Fig. 6-8	Decrease of influence of Cr in steels on formation of Fe-Cr oxide layer in liquid Pb-Bi	147
Fig. 6-9	Schematic of Pb-Bi forced convection test loop	148
Fig. 6-10	Diagram of oxygen potential; oxygen condition in 500-hour and 1,000-hour test was shown in black square; oxygen condition in 2000-hour test was shown in vacant triangle	148
Fig. 6-11	Appearance of SUH3, Recloy10 and NTK04L specimens in Mo-test piece holder after exposure to flowing Pb-Bi for 500,1,000 and 2,000 hours	149
Fig. 6-12	Weight loss of SUH3, Recloy10 and NTK04L steels in flowing Pb-Bi	149

Fig. 6-13	Si-enriched single oxide layer formed on SUH3 surface in 500 hour-exposure to flowing Pb-Bi	150
Fig. 6-14	Double oxide layer consists of outer [O] layer and inner [I] layer formed on SUH3 surface in 1,000 hour-exposure to flowing Pb-Bi	151
Fig. 6-15	Cracked oxide layer formed on SUH3 surface in 2,000 hour-exposure to flowing Pb-Bi	152
Fig. 6-16	Al-enriched oxide layer formed on NTK04L steel in 500-hour test	153
Fig. 6-17	Al-enriched layer formed on NTK04L steel in 2,000-hour test	154
Fig. 6-18	Al-enriched thin layer formed on Recloy10 steel in 500 hour-exposure to flowing Pb-Bi	155
Fig. 6-19	Al-enriched thin layer formed on Recloy10 steel in 2,000 hour-exposure to flowing Pb-Bi	156
Fig. 6-20	Formation of Al- and Si- rich oxide layers on steels in flowing Pb-Bi	157
Fig. 6-21	Corrosion rates of corrosion resistant steels in flowing Pb-Bi	157
Fig. 7-1	Schematic of Pb-Bi forced convection loop	165
Fig. 7-2	Weight change of SiC and Si ₃ N ₄ specimens compared with other steel specimen	165
Fig. 7-3	SiC and Si ₃ N ₄ surfaces before and after corrosion test	166
Fig. 7-4	FE-SEM image of SiC specimen; (a) initial SiC surface; (b) after immersion in Pb-Bi for 2000 hours	166
Fig. 7-5	FE-SEM image of Si ₃ N ₄ specimen; (a) initial SiN surface; (b) SiN surface after immersion in Pb-Bi for 2000 hours	166
Fig. 7-6	Fe-SEM image and EDX analysis for surface cross section of SiC	167
Fig. 7-7	Fe-SEM image for surface cross section of Si ₃ N ₄	167
Fig. 7-8	Fe-SEM image and EDX analysis for dent part (a) in Si ₃ N ₄	168
Fig. 8-1	Pb-Bi forced convection test loop	183
Fig. 8-2	Schematic and photo of Pb-Bi sampling line in Pb-Bi forced convection test loop	184
Fig. 8-3	View of ruptured tube	185
Fig. 8-4	Size of fracture crack and deformation of ruptured tube	185
Fig. 8-5	SEM image of fractured face	185
Fig. 8-6	Dimple marks observed on the outer side of fractured face	186
Fig. 8-7	SEM images and component profiles: analysis point (a) distant from ruptured part; analysis point (b): near ruptured part	186

Fig. 8-8	Schematic of experimental apparatus, (a) Pb-Bi forced convective loop, (b) Electrodes and electromagnetic flow meter, (c) Circular duct and core of electromagnetic pump	187
Fig. 8-9	(a) EMF calibration curves before and after the operation for the third corrosion test and after test; (b) and (c) Corrosion and precipitation on the surface of electrode of electro-magnetic flow meter after the operation for the third corrosion test	187
Fig. 8-10	Decreases in Pb-Bi flow rate during operations for (a) third corrosion test and (b) fourth corrosion test	188
Fig. 8-11	Appearance of EMP core after fourth corrosion test, (a) EMP core part, (b) frontal view of EMP core head, (c) top view of EMP core head	188
Fig. 8-12	Corrosion and precipitation of EMP core head, (a) erosion at top of core head, (b) erosion at the bottom of spacer, (c) Pb-Bi penetration along welded part, (d) enlarged view of (c), (e) lump of corrosion products adhered on surface of ring spacer, (f) lump of corrosion products adhered on surface of EMP core	189
Fig. 8-13	Corrosion products on surface of EMP core down stream, (a) double layer corrosion products in adhered Pb-Bi, (b) corrosion products adhered on surface of EMP core downstream.	189

Chapter 1

Introduction

1.1 Background

Great amount of electricity has been generated and supplied by nuclear power plants in many industrialized countries. Nuclear energy is one of the solutions for the critical issues of energy security, economic growth and environmental protection [1].

Currently, the contribution of the light water reactor (LWR) is very large in the world. However, the importance of the fast breeder reactor (FBR) will increase in near future, since the uranium resources for the LWR fuels are limited and the reduction of LWR spent fuels are important to promote the peaceful use of nuclear technology. According to Yamaji *et al.* [1-3], the environmental protection is also promoted by the stabilization of the CO₂ emission in case the FBR is introduced after they may be available.

The lead alloy (Pb-Bi)-cooled fast reactor (LFR) is one of the candidates for the long-life, safe, simple and proliferation resistant fast reactors (FRs). Research of the LFR has been extensively performed in Russia [4, 5]. In the early 1950s in Russia at Institute of Physics and Power Engineering (IPPE), research and design study for the use of liquid Pb-Bi coolant in nuclear reactors were initiated. Full-scaled prototypes of the reactor installations were put into operation in 1959 and the first nuclear submarine with the Pb-Bi coolant was put into operation in 1963. Continuously, some reactors and submarines with the Pb-Bi coolant were constructed and put into the operation. However, some troubles occurred on the operation of Pb-Bi cooled reactors and submarines due to corrosion of steels in the flowing Pb-Bi. Thus, the corrosion of cladding and structural materials in the flowing Pb-Bi is a critical issue for the development of the Pb-Bi-cooled FRs.

1.2 Lead-Bismuth Cooled Fast Reactor

The use of the liquid Pb-Bi as the reactor coolant has some advantages even though there are some disadvantages as explained in next chapters. Applying the advantages, the design study on the Pb-Bi-cooled reactor has been performed.

Various types of small reactors with Pb-Bi coolant have been designed. This is since the small reactor has the advantages of easy operation, easy construction and proliferation resistance even though there is a scale demerit. Sekimoto *et al.* has designed LSPR (LBE-cooled Long life Safety Simple Small Portable

Proliferation-Resistant Reactor) [6]. This type of reactor is suitable for special uses, e. g., use in an isolated island such as Indonesia [7]. Moreover, in case of the Self-fuel-providing reactor (SFPR), the natural (or depleted) uranium is used as a reload core fuel, plutonium recycling by fuel reprocessing is not required [8, 9].

A direct contact type Pb-Bi cooled FBR (PBWR) was proposed by Buongiorno *et al.* [10]. Then, a design concept of PBWFR (Pb-Bi cooled direct contact boiling water small reactor) has been formulated with some design parameters by Takahashi *et al.* [11, 12]. The design of the PBWFR allows us to eliminate the coolant circulation pump, intermediate heat exchangers, intermediate circulation loops and steam generators since the direct contacts of water with hot Pb-Bi flow made lift pump and generated steam goes to turbine. Then, the reactor is simplified and this increases safety.

An LMR, named PEACER (Proliferation-resistant, Environmental-friendly, accident-tolerant, Continueable-energy, Economic Reactor) is being designed at the Seoul National University [13-15]. This reactor produces 1560MWth power, and the lifetime of the reactor is predicted as 60 years.

1.3 Merit of Lead-Bismuth as FR or FBR Coolant

The characteristics of the liquid Pb-Bi are presented in **Table 1-1** with those of major liquid metals and molten salts in the field of nuclear technology [16-32]. The advantages of the liquid Pb-Bi are as follows:

1) High boiling point of 1670°C

The Pb-Bi has higher boiling point of 1670°C than that of 883°C in sodium (Na), which is considered as the best coolant for fast reactors. The possibility of the boiling of the Pb-Bi seems negligible.

2) Low melting point of 125°C

The liquid Pb has high melting point of 327°C, this seems relatively high as the coolant of the FBR while that of 125°C in the Pb-Bi is low enough.

3) Small volume shrinkage at coagulation [33]

Volume shrinkage at coagulation of the Pb is 3.44%, while that of the Pb-Bi is uncountable.

4) Non violent reaction with water and air

In case of the Na-cooled reactor, any defects in the structural material will cause a steam come into contact with sodium. The resulting sodium-water reaction is exothermic and the caustic nature of the products can lead to propagation of the leak resulting in catastrophic accident conditions [34]. However, the liquid Pb-Bi does not react with water although the oxygen content in the water affects on the control of the oxygen potential in the melt, which is important factor for the corrosion control.

5) Favorable neutronic properties [7]

For the small fast reactor, it is expected that LBE coolant shows much better performance on the neutron economy than Na coolant because of its large scattering cross section and heavy nuclide mass.

The radioactive materials produced in the coolant during operation are also important. For Na, ^{24}Na should be considered. Its half-life time is 15 hrs and emits high energy gamma-rays (2.8MeV and 1.4MeV). Therefore, the primary loop of sodium cooled reactor shows very high dose rate. On the other hand, LBE does not produce so much gamma ray emitters, though Polonium is produced, which is an alpha ray emitter.

1.4 Weak Point of Liquid Lead-Bismuth as FR or FBR Coolant

Weak point of the liquid Pb-Bi could be summarized as follows:

1. High density of Pb-Bi

The density of the Pb-Bi is 10g/cm^3 and this is about 12 times higher than that of Na. The high density and the large viscosity of the Pb-Bi cause a large pressure drop. This affects the coolability of the Pb-Bi, and power density of the reactor must be decreased [7].

2. Corrosion of cladding and structural materials in flowing Pb-Bi

The corrosion of the cladding and structural materials makes the reactor-life time shorter, and this consequently affects the cost for the reactor construction and maintenance. Corrosiveness of the liquid Pb alloy for the steels is high even though that of the liquid Na are relatively low [16-20]. The corrosion rates of the

austenitic steels in the liquid Na are shown in **Fig.1-1** [20].

It can be considered that the corrosion characteristics of the steels in the liquid Pb-Bi are similar to those in the liquid Pb [6, 31, 32, 35]. The well known diagram for the corrosion of steel in the liquid Pb is shown in **Fig. 1-2** [6]. In the diagram, the corrosion behaviors of two types of austenitic steels were shown. These steels caused two types of corrosion depending on the oxygen concentration in the liquid Pb-Bi. These are a liquid metal corrosion (LMC) at low oxygen concentration and an oxidation corrosion at high oxygen concentration. In both types of corrosion, the oxygen concentration in the liquid Pb influenced on the intensity of the corrosion. Thus, the oxygen concentration in the liquid lead Pb alloy is of great importance as regards the corrosion behavior of the steels.

3. Liquid metal embrittlement of steels in flowing Pb-Bi

Liquid metal embrittlement (LME) phenomenon in the liquid Pb-Bi are rarely reported so far [36-38]. Liquid Pb alloy may cause LME of steels, *i.e.* the ductility may decrease in steels in contact with liquid Pb-Bi and they may become stressed.

4. Problem of Polonium Formation

The Bi, which is the main element of the Pb-Bi, has the property of polonium production. Polonium-210 is a radioactive nuclide, which emits 5.3MeV α -rays with 138 day half time. Obara *et al.* investigated about the removal of polonium by baking method [39]. The polonium evaporated from the LBE can be removed by baking samples at temperatures of 300°C and above. Miura *et al.*, investigated about the unfolding of polonium distribution in depth of irradiated lead-bismuth eutectic from α -particle pulse-height distribution [40]. In the work, the vertical polonium distribution in irradiated LBE is calculated from the measured α -particle pulse-height distribution with unfolding code UFOQ and three sets of response. The evaporation behavior of the polonium was examined by Glasbrenner *et al.* [41] and the alkaline extraction method for the removal was investigated by Lowen [42].

1.5 Review of Previous Studies on Lead-Bismuth Corrosion and Coolant Technology

The studies on the Pb-Bi corrosion have been performed for the development of the Pb-Bi cooled FRs. In the same way, the corrosion study has been performed for the development of accelerator driven system (ADS) with Pb-Bi target [43]. These studies have been mainly performed by the institutes of Russia, America, Europe and Japan with various type Pb-Bi corrosion test apparatus as shown in Tables 1-2 and 1-3.

1.5.1 Control of Oxygen Concentration in Liquid Lead-Bismuth

For the investigations on the corrosion characteristics of steels in the liquid metal, it is important to develop the oxygen control method since the oxygen in the melt influenced well on the corrosion characteristics [6, 28-32].

In case of the liquid Na, the oxygen concentration can be controlled within corrosion inhabitable condition by the cold trapping method [16-20]. The liquid Na with lower oxygen concentration causes weaker corrosion. However, as mentioned in the previous chapter, it is not easy to control the oxygen concentration in case of the liquid Pb alloy. This is since the preferable oxygen concentration in the melt is expected as much lower than that in the liquid Na, and the concentration has to be kept in the certain condition in order to prevent the occurrence of the LMC. Therefore, it is important to establish the method of the oxygen measurement and control with high accuracy.

For the measurement of the oxygen concentration in the melt, solid electrolyte type oxygen sensor has been developed. The performance of these sensors in the liquid Pb-Bi has been reported in some articles so far. According to Fernandez *et al.* the sensor output was agreed well with the results of the theoretical calculation. Also, it was found that the sensor response for the change of oxygen partial pressure in the liquid Pb-Bi was rapid enough [44]. Then, Konys *et al.* evaluated the response speed as in the range of minutes [45].

Two types of the oxygen control method in the liquid Pb alloy have been reported. The first one is the control by oxidation and reduction by injecting a gas mixture of H₂, steam and Ar into the melt, and the controllability was reported in ref [46-49]. The other method is the control by using mass exchanger where oxygen dissolves from solid lead oxide particles into the Pb-Bi flow and precipitates from the Pb-Bi on the solid PbO particles depending on the temperature [50, 51].

1.5.2 Corrosion in Static Condition

Static test method is appropriate to investigate the trend of corrosion behaviors [52-59].

Benamati and Fazio *et al.* investigated the corrosion characteristics of steels in the static Pb-Bi at the temperature of 573, 673 and 823K [52]. It was found that thin oxide layer formed and the layer protected the steel matrix from the LMC attack in the liquid Pb-Bi at lower temperature of 573 and 673K. However, the LMC occurred in the melt at 823K.

Ballinger *et al.* investigated the corrosion characteristics of the original components Fe-Cr-Si steels in the static Pb-Bi for 500 hours [53-54]. In the work, it was indicated that the Cr and Si in steels beneficially influenced on the formation of stable oxide layer, and this suppressed the oxidation corrosion and LMC due to the Si-Cr rich stable oxide layer formation.

Kurata *et al.* (JAERI) reported about the excellent corrosion resistance of 18Cr-20Ni-5Si steel in static Pb-Bi [55]. The 5wt% of Si in the austenitic steel, SX beneficially influenced on the formation of stable protection layer for the LMC attack, even though the Ni in the steel could easily dissolve into the melt due to the high dissolution rate [6].

Crespo *et al.* did the corrosion tests in the static conditions for the investigation on the effect of pre-oxidation of steels on the corrosion resistance in the early stage of the corrosion behavior [56]. The existence of the oxide layer preliminary formed was effective to suppress the initial corrosion. From these facts, the existence of the oxide layer on the steel surface is supposed to be effective to suppress the LMC in Pb-Bi.

Thus, it can be summarized that the LMC attack in the static Pb-Bi can be avoided if the stable protection layers, which were improved by the use of Cr and Si, could be formed.

Lowen *et al.* suggested that the corrosion characteristics of steels in the Pb-Bi can be influenced by the corrosion of container material in the corrosion test apparatus [57]. Furukawa *et al.* in JNC investigated the effect of oxygen concentration and temperature of liquid Pb-Bi on compatibility of ODS steel with liquid, stagnant Pb-Bi [58]. Hata *et al.* (Tokyo Tech) performed the experimental studies on steel corrosion in Pb-Bi with steam injection [59].

By the review of the above three papers of ref. [57-59], it was found that the corrosion conditions, such as oxygen concentration in the melt, liquid

temperature and dissolved hydrogen concentration, influenced on the corrosion characteristics of steels in liquid Pb-Bi.

1.5.3 Corrosion in Flowing Condition

The corrosion characteristics of steels in the flowing Pb-Bi are different from those in the static conditions, since the heavy density Pb-Bi flow causes shear and frictional stress which act on the surfaces of the steels or the formed oxide layers. Therefore, the results of the flowing corrosion tests are important to predict the corrosion characteristics and the corrosion rates of the materials in the actual reactors.

In the Los Alamos National Laboratory (LANL), there was the loop for the investigations on corrosion and thermal hydraulics in the flowing Pb-Bi [60, 61]. Barbier and Rusanov investigated the relation between the corrosion rate and the test time by means of the corrosion tests in the flowing Pb-Bi [62]. The test temperature was 470°C, and this is not sufficient for the conditions of LFR cladding and structural materials.

Aiello *et al.* (ENEA) found that the austenitic steel had corrosion resistant in the flowing Pb-Bi at the temperature of 400°C rather than martensitic steels [63]. Muller and Heinzl *et al.* performed long time corrosion test with three test steels for 2000- 7200 hours [64, 65]. The oxide layer protected the steel matrix for 7200- hours in the liquid Pb-Bi at 550°C. However, the LMC attack occurred in the melt at 600°C. Kikuchi *et al.* (JAERI) performed the corrosion test using tube shape specimen in the flowing Pb-Bi [66]. Sawada *et al.* found that Ni in steels dissolved into the melt and finally promoted the corrosion in the flowing Pb-Bi [67].

Corrosion-erosion occurrence was reported several times [47, 66, 67]. When the corrosion-erosion occurred on the steel surfaces, the corrosion rate of the steels can be increased drastically. Therefore, it is important to make clear the mechanism and process of the corrosion-erosion of the steels in the flowing Pb-Bi. Then, the countermeasure for the corrosion-erosion has to be discussed.

The corrosion in the flowing condition was reported although the volume of the data of the corrosion in the flowing condition was less than that in the static condition.

1.6 Unknown Factors on Lead-Bismuth Corrosion

By the review of the previous studies on the Pb-Bi corrosion, the unknown factors for the corrosion were summarized as follows:

- 1) The performance of the solid electrolyte type oxygen sensor in the flowing Pb-Bi is not sufficiently investigated. This is since the performance of the oxygen sensor in the long-term operation in the flowing Pb-Bi and the corrosion of sensor materials in the flow was not investigated.
- 2) The controllability of oxygen content in the melt by using a mass exchanger type oxygen control system is not made clear so far. This is since the performance of the mass exchanger type oxygen control method in the flowing Pb-Bi at low temperature for the appropriate oxygen concentration was not reported. The stability of the mass exchanger system should be investigated in the long term test in the flowing Pb-Bi.
- 3) The analysis for the corrosion-erosion phenomenon on the steel surfaces [47, 49] was not sufficient to determine the mechanism or the process of the corrosion-erosion of steels in the flowing Pb-Bi. The countermeasure to avoid the occurrence of the corrosion-erosion has not been discussed.
- 4) The results of the flowing corrosion tests were not sufficient to discuss the influence of the oxygen in the liquid Pb-Bi on the corrosion characteristics of steels.
- 5) The effects of surface treatment and roughness of steels on the corrosion in the flowing Pb-Bi was not made clear even though these effects on general corrosion, such as the corrosion of steels in a vapor or water, were well studied [69].
- 6) Effects of oxidation resistant element of Al in steel on the corrosion resistances in the flowing Pb-Bi were not investigated, even though the effects of Cr and Si in steels on the corrosion resistance in the static Pb-Bi were partly investigated [52, 53].
- 7) The use of ceramic materials as reactor cladding or structural materials of the Pb-Bi cooled FRs can increase the operation temperature and thermal efficiency. However, corrosion characteristics of the ceramic materials in the flowing Pb-Bi were not investigated.
- 8) Precipitation behavior of corrosion products in the flowing Pb-Bi was not investigated.

1.7 Purpose

Considering above-mentioned unknown factors for the Pb-Bi corrosion, the purpose of the thesis work is determined to outline the corrosion control by using corrosion resistant materials and chemical control method in the flowing Pb-Bi. To fulfill this purpose, the thesis study divided into seven stages. Each stage has individual purpose and motivation as follows;

1) Development of oxygen monitor and control system

The oxygen concentration in the flowing Pb-Bi must be monitored during the corrosion test operation, since the oxygen concentration in the flowing Pb-Bi may influence on the corrosion of steels [16]. For the application of the sensing technique to the actual coolant loop, sensor performance should be investigated by means of the performance tests at high temperature for long term. Then, the corrosion of the sensor materials should be analyzed. As for the oxygen control system, it is required that the oxygen concentration can be easily maintained in the adequate conditions. Thus, the development of the simple system for the oxygen control in the flowing Pb-Bi is important.

2) Investigation on the mechanism of erosion and corrosion in flowing Pb-Bi

The mechanism for the erosion/corrosion phenomena was not made clear so far. Then, the analysis for the eroded specimens should be carried out in detail. From the analysis results, the cause and process of the erosion in the flowing Pb-Bi should be made clear, and the counter measure for the erosion occurrence should be made clear.

3) Investigation on corrosion resistant of oxide layer in the flowing Pb-Bi

The property of the oxide layers formed on the steel surfaces in the flowing Pb-Bi should be investigated to make clear the relation between the layer property and the corrosion resistance. In addition, the characteristic of the oxidation corrosion of various steels should be investigated. The properties of protective oxide layers in the flowing Pb-Bi should be investigated.

4) Investigation on effects of surface treatment and condition of steels on corrosion resistance in flowing Pb-Bi

The effects of surface treatment and roughness of steels on the general corrosion, such as the corrosion of steels in a vapor or water, was well-known phenomenon [39]. However, these effects on the corrosion in the flowing Pb-Bi was not made clear yet. Thus, these effects in the flowing Pb-Bi should be investigated, and the ideal conditions of steel surfaces to be a corrosion resistant in the flowing Pb-Bi should be investigated.

5) Investigation on effect of Alloying Elements of Steels on Corrosion Resistance in Flowing Pb-Bi

The effect of Cr, which is major alloying element in the steels, on the corrosion resistant in the flowing Pb-Bi should be investigated. Furthermore, the effect of Si and Al, which are the steel alloying elements for the increase of the oxidation resistance, on the formation of stable oxide layer in the flowing Pb-Bi should be investigated.

6) Investigation of the corrosion resistance of ceramic materials, SiC and Si₃N₄, in the flowing Pb-Bi.

The corrosion characteristics of ceramic materials in the Pb-Bi should be investigated to know their possibility as the cladding material of the LFR which could be operated at higher temperature for higher thermal efficiency. The corrosion resistance of the ceramic materials should be compared with those of the other steels.

7) Investigation on the phenomena which involve corrosion in the flowing Pb-Bi

The corrosion involving phenomena, such as liquid metal embrittlement [36-38] or the precipitation of corrosion products [66] in the flowing Pb-Bi was rarely reported so far. By the analysis of the ruptured tube in the liquid Pb-Bi, the possibility of the corrosion influence of the tube wall on the liquid metal embrittlement should be investigated. The performance-worsened loop instruments should be taken off from the loop, and the cause for the performance decreasing should be investigated. Then, the corrosion products precipitated on the low temperature region of the loop should be analyzed.

1.8 Outline of The Thesis

According to the purpose explained in the previous chapter, this thesis consists of nine chapters. They are briefly outlined as follows:

Chapter 2 – Chemical Control of Liquid Alloy consists of *Chapter 2.1- Performance of Solid Electrolyte Type Oxygen Sensor in Flowing lead-bismuth* and *Chapter 2.2- Performance of Mass Exchanger Type Oxygen Control System in Flowing Pb-Bi*. In the *Chapter 2.1*, the performance of the solid electrolyte type oxygen sensor in the flowing Pb-Bi was described. The stability and reliability of the sensor was investigated by the means of the performance tests of sensors in the flowing Pb-Bi at various conditions. The corrosion of the sensor materials on the performance was metallurgically investigated. In the *Chapter 2.2*, the performance tests for the mass exchanger type oxygen control system were performed at various conditions in the flowing Pb-Bi. In the work, the oxygen sensing technique developed in *the Chapter 2.1* was used for the monitor of oxygen concentration. From the obtained results, stability and controllability of the mass exchanger type system were discussed. The experimental equation, which was drawn from the results of the performance tests, were compared with the conventional equation provided by Gromov *et al.* [6] and Muller *et al.* [70].

In *Chapter 3– Liquid Metal Corrosion and Erosion Behaviors of Steels in Flowing Lead-Bismuth*, the mechanism of erosion and corrosion of steels in the Pb-Bi flow was investigated. Nine steels were simultaneously exposed to the Pb-Bi flow at the temperature of 550°C for 1,000 hours [47, 49]. The behaviors of liquid metal corrosion (LMC) and Pb-Bi penetration into steels were analyzed metallurgically. The analysis results of the corroded steels were compared each other. Then, the general erosion mechanism of steels in the flowing Pb-Bi was schematically explained. The countermeasure for the erosion was discussed.

In *Chapter 4- Oxidation Corrosion Behaviors of Steels in Flowing Lead-Bismuth*, the results of steel corrosion test performed in a flowing Pb-Bi at high oxygen concentration were reported. In the corrosion test, the oxygen concentration was measured by the oxygen sensor explained in the *Chapter 1*. Oxidation corrosion characteristics of various steels in the flowing Pb-Bi were investigated by means of SEM/EDX analysis for the surface cross sections of

exposed steels. Then, the properties of the protective oxide layers were investigated. The measured weight loss of the steels was compared with that of severe LMC case explained in *Chapter 3*. The effect of the oxide layer formation on the LMC resistance was discussed. The mechanism for the layer formation in the flowing Pb-Bi was schematically explained.

Chapter 5– Effect of surface treatment of steels on corrosion resistance consists of *Chapter 5.1- Effect of Pre-Oxidation of Steels on Corrosion Resistance of Steels in Flowing Lead-Bismuth* and *Chapter 5.2- Effect of Surface Roughness of Steels on Corrosion Resistance of Steels in Flowing Lead-Bismuth*. In *Chapter 5.1*, the effect of pre-oxidation treatment of the steel surfaces on the initial corrosion in the flowing Pb-Bi was explained. Several steels were pre-oxidized in moist air, and the pre-oxidized steel was immersed in the flowing Pb-Bi at 550°C for 500 hours. In *Chapter 5.2*, the effect of surface roughness of the steels on the corrosion behaviors is explained. The specimens of 12-Cr and 9-Cr steels, which had the surface of smooth, rough and their middle roughness, were exposed into the Pb-Bi flow. The trend of crack occurrence in the layer and the layer detachment in the flowing Pb-Bi was discussed based on the corrosion experiment results.

Chapter 6- Effect of Alloying Elements in Steels on Corrosion Resistance consists of *Chapter 6.1- Effect of alloying element, Chromium (Cr) in steels on corrosion resistance* and *Chapter 6.2- Effect of alloying elements, silicon (Si) and aluminum (Al), in steels on corrosion resistance*. In the *Chapter 6.1*, the corrosion characteristics of high Cr steels were investigated by means of corrosion tests in the flowing Pb-Bi up to 2000 hours. In this chapter, corrosion resistance of SS430 (18-Cr steel) was highlighted by comparing with those of the other 12-Cr and 9-Cr steels. In the *Chapter 6.2*, corrosion resistance of Si- and Al-rich steels in the Pb-Bi flow was metallurgically investigated. The excellent corrosion resistance due to the formation of the Si- and Al- rich oxide layer was highlighted.

In ***Chapter 7- Corrosion Characteristics of Ceramic Materials, SiC and Si₃N₄ in Flowing Lead-Bismuth***, corrosion characteristics of SiC and Si₃N₄ ceramic materials in a flowing lead-bismuth were described. The corrosion on these specimens was metallurgically analyzed. The weight loss of SiC and Si₃N₄ specimens were compared with those of the other steels.

Chapter 8- Effect of Corrosion on Tube Rupture Behavior and Liquid Contamination consists of *Chapter 8.1- Effect of Corrosion on Tube Rupture Behavior in Liquid Lead-Bismuth* and *Chapter 8.2- Effect of Corrosion on Performance of Electro Magnetic Pump and Flow Meter in Flowing Lead-Bismuth*. In *Chapter 8.1*, results of investigation on the major factor of the tube rupture in the liquid Pb-Bi were reported. Effect of the corrosion on the tube rupture behavior in liquid Pb-Bi was investigated by means of metallurgical analysis for the corrosion of the ruptured part. In *Chapter 8.2*, the factor for the decreasing of the electro magnetic pump (EMP) and flow meter (EMF) were investigated by means of metallurgical analysis for the immersion part of the performance worsened EMP and EMF. Then, the precipitated materials on their surfaces were analyzed in detail.

In **Chapter 9- Conclusions**, conclusions are drawn from the study that was done.

References

- [1] K. Yamaji *et al.*, “Nuclear Power in the Global Energy-Environmental System”, Prog. in Nucl. Energy, vol. 32, No. 3/4. 235-241 (1998).
- [2] K. Yamaji *et al.*, “Global Energy Strategy”, Denryoku-Shimpo-sha (1995) [in Japanese]
- [3] K. Yamaji *et al.*, “Long-range Optimal Strategy of Plutonium Utilization”, Energy Systems, Management and Economics: Selected papers from the IFAC/IFORS/IAEE Symposium, Tokyo Japan Oct.25-27 (1989).
- [4] B. F. Gromov *et al.*, “Designing the Reactor Installation with Lead-Bismuth Coolant for Nuclear Submarines. The Brief story. Summarized Operation Results”, Proc. of HLMC1999, P14-17 (1998).
- [5] B. F. Gromov, Y. I. Orlov, P. N. Martynov, V. A. Gulevski, “The Problems of Technology of the Heavy Liquid Metal Coolants (Lead-bismuth, Lead)”, Proc. of HLMC1999, P87-100 (1998).
- [6] H. Sekimoto *et al.*, “Small LBE-cooled fast reactor for expanding market” Proc. of 10th Int. Conf. on Nucl. Eng. ICONE10, ICONE10-22049, Apr. 14-18, Arlington, VA (2002).
- [7] H. Sekimoto and Z. Su’ud, “Design Study of Lead- and Lead- Bismuth-Cooled Small Long-Life Nuclear Power Reactors Using Metallic and Nitride Fuel”, J. Nucl. Technol. Vol. 109, 307-313 (1994).
- [8] V. I. Subbotin, Proc. Int. Top. Meet. on Advanced Reactor Safety, Pittsburgh, PA, vol.2. P.636 (1994).
- [9] V. G. Toshinsky *et al.*, “Multi Objective Fuel Management Optimization for Self-Fuel-Providing LMFBR Using Genetic Algorithms”, Annals of Nucl. Eng. 26, 783-802 (1999).
- [10] J. Buongiorno *et al.*, “Conceptual Design of a Lead-Bismuth Cooled Fast Reactor with In-vessel Direct-Contact Steam Generation” MIT-ANP-TR-079, Center for Advanced Nuclear Energy Systems, Massachusetts Institute of Technology.
- [11] M. Takahashi *et al.*, “Pb-Bi Cooled Direct Contact Boiling Water Small Reactor”, Prog. in Nucl. Energy, vol.47, pp. 190-201 (2005).
- [12] M. Takahashi *et al.*, “Study on Pb-Bi-Water Direct Contact Boiling Two-Phase Flow and Heat Transfer”, Prog. in Nucl. Energy, vol.47, No.1-4, pp. 569-576 (2005).

-
- [13] I. S. Hwang *et al.*, “Conceptual Design Study of Proliferation-Resistant Transmutation Reactor”, Ministry of Science and Technology, Seoul, Korea (1999).
- [14] I. S. Hwang *et al.*, “The Concept of Proliferation-Resistant, Environmental Friendly, Accident-Tolerant, Continual and Economical Reactor (PEACER)”, *Prog. in Nucl. Energy*, vol. 37, No. 1-4, 217-222, (2000).
- [15] J. E. Chang *et al.*, “Natural Circulation Capability of Pb-Bi Cooled Fast Reactor: PEACER”, *Prog. in Nucl. Energy*, vol. 37, No. 1-4, 211-216, (2000).
- [16] J. R. Weeks and C. J. Klamut, “Liquid Metal Corrosion Mechanisms”, *Proc. of the Conf. on corrosion of reactor materials*, Salzburg, Austria, June 4-9 (1962).
- [17] V. Ganesan, V. Ganesan and H. U. Borgstedt, “Analysis of CRENOVA Sodium Loop Material” *J. Nucl. Mater.*, 312, 174-180 (2003).
- [18] E. Yoshida and S. Kato, “Sodium Compatibility of ODS Steel at Elevated Temperature”, *J. Nucl. Mater.*, 329-333, 1393-1397 (2004).
- [19] H. U. Borgstedt, “Compatibility of Steel No. 1.4970 with Liquid Sodium at High Temperatures”, *J. Nucl. Mater.*, 317, 160-166 (2003).
- [20] A. Maruyama *et al.*, Corrosion rate equation of austenitic steels in liquid Na at high temperature, *Nihon Genshiryoku Gakkaishi*, Vol. 26, No. 4 (1984).
- [21] H. Moriyama, A. Sagara, S. Tanaka, R. W. Moir, D. K. Sze, “Molten Salts in Fusion Nuclear Technology”, *Fusion Engineering and Design*, 39-40, 627-637 (1998).
- [22] H. Nishimura, T. Terai, T. Yoneoka, S. Tanaka, A. Sagara and O. Motojima, “Compatibility of Structural Candidate Materials with LiF-BeF₂ Molten Salt Mixture”, *J. Nucl. Mater.*, 283-287, 1326-1331 (2000).
- [23] H. Nishimura, T. Terai, M. Yamawaki, S. Tanaka, A. Sagara and O. Motojima, “Compatibility of Ferritic Steels with Li₂BeF₄ Molten Salt Breeder”, *J. Nucl. Mater.*, 307-311, 1355-1359 (2002).
- [24] O. I. Eliseeva, V. N. Fedirko, V. M. Chernov, L. P. Zaviatsky, “Corrosion of V-Ti-Cr Alloys in Liquid Lithium: Influence of Alloy Composition and Concentration of Nitrogen in Lithium”, *J. Nucl. Mater.*, 283-287, 1282-1286 (2000).

- [25] V. A. Evtikhim, I. E. Lyublinski, A. V. Vertkov, "Compatibility of Vanadium Alloys and Its Weld Joints in Homogeneous and Heterogeneous Liquid Lithium Systems", *J. Nucl. Mater.*, 258-263, 1487-1491 (1998).
- [26] A. Suzuki, T. Muroga, T. Yoneoka, S. Tanaka, "Compatibility of Compound Oxides with Liquid Lithium for Fusion Reactor Blanket Application", *J. Phys. and Chem. of Solids*, 66, 690-693 (2005).
- [27] S. Malang and R. Mattas, "Comparison of Lithium and the Eutectic Lead-Lithium Alloy, Two Candidate Liquid Metal Breeder Materials for Self-Cooled Blankets", *Fus. Eng. Des.*, 27, 399-406 (1995).
- [28] H. Glasbrenner, J. Konys and Z. Vob, "Corrosion Behavior of Low Activation Steels in Flowing Pb-17Li", *J. Nucl. Mater.*, 281, 225-230 (2000).
- [29] Ph. Deloffre, A. Terlain, A. Alemany, A. Kharicha, "Corrosion Study of an Austenitic Steel in Pb-17Li Under Magnetic Field and Rotating Flow", *Fus. Eng. Des.*, 69, 391-396 (2003).
- [30] J. Konys, W. Krauss, Z. Voss, O. Wedemeyer, "Corrosion Behavior of EUROFER Steel in Flowing Eutectic Pb-17 Li Alloy ", *J. Nucl. Mater.*, 329-333, 1379- 1383 (2004).
- [31] G. Muller, G. Schumacher and F. Zimmermann, "Investigation on Oxygen Controlled Liquid Lead Corrosion of Surface Treated Steels", *J. Nucl. Mater.*, 278, 85-95 (2000).
- [32] H. Glassbrener, J. Konys, G. Muller and A. Rusanov, "Corrosion Investigations of Steels in Flowing Lead at 400°C and 550°C", *J. Nucl. Mater.*, 296, 237-242 (2001).
- [33] E. H. Pylchenkov "The Issues of Freezing-Defreezing Lead-Bismuth Liquid Metal Coolant in Reactor Facilities Circuits", *Proc. of HLMC1999*, P110-120 (1998).
- [34] T. Gnanasekaran, "Thermo-Chemistry of Binary Na-NaH and Ternary Na-O-H Systems and the Kinetics of Reaction of Hydrogen/Water with Liquid Sodium- a Review", *J. Nucl. Mater.*, 274, 252-272 (1999).
- [35] I. V. Gorynin, G. P. Karzov, V. G. Markov, V. S. Lavrukhin and V. A. Yakovlev, "Structural Materials for Power Plants with Heavy Liquid Metals as Coolants", *Proc. of HLMC1999*, P120-124.
- [36] A. Legis, G. Nicaise, J.-B. Vogt, J. Foct, "Liquid Metal Embrittlement of the Martensitic Steel 91: Influence of the Chemical Composition of the

- Liquid Metal Experiments and Electronic Structure Calculations”, J. Nucl. Mater., 301, 70 (2002).
- [37] H. Glasbrenner, D. Viol, “Tensile Testing of MANET II in Flowing Pb-Bi Alloy at Elevated Temperature”, Fusion Eng. and Design, 61, 691 (2002).
- [38] A.G. Nicholas and C.F. Old, “Review of Liquid Metal Embrittlement”, Journal of material science, 14, 1 (1979).
- [39] T. Obara, T. Miura and H. Sekimoto, “Fundamental Study of Polonium Contamination by Neutron Irradiated Lead-Bismuth Eutectic”, J. Nucl. Mater., 343, 297-301 (2005).
- [40] T. Miura, T. Obara and H. Sekimoto, “Unfolding of Polonium Distribution in Depth of Irradiated Lead-Bismuth Eutectic from α -particle Pulse-Height Distribution”, Applied Radiation and Isotopes, 61, 1307-1311 (2004).
- [41] H. Glasbrenner, J. Eikenberg, F. Groschel, L. Zanini, “Polonium Formation in Pb-55.5Bi Under Proton Irradiation”, J. Nucl. Mater., 335, 270-274 (2004).
- [42] E. Lowen, “Investigation of polonium removal systems for lead-bismuth cooled FBRs”, Progress in Nuclear Energy, Vol. 47, No.1-4, pp. 586-595 (2005).
- [43] M. Takahashi, M. Igashira, T. Obara, H. Sekimoto, K. Kikuchi, K. Aoto and T. Kitano, “Studies on Materials for Heavy-Liquid-Metal-Cooled Reactors in JAPAN”, Proc. of 10th Int. Conf. Nuc. Eng., Arlington, Virginia, VA, Apr. 14-18, ICONE10-22166 (2002).
- [44] J. A. Fernandez, J. Abella, J. Barcelo and L. Victori, “Development of an Oxygen Sensor for Molten 44.5% Lead- 55.5% Bismuth Alloy”, J. Nucl. Mater., 301, 47-52 (2002).
- [45] J. Konys, H. Muscher, Z. Vob and O. Wedemeyer, “Development of Oxygen Meters for the Use in Lead-Bismuth”, J. Nucl. Mater., 296, 289-294 (2001).
- [46] M. Kondo, M. Takahashi, T. Suzuki, K. Ishikawa, K. Hata, S. Qiu and H. Sekimoto, “Metallurgical Study on Erosion and Corrosion Behaviors of Steels Exposed to Liquid Lead-Bismuth Flow”, J. Nucl. Mater., 343, 349 (2005).
- [47] K. Ishikawa, Master’s thesis at Tokyo Institute of Technology (2002).
- [48] T. Kumagai, Master’s thesis at Tokyo Institute of Technology (2006).

-
- [49] M. Takahashi *et al.*, “Experimental Studies on Flow Technology and Steel Corrosion of Lead Bismuth”, Proc. of 10th Int. Conf. Nuc. Eng., Arlington, Virginia, VA, Apr. 14-18, ICONE10-22226 (2002).
- [50] Z. I. Yemelyantseva, V. N. Lenonv, A. D. Yefanov, Y. I. Orlov, P. N. Martynov and V. A. Gulevsky, “Validation of the Lead Coolant Technology for BREST Reactor”, Proc. of 11th International Conf. Nucl. Eng., Tokyo, Japan, Apr. 20-23, ICONE11-36408 (2003).
- [51] G. Ilincev, “Research Results on the Corrosion Effects of Liquid Heavy Metals Pb, Bi and Pb-Bi on Structural Materials with and without corrosion Inhibitors”, J. Nucl. Eng. and Sci., 217, 167-177 (2002).
- [52] G. Benamati, C. Fazio *et al.*, “Temperature Effect on the Corrosion Mechanism of Austenitic and Martensitic Steels in Lead-Bismuth”, J. Nucl. Mater., 301, 23-27 (2001).
- [53] R. G. Ballinger, J. Lim, E. Lowen, “The Effect of Si on the Corrosion of Iron on Lead Bismuth Eutectic”, Proc. of 11th Int. Conf. on Nucl. Eng. ICONE11, ICONE11-36531, Apr. 20-23, Tokyo, Japan (2003).
- [54] J. Lim, R. G. Ballinger, P. W. Stable, Proc. of Int. conf. of Global-2003, Nov. 16-20, New Orleans, LA , 2100 (2003).
- [55] Y. Kurata and M. Futakawa, “Excellent Corrosion Resistance of 18Cr-20Ni-5Si Steel in Liquid Pb-Bi”, J. Nucl. Mater., 325, 217-222 (2004).
- [56] L. Soler. Crespo, F.J.Martin Munoz, D. Gomez Briceno, “Short Term Static Corrosion Tests in Lead-Bismuth”, J. Nucl. Mater., 296, 273-281 (2001).
- [57] E. P. Lowen, H. J. Yount, K. Volk and A. Kumar, “Layer Formation on Metal Surfaces in Lead-Bismuth at High Temperatures in Presence of Zirconium”, J. Nucl. Mater., 321, 269-280 (2003).
- [58] T. Furukawa, G. Muller, G. Schumacher, A. Weisenburger, A. Heinzl and K. Aoto, “Effect of Oxygen Concentration and Temperature on Compatibility of ODS Steel with Liquid, Stagnant Pb-Bi”, J. Nucl. Mater., 335, 189-193 (2004).
- [59] K. Hata, K. Hara and M. Takahashi, “Experimental Studies on Steel Corrosion in Pb-Bi with Steam Injection”, Progress in Nuclear Energy, Vol. 47, 596-603 (2005).
- [60] T. R. Allen *et al.*, “Corrosion and Radiation of Advanced Ferritic-Martensitic Steels for Generation IV Application”, Proc. of Global 2005,

- Oct. 9-13, Tsukuba, Japan (2005).
- [61] J. Zhang and Ning Li, "Corrosion/Precipitation in Non-isothermal and Multi-modular LBE Loop Systems", *J. Nucl. Mater.*, 326, 201-210 (2004).
- [62] F. Barbier and A. Rusanov, "Corrosion Behavior of Steels in Flowing Lead-Bismuth", *J. Nucl. Mater.*, 296, 231-236 (2001).
- [63] A. Aiello, M. Azzati, G. Benemati, A. Gessi, B. Long and G. Scaddozzo, "Corrosion Behavior of Stainless Steels in Flowing LBE at Low and High Oxygen Concentration", *J. Nucl. Mater.*, 335, 169-173 (2004).
- [64] G. Muller *et al.*, "Results of steel corrosion tests in flowing liquid Pb/Bi at 420-600°C after 2000 h", *J. Nucl. Mater.*, 301, 40-46 (2002).
- [65] G. Muller *et al.*, "Results of Steels in Flowing Liquid PbBi Eutectic Alloy at 420°C-600°C After 4000-7200 h", *J. Nucl. Mater.*, 335, 163-168 (2004).
- [66] K. Kikuchi *et al.*, "Corrosion-Erosion Test of SS316 in Flowing Pb-Bi, *J. Nucl. Mater.*, 318, 348-354 (2003).
- [67] N. Sawada, Master's thesis at Tokyo Institute of Technology (2001).
- [68] K. Kamata, T. Kitano, H. Ono and M. Ono, "Studies of Corrosion Resistance of Japanese Steels in Liquid Lead-Bismuth, Proc. of 11th Int. Conf. on Nucl. Eng. (ICONE12), ICONE11-36204, April 20-23, Tokyo, Japan (2003).
- [69] High Temperature Oxidation of Metal, Japan Society of Corrosion Engineering, (1882) (*in Japanese*).
- [70] G. Muller *et al.*, "Investigation on Oxygen Controlled Liquid Lead Corrosion of Surface Treated Steels", *J. Nucl. Mater.*, 278, 85-95 (2000).

Table 1-1 Comparison of properties of liquid metals

Liquid metals	Na [16-20]	Flibe [21-23]	Li [24-27]	Pb-17Li [28-30]	Pb [31-32]	Pb-Bi
Melting point (°C)	98	459	180	235	327	125
Density (g/cm ³)	0.85	2.0	0.48	8.98	11.34	10
Thermal conductivity (W/m K)	70.8	1.00	49.9	13.2	35.2	12.9
Viscosity (mm ² /s)	0.274	7.44	0.83	0.17	0.23	1.83
Major impurity which affects material corrosion	Oxygen	TF	Nitrogen	Oxygen	Oxygen	Oxygen
Preferable concentration of impurities	Less than 0.0025 (%)	-	0.0015-0.67 (at%)	-	10 ⁻⁷ (wt%)	-
Method of impurity control	Cold trapping	-	Cold trapping Getter trapping	-	Gas injection	-
Corrosion	Low (Corrosion depth of 304 steel was 10-20µm for 80000-hour immersion in flowing Sodium [2])	Low (Corrosion depth of the steels is of the order of nanometer [6].)	Active (Corrosion depth of ceramic materials is of the order of micrometer [10])	Active (Corrosion rate of 9Cr steels is of the order of about 90µm per year [14])	Active (Corrosion rates of austenitic steels are of the order of about 200 µm per year [15])	-

Table 1-2 Pb-Bi test apparatus (Static system)

	America		Europe			Japan	
	MIT [53, 54]	INEEL [56]	CIEMAT [57]	ENEA [52]	JNC [58]	JAERI [55]	Tokyo Tech [59]
Test temperature (°C)	600	650	600	300-400	650	550	400-500
System	Rotating system	Static	Static	Static	Static	Static	Static
Control system of oxygen potential in Pb-Bi	Gas injection (Ar/Steam/H ₂)	Gas injection (Ar/O ₂)	Gas injection (Ar/H ₂)	Oxygen saturated	Gas injection (Ar/Steam/H ₂)	Oxygen saturated	Steam injection
Monitor technique of oxygen potential in Pb-Bi	-	Monitor for the gas injection and estimation	-	Estimation	Oxygen sensor (solid electrolyte)	Estimation	Oxygen sensor (solid electrolyte)
Corrosion test material	Fe-Cr-Si	HT-9	F82H mod	MANET2 (10Cr) EP823 (12Cr-1.8Si)	P122 (11Cr-2W)	SX steel	HCM12A

Table 1-3 Pb-Bi test apparatus (Dynamic system)

	America	Russia		Europe		Japan	
Institute (loop name)	LANL [60, 62] (DELTA)	IPPE [62] (CU-1M)	IPPE (2M)	ENEA [63] (LECOR loop)	Tokyo Tech [67]	JAERI [66]	MES [68]
Pb-Bi test temperature (°C)	460	479	550	400	550	450	550
Temperature gap (°C)	-	300	-	250	150	50	100
Flow velocity (m/s)	1.2m/s	1.9	2	1	2	1	2
Control system of oxygen potential in Pb-Bi	-	-	Oxygen saturated	Gas injection (Ar/H ₂) Adding Mg for deoxide	Gas injection (Ar/Steam/H ₂)	Oxygen saturated	-
Monitor technique of oxygen potential in Pb-Bi	Oxygen sensor	Oxygen sensor (solid electrolyte: Yttria stabilized zirconia)	Oxygen saturated	Oxygen sensor (solid electrolyte: Yttria stabilized zirconia)	Oxygen sensor (solid electrolyte)	-	Oxygen sensor (solid electrolyte)
Pump	-	Centrifugal pump	-	Mechanical pump	Electro-magnetic pump	Electro-magnetic pump	Mechanical pump
Test material	HCM12A	1.4970 (15Cr-14Ni-1.8 Mo) T91 (8.26Cr-1Mo) EP823 (12Cr-2Si)	-	-	NTK04L, SUH3, Recloy10, HCM12A, SUS405 and so on	SUS316 ,SX Austenitic steel	SUH3, 9Cr steel 2.25Cr steel and so on

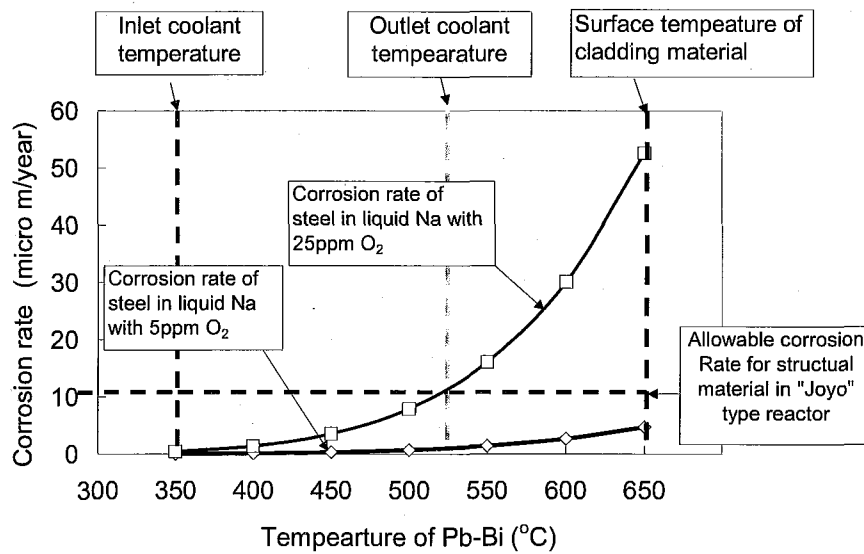


Fig. 1-1 Corrosion rates of steels in flowing Na calculated using equation of corrosion rate for structural material in Joyo type reactor

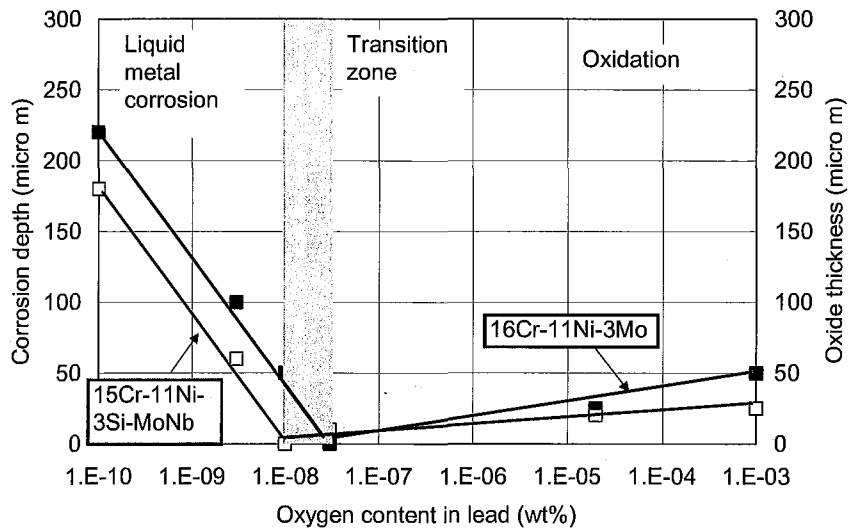


Fig. 1-2 Diagram showing corrosion behavior of steels in flowing oxygen containing Pb for 3000 hours at 550°C [35]

Chapter 2

Chemical Control of Liquid Alloy

2.1 Performance of Solid Electrolyte Type Oxygen Sensor in Flowing Lead-Bismuth

2.1.1 Introduction

For the development of fast reactors (FRs) with lead-55bismuth (Pb-Bi) coolant, corrosion of cladding and structural materials is one of the critical issues [1]. An oxygen concentration in the liquid Pb-Bi is important parameter to determine the corrosion of the materials as the same as that in liquid Pb [2].

For the monitor of the oxygen concentration in the flowing Pb-Bi, the solid electrolyte type oxygen sensor has been developed. The performance of these sensors in the liquid Pb-Bi is well reported in the journals. According to Fernandez *et al.* the sensor output was agreed well with the results of the theoretical calculation. Also, it was found that the sensor response for the change of oxygen partial pressure in the liquid Pb-Bi was rapid enough [3]. Then, Konys *et al.* evaluated the response speed as in the range of minutes [4].

However, the results of long -term use of this type of sensors in the flowing Pb-Bi was not reported so far. The corrosion of the sensor materials and how this influence on the sensor performance should be investigated.

In this chapter, the performance of the oxygen sensor in the flowing Pb-Bi was reported with the basic theory for the measurement. The reliability and repeatability of the sensor were investigated. The corrosion of the sensor-cell materials in the flowing Pb-Bi was analyzed to make clear whether this type of the sensor can be use in the flowing Pb-Bi for long term or not.

2.1.2 Experimental apparatus and procedure

Pb-Bi Forced Convection Loop

The long-term performance tests for the oxygen sensor were performed by using the Pb-Bi forced convection loop. **Figure 2-1** shows a schematic of a Pb-Bi forced convection test loop used in the present study. The volume of the liquid Pb-Bi in the loop was 22L. The loop can be classified to a high temperature region made of high Cr steel (9Cr-1Mo) and a low temperature region made of SS-316 (18Cr-12Ni-2Mo). The corrosion test section and the oxygen sensor were in the high temperature region, and the expansion tank, the electromagnetic pump and the electromagnetic flow meter were in the low temperature region.

The PbO reaction vessel was installed as a mass exchanger in a by-pass line of the low temperature region (This is explained in detail in *Chapter 2.2*). An oxygen concentration in the Pb-Bi loop can be controlled by changing the temperature of solid

PbO particles in the PbO reaction vessel. The electromagnetic flow meter and the bellow valves for material test were also installed in the by-pass line.

Liquid Pb-Bi was circulated by the electromagnetic pump, and the flow rate was measured by the main and by-pass electromagnetic flow meters. The Pb-Bi temperature at several points of the loop were monitored using sheathed thermocouples inserted into the flow.

Oxygen Sensor

Figure 2-2 shows a schematic of the oxygen sensor. The sensor equipped two reference electrode cells. The temperature of the Pb-Bi around the sensor cells was measured by the thermocouples directory inserted in the Pb-Bi. The weight made of a SS-304 cylinder prevents the sensor cells from floating up by buoyancy force. The liquid level was controlled by the cover gas pressurized with Ar gas of 99.999% purity.

Figure 2-3 shows the schematic of the sensor cell. The reference electrode cell consists of a solid electrolyte conductor, a Mo wire as electrical lead and an oxygen saturated bismuth as reference fluid (**Fig. 2-3 (a)**). Two types of the solid electrolyte conductor, yttria stabilized zirconia (YSZ: $Y_2O_3-ZrO_2$) and magnesia stabilized zirconia (MSZ: $MgO-ZrO_2$), were used. The mechanical characteristics of these solid electrolyte cells were shown in **Table 2-1**. Reference fluid in the sensor cells was an oxygen saturated Bi. These solid electrolyte cells were supplied from NIKKATO corporation.

The powder of bismuth oxide (Bi_2O_3) and bismuth metal (Bi) was mixed well and poured into the cell (**Fig. 2-3 (b)**). The weight ration of Bi to Bi_2O_3 was 95wt% to 5wt%. The powder of the Bi and Bi_2O_3 had the purity of 99.9% and 98%, respectively. The Mo wire was inserted into the cell as an electrical lead. An electromagnetic force (EMF), or electrical potential between the Mo lead and Pb-Bi (steel vessel wall) was measured using electrometer with high input impedance of $10^{12}\Omega$. The system of the sensor can be expressed as



In the system, O^{2-} dissolves in Bi- Bi_2O_3 at saturation condition, and it dissolves in Pb-Bi. The EMF between inside and outside surfaces of the sensor cell is induced by the difference of the chemical potential of oxygen in the reference fluid Φ_{ref} and that in Pb-Bi Φ_{Pb-Bi} . The EMF is expressed by the Nernst equation:

$$E = \frac{1}{2F} [\Phi_{ref} - \Phi_{Pb-Bi}] \quad (2.2)$$

where F is the Faraday constant. The chemical reactions are as follows:



in the reference fluid,



in Pb-Bi. If $\Delta G_{Bi_2O_3}^0$ and ΔG_{PbO}^0 are the formation energies of Bi_2O_3 and PbO , respectively, the oxygen potentials are given as reported in ref [5]:

$$\Phi_{ref} = \Delta G_{Bi_2O_3}^0 / 3. \quad (2.5)$$

$$\Phi_{Pb-Bi} = \Delta G_{PbO}^0 - RT_{sensor} \ln \frac{C}{C_s}. \quad (2.6)$$

where C is the oxygen concentration in the liquid Pb-Bi, C_s is the saturated concentration or the solubility of the oxygen in Pb-Bi, and T_{sensor} is the temperature of the liquid Pb-Bi at the sensor in the unit of K. Then, the Eqs. (2-2), (2-5) and (2-6) are combined as follow:

$$E = \frac{1}{2F} \left[\frac{\Delta G_{Bi_2O_3}^0}{3} - \Delta G_{PbO}^0 - RT_{sensor} \ln \frac{C}{C_s} \right]. \quad (2.7)$$

If Bi of 55wt% in the melt plays a particular role in the oxidation process, then, the Nernst equation is given by

$$\begin{aligned} E &= \frac{1}{2F} \left[\frac{\Delta G_{Bi_2O_3}^0}{3} - (0.45\Delta G_{PbO}^0 + 0.55\frac{\Delta G_{Bi_2O_3}^0}{3} + RT_{sensor} \ln \frac{C}{C_s}) \right] \\ &= \frac{1}{2F} \left[0.45\frac{\Delta G_{Bi_2O_3}^0}{3} - 0.45\Delta G_{PbO}^0 - RT_{sensor} \ln \frac{C}{C_s} \right]. \end{aligned} \quad (2.8)$$

The oxygen solubility in the liquid Pb-Bi was calculated using the equations:

$$\log C_s = 1.2 - 3400/T \quad (673K < T < 973K) \quad (2.9)$$

provided by Gromov *et al.* [2]. This equation was used with fitting in the low

temperature ranges ($T < 673\text{K}$). And according to Muller *et al.* [5], theoretical equation was given as

$$\log C_s = 2.52 - 4803/T \quad (2.10).$$

Test Conditions

The conditions of the sensor performance tests is presented in **Table 2-2**. The performance tests were named as T-1 to T-5. In the tests, liquid Pb-Bi was charged into the loop at 250 °C. Then, the temperature of the flowing Pb-Bi was increased up to 550 °C in the high temperature region and 400°C in the low temperature region. After the each performance tests, the liquid Pb-Bi was cooled down and drained from the loop into the dump tank at 250 °C. Then, the Pb-Bi was removed from the sensor surface. Simultaneous to the performance tests of T-1, T-2 and T-4, steel corrosion tests were performed in the corrosion-test section in the loop (**Fig. 2-1**). Before the T-2 test, new MSZ and YSZ cell was installed in the sensor. These sensor operated for 100 hours at 400°C for the performance tests of the electromagnetic pump and flow meter (This is described in *Chapter 8-2*). In the T-3 test, the oxygen control test using PbO mass exchanger was performed. The oxygen concentration in the Pb-Bi was controlled at high potentials. Test T-5 was carried out to analyze initial condition of the MSZ sensor.

Analysis Procedure of Sensor Corrosion

After the tests T-1 and T-4, the sensor cells were extracted from the loop to analyze the corrosion of sensor cell surfaces. The removal of the adherent Pb-Bi or corrosion products was not performed, since the authors interested in adhesive materials on the sensor surfaces. The sensor cells were cut as cross section around the free surface of the Pb-Bi flow. Also, the sensor cells were cut as cross section at the part immersed deeply into the Pb-Bi flow. These cross sections were analyzed using 3D laser microscope at low magnification. Then, the corroded part or adherent corrosion products was analyzed using FE-SEM/EDX.

2.1.3 Performance of Oxygen Sensor in Flowing Lead-Bismuth

Sensor Performance

Figure 2-4 shows the initial EMF output of the MSZ sensor in the flowing Pb-Bi. Although the Pb-Bi temperature became constant at 550°C after 25 hours passed, the sensor output kept to increase with time initially. After 200 hours passed, the sensor output became stable and constant at 0.43V, and the noise level error was detected possibly due to the temperature fraction in the flowing Pb-Bi. This value corresponds to the oxygen concentration of 1×10^{-8} wt% by the calculation using eqs. (2.1)-(2.10). This oxygen potential was higher than that required for the Fe oxide formation in the liquid Pb-Bi. As the sensor output indicated the formation of Fe-oxide, the Fe oxide formed on the low Cr steels in the steel corrosion test (*Chapter 4*).

Figure 2-5 shows the initial performance of the MSZ and YSZ sensors in the test T-2. The stable performance of the sensors was obtained shortly after the immersion. The output of the MSZ and the YSZ sensors became nearly equal to each other as the Pb-Bi temperature increased. Finally, the EMF output became the same at 0.43V at the temperature of 550°C, and this value was the same to that in the test T-1. This indicates that the sensors have repeatability. The oxygen concentration in the T-1 and T-2 tests must be the same, since the oxygen concentration was not controlled in these tests.

In the test T-3, the sensor responded to the change of the oxygen concentration in the flowing Pb-Bi. These results in detail were reported in *Chapter 2-2*.

Figure 2-6 shows the initial performance of the YSZ sensor in the test T-4. The sensor output was not stable for initial 200 hours. This is possibly because there was the fraction of the oxygen concentration in the flowing Pb-Bi due to the influence of the oxygen control test in the test T-3.

Influence of Metallurgical State of Sensor on Performance

In the test T-1, the sensor kept to increase the EMF output after the Pb-Bi temperature became constant. The Pb-Bi contained certain oxygen concentration (**Fig. 2-4**). This implies that the metallurgical state of the sensor changed initially. The initial condition of the sensor cell was investigated, by means of the microscope observation of the sensor cell which was only immersed in the Pb-Bi for 4 hours in the test T-5. **Figure 2-7 (a)** shows the cross section of the sensor cell. The reference fluid of the oxygen saturated Bi was not compact. The reference fluid did not contact well with the inner surface of the MSZ conductor. **Figure 2-7 (b)** shows the cross section of the MSZ cell used in the Test T-1. The reference fluid was compact and well contacted with the inner surface of the solid electrolyte conductor. The influence of the Pb-Bi was not detected on the outer surfaces of the sensor cell in both case. Thus, the initial un-stable work of the sensor was because the reference fluid was not mixed well and

did not contact with inner surface of the sensor cell. The sensor must have well-mixed reference fluid before the measurement of oxygen concentration. One idea to remove this influence is to heat the sensor cell at the higher temperature than the melting point of Bi, 271.9°C for 100-200 hours before the measurement of oxygen concentration in the liquid Pb-Bi.

2.1.4 Corrosion of Sensor Materials in Flowing Lead-Bismuth

MSZ cell

Figure 2-8 shows the MSZ and YSZ cells used in the flowing Pb-Bi for 3500 hours through the tests T-2 to T-4. In the MSZ cell, the surface color was changed from initial silky white to black after the exposure. This indicated that corrosion products adhered on the sensor surface in the Pb-Bi. Pb-Bi particles of silver color was partially adhered on the sensor surface.

Figure 2-9 shows the cross section of MSZ sensor cells. The MSZ outer surface was smooth without erosion. The reference fluid of the oxygen saturated Bi was compact and well contacted with the inner surface of the sensor cell.

The cross section of the MSZ surface which had black color was analyzed using FE-SEM and EDX. The analysis results shows that Fe-oxide was partly detected on the sensor surface (**Fig.2-10**). The thickness of the adhered Fe-oxide is 10 μ m in average. This implies that the black color of the MSZ surface is due to the adherence of Fe-oxide.

From the visual inspection (**Fig. 2-8**), the adherent of Pb-Bi was partially detected. The interface between the adhered Pb-Bi and the MSZ cell surface was metallurgically analyzed (**Fig. 2-11**). In the interface, the Fe was detected. The thickness of the Fe-layer was 2 μ m. In the adherent Pb-Bi, the Fe was dissolved partially. These results implies that the adherence of the Pb-Bi was promoted by the chemical reaction between the adhered Fe and the Pb-Bi. The change of the chemical components was not detected in the MSZ surface.

The reason of the adherence of Fe and Fe-oxide on the MSZ sensor surface can be consider as follows; the formation of the Fe-oxide was caused by the reaction between the Fe and oxygen supplied from the Pb-Bi and the sensor surface. Then, the Fe was generated in the corrosion test section, which was installed in the upstream of the oxygen sensor. The Fe might be dissolved from the corrosion specimens into the Pb-Bi, since the Fe had high dissolution rate as reported in ref. [2]. The sensor output in the performance tests indicated that the Fe can be oxidized in the Pb-Bi, since the oxygen potential was higher than that required for the Fe-oxide.

YSZ cell

In the YSZ cell, the surface kept the color of initial silky white in the flowing Pb-Bi for 3500 hours (**Fig. 2-8**). **Figure 2-12** shows the cross section of YSZ surface. The outer surface was partially eroded. The erosion depth was measured as 100 μ m. Adherent Pb-Bi was not detected.

Figure 2-13 shows FE-SEM image and EDX analysis results for the eroded surface of the YSZ sell after the use in the flowing Pb-Bi for 3500 hours. In the outer surface,

crack layer with the depth of 50 μm was detected. In the cracked layer, there was no change of chemical components. Thus, the surface of the YSZ caused crack by the shear and/or normal stress of heavy density Pb-Bi flow. The cracked surface might be eroded mechanically

The Fe and/or Fe oxide was not detected on the YSZ surface. This is since the YSZ surface was eroded together with adhered Fe and/or Fe oxide in the flowing Pb-Bi. The reason for the erosion occurrence was possibly because the mechanical property of the YSZ cell was weaker than that of MSZ one.

2.1.5 Summary

The performance tests of the solid electrolyte type oxygen sensors in the flowing lead-bismuth (Pb-Bi) was carried out for long term. The stability and repeatability of the sensor were investigated. The corrosion of the sensor materials was analyzed. The work is summed up as follows:

- (1) The performance of solid electrolyte type oxygen sensor in the flowing Pb-Bi was stable and reliable.
- (2) The sensor showed repeatability in the long term use in the flowing Pb-Bi.
- (3) The EMF output obtained from the yttria stabilized zirconia cell was the same with that from the magnesia stabilized zirconia one in the flowing Pb-Bi.
- (4) The initial performance of the sensors was not reliable. This is since the reference fluid of the oxygen saturated bismuth in the cell was not mixed well and did not contact with inner surface of the solid electrolyte cell.
- (5) The corrosion of the sensor cells were investigated metalurgically. The surface of the YSZ cell was cracked and eroded after 3500 hour- exposure in the flowing Pb-Bi. The MSZ cell showed smooth surface, although the Fe and Fe-oxide were partially adhered on the surface.

2.2 Performance of Mass Exchanger Type Oxygen Control System in Flowing Lead-Bismuth

2.2.1 Introduction

A self-healed oxide layer formed on steel surface inhibits a liquid metal corrosion and reduces the corrosion rate in the flowing Pb-Bi [7-9]. In order to keep a stable condition of the self-healed layer, the oxygen content in the Pb-Bi should be controlled adequately by an oxygen control system.

The performance of the sensor in the liquid Pb-Bi was investigated in the *Chapter 2-1*. From the measured electromotive force (EMF) of the sensor, the oxygen concentration in the melt could be estimated using the correlation of oxygen solubility by Gromov *et al.* [2] and Muller *et al.* [6]. However, there is no experimental data of the oxygen solubility at low temperature.

The oxygen concentration in liquid alloy could be controlled by oxidation and reduction by injecting a gas mixture of H₂, steam and Ar into the melt, and the controllability was reported in ref [10]. The other oxygen control method is a mass exchanger where oxygen dissolves from solid lead oxide (PbO) particles into the Pb-Bi flow and precipitates from the Pb-Bi on the solid PbO particles depending on the temperature [11, 12]. The advantage of this method is to simplify the loop by eliminating some gas lines used in the gas injection method, which increase the safety of the operation. Also in this method, the oxygen solubility in the liquid Pb-Bi can be obtainable, since the oxygen concentration is controlled via the reaction of oxygen dissolution and oxide precipitation.

In the present study, a series of oxygen control test using the PbO mass exchanger was carried out in a Pb-Bi non-isothermal loop. The dynamic shift of the oxygen concentration in the Pb-Bi was measured by the solid electrolyte type oxygen sensor. The purpose is to investigate the controllability of oxygen concentration in the flowing Pb-Bi by means of the PbO mass exchanger and the oxygen solubility in the liquid Pb-Bi.

2.2.2 Experimental Apparatus and Procedure

Pb-Bi forced convection loop and oxygen sensor

The Pb-Bi forced convection loop and oxygen sensor, which were explained in detail in *Chapter 2.1.1* (Figs. 2-1 and 2-2), were used in the present work.

Oxygen control system

The oxygen control system was installed as a mass exchanger in a by-pass line of the low temperature region of the Pb-Bi forced convection loop (**Fig. 2-1**). An oxygen concentration in the Pb-Bi loop was controlled by changing the temperature of solid PbO particles in the PbO reaction vessel. The electromagnetic flow meter and the bellow valves for material test were also installed in the by-pass line. **Figure 2-15** shows a schematic of the mass exchanger with PbO particles. 360 pieces of spherical PbO particles were mounted in each of the meshed container of the PbO reaction vessel. The temperature of the Pb-Bi melt and the PbO particles was controlled by the inserted sheathed heater and the air cooler, and monitored by inserted thermocouples.

Table 2-3 shows the major specifications of the PbO particle. The particles were made in a following procedure: the powder of PbO which has a melting point of 888°C was sintered into lumps at the temperature of 800°C; and then, the lumps were broken into small pieces by hammers. Therefore, the surfaces of the particles were rough. Total surface area of PbO particles in the vessel was estimated as $9.08 \times 10^{-2} \text{m}^2$.

Experimental

The oxygen control test was performed at the conditions shown in **Table 2-4**. The circulation loop was heated up to 250 °C, and the liquid Pb-Bi was charged from the dump tank into the loop at a flow rate of approximately 0.5 l/min by the pressurizing the dump tank at 0.18 MPa with the loop pressure of 0.02 MPa. When the loop was filled with the Pb-Bi, temperatures of the melt were increased up to the experimental condition. The liquid Pb-Bi in the PbO reaction vessel was kept at 250°C using the air cooler during the heat up operation of the loop. In the test, the Pb-Bi temperature at the oxygen sensor was kept constant, and the temperature in the PbO reaction vessel was changed.

2.2.3 Performance of Mass Exchanger Type Oxygen Control System in Flowing Pb-Bi

Figures 2-15 (a) through (c) show the transient of the sensor signal due to the temperature change of the Pb-Bi in the PbO reaction vessel.

In order to evaluate the performance of the mass exchanger type oxygen control system, the response of the oxygen sensor to the PbO reaction temperature was measured with various temperatures at short intervals as shown in **Figures 2-15 (a)**. The EMF output was constant at 0.18V at the constant reaction temperature of 320°C. Shortly after the Pb-Bi was heated up to 330°C in the reaction vessel, the EMF began to decrease to 0.17V. And, the EMF reached constant within 3 hours. When the temperature was decreased from 330°C to 320°C, the EMF increased up to 0.195V. Similarly, when the liquid Pb-Bi in the reaction vessel was cooled down from 320°C to 310°C at the time of 35 hours, the EMF increased to nearly 0.22V and then reached constant value within 8 hours.

In the cooled down process at the time of 45 hours, the EMF of app 0.21 lower than that at the time of app.40 hours was obtained. After the 5 hours, the signals reached constant. At the time of 60 hours, Pb-Bi in the reaction vessel was heated up to 315°C. The negative curve was similar to the former one.

The oxygen control test was performed with longer intervals to investigate the stability of the oxygen control system. The result is shown in **Figure 2-15 (b)**. The electromotive force transited from 0.19V to 0.23V following the Pb-Bi temperature shift from 315°C to 290°C, and became constant in 5 hours. Then, under constant conditions the signal was constant for 40 hours, although the EMF changed within noise level possibly due to the temperature control capability.

In the heat up process from 290°C to 315°C, the EMF decreased to the value lower than the previous one at 315°C, which lead to an increase in oxygen concentration. After 3 hours, the EMF reached constant.

Figure 2-15 (c) shows the result of the mass exchanger operation at the temperature of about 260°C with the temperature difference of 240°C in the loop. At the operation time of 10 hours, the Pb-Bi in the reaction vessel was heated up to 275°C from 260°C. Then the EMF changed from 0.27V to 0.24V. The signals reached constant within 3 hours. After the time of 60 hours when Pb-Bi in the reaction vessel was cooled down from 275°C to 265°C, the EMF increased from 0.24V to 0.27V, and the signals reached constant within 10 hours.

According to a calculation applying the Nernst equation (Eqs. 2.7 or 2.8) to the EMF signals, the oxygen concentration was controlled between 1×10^{-5} wt% (temperature of PbO sinter: 315°C) and 3×10^{-6} wt% (temperature of PbO sinter: 280°C), where is the corrosion-inhibition region.

Response of PbO reaction to oxygen sensor

The sensor signal quickly responded to the temperature change of the mass exchanger. The increase in the oxygen concentration in the heat up process was more rapid than that in the cool down process as shown in **Figures 2-15** (a) through (c). It suggests that the dissolution of oxygen from the PbO surfaces to liquid Pb-Bi is more rapid than the oxide precipitation on the PbO surface. However, the response of both of them is fast enough to keep the oxygen concentration in the adequate region for the formation of the protective oxide layer.

2.2.4 Experimental Equation of Oxygen Solubility in Liquid lead-bismuth

Figure 2-16 depicts the relation between the temperature of the liquid Pb-Bi and PbO particles and the EMF. The EMF decreased linearly with the temperature. By least square method, the empirical correlation of the EMF with the temperature of the Pb-Bi which contacted with the PbO particles T_{pbO} (in the unit of K) was derived as

$$E_{\text{experiment}} = 0.013T_{pbO} + 0.9561, \quad (2-11)$$

in the inaccuracy of 17.7%. This is possibly due to the temperature fraction in the vessel. The EMF in the Eq. (2-11) was obtained by the sensor operated in the Pb-Bi flow at temperature of 500°C. The measured electromotive force was compared with the theoretically calculated result using the Eqs. (2-7)-(2-10).

The measured EMF agreed better with the calculated ones using Eq.(2-8) than that using Eq.(2-7). This suggested that Bi might play a certain role in the oxidation or the oxide precipitation in the liquid Pb-Bi. It is probable that Bi oxide was partly generated in the reaction of oxygen dissolution and precipitation, since the oxygen potential locally around the PbO particles can be higher than that required for the Bi oxide formation by the temperature change. Then, using Eqs.(2-8) and (2-11), the measured EMF can be expressed by;

$$\begin{aligned} E_{\text{experiment}} &= -0.0013T_{pbO} + 0.956 \\ &= \frac{1}{2F} \left[0.45 \frac{\Delta G_{Bi_2O_3}^0}{3} - 0.45 \Delta G_{PbO}^0 - RT_{\text{sensor}} \ln \frac{C}{C_s} \right], \end{aligned} \quad (2-12)$$

where, the oxygen solubility C_s in the melt at the oxygen sensor is generally given by

$$\log C_s = A + \frac{B}{773} \quad (2-13)$$

The oxygen concentration C in the melt at the sensor is the same as the saturated oxygen content in the PbO reaction vessel expressed by

$$\log C = A + \frac{B}{T_{Pbo}} \quad (2-14)$$

Then, substituting Eqs.(2-13) and (2-14) into Eq.(2-12), the EMF can be written as follows:

$$\begin{aligned} E_{\text{experiment}} &= -0.0013T_{\text{PbO}} + 0.956 \\ &= 0.057685 - 0.033307 \left(\ln 10^{\frac{B}{T_{\text{PbO}} - 773}} \right), \end{aligned} \quad (2-15)$$

where the constant B can be obtained as shown in **Fig. 2-17**.

From **Fig.2-16**, it was found that the measured EMF data was arranged between the calculated EMF applying Eqs.(2-9) and (2-10). Thus, it can be expressed as:

$$E_{\text{(Eqs.(2-8) and (2-9))}} < E_{\text{(Experiment)}} < E_{\text{(Eq.(2-8) and (2-10))}} \quad (2-16)$$

and using the Eqs. (2-8), (2-9) and (2-10), the Eq.(2-16) can be expressed by the latter part of the Eq.(2-7) as :

$$\ln \frac{C}{C_{S \text{(Eq.(2-10))}}} < \ln \frac{C}{C_{S \text{(Experiment)}}} < \ln \frac{C}{C_{S \text{(Eq.(2-9))}}} \quad (2-17)$$

Where, the oxygen concentration C should be the same. Then, the constant A in the **Eq. (2-13)** can be given as a region in **Fig. 2-18**. Then, the oxygen solubility C_s at the temperature between 260°C and 330°C is obtained as shown in **Fig. 2-19**.

2.2.5 Summary

The work for the oxygen concentration control is summed up as follows:

- (1) The electromotive force of the oxygen sensor responded to the temperature change of the mass exchanger in short times.
- (2) In oxygen dissolving process by temperature increase, the transition of electromotive force was completed within 5 hours, and that occurred more rapidly than that in oxygen precipitation or reduction process by temperature decrease.
- (3) The electromotive force depended on the PbO temperature linearly. The measured data could be expressed by $E_{\text{experiment}} = 0.013T_{\text{PbO}} + 0.9561$ with T_{PbO} in K within an accuracy of 17%.
- (4) The measured electromotive force agreed with the calculated results from the Nernst equation using $\Delta G^{\circ}_{\text{Pb-Bi-O}}$ equation.
- (5) The oxygen solubility in liquid lead bismuth was expressed by $\log C_s = A + B/T$, where the constant A ranged from -4000 to -4600 , and the constant B ranged from 1 to 3.5 depending on the reaction temperature.

2.3 Conclusions

In the *chapter 2-1*, it is concluded that the oxygen concentration in the flowing Pb-Bi can be monitored by using solid electrolyte type oxygen sensor.

In the *chapter 2-2*, it is concluded that the oxygen concentration in the flowing Pb-Bi can be controlled by the immersion of PbO particles in the by-pass line of the loop. Then, the oxygen concentration in the flowing Pb-Bi can be maintained in the adequate region for the oxygen inhibition, in which Fe oxide can be formed on the steel surface but PbO never form in the liquid Pb-Bi.

References

- [1] M. Takahashi, M. Igashira, T. Obara, H. Sekimoto, K. Kikuchi, K. Aoto and T. Kitano, "Studies on Materials for Heavy-Liquid-Metal-Cooled Reactors in JAPAN", Proc. of 10th Int. Conf. Nuc. Eng., Arlington, Virginia, VA, Apr. 14-18, ICONE10-22166 (2002).
- [2] B. F. Gromov, Y. I. Orlov, P. N. Martynov and V. A. Gulevski, Proc. of HLMC1999, 87-100 (1999).
- [3] J. A. Fernandez, J. Abella, J. Barcelo and L. Victori, "Development of an Oxygen Sensor for Molten 44.5% Lead- 55.5% Bismuth Alloy", J. Nucl. Mater., **301**, 47-52 (2002).
- [4] J. Konys, H. Muscher, Z. Vob and O. Wedemeyer, "Development of Oxygen Meters for the Use in Lead-Bismuth", J. Nucl. Mater., **296**, 289-294 (2001).
- [5] Ning Li, "Active Control of Oxygen in Molten Lead-Bismuth Eutectic Systems to Prevent Steel Corrosion and Coolant Contamination", J. Nucl. Mater., **300**, 73-81 (2002).
- [6] G. Muller, A. Heinzl, G. Schumacher and A. Weisenburger, "Control of oxygen concentration in liquid lead and lead bismuth", J. Nucl. Mater., **321**, 256-262 (2003).
- [7] C. Fazio, G. Benamati, C. Martini and G. Palombarini, "Compatibility tests on steels in molten lead and lead-bismuth", J. Nucl. Mater., **296**, 243-248 (2001).
- [8] G. Benamati, C. Fazio, H. Piankova and A. Rusanov, "Temperature effect on the corrosion mechanism of austenitic and martensitic steel in lead-bismuth," J. Nucl. Mater., **301**, 23-27 (2002).
- [9] F. Barbier and A. Rusanov, "Corrosion Behavior of Steels in Flowing Lead-Bismuth", J. Nucl. Mater. **296**, 231-236 (2001).
- [10] M. Kondo, M. Takahashi, T. Suzuki, K. Ishikawa, K. Hata, S. Qiu and H. Sekimoto, "Metallurgical Study on Erosion and Corrosion Behaviors of Steels Exposed to Liquid Lead-Bismuth Flow", J. Nucl. Mater., **343**, 349 (2005).
- [11] Z. I. Yemelyantseva, V. N. Lenov, A. D. Yefanov, Y. I. Orlov, P. N. Martynov and V. A. Gulevsky, "Validation of the Lead Coolant Technology for BREST Reactor", Proc. of 11th International Conf. Nucl. Eng., Tokyo, Japan, Apr. 20-23, ICONE11-36408 (2003).
- [12] Georgi Ilincev, "Research Results on the Corrosion Effects of Liquid Heavy Metals Pb, Bi and Pb-Bi on Structural Materials with and without corrosion Inhibitors", J. Nuc. Eng. and Sci., **217**, 167-177 (2002).

Table 2-1 Mechanical characteristics of solid electrolyte conductors MSZ and YSZ

Components		MgO-ZrO ₂ (MSZ)	Y ₂ O ₃ -ZrO ₂ (YSZ)
Density	(g/cm ³)	5.4	5.4
Bending strength	(MPa)	250	150
Thermal expansion coefficient	(x10 ⁻⁶ /k)	6.2	10.2
Conductance (550°C)	(Log σ [S·cm])	-3	-5

Table 2-2 Conditions of sensor performance tests

Performance test	T-1	T-2	T-3	T-4	T-5
Operation time (h)	1000	500	1000	2000	4
Pb-Bi temperature at oxygen sensor (°C)			550		400
Pb-Bi temperature in low temperature region (°C)			400		400
Pb-Bi charge temperature (°C)			250		250
Oxygen concentration in Pb-Bi (wt%)	1x10 ⁻⁸	1x10 ⁻⁸	1x10 ⁻⁶	1x10 ⁻⁶	-
Flow rate (L/min)	3				
Active oxygen control	X	X	O	X	X
Steel corrosion test	O	O	X	O	X
Sensor cell material	MSZ	MSZ and YSZ			MSZ

Table 2-3 Specifications of PbO particle

Diameter (m)	2-4x10 ⁻³
Density (g/m ³)	6.94
Weight (g)	2.91x10 ⁻²
Volume (m ³)	4.19x10 ⁻⁹

Table 2-4 Experimental conditions of oxygen control test

Temperature of Pb-Bi in high temperature region (°C)	500
Temperature of Pb-Bi in low temperature region (°C)	400
Temperature of Pb-Bi in PbO reaction vessel (°C)	280-350
Flow rate in circulation loop (L/min)	3
Flow rate in diverged PbO reaction vessel (L/min)	0.5

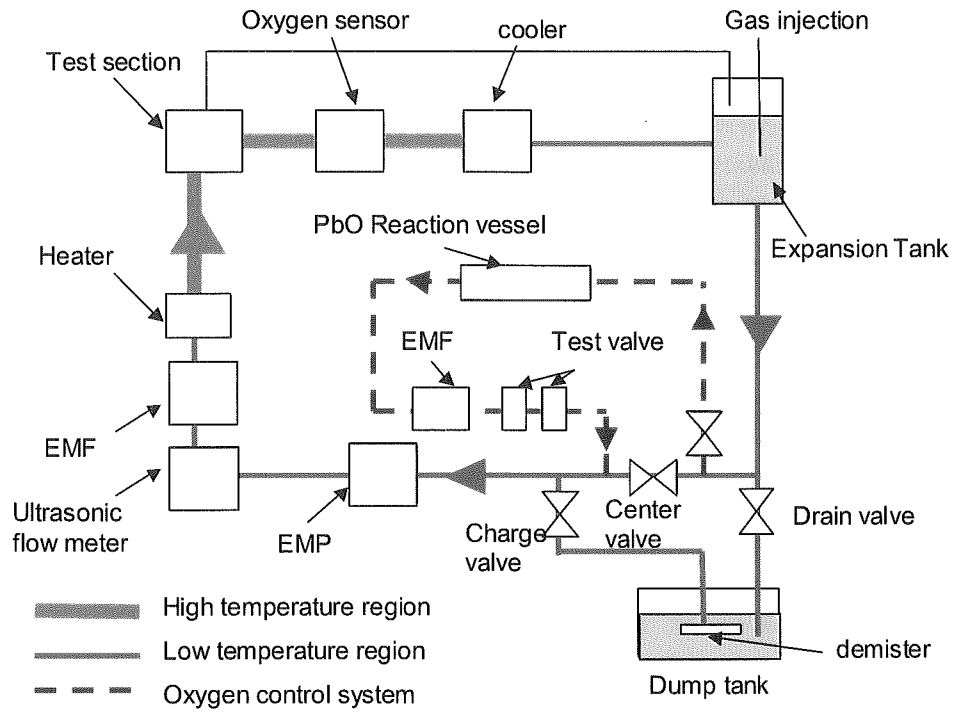


Fig. 2-1 Schematic of Pb-Bi forced convection loop

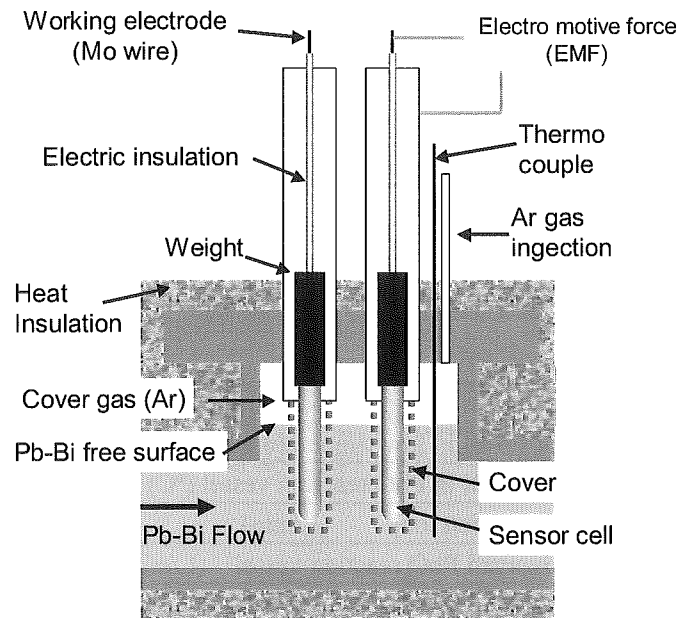


Fig.2-2 Schematic of oxygen sensor

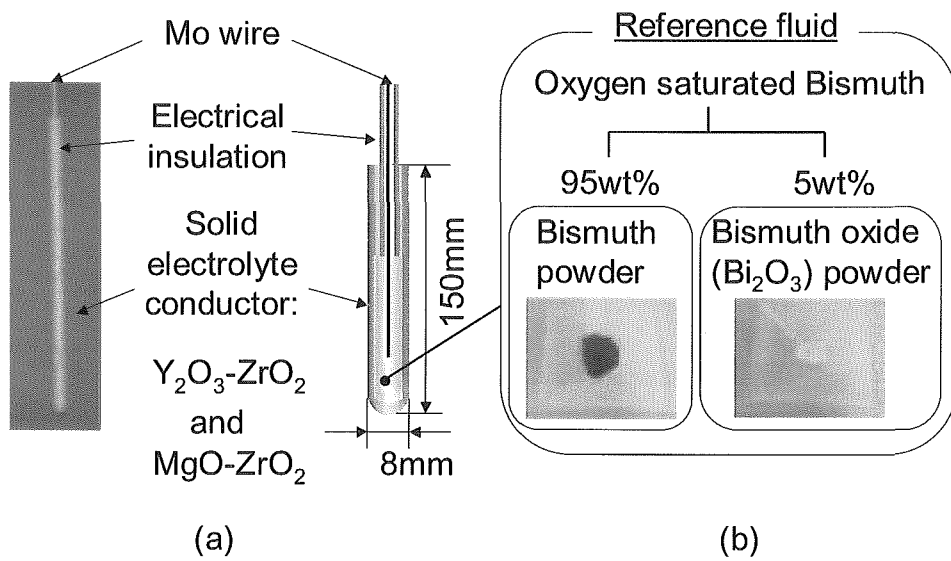


Fig.2-3 Schematic of sensor cell

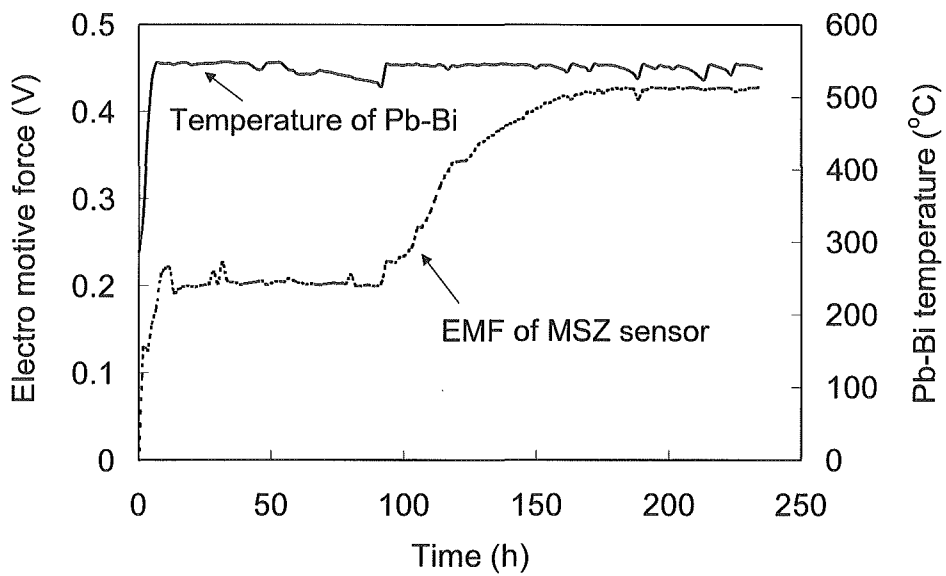


Fig. 2-4 Initial EMF output of sensors with MSZ cell in T-1 operation

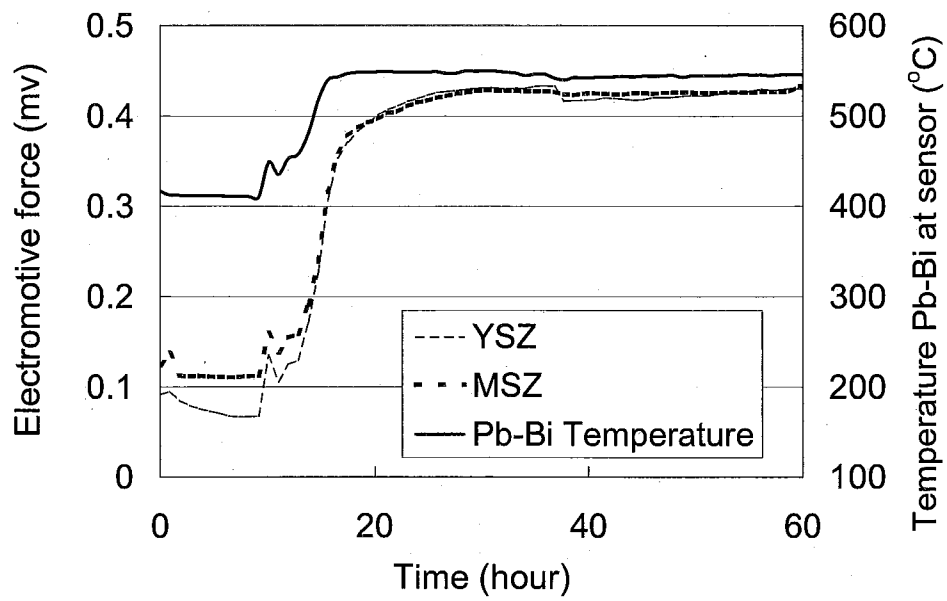


Fig.2-5 Initial EMF output of sensors with MSZ and YSZ cells in T-2 operation

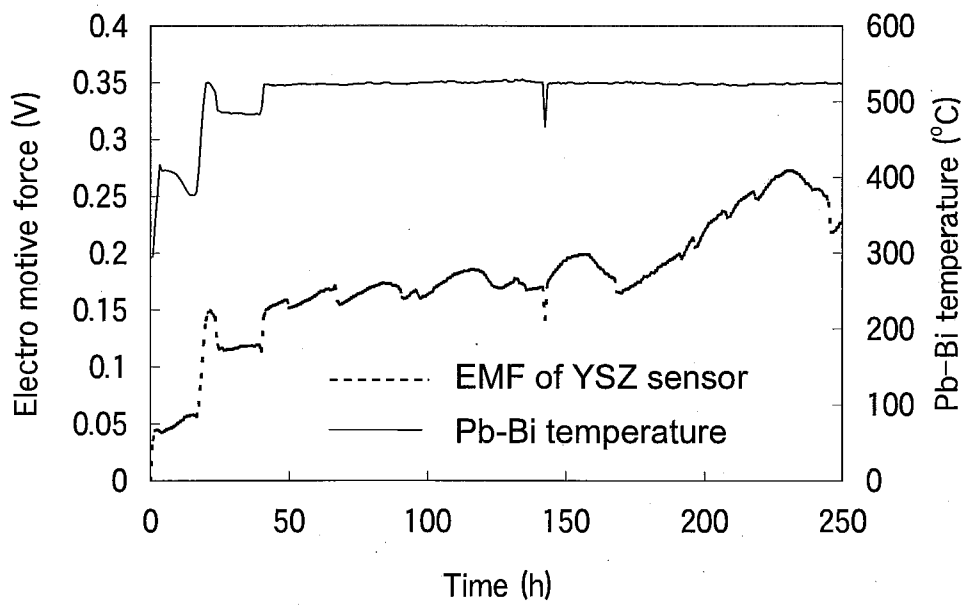


Fig. 2-6 Initial EMF output of sensor with YSZ cell in T-4 operation

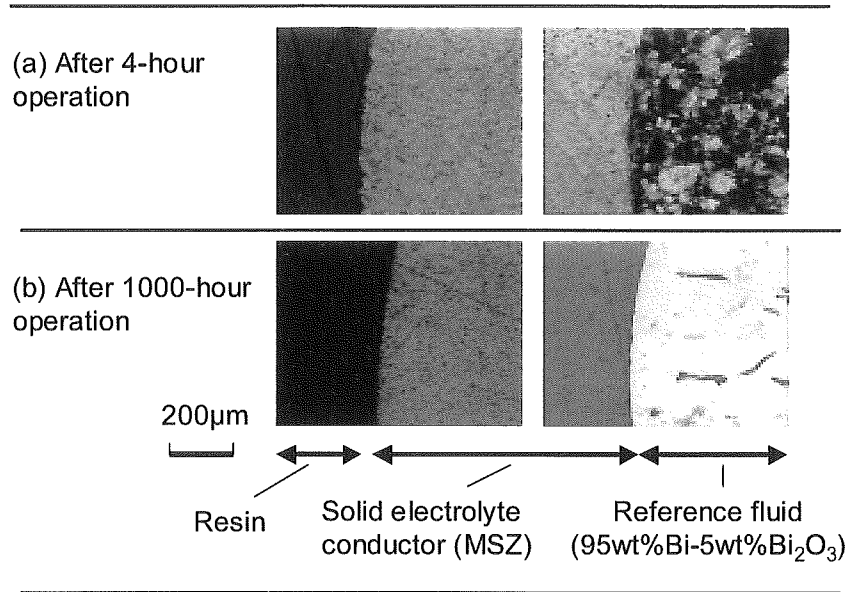


Fig. 2-7 Metallurgical conditions of MSZ sensor (a) used in Pb-Bi for 4 hours; (b) for 1000 hours

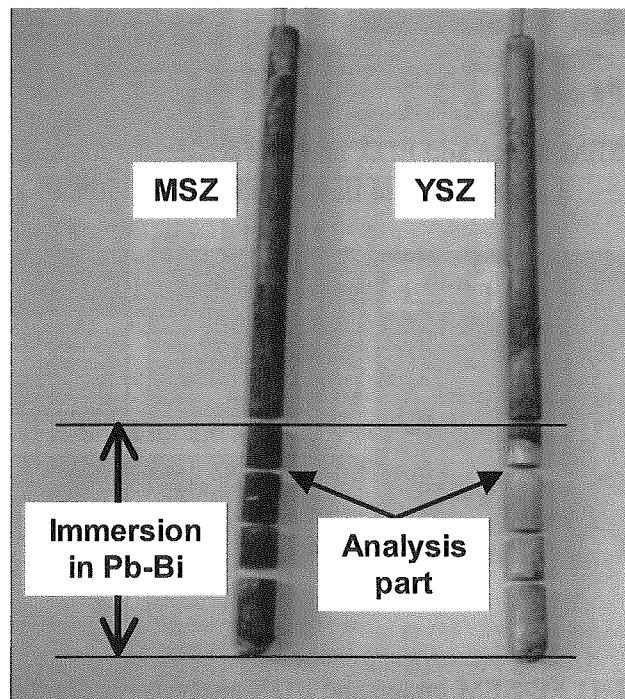


Fig. 2-8 MSZ and YSZ sensor surfaces after 3500-hour use in flowing Pb-Bi

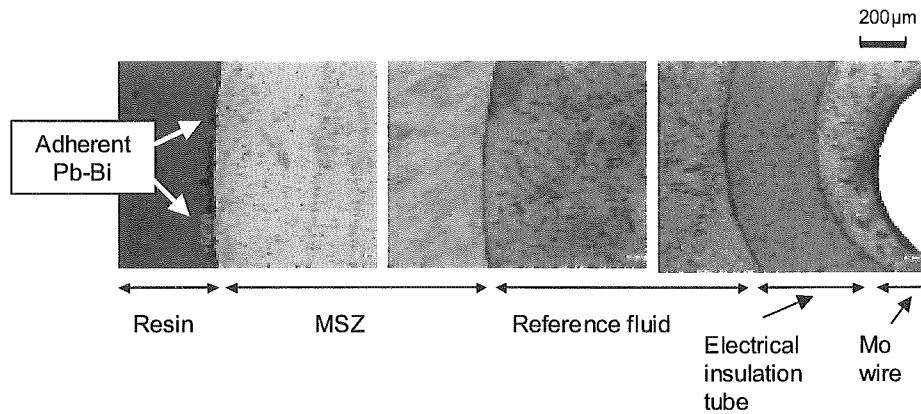


Fig.2-9 Cross sections of MSZ sensor cells used in flowing Pb-Bi for 3500 hours

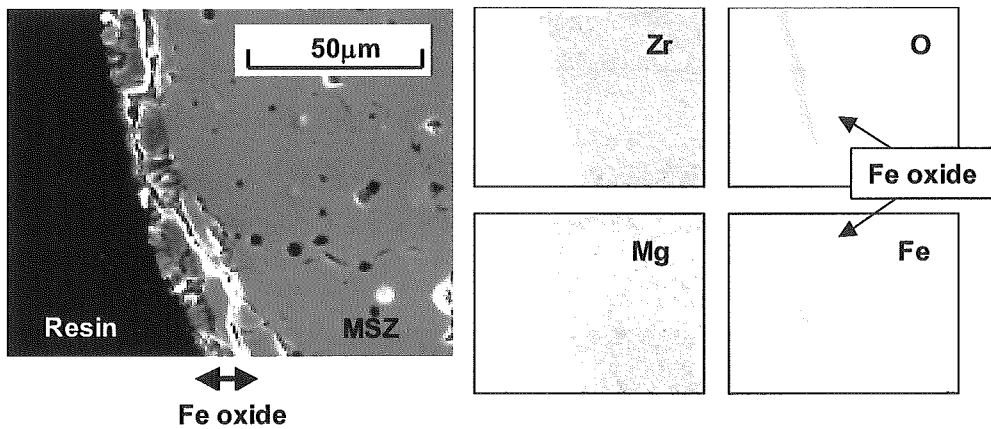


Fig.2-10 FE-SEM image and EDX analysis results for the surface of MSZ sell surface after use in flowing Pb-Bi for 3500 hours

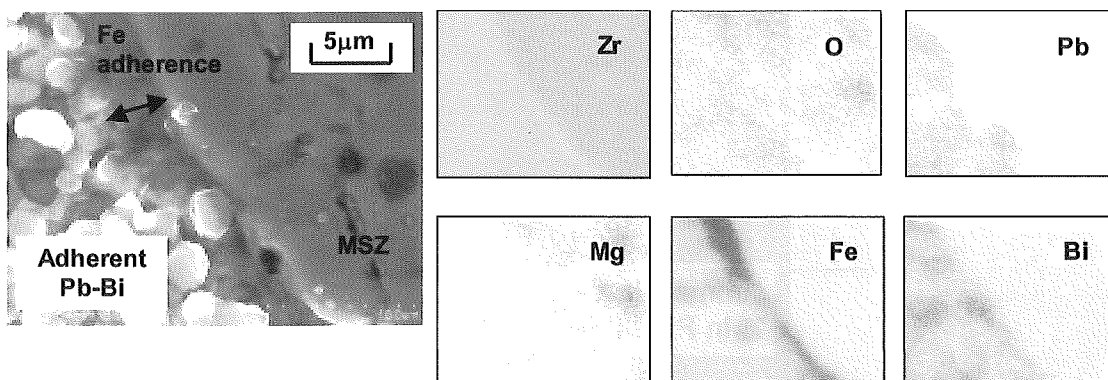


Fig. 2-11 FE-SEM image and EDX analysis results for adherent Pb-Bi on surface of MSZ sell after use in flowing Pb-Bi for 3500 hours

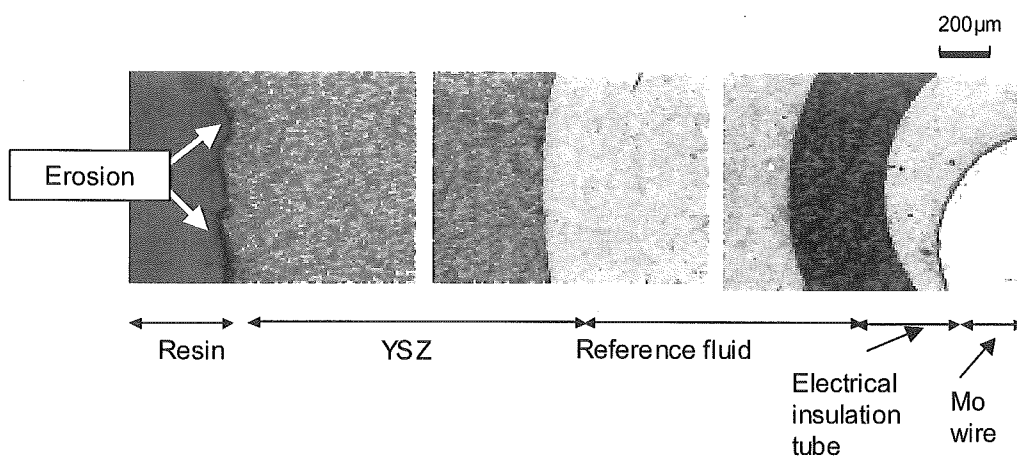


Fig. 2-12 Cross sections of YSZ sensor cells used in flowing Pb-Bi for 3500 hours

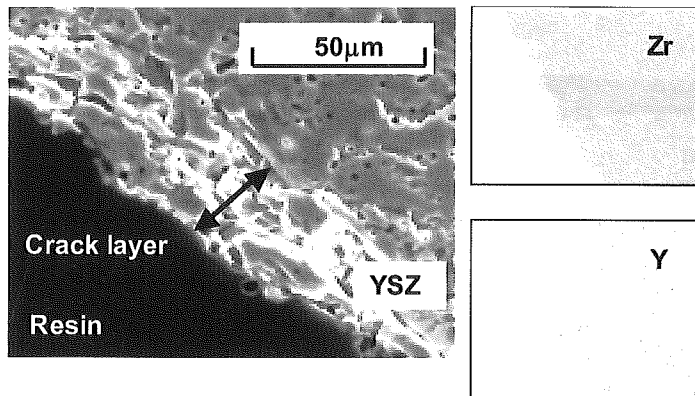


Fig. 2-13 FE-SEM image and EDX analysis results for surface of YSZ cell after use in flowing Pb-Bi for 3500 hours

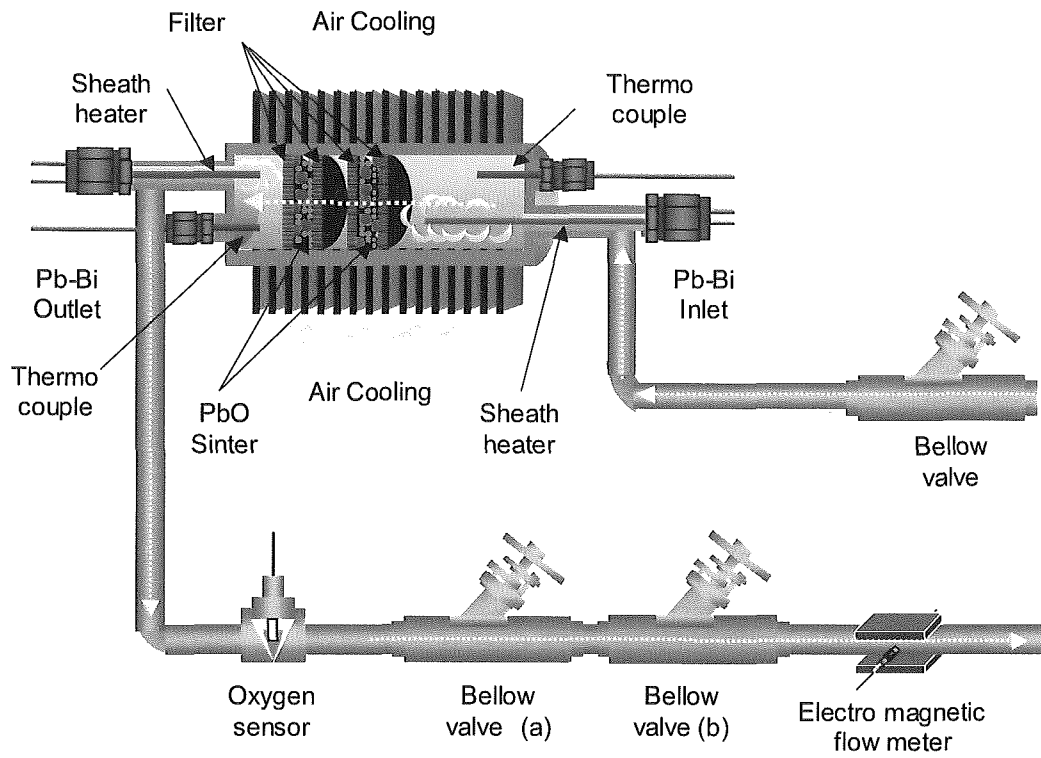


Fig.2-14 Schematic of MX with PbO particles

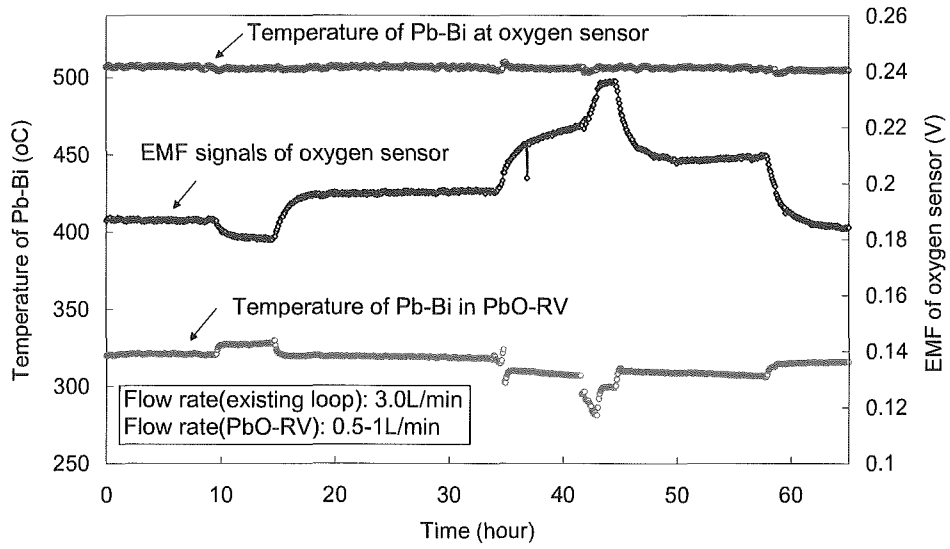


Fig.2-15 (a) EMF transient due the change of reaction temperature between 275°C and 330°C

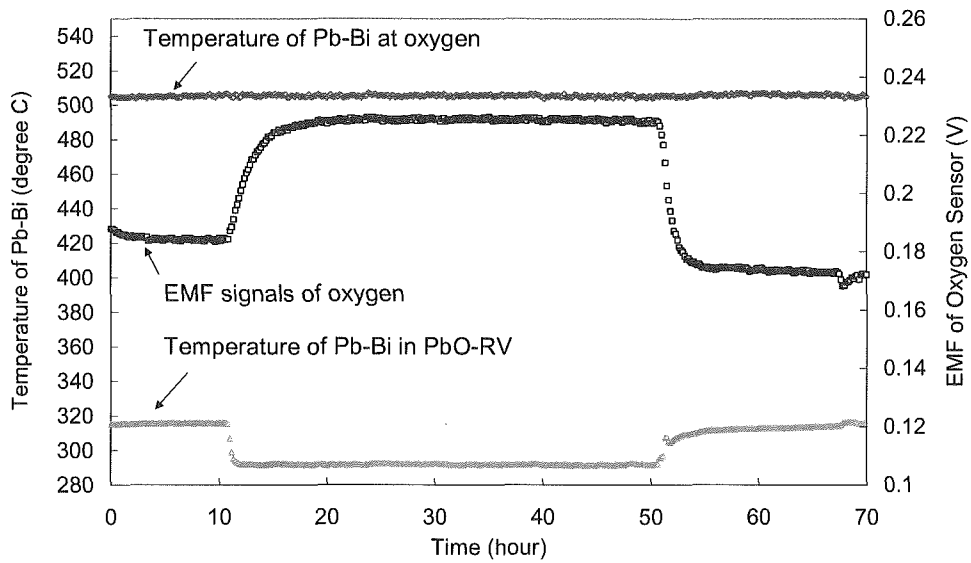


Fig.2-15 (b) Stable EMF transient according to the change of reaction temperature between 275°C and 320°C

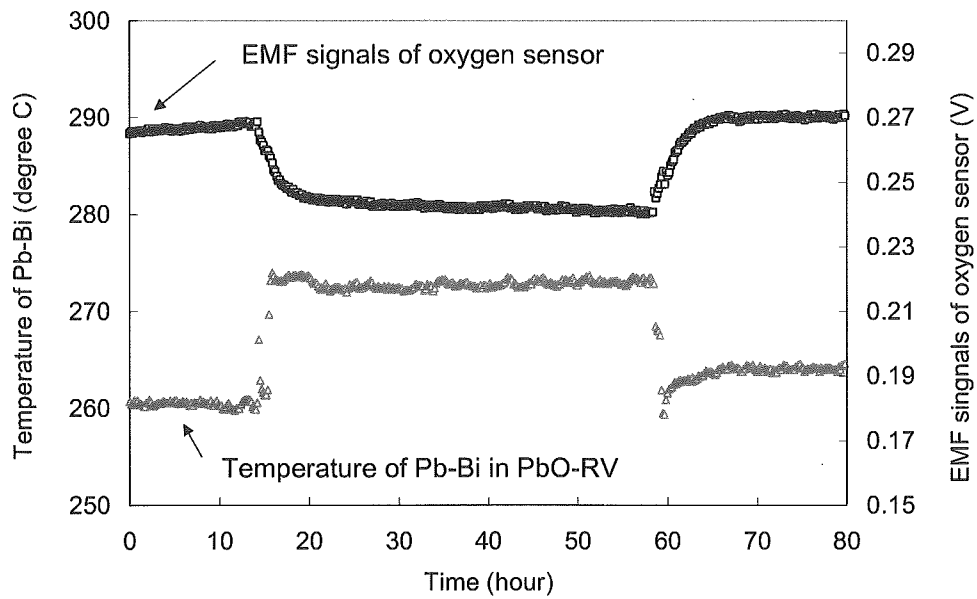


Fig.2-15 (c) EMF signals of oxygen sensor and temperature of PbO

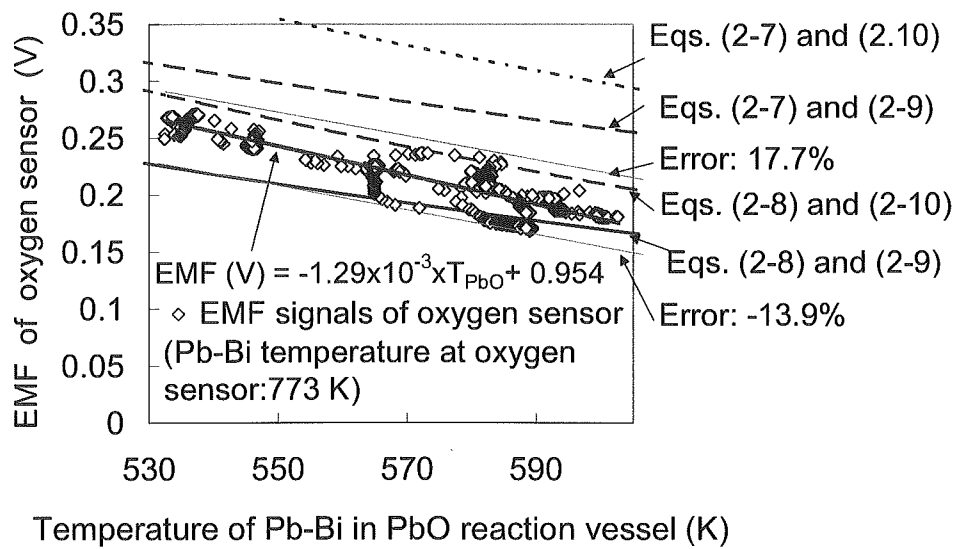


Fig.2-16 Comparison of calculated and measured EMF

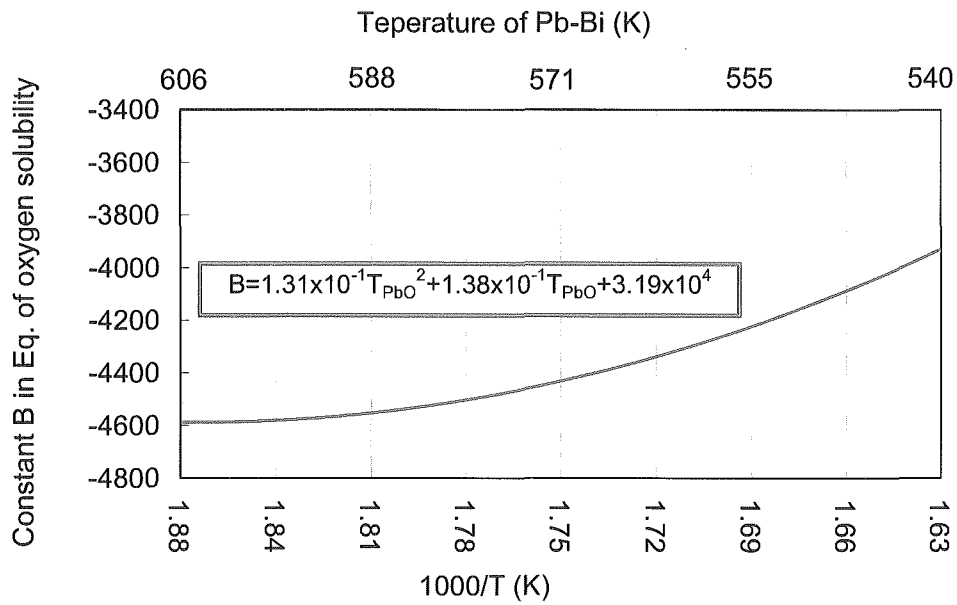


Fig.2-17 Const B

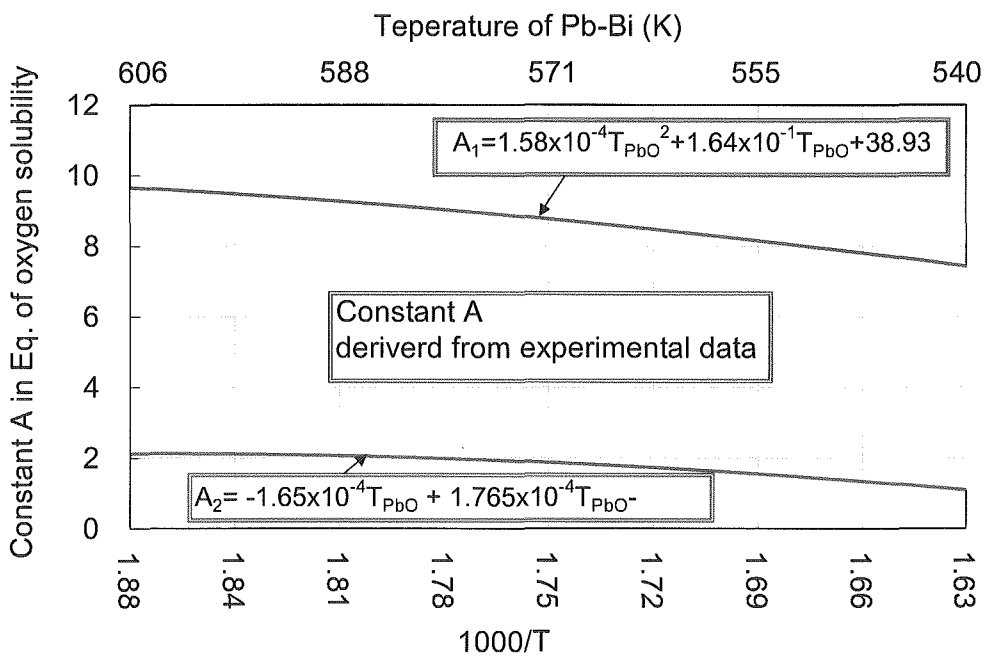


Fig. 2-18 Const A

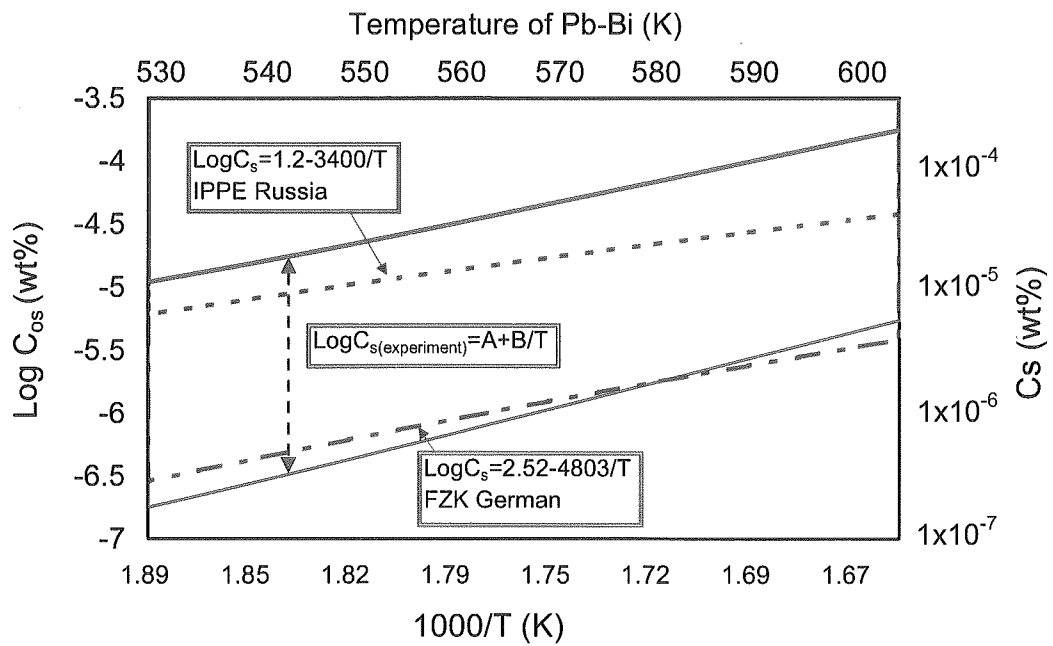


Fig.2-19 Comparison between oxygen solubility obtained from experiment and preliminary reported equations [2,6]

Chapter 3

Liquid Metal Corrosion and Erosion Behaviors of Steels in Flowing Lead-Bismuth

3.1 Introduction

The compatibility of steels in liquid lead₄₅-bismuth₅₅ (Pb-Bi) flow is one of the key issues for the development of accelerator driven systems (ADS) with a target of Pb-Bi and Pb-Bi cooled fast breeder reactors (FBRs)[1]. It has been expected to have a corrosion resistance of steels if stable oxide films are formed on the surface of the steels as protective layers by controlling oxygen potential in the Pb-Bi adequately.

However, it is probable that some the spallation products in the target of the ADS may decrease the oxygen potential in the Pb-Bi to a value of less than that necessary for the formation of Fe₃O₄. As a result, iron oxide films covering the steels are reduced, and the steel surface is directly exposed to Pb-Bi flow, which leads to the liquid metal corrosion (LMC) where steel elements are dissolved into Pb-Bi. An aluminum coating on the steel surface is expected to be effective for the formation of a protective oxide layer, since the aluminum is easily oxidized at low oxygen potential. Kurata et al., reported that the effectiveness of Al oxide layer by the coating of aluminum on the steel surfaces. However, the If the protective oxide layer or the alumina coating was not formed successfully, the steel corrosion is not inhibited.

The LMC may accompany Pb-Bi penetration into the steel where mechanical strength may be weakened. As the dynamic pressure and shear stress of the Pb-Bi flow acting on the steel surfaces are ten times as high as those of ordinary fluids such as water, the mechanically weakened parts may be broken by the fluid-mechanical forces. This type of fluid-mechanical damage is called "erosion". The erosion should be avoided since it causes serious damage of material and a large weight loss. The erosion of steels exposed to a Pb-Bi flow has been reported so far [2,3,4]. The erosion can be classified to the widely damaged surface along the flow as if fluid carries out the surface material by a strong dynamic pressure and the pitting type erosion where material is deeply lost from narrow surfaces.

Although the apparent feature of the erosion, such as damaged surface shapes, has been reported so far, the mechanism of the erosion has not been made clear yet. In order to know the mechanism, the behavior of the eroded parts must be observed metallurgically. In the present study, the corrosion/erosion test of nine steels in a Pb-Bi flow was carried out at low oxygen potential and high velocity, and the behavior of erosion and that of corrosion around the eroded region was investigated metallurgically.

3.2 Experimental apparatus and procedure

Experimental apparatus and conditions

Figure 3-1 shows the Pb-Bi forced convection-type corrosion test apparatus used for the present test. The apparatus consists of an electromagnetic pump, the electromagnetic flow meter, electrical heater, the test section, air cooler, expansion tank, and dump tank. The circulation loop has Pb-Bi inventory of 0.022 m³, and consists of a hot loop region

(550 °C) from the heater to the cooler made of STBA26 (9Cr-1Mo steel) to avoid corrosion and a cold loop region (400 °C) made of SS-316. Inside of the test apparatus was kept clean by being burned by heaters, evacuated and filled with argon having a purity of 99.999% to achieve clean condition. The Pb-Bi was melted in the dump tank up to 180 °C for several days and then Pb-Bi at the temperature of 250°C was charged with a rate of approximately 0.5L/min from dump tank to the circulation loop which was heated up to 250 °C. Pb-Bi was circulated by the electro-magnetic pump at the rated operation flow rate, and heated up to 400 °C. At the inlet of the hot region, an electrical heater operated to heat Pb-Bi to the temperature of 550 °C. And at the outlet of the hot region, cooler operated to cool down Pb-Bi at the temperature of 550 °C. to the temperature of 400 °C.

The 2.3 mm-thick plates of test pieces were mounted in the cylindrical holder made of molybdenum as shown in **Fig. 3-2**. The holder was inserted in the test section of the corrosion test loop as shown in **Fig. 3-3**. The Pb-Bi flows in two Pb-Bi flow channels of 13mm in width, 2mm in height and 425 mm in length above and below the test pieces.

Test conditions are summarized in **Table 3-1**.

Measurement and control of oxygen potential in Pb-Bi

The oxygen sensor was mounted downstream from the test section. The sensor was made of a cylindrical solid electrolyte conductor, $ZrO_2\text{-}Y_2O_3$ with the reference electrode of platinum pasted inner surface in a purged air flow. The sensor was placed in an argon cover gas space during the normal operation, and was immersed in the Pb-Bi melt by increasing the Pb-Bi free surface level by the control of pressure in Ar cover gas space when the oxygen potential was measured.

During the corrosion test, the oxygen potential was controlled by the injection of a mixture gas of argon, hydrogen and moisture into Pb-Bi in the expansion tank. The hydrogen and argon flow rates were measured with purge meters, the moistured steam concentration was measured to be 93 %, and the temperature of the water bath was measured with a sheathed type-K thermocouple. The partial pressure ratio of hydrogen to steam was estimated from the saturation pressure of the steam at the temperature in the water bath and flow rates. The mixture gas was heated up in the supply tube and then injected into circulating Pb-Bi flow in the expansion tank at the temperature of 400 °C through a vertical 1/4 in. steel tube. The injection gas flow rate was chosen in the range of 70-100ml/min. The mixture gas remained in the cover gas space of the expansion tank, and then went out to the atmosphere.

In the present study, the formation of protective oxide layer as described in **Ref. [4-7]** on the steel surface was inhibited to investigate the erosion and corrosion behaviors in a Pb-Bi at low oxygen. **Figure 3-4** shows the diagram of the Gibbs free energy of oxide formation and oxygen potential. If the oxygen concentration of Pb-Bi is kept to be lower than the Fe_3O_4 formation potential, the steel may have no protective outer oxide films of Fe_3O_4 and no internal layer of $(Fe, Cr)_3O_4$. The oxygen potential, $(RT/2)\ln P_{O_2}$, is expressed by

$$\begin{aligned} \frac{RT}{2} \ln P_{O_2} &= \Delta G^0_{Pb_{0.45}Bi_{0.55}O_{1.275}} + RT \ln\left(\frac{C}{C_s}\right) \\ &= \Delta G^0_{H_2O} + RT \ln\left(\frac{P_{H_2}}{P_{H_2O}}\right) \end{aligned} \quad (3-1)$$

where C is the oxygen concentration in the Pb-Bi, and the saturated concentration or the solubility of oxygen in Pb-Bi at the temperature of T in the unit of wt.%, C_s , is provided by [8]

$$\log C_s = 1.2 - 3400/T \quad (673K < T < 973K) \quad (3-2)$$

The curves of constant oxygen concentration and constant partial pressure ratio of H_2 to H_2O are shown in Fig.3-4. The partial pressure ratio of P_{H_2}/P_{H_2O} in the mixture gas was chosen to be 0.217. From the value of P_{H_2}/P_{H_2O} in the injected gas, the oxygen potential and the oxygen concentration in the expansion tank was determined from Eqs. (3-1) and (3-2). Although the temperature increased, i.e. from the expansion tank to the test section, the oxygen concentration in the Pb-Bi is kept constant along the thick curve. Therefore, the oxygen concentration in the test section was estimated to be 2×10^{-9} wt%; at 550°C, Cr_2O_3 is stable but Fe oxide is not formed.

During the corrosion/erosion test, the oxygen concentration downstream from the test section was measured using the oxygen sensor. It was confirmed that the electromotive force of the oxygen sensor reached equilibrium after 80-hour gas injection.

Measurement of weight change and SEM/EDX observation and analysis

After the exposure to the Pb-Bi flow for 1,000 hours, the test piece holder was immersed in a glycerin pool at temperature of 200 °C to remove adhered Pb-Bi on the test piece surfaces [7] and to observe the occurrence of the LMC. The surface of the steels had metallic luster before the test. The change of surface color was checked after the exposure, and the occurrence of erosion and the existence of adhered Pb-Bi were inspected by microscopy.

For the measurement of weight change, metal elements dissolved in Pb-Bi with higher melting point than that of pure Pb-Bi were removed by applying nitric acid to the test pieces (c). An electronic reading balance with the accuracy of 0.1mg was used for the measurement of weight change.

The test pieces (a) were cut across the eroded regions and molded into a resin as shown in Fig. 3-5. The faces of the cross section were polished with a mechanical grinder with polishing agent of polycrystalline diamond and lubricant of ethanol, and observed and analyzed using the SEM/EDX.

3.3 Test materials

Alloying components of the test pieces are presented in **Table 3-2**. SCM420 is a low alloy steel, STBA28, NF616 and STBA26 were developed for supercritical pressure boilers, HCM12 and HCM12A are candidates as for structural materials of fossil fuel power plants, ODS is a cladding steel strengthened for the use at high temperature and high radiation condition in sodium cooled FBRs, and F82H is foreseen to be used as blanket material in the fusion reactors.

The test pieces were mounted in the test piece holder in the following order from upstream to downstream: (1) SCM420, (2) ODS, (3) F82H, (4) STBA26, (5) NF616, (6) HCM12, (7) HCM12A and (8) SS-316.

The test pieces were 15mm wide, 10mm long and 2.3 mm in thickness. And in total, four test pieces exposed of each steel. Analysis method is shown in Fig.4, that is, the test piece (a) was prepared for metallurgical analysis, the test piece (c) was for the measurement of weight change and the test piece (b) and (d) was a spare of (a) and (c), respectively.

3.4 Liquid Metal Corrosion and Erosion of Steels

Corroded surface

The photographs of the test piece in the molybdenum holder are shown in **Table 3-3**. The surface of SCM420 exhibited severe erosion, particularly on the upstream end of the test piece (a) where dynamic pressure acted (**Table 3-3**, the left end of SCM420). All of the surface of ODS was covered with Pb-Bi. F82H exhibited severe erosion, particularly at the sides and corners of the test pieces. Although STBA26 exhibited strong erosion, particularly in the test piece (b), no erosion was observed in the test pieces of STBA28 and NF616 in spite that their alloying components are similar to those of STBA26. HCM12 exhibited crack-like erosion, while HCM12A with similar alloying components to those of HCM12 exhibited smooth surface without erosion. The surface of SS-316 was completely covered with Pb-Bi.

Corrosion Analysis using SEM/EDX

Corrosion/erosion behaviors in SCM420, ODS and F82H

Figure 3-7 shows the results of SEM/EDX observation and analysis for the cross-section of SCM420. A large amount of surface material was lost by erosion, and Pb-Bi penetrated into the steel matrix, probably into grain boundaries. The penetration depth was approximately (app.) 40 μ m. According to EDX analysis, app.80wt% of Bi (**Fig.3-7**, point no.2 and 5) was detected in the penetration region, and the content of Fe was app.10 wt% in the interface of the penetrated region and the steel matrix.

Figure 3-8 (a) shows the behavior of corrosion in ODS in Pb-Bi. It is found that the ODS did not exhibit severe LMC and the Pb-Bi penetration depth was only app.5 μ m.

The content of Pb was a little higher than that of Bi in the penetration region, and small amounts of Fe and Cr were detected in the adhered Pb-Bi.

Figure 3-8 (b) shows the behavior of corrosion in F82H which exhibited Pb-Bi penetration into grain boundary with a depth of up to 22 μ m. Some vacancies are observed around the interface between the Pb-Bi penetration region and the steel matrix. The content of Bi was higher than that of Pb in the Pb-Bi penetrated region as it was in SCM420.

Figures 3-9 (a) and **(b)** show two types of erosion in F82H, respectively: narrow erosion like pitting and wide erosion. It is found that the pitting was app.35 μ m in depth and app.100 μ m in width and Pb-Bi penetrated deeply from the bottom of the pitting. The erosion was app.2mm in width and 200 μ m in depth in **Fig. 3-9 (b)**. The enlarged view of the local erosion is shown in **Fig. 3-9 (c)**. It is found that Pb-Bi penetrated so as to envelop a lump of steel, which suggests the mechanism of erosion, that is, the lump of steel may be carried away easily from the steel matrix by the Pb-Bi flow because the strength of the penetration region decreases.

Corrosion/erosion behaviors in STBA26, STBA28 and NF616

Figures 3-10 (a) shows the corrosion behavior of STBA26. The surface became rough and Pb-Bi penetrated into the steel matrix up to a depth of app.16 μ m. The content of Pb was higher than that of Bi near the interface of the penetration region and the steel matrix as shown in point No.4 of **Fig.3-10 (a)**, while Fe was detected in the Pb-Bi penetration region as shown in point No.1-3 of **Fig.3-10 (a)**.

Figure 3-10 (b) shows the corrosion behavior of STBA28. It exhibited similar corrosion behavior to that of STBA26 possibly because of nearly the same contents of alloying components as those of two steels. The depth of Pb-Bi penetration was app. 20 μ m. The content of Bi was much higher than that of Pb in the penetration region as indicated by point No.1-3 of the EDX analysis in **Fig. 3-10 (b)**, although the content of Pb was app.40 wt% in the interface between the penetration region and the steel matrix.

Figure 3-11 (a) shows the erosion in STBA26 which is 120 μ m in depth and 500 μ m in width. It is found that Pb-Bi penetrated into the steel matrix, and there appeared some defects in the edge regions shown in **Figs. 3-11 (b) and (d)**. Pb-Bi penetrated more deeply into the steel matrix from the bottom of the eroded region as shown in **Fig. 3-11 (c)**. The result of the EDX analysis in **Fig. 3-11 (c)** shows that the contents of Pb and Bi were high in the penetration region. The Pb-Bi penetration behavior in the eroded region was similar to that in the corroded region shown in **Fig.3-10 (a)**.

Figures 3-12 (a) to (c) show the results of SEM/EDX observation and analysis for cross sections of NF616. Although erosion in NF616 could not be observed in the surface observation due to the cover of Pb-Bi, the result of SEM observation indicated the occurrence of erosion in NF616. In the eroded region, some lumps of steel were detached from the surface. **Figure 3-12 (b)** shows that Pb penetrated into the steel matrix in the depth of app.15 μ m from the interface between adhered Pb-Bi and steel matrix. The content of Pb was much higher than that of Bi in the penetrated region as indicated by No.3-4 in **Fig. 3-12 (b)**. **Figure 3-12 (c)** shows the penetration behavior in corroded region in NF616. It is found that the penetration behavior in the corroded region was similar to that in the eroded region.

Corrosion/erosion behaviors in HCM12 and HCM12A

Figure 3-13 (a) shows the corrosion behavior in HCM12. The Pb-Bi penetrated into the steel matrix and grain boundary in the depth of app.21 μ m from a rough interface between steel and adhered Pb-Bi. The content of Pb was higher than that of Bi around the interface as shown in the result of EDX analysis. The adhered Pb-Bi contained Fe and a little amount of Cr. Pb-Bi penetration into grain boundary was observed clearly. **Figure 3-13 (b)** shows the Pb-Bi penetration behind some lumps of steel which might be detached easily, and **Fig. 3-13 (c)** shows the deep Pb-Bi penetration with adhered Pb-Bi in the eroded region. The penetration region was between app.100 μ m deep and app.200 μ m wide.

Figure 3-13 (d) shows the corrosion behavior in HCM12A where Pb-Bi penetrated into a depth of app.15 μ m. Some continuous holes were observed along the Pb-Bi penetration region. The content of Bi was higher than that of Pb in the Pb-Bi penetration region. There was a little amount of Cr although the content of Fe did not decreased.

Corrosion/erosion behaviors in SS-316

SS-316 is corroded up to a depth of app. 100 μ m and erosion has already started (See. **Fig. 3-14(a)**). The corroded region can be distinguished into two layers from the Pb-Bi penetration behavior into grain-boundaries and the results of EDX line analysis. Pb penetrated into a depth of app. 42 μ m in the outer region (A), while Pb-Bi penetrated in the depth of 208 μ m in the intermediate region (B). The contents of Ni and Cr decreased in the Pb-Bi penetration region.

3.5 Weight changes of Steels on Liquid Metal Corrosion and Erosion

Figure 3-15 shows the result of the weight change measurements of the test pieces. The weight loss of SCM420 was the highest, and those of F82H and NF616 were high. This is probably because these steels contained low Cr concentration. The weight losses of SCM420, F82H, STBA26, NF616, HCM12 and SUS316 that were eroded were higher than those of ODS, STBA28 and HCM12A that were not eroded. The weight loss of STBA26 was two times as high as that of STBA28, and the weight loss of HCM12 was five times as high as that of HCM12A, although the contents of alloying components were nearly as the same as each other in both cases.

3.6 Erosion mechanism

Under the present oxygen potential, the LMC, particularly Pb-Bi penetration, took place in all the steels, and severe erosion occurred in some of the test pieces. In a previous test using Pb-Bi with an oxygen concentration of 5×10^{-7} wt% [2], LMC and erosion did not occur on the same steels and comparable conditions. Therefore, it has been confirmed that oxygen concentration in Pb-Bi lower than the formation potential of Fe_3O_4 suppresses the formation of protective oxide layers and enhances the LMC, and as consequence the erosion well.

The degree of LMC, or Pb-Bi penetration depth, and erosion may be related to each other, depending on the types of steels: Pb-Bi penetration was deep and erosion occurred in SCM420, F82H and HCM12 as shown in Fig. 3-16. This may be attributed to low content of Cr, particularly in SCM420 where protective Cr oxide films cannot be formed easily. SS-316 which has high contents of Cr caused severe Pb-Bi penetration and erosion possibly due to that Ni is dissolved out of the steel surface [8] and porous layer remained which underwent a phase transformation into a ferrite structure. Pb-Bi can easily penetrate into the porous layers.

The depth of Pb-Bi penetration was almost the same among STBA26, STBA28 and NF616 possibly because of nearly the same contents of alloying components. The Pb-Bi penetration was not so deep in ODS and HCM12A that subjected no erosion. In the case of ODS, the grain boundary with unique structure [9, 10] might beneficially influenced to that.

The process from corrosion to erosion can be explained schematically in Fig. 3-17. It is described as follows: at first, the LMC occurred on the steel surface exposed to high temperature Pb-Bi, where Pb-Bi penetrates into grain boundaries. The grain boundaries are weakened, and consequently, some grains are taken away from the steel matrix by the hydrodynamic shear forces of the Pb-Bi flow. Some defects formed by dissolution of alloying elements into Pb-Bi may enhance the detachment of a lump of steel from the steel matrix. Therefore, the Pb-Bi penetration might cause large-scale erosion.

6. Conclusion

The corrosion/erosion behaviors of 9 existing steels were investigated by means of corrosion test for 1,000 at low oxygen concentration of 2×10^{-9} wt% under the conditions of the temperature of 550°C, the non-isothermal loop temperature difference of 150°C, and the flow velocity of 2m/s. Conclusions are as follows:

- (1) Pb-Bi penetration-type corrosion and, in some steels erosion, occurred on the test piece surfaces because no protective oxide layers were formed under the present low oxygen concentration less than the Fe_3O_4 formation potential.
- (2) A relation between LMC and erosion has been confirmed. The degree of LMC could be evaluated from the depth of the Pb-Bi penetration into steel matrix. The Pb-Bi penetration was deeper in the relatively low Cr steels of SCM420 and F82H than in the high Cr steels: ODS, HCM12, and HCM12A.
- (3) The austenitic steel, SS-316, was a special case where Pb-Bi penetration was deep in spite of high Cr content because of high content of Ni in the steel that dissolves into Pb-Bi and promotes the Pb-Bi penetration. The test steels which were more deeply penetrated by Pb-Bi exhibited more severe erosion.
- (4) Low Cr steel and austenitic steel are more readily eroded under the low oxygen potential as in this study.

References

- [1] M. Takahashi, M. Igashira, T. Obara, H. Sekimoto, K. Kikuchi, K. Aoto and T. Kitano, "Studies on Materials for Heavy-Liquid-Metal-Cooled Reactors in JAPAN", Proc. of 10th Int. Conf. Nuc. Eng., Arlington, Virginia, VA, Apr. 14-18, ICONE10-22166 (2002).
- [2] M. Takahashi, M. Sekimoto, K. Ishikawa, T. Suzuki, K. Hata, S. Que, S. Yoshida, T. Yano and M. Imai, "Experimentally Study on Flow Technology and Steel Corrosion of Lead Bismuth," Proc. of 10th Int. Conf. on Nucl. Eng. (ICONE10), April 14-18, Arlington, Virginia, VA, ICONE10-22226 (2002).
- [3] K. Kamata, T. Kitano, H. Ono and M. Ono, "Studies of Corrosion Resistance of Japanese Steels in Liquid Lead-Bismuth", Proc. of 11th Int. Conf. on Nucl. Eng. (ICONE12), April 20-23, Tokyo, Japan, ICONE11-36204 (2003).
- [4] J. Zhang, N. Li, Y. Chen, A. E. Rusanov, "Corrosion Behaviors of US Steels in Flowing Lead-Bismuth Eutectic (LBE)", *J. Nucl. Mater.*, **336**, 1-10, (2006).
- [5] C. Fazio, G. Benamati, C. Martini and G. Palombarini, "Compatibility Tests on Steels in Molten Lead and Lead-Bismuth", *J. Nucl. Mater.* **296**, 243-248 (2001).
- [6] G. Benamati, C. Fazio, H. Piankova and A. Rusanov, "Temperature Effect on the Corrosion Mechanism of Austenitic and Martensitic Steel in Lead-Bismuth," *J. Nucl. Mater.*, **301**, 23-27 (2002).
- [7] F. Barbier and A. Rusanov, "Corrosion behavior of Steels in flowing lead-bismuth", *J. Nucl. Mater.*, **296**, 231-236 (2001).
- [8] B. F. Gromov, Y. I. Orlov, P. N. Martynov, V. A. Gulevski, Proc. of HLMC1999, 87-100 (1999).
- [9] S. Jitsukawa, M. Tamura, B. van der Schaaf, R.L. Klueh, A. Alamo, C. Peterson, M. Schirra, P. Spaetig, G. R. Odette, A. A. Tavassoli, K. Shiba, A. Kohyama and A. Kimura, "Development of an extensive database of mechanical and physical properties for reduced-activation martensitic steel F82H", *J. Nucl. Mater.*, **307-311**, 179 (2002).
- [10] S. Ukai, M. Fujiwara, "Perspective of ODS alloys application in nuclear environments", *J. Nucl. Mater.*, **307-311**, 749 (2002).

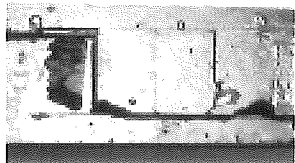
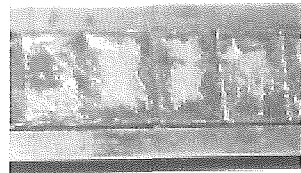
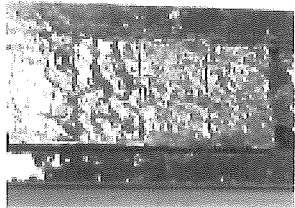
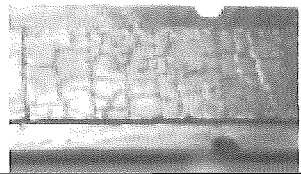
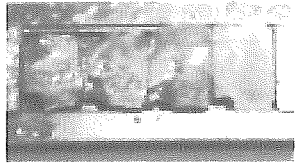

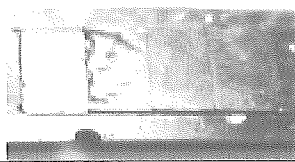
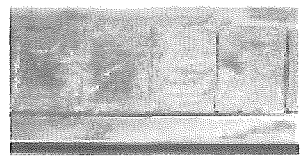

Table 3-1 Test conditions.

Flow rate (L/min)	6
Flow velocity (m/s)	2
Temperature of hot region (°C) (Test temperature)	550
Temperature of cold region (°C)	400
Test time (h)	1000

Table 3-2 Contents of alloying components in test steels.

	Cr	Mo	W	Si	Others
SCM420	1.2	0.2	-	0.2	
F82H	7.7	1.94	1.94	0.1	0.01Ti-0.01Cu
STBA28	8.8	1	-	0.4	
NF616	9	0.5	1.8	0.3	
STBA26	9	1	-	0.2	
ODS	11.7	-	1.9	-	0.29Ti-0.23Y ₂ O ₃ -0.18Y
HCM12A	12	0.3	1.9	0.3	0.9Cu
HCM12	12.1	1.1	1.0	0.3	
SS-316	18	2-3	-	0.1	10-14Ni

Table 3-3: Photographs of test piece surfaces in molybdenum holder.

Steel	Surface observation		
SCM420 (1Cr) -Erosion-		NF616 (9Cr-0.5Mo-8W) -Covered with Pb-Bi-	
ODS (11.7Cr-1.9W-0.29Ti-23Y ₂ O ₃ -0.18Y) -Covered with Pb-Bi-		HCM12 (12.1Cr-1.1Mo 1.0W) -Erosion-	
F82H (7.7Cr-1.94Mo -1.94W -0.01Ti-0.01Cu) -Erosion-		HCM12A (12Cr-0.3Mo 9W) -Smooth-	
STBA26 (9Cr-1Mo) -Erosion-		SS-316 (18Cr-2Mo -12Ni) -Rough surface-	
STBA28 (8.8Cr-1Mo-0.4Si) -Smooth-			

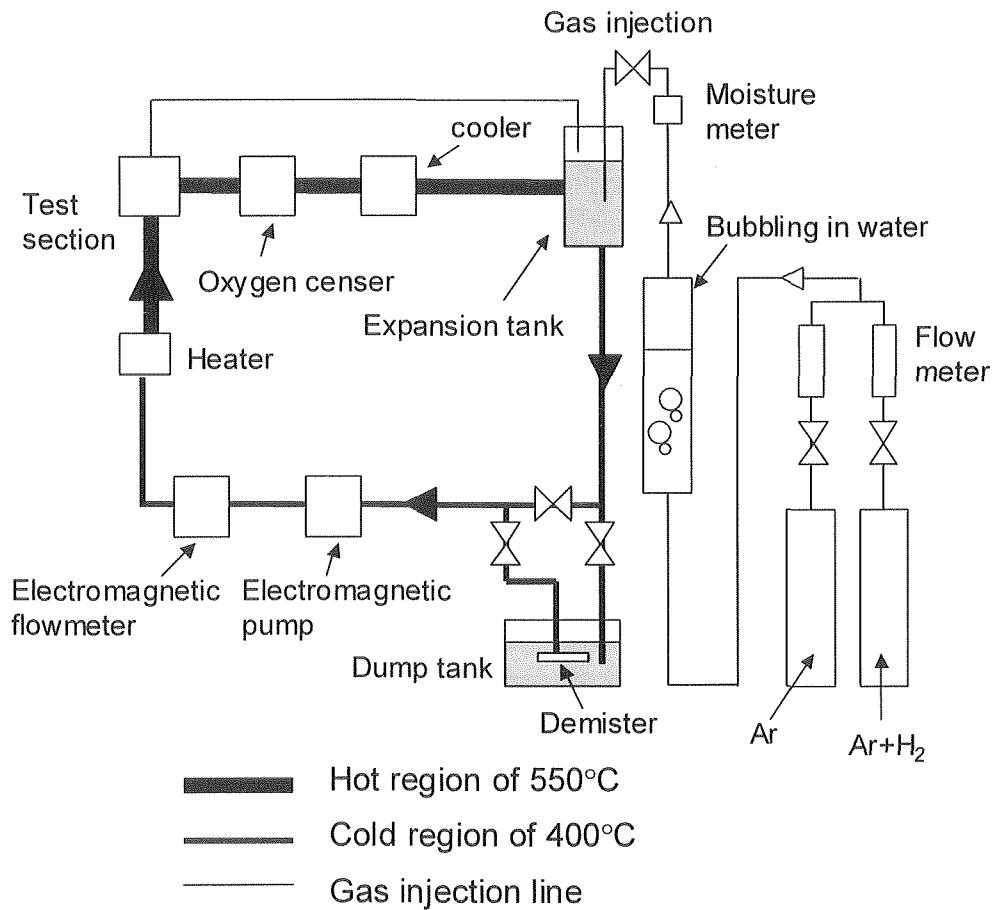


Fig. 3-1 Lead-bismuth corrosion test loop.

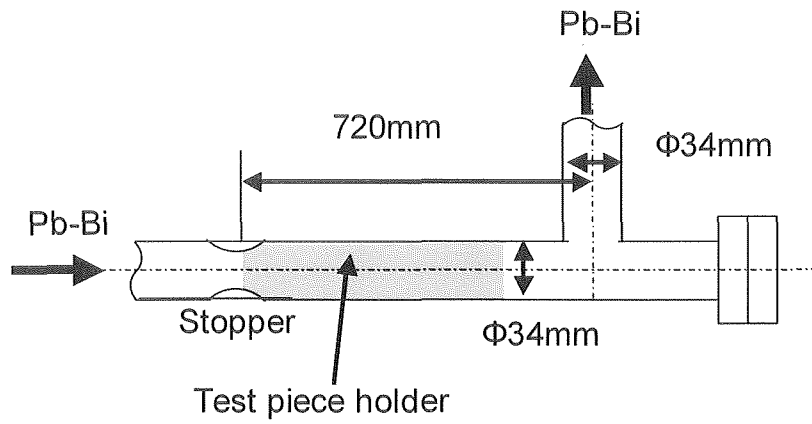


Fig. 3-2 Schematic of test section.

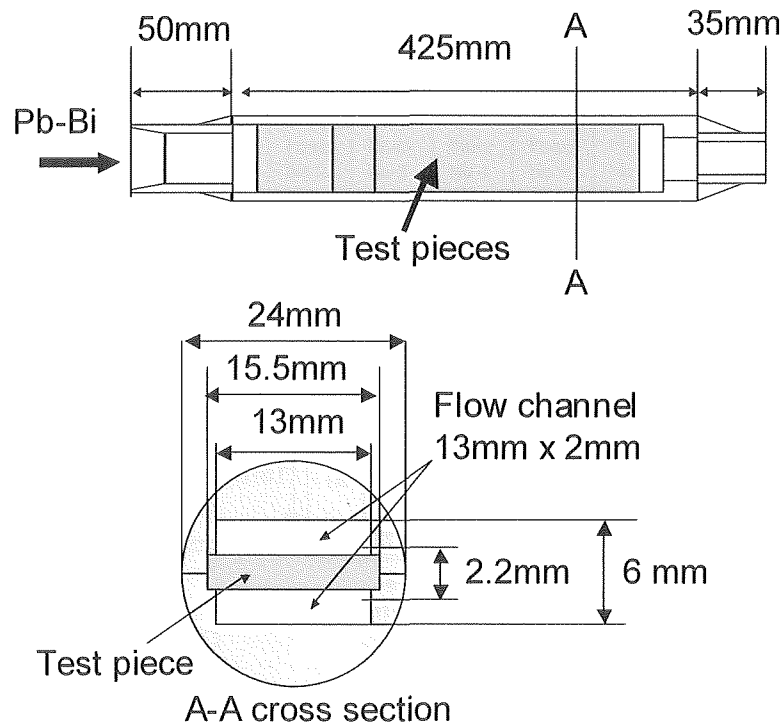


Fig. 3-3 Schematic of test piece holder.

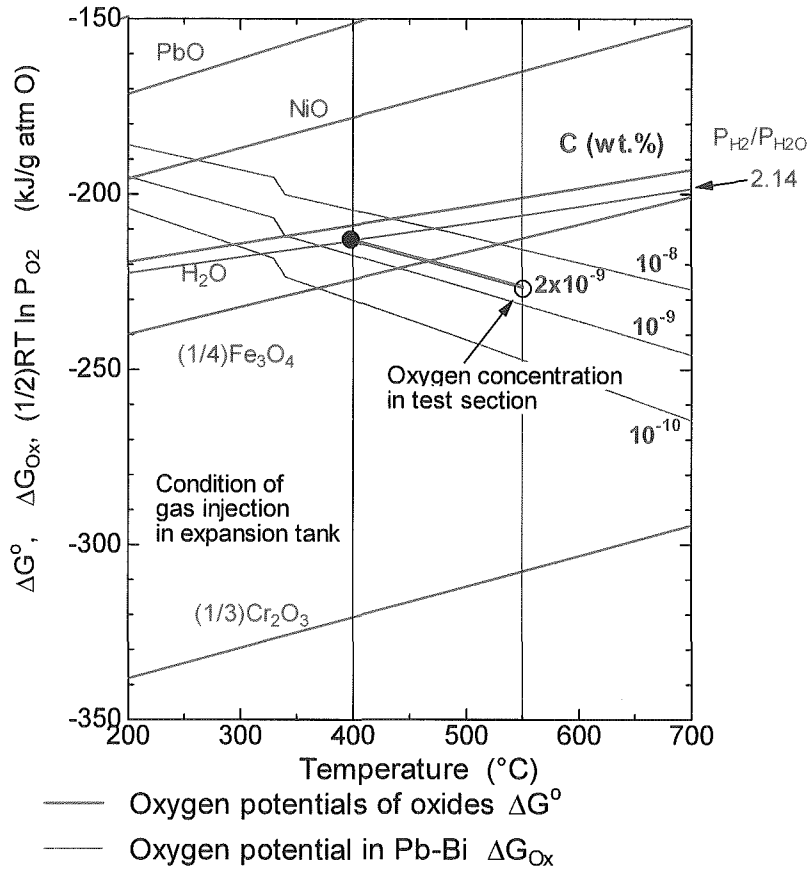


Fig. 3-4 Diagram of oxygen potential

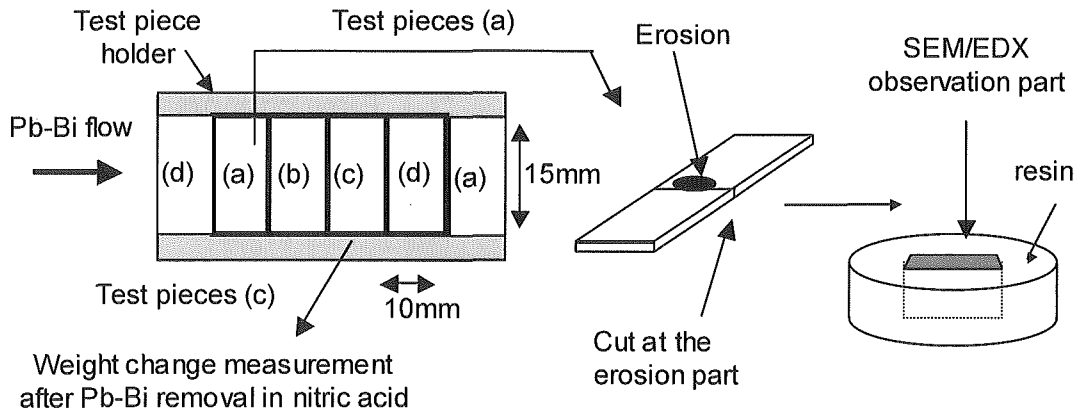
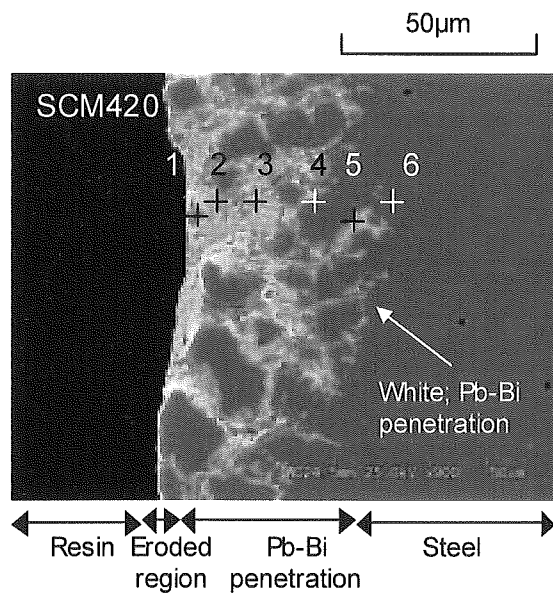


Fig.3-5 Test pieces in molybdenum holder and preparation for SEM/EDX observation and analysis.



	Point No 1	Point No 2	Point No 3	Point No 4	Point No 5	Point No 6
Fe	72.83	0.23	0.66	99.38	9.88	81.4
Cr	0.37	0	0	0.62	0	0.49
Pb	13.89	8.53	65.26	0	7.69	3.82
Bi	12.9	91.24	33.29	0	82.96	14.32

Unit: wt%

Fig. 3-6
in SCM420.

SEM/EDX observation and analysis for cross section of eroded region

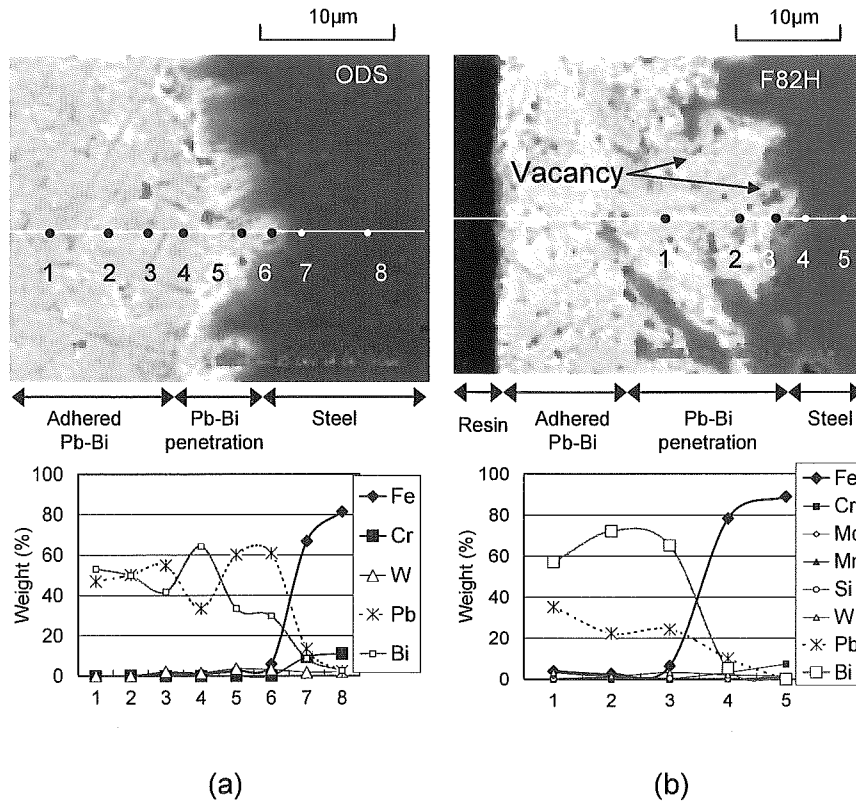


Fig.3-7: SEM/EDX observation and analysis for cross section of corroded region in (a) ODS and (b) F82H.

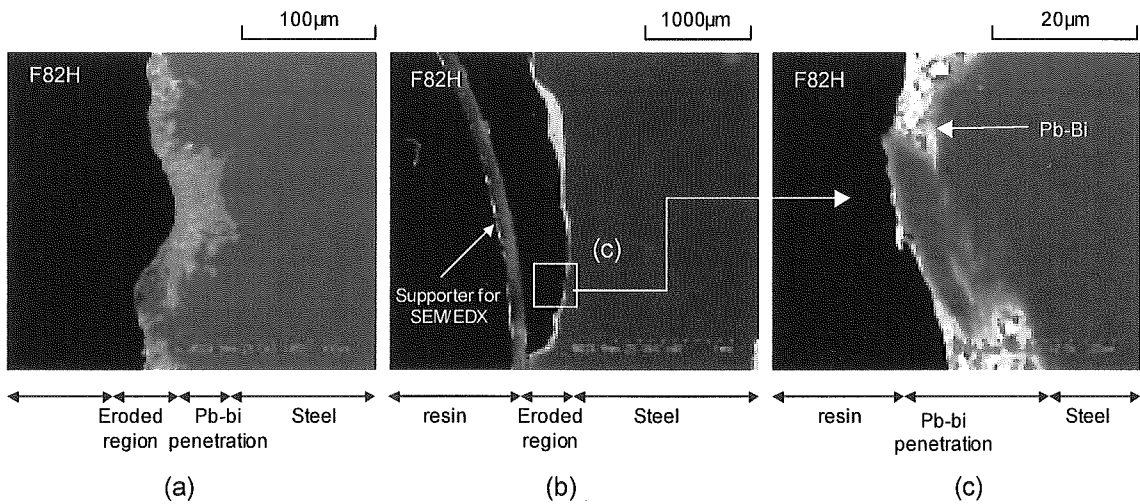


Fig. 3-8: SEM observation for cross section of eroded region in F82H (a) Pb-Bi penetration along narrow erosion, (b) Wide erosion, (c) Pb-Bi penetration in widely eroded region.

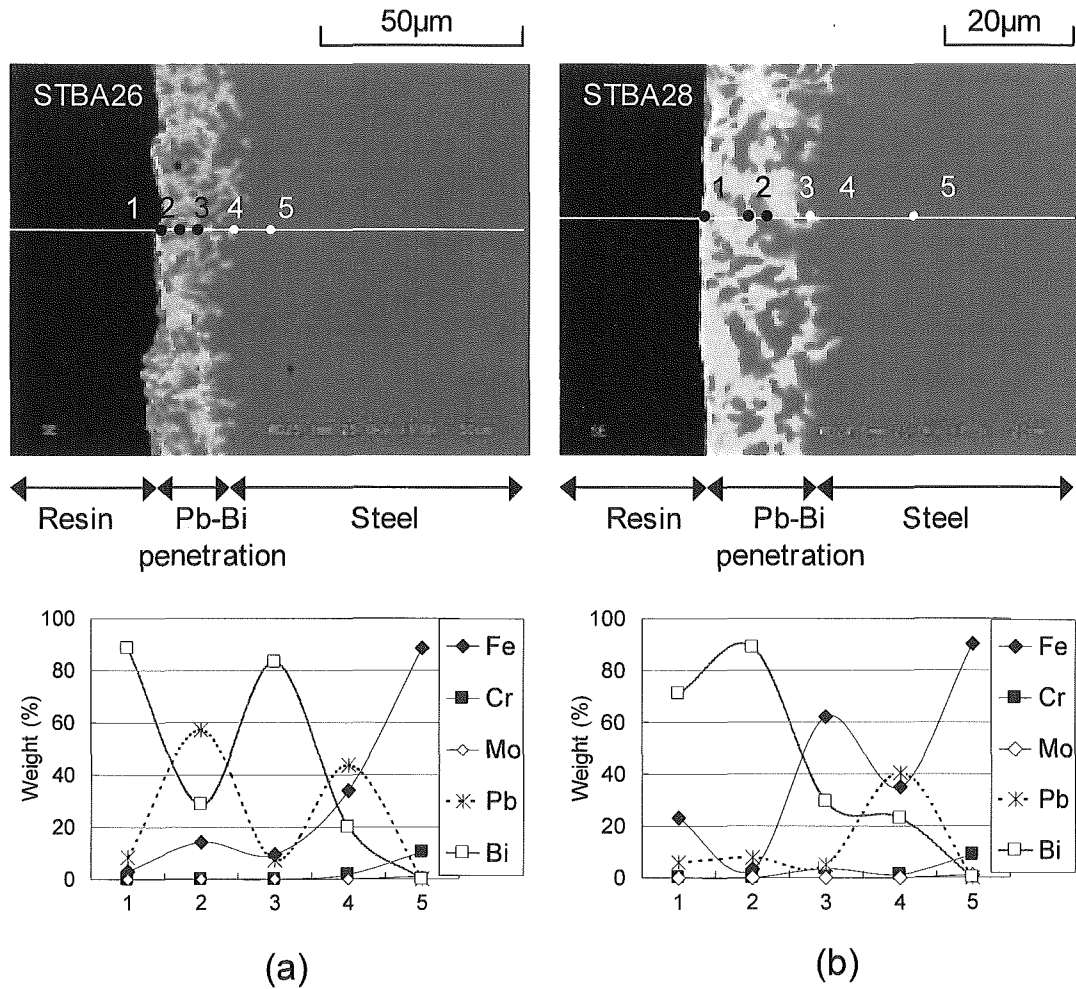


Fig. 3-9 SEM/EDX observation and analysis for cross section of corroded region in (a) STBA26 and (b) STBA28.

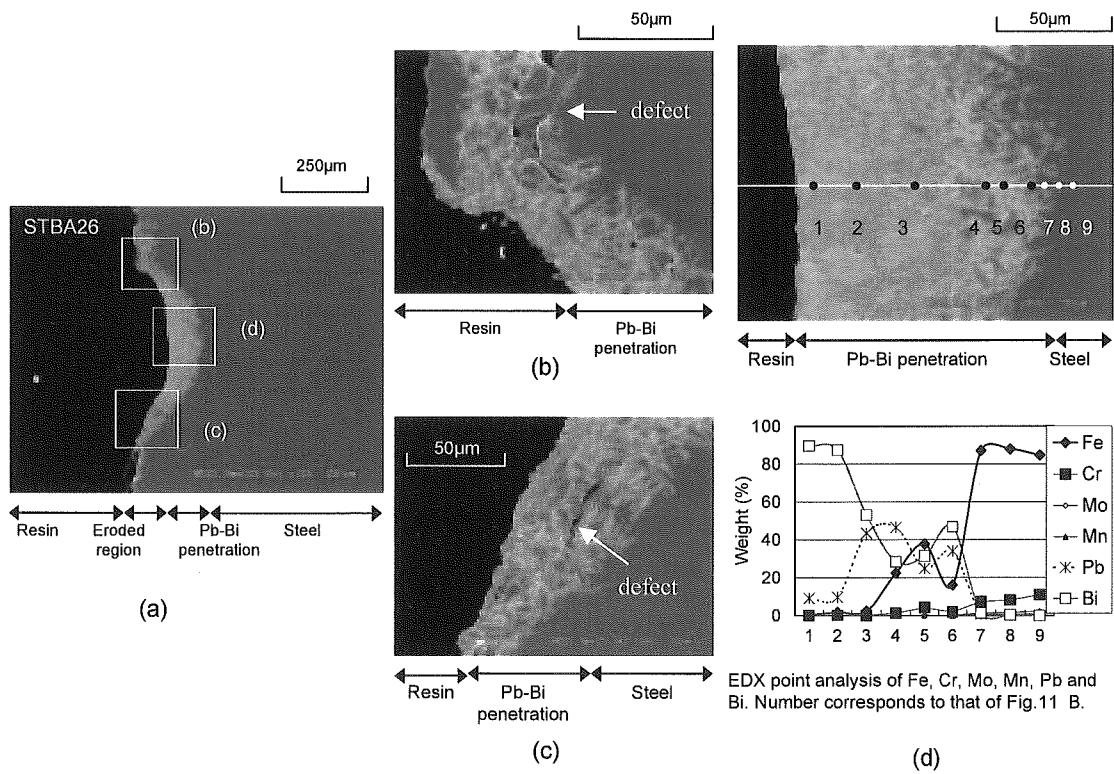


Fig. 3-10 SEM/EDX observation for cross section of eroded region in STBA26: (a) erosion, (b) end of eroded region, (c) end of eroded region, (d) Pb-Bi penetration and EDX analysis.

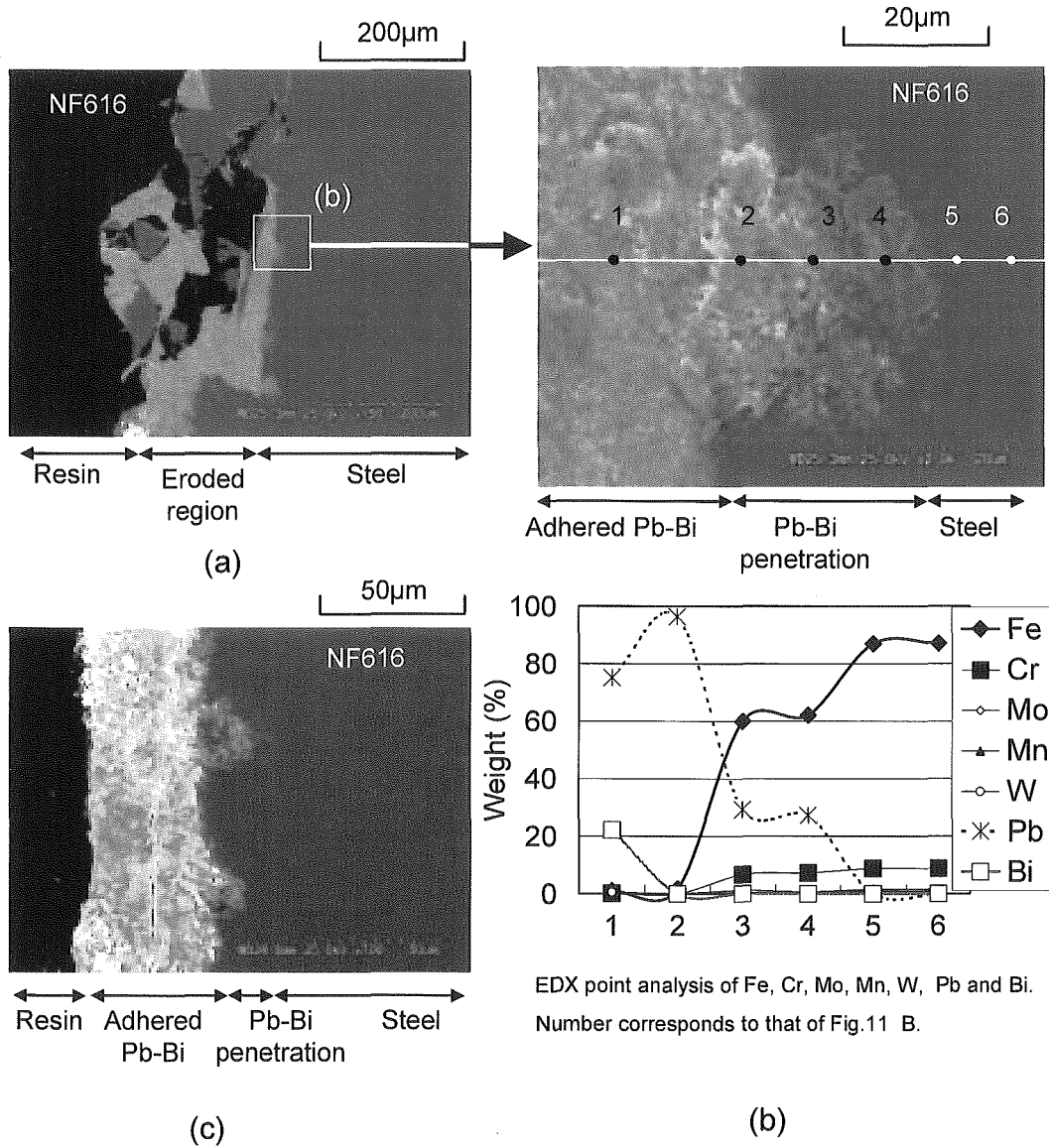


Fig. 3-11 SEM/EDX observation and analysis for cross section in NF616: (a) erosion, (b) Pb-Bi penetration in eroded region and EDX analysis, (c) Pb-Bi penetration in corroded region.

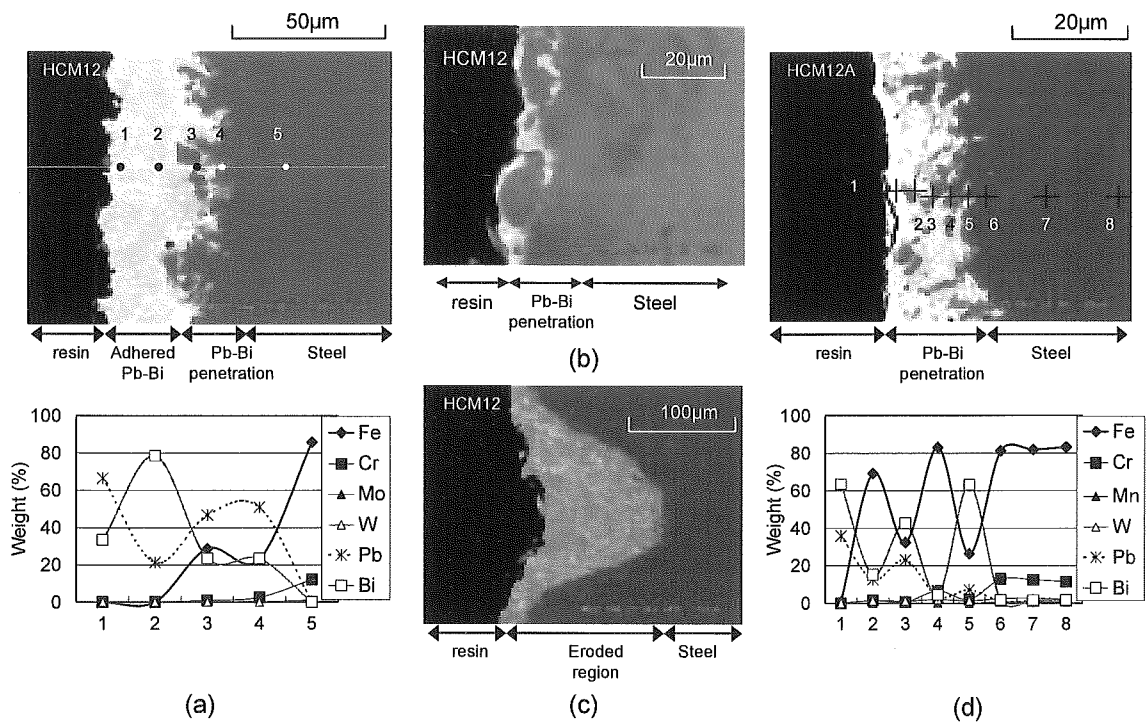


Fig.3-12 SEM/EDX observation and analysis for cross section of HCM12 and HCM12A : (a) corrosion and EDX analysis in HCM12, (b) Pb-Bi penetration in HCM12, (c) erosion in HCM12, (d) corrosion and EDX analysis in HCM12A.

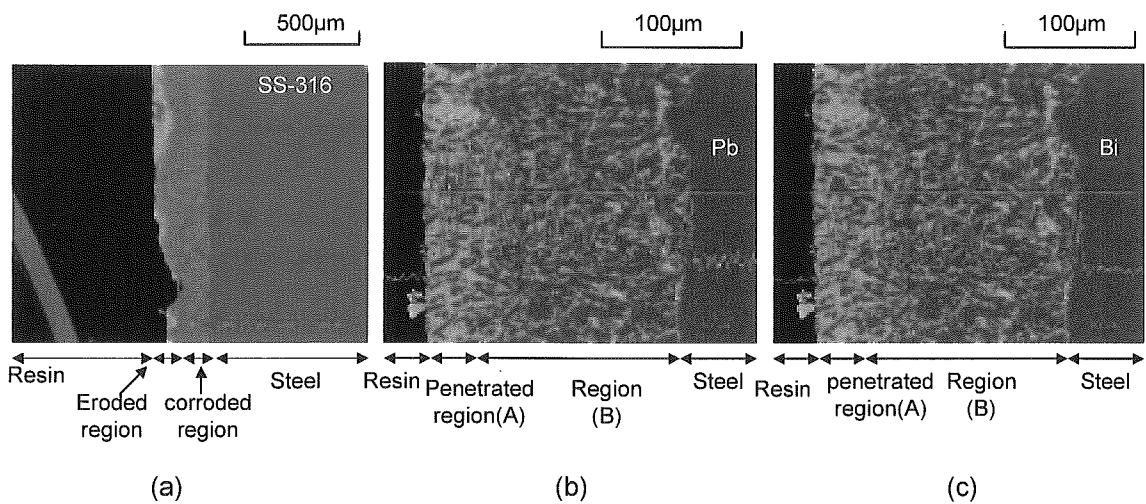


Fig.3-13: SEM/EDX observation and analysis for cross section of eroded region in SS-316: (a) erosion, (2) EDX analysis of Pb content in penetrated region (3) EDX analysis of Bi content in penetrated region.

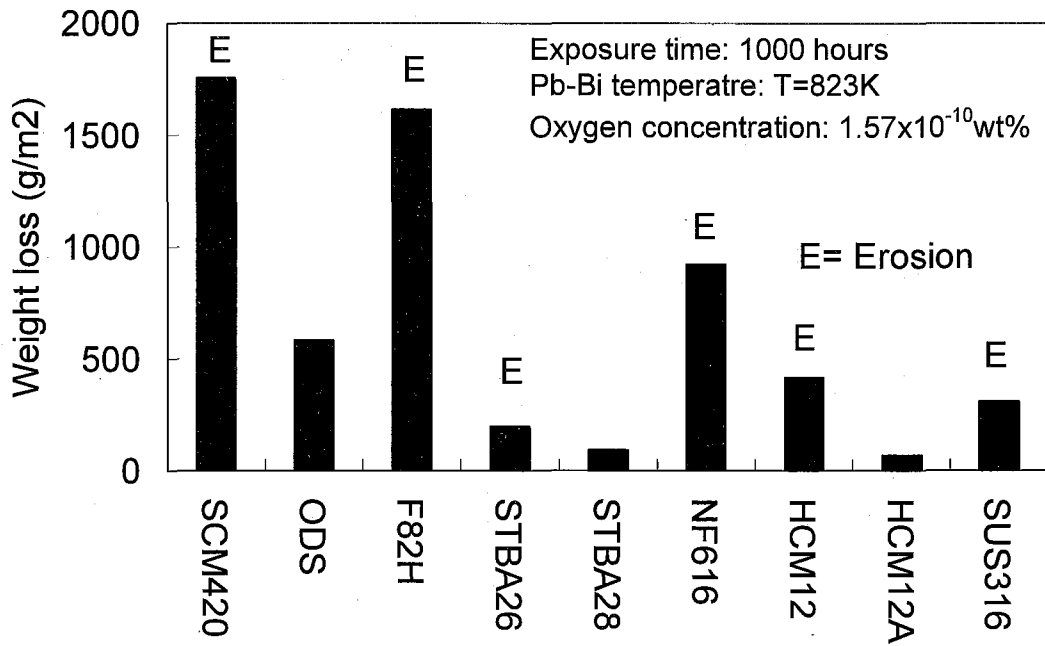


Fig.3-14 Weight change of test pieces during 1000-hour exposure to Pb-Bi flow

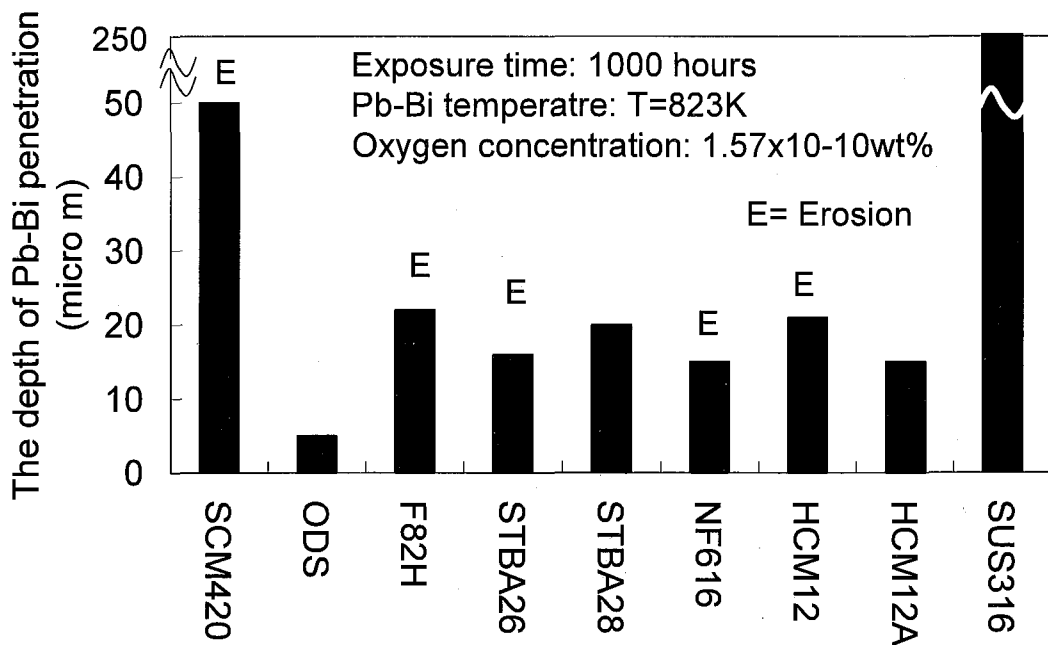


Fig.3-15 Depth of Pb-Bi penetration layers in steels

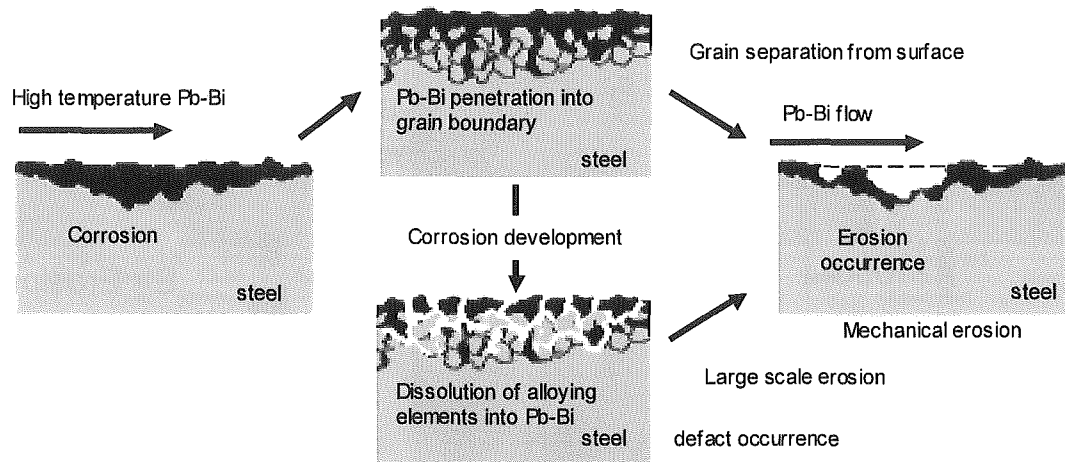


Fig. 3-16 Schematic of erosion mechanism

Chapter 4

Oxidation Corrosion Behaviors of Steels in Flowing Lead-Bismuth

4.1 Introduction

One of the key issues to develop lead-bismuth (Pb-Bi) cooled fast breeder reactors (FBRs) [1] is the compatibility of core and structural materials with Pb-Bi flow at high temperatures [2, 3].

Gorynin et al. [4] reported that the compatibility of steels with liquid Pb is dominated by two types of corrosion, i.e. oxidation in the liquid Pb with high-oxygen concentration and so-called liquid metal corrosion (LMC) in the liquid Pb with low-oxygen concentration (*Chapter 1, Fig. 1-2*). It can be expected that the corrosion behaviors of steels in the liquid Pb-Bi are similar to that in the liquid Pb. The LMC behaviors of steels in the liquid Pb-Bi was reported in *Chapter 3*.

The study on the oxidation characteristics of steels in liquid Pb-Bi was carried out. The purpose of the present study is to investigate the corrosion characteristics of the steels in the flowing Pb-Bi.

4.2 Experimental Apparatus and Procedure

Pb-Bi forced convection loop

Figure 4-1 shows the schematic of the forced convective Pb-Bi circulation loop used in the present corrosion test. The working fluid was Pb-Bi with a melting point of 125°C. The loop consists of a high temperature region made of 9Cr steel and a low temperature region made of SUS316 steel. The high temperature region has the electric heater, the corrosion test section and the oxygen sensor, and the low temperature region has the air cooler, the expansion tank, the electro-magnetic pump, and the electro-magnetic flow meter (explained in detail in *Chapter 8-2*). The cover gas of the expansion tank and the dump tank was argon having purity of 99.999%. Major specification of the loop is shown in **Table 4-1**.

The Pb-Bi in the dump tank was heated up to 180°C and melted. The circulation loop was heated up to 180 °C, and the Pb-Bi was charged from the dump tank into the circulation loop at a flow rate of approximately 0.5 l/min by the pressurizing the dump tank at 0.18 MPa with the loop pressure of 0.02 MPa. The Pb-Bi was circulated by the electro-magnetic pump at the rated operation flow rate, and the flow rate was measured by the electromagnetic flow meter. During the corrosion test, Pb-Bi was heated by the electric heater to the temperature of 550 °C at the inlet of the test section, and cooled down by the air cooler to the temperature of 400°C at the outlet of the cooler. Due to the loop temperature difference, dissolved steel alloying elements in the hot region were transported to the low temperature region, and then precipitated there because of the lower solubility of the elements at the lower temperature. Therefore, a steady condition of dissolved element concentrations in the hot and cold regions were achieved without the saturation of the elements in the hot region¹⁴⁾.

Figure 4-2 shows schematics of rectangular plate-type steel specimens mounted in a cylindrical molybdenum specimen holder. The holder was wound by a Mo wire, and

inserted into the test section as shown in **Fig. 4-3**. Then, Pb-Bi flowed in two flow channels above and below the specimens which were 13 mm wide, 2 mm high and 425 mm long.

The oxygen concentration in Pb-Bi was measured with the oxygen sensor which was mounted at the outlet of the corrosion test section. The oxygen sensor was a solid electrolyte conductor made of a cylinder of magnesia stabilized zirconia (Zr_2O-MgO) with the reference fluid of oxygen-saturated bismuth, that is, a mixture of 95wt%Bi and 5wt% Bi_2O_3 . Electro-motive force between Pb-Bi and the reference fluid was measured and the oxygen potential in Pb-Bi was estimated from the Nernst equation.

Experimental conditions

Experimental conditions are summarized in **Table 4-2**. The specimens were exposed to Pb-Bi flow for 1,000 hours.

In order to form the protective oxide layer of Fe_3O_4 on the steel surface that can suppress LMC, the oxygen potential in Pb-Bi was controlled to be slightly higher than Fe_3O_4 formation potential on the diagram of Gibbs free energy of oxide formation in **Fig. 4-4**. The electromotive force measured using the oxygen sensor at 550°C was 0.43V during the operation. From the electromotive force, the oxygen concentration in Pb-Bi was calculated using the Nernst equation and oxygen solubility in Pb-Bi by Gromov *et al.* [5] as 3.7×10^{-8} wt% and 1.7×10^{-8} wt% using PbO and $Pb_{0.45}Bi_{0.55}O_{1.275}$ for ΔG^0 , respectively. It is found in **Fig. 4-4** that the measured oxygen concentration was slightly higher than the Fe_3O_4 formation potential. With this oxygen content, it is expected that an outer oxide layer of Fe_3O_4 and an inner layer of Fe (Fe_{1-x}, Cr_x) $_2O_4$ are formed for high Cr steels according to the report of Fazio *et al.* [6].

Procedure of specimen analysis

In order to evaluate corrosion rate of the steels in the flowing Pb-Bi, the weight loss of specimens caused by the dissolution of the alloying elements into Pb-Bi or detachment of unstable oxide layer during the exposure into Pb-Bi has been measured. For the measurement of the weight loss, it is necessary to remove adherent Pb-Bi to the specimens, although the oxide layers should not be removed for subsequent metallurgical analysis. However, in the previous experiment [7], adherent Pb-Bi was removed together with the oxide layers by immersing specimens in a hot sodium pool. According to F. Barbier and A. Rusanov, the immersion of the specimens in a hot glycerin pool is adequate for the removal of adhered Pb-Bi without removing the oxide layers [8]. Thus, in the present study, the adherent Pb-Bi was removed by using a hot glycerin pool for the measurement of weight loss.

After the 1,000-hour exposure of the specimens to the Pb-Bi flow, the specimen holder was demounted from the test loop, and immersed in a glycerin pool at the temperature of 180°C to remove adherent Pb-Bi from the outside and inside of the holder. Then, the holder was opened and the specimens were taken out of the holder, and rinsed again in glycerin pool at the temperature of 180°C to melt and remove

adherent Pb-Bi from the specimen surfaces without removal of the oxide layers. Finally, glycerin on the specimen surface was removed in warm water at the temperature of 70°C.

The surfaces of the specimens were observed before and after the exposure to inspect the occurrence of erosion. In order to determine the corrosion rate, weight losses of the specimens were measured using an electro reading balance with an accuracy of 0.1mg. The specimens were cut at the span wise center. The cross sections were polished, and then analyzed by a scanning electron microscope (SEM)/energy-dispersive X-ray spectrometer (EDX).

4.3 Test materials

Various steels were chosen as test material for the comparison of corrosion characteristics. Chemical components of test material are presented in **Table 4-3**. Low Cr steel, SCM420, is for structural material. Martensitic steel, F82H, has been developed as fusion blanket material [9]. STBA26 and NF616 are for boiler at high temperature. Martensitic steel, SUH3, has been developed for inner combustion material. Martensitic steel, ODS, has been developed as cladding material of fuel rods in sodium cooled fast breeder reactor [10]. HCM12A and HCM12 have been developed for the structural material of supercritical thermal power plant [11]. Ferritic steel, SUS405 and SUS430, and austenitic steel, SUS316, have been used as structural materials for chemical plant.

The sizes of the specimens are shown in **Table 4-4**. In order to remove the effect of surface roughness on corrosion behavior of each specimen when they were compared with each other¹⁸⁾, the surfaces were polished to be at the same smooth condition of arithmetical mean surface roughness Ra of 1.5 μ m. The polish is also needed to remove oxide layers as an initial surface condition.

The specimens were mounted in the specimen holder in the flow direction in the following order: (1) HCM12A, (2) SUH3, (3) STBA26, (4) NF616, (5) SUS430, (6) SUS405, (7) SUS316, (8) F82H, (9) ODS, (10) SCM420. The steels mounted in upstream region were chosen to be more corrosion resistant based on the previous study in order to prevent the influence of metal dissolution from specimens upstream on corrosion of specimens downstream.

4.4 Oxide Layers on Steels

Surface observation

The surfaces of the specimens after the 1,000-hour exposure are shown in **Fig. 4-5**. It can be seen that no appreciable traces of erosion existed on all of the steel surfaces. The surface state was similar to each other in all the specimens. The colors of the steel surfaces changed from initial metallic luster before the exposure into black after the exposure, which suggested the formation of corrosion products or oxide layers on the surfaces.

Oxide layer analysis using SEM/EDX

HCM12A and HCM12

On the surfaces of HCM12A, triple oxide layers were formed as shown in **Fig. 4-6 (a)**. These layers can be classified into the outer layer (O), the middle layer (M) and the inner layer (I). The Fe-rich outer layer (O) was broken into some pieces and peeled from the substrate, while the Cr-rich middle and inner layers stuck to the substrate stably (**Fig. 4-6 (a)** No.1, 2 and 3). The thickness of the each layer is shown in **Table 4-5**.

It was observed in HCM12 (**Fig. 4-6 (b)**) that double oxide layer formation. The outer layer (O) consisted of the small fragments. The inner layer (I) was compact and stuck to the substrate. The weight ratio of Fe to Cr in the outer layer and inner layer was app. 2:1 and 7.2, respectively (**Fig. 4-6 (b)** No1, 2 and 3).

The major difference between the layers in HCM12A and HCM12 is that the crack existed in the outer layer on the former steels. In both of the steels, no sign of Pb-Bi penetration was observed beneath these layers.

NF616 and STBA26

Triple oxide layer was observed on NF616 surface (**Fig. 4-6 (c)**). There were some cracks in the outer layer where Fe was poor and Cr was slightly enriched compared with that of the matrix (**Fig. 4-6 (c)** No.1). Fe content was poor and Cr and W were enriched in the middle layer (**Fig. 4-6 (c)** No.2) which might be effective together with the quite thin oxide layer close to the surface of the inner layer to protect the steel from corrosion.

The surface of STBA26 was covered by the oxide layer with double layer structure: (**Fig. 4-6 (d)**). The outer layer (O), where Cr was enriched (**Fig. 4-6 (d)** No.1), seemed to correspond to the middle layer in NF616 (**Fig. 4-6 (c)** No.2) since a developing scale could be observed on the outer layer. The inner layer was very thin as it merged with the steel matrix. Beneath the layers, Pb-Bi penetration was not detected. From these facts, the outer layer inhibits Pb-Bi penetration even though the oxygen penetrated through the outer layer.

SUS430 and SUS405

Double oxide layer was observed on the surface of SUS430 as shown in **Fig. 4-6(e)**. The Cr-enriched outer layer (O) had some cracks. Inner layer (I) consists of the small pieces.

On the SUS405 surface (**Fig. 4-6 (f)**), the app.6.7 μm thick outer layer (O) and app.4 μm thick inner layer (I) were observed. In the outer layer A, Cr was enriched (**Fig. 4-6 (f) No.1**), and there were some cracks particularly on the rough part of the steel surface²¹⁾.

ODS

It was observed in ODS that the oxide layers were formed and that composed of two layers: outer layer (O) of app.7 μm in thickness and inner layer (I) of app.11 μm in thickness (**Fig. 4-6 (g)**). The Cr-enriched outer layer was broken to small fragments and peeled from the inner layer. In the thick inner layer which stuck to the matrix stably, Cr was enriched only slightly compared with that of the steel matrix (**Fig. 4-6 (g) No.2**). Some transverse cracks existed on the convex part of the steel surfaces²²⁾.

F82H

Double oxide layer: app.8.3 μm thick outer layer (O) and app.4 μm thick inner layer (I) were observed (**Fig. 4-6 (h)**). The Cr-enriched outer layer was peeled from the inner layer. The W enriched inner layer was also peeled from the surface (**Fig. 4-6 (h) No. 2**). Beneath the inner layer, Pb-Bi penetrated into the steel matrix.

SUS316

Single oxide layer was formed on the surface of SUS316. Fe was poor and Cr was enriched in the layer (**Figs. 4-6 (i) and (j)**). The Pb-Bi penetration was partially caused by the dissolution of Ni and Cr into Pb-Bi. However, the depth was app.15 μm which was much shallower than that caused erosion without the formation of the oxide layer in previous study (see *Chapter 3-3*).

SUH3

There were two layers on the surface of SUH3 as shown in **Fig. 4-6 (k)**. The outer oxide layer was peeled from the steel surface. The inner layer was thin and the surface is smooth without damage. It has been found by EDX analysis that Si was enriched only in the inner layer.

SCM420

Figure 4-6 (l) shows that SCM420 characterized by low-alloy steel has only single layer with cracks. In the layer, Cr was not enriched.

4.5 Weight Changes of Steels in Flowing Pb-Bi at High Oxygen Concentration

Figure 4-7 shows the measured weight losses of the specimens. All the steels lost their weight during the exposure. The weight loss in SCM420 was the largest among all the steels. The weight loss of F82H, ODS and HCM12A were also large. The weight losses of SUH3 and SUS430 were less than the other steels. Although the HCM12A specimen decreased the weight, HCM12 which has chemically similar components increased the weight in the Pb-Bi. That is possibly because HCM12 formed the compact oxide layer and did not caused the oxidation corrosion (Fig. 4-6 (b)), while the HCM12A caused the oxidation corrosion due to the detachment of unstable outer oxide layer (Fig. 4-6 (a)).

The weight loss of SUS316 was not able to evaluate in the present experiment. That was because Pb-Bi penetrated into the porous layer formed by the dissolution of Ni and Cr into Pb-Bi was not completely removed in the glycerin. The weight loss of F82H might be larger than the measured one since Pb-Bi that rarely penetrated into steel matrix could not be completely removed by glycerol.

4.6 Effect of Oxide Layer Formation on Corrosion Resistance

All the test steels formed the oxide layers in the Pb-Bi flow. Although the LMC occurred in F82H and SUS316, the intensities of the LMC in F82H and SUS316 were much weaker than those in the pervious results (see *Chapters 3-3 and 3-4*) where the oxide layers were not formed because of low oxygen content in Pb-Bi. Therefore, the formation of the oxide layers seemed to be effective to inhibit the LMC.

The structures of the oxide layers depended on the type of the steels as shown in Fig. 4-6. Except for the single layers formed on SCM420 and SUS316, the layers on the other steels could be observed as multiple which were composed of different chemical composition as the same as reported by some researchers [6, 8, 12].

As for the property of the multiple layers, the most of the outer layers were cracked and broken into some pieces. In other words, it is not be effective as barrier for the corrosion. On the contrary, the inner one was compact and stuck to the steel surface. Thus, the formation of the compact inner layer was more important to inhibit the LMC. The formation mechanism of multiple oxide layers on the steels in Pb-Bi could be explained as follows. Fe-rich oxide layer as the outer layer was formed by the reaction of Fe and oxygen in Pb-Bi. Then, oxygen diffused from the Pb-Bi into the steel matrix across the outer layer and reacted chemically with Fe with a condensed Cr. This is since the Fe was used to form the oxide layer while Cr was remained on the surface. This might produce a thin and stable oxide layer close to the surface of the steel matrix. Once the Cr-rich oxide layer was formed, Fe could not be dissolved easily into the Pb-Bi because of the barrier of the Cr-rich oxide layer.

4.7 Oxidation Corrosion in Flowing Pb-Bi

The oxide layers were formed on the steels in the liquid Pb-Bi at the oxygen concentration higher than the formation potential of Fe_3O_4 , even though the Cr oxide layer was not formed at the oxygen concentration lower than that of Fe-oxide formation but higher than that of Cr-oxide formation (*Chapter 3*). This is since the corrosion behavior was well influenced by the alloying elements of Fe, which occupied app. 80% in the steel matrix. If Fe on the surface does not formed oxide layers, Fe may be dissolved into the liquid alloy. In the same time, Cr is also dissolved into the liquid alloy.

Due to the formation of the oxide layers on the steel surfaces, the LMC was inhibited by the existence of the layer as the corrosion barrier. However, some steels formed the unstable oxide layers, and caused a break away of the layers. Then, the corrosion pattern of the steels in the liquid Pb-Bi was changed from the LMC to the oxidation corrosion. **Fig. 4-8** shows the patterns of corrosion which generally occurs on the steels. The oxidation corrosion of steels in the liquid Pb-Bi is possibly similar to the oxidation corrosion in the so-called dry corrosion.

4.8 Pilling-Bedworth Ratio (PB ratio) of Oxide Layers Formed on Steels in Liquid Pb-Bi

The oxidation corrosion in the so-called dry corrosion is caused by the break away of the unstable oxide layers. Pilling-Bedworth ratio (PB ratio) is well-known dimensionless number to determine the stability of the formed oxide layers. When the oxygen in the liquid Pb-Bi diffuses into the steel matrix and formed a metal oxide, the metal may increase or decrease the volume. Then, the change of the volume in the metal oxidation process can be expressed by PB ratio ϕ

$$\phi = \frac{Md}{mD} \quad (4-1)$$

where M is the molecular weight of the metal oxide, m is the weight of the metal, D is the density of the metal oxide and d is the density of the metal. The PB ratio less than 1 indicates the formation of porous oxide layer, and this condition may cause the oxidation corrosion on steel due to the oxide diffusion through the porous layer. The PB ratio much higher than 2 indicates the occurrence of the cracks in the oxide layer due to the stress caused by the great increase of the volume in the oxidation process. Thus, the PB ratio between 1 and 2 is preferable for the formation of the compact oxide layer due to the brief stress caused by the slight increase of the volume in the process.

Table 4-6 shows the PB ratio provided in ref. [13]. It was found that the metals increased the volume in the oxidation process in the present study. The PB ratio of the Cr or Fe-Cr oxide formation is higher than that in Fe oxide formation. The PB ratio of

the Si oxide formation is higher than these Fe-Cr oxide formation, while that of the Al oxide formation is much less than those of Fe-Cr or Si oxide formation. Thus, the oxide layer formed on the Fe-Cr steels and Si rich steel such as HCM12A or SUH3 had stress in the layer slightly larger than the low alloy steel SCM420.

Table 4-7 shows the self-diffusion coefficient of the metal in the metal oxide at 1000 °C [13]. It was found that the Cr, Si and Al oxide had lower diffusion coefficient. This indicates that the these oxides have higher oxidation resistance than the Fe oxide.

The stability of the formed oxide layers may be determined by these factors. It can be summarized that the PB ratio of the oxidation of the structural materials in the liquid Pb-Bi was agreed with the condition for the compact oxide layer formation. The self-diffusion coefficient may be influenced on the stability.

4.9 Conclusion

Corrosion characteristics of the steels in flowing lead bismuth were investigated by means of the steel corrosion test performed in flowing lead bismuth. Conclusions are as follows:

- (1) The oxide layers were formed on all the test steels in flowing Pb-Bi at the oxygen potential higher than that required for the formation of Fe_3O_4 .
- (2) Beneath the oxide layers, the trace of liquid metal corrosion was not observed except for austenitic steel SUS316 and martensitic steel F82H.
- (3) The oxide layers had a multiple layer structure. The existence of the thin and compact inner oxide layer was important for the steels to be more corrosion resistant in Pb-Bi flow.
- (4) In the oxide layers which were formed on high Cr steels: HCM12, HCM12A, SUS405, SUS430, Cr was enriched.

References

- [1] S. Uchida, H. Osada, Y. Kasahara, M. Takahashi and K. Hata, "A Feasibility Study on the Lead-bismuth Cooled Direct Contact Boiling Water Fast Reactor", Proc. of 11th Int. Conf. Nuc. Eng., Tokyo, Japan, Apr. 20-23, ICONE11-36320 (2003).
- [2] M. Takahashi, M. Igashira, T. Obara, H. Sekimoto, K. Kikuchi, K. Aoto and T. Kitano, "Studies on Materials for Heavy-Liquid-Metal-Cooled Reactors in JAPAN", Proc. of 10th Int. Conf. Nuc. Eng., Arlington, Virginia, VA, Apr. 14-18, ICONE10-22166 (2002).
- [3] B. F. Gromov, Y. I. Orlov, P. N. Martynov, V. A. Gulevsky and V. A. Yakolev, "The problems of technology of the heavy liquid metal coolants (Lead-bismuth, Lead)", Proc. of HLMC1998, Obninsk, Russia, Oct. 5-9, 87 (1998).
- [4] I. V. Gorynin, G. P. Karzov, V. G. Markov, V. S. Lavrukhin and V. A. Yakolev, "STRUCTURAL MATERIALS FOR POWER PLANTS WITH HEAVY LIQUID METALS AS COOLANTS", Proc. of HLMC1999, 87-100 (1999).
- [5] B. F. Gromov, Y. S. Belomitcev, E. I. Yefimov, M. P. Leonchuk, Y. I. Orlov, Y. I. Pankratov, Y. G. Pashkin, G. I. Toshinski, V. V. Chekunov, B. A. Shmatko and V. S. Stepanov, "Use of lead-bismuth coolant in nuclear reactors and accelerator-driven systems", Nucl. Eng. Design, **173**, 207 (1997).
- [6] C. Fazio, G. Benamati, C. Martini, G. Palombarini, "Compatibility tests on steels in molten lead and lead-bismuth", J. Nucl. Mater., **296**, 243 (2001).
- [7] M. Takahashi, M. Sekimoto, K. Ishikawa, T. Suzuki, K. Hata, S. Que, S. Yoshida, T. Yano, M. Imai, "Experimentally Study on Flow Technology and Steel Corrosion of Lead Bismuth," Proc. of 10th Int. Conf. on Nucl. Eng. (ICONE10), April 14-18, Arlington, Virginia, VA, ICONE10-22226 (2002).
- [8] F. Barbier, A. Rusanov, "Corrosion behavior of Steels in flowing lead-bismuth", J. Nucl. Mater. **296**, 231-236 (2001).
- [9] S. Jitsukawa, M. Tamura, B. van der Schaaf, R.L. Klueh, A. Alamo, C. Peterson, M. Schirra, P. Spaetig, G. R. Odette, A. A. Tavassoli, K. Shiba, A. Kohyama and A. Kimura, "Development of an extensive database of mechanical and physical properties for reduced-activation martensitic steel F82H", J. Nucl. Mater., **307-311**, 179 (2002).
- [10] S. Ukai, M. Fujiwara, "Perspective of ODS alloys application in nuclear environments", J. Nucl. Mater., **307-311**, 749 (2002).
- [11] K. Rodak, A. Hernas, A. Kielbus, Nucl. Chem. and Phys., **81**, 483-485 (2003).
- [12] G. Benamati, C. Fazio, H. Pinakova, A. Rusanov, "Temperature effect on the corrosion mechanism of austenitic and martensitic steels in lead-bismuth", J. Nucl. Mater., **301**, 23 (2002).
- [13] High temperature oxidation of steel, Hushoku-Boushoku kyokai (1982). [In Japanese]

Table 4-1 Specifications of forced convective Pb-Bi corrosion test loop

Pb-Bi inventory in loop	0.022 m ³
Volume in dump tank	0.066 m ³
Maximum test temperature	823 K
Maximum system pressure	0.4 MPa
Maximum flow rate	6 l/min
Maximum velocity in test section	2 m/s
Heater and cooler power	22 kW
Structural material in hot region	9Cr-1Mo steel
Structural material in cold region	SUS316

Table 4-2 Experimental conditions

Exposure time	1,000 hrs	
Pb-Bi temperature in test section	550 °C	
Pb-Bi temperature in low temperature sections of loop	400 °C	
Pb-Bi velocity in test section	1 m/s	
Pb-Bi flow rate	3 l/min	
Oxygen concentration in Pb-Bi	ΔG^0 of PbO	3.7×10^{-8} wt%
	ΔG^0 of $\text{Pb}_{0.45}\text{Bi}_{0.55}\text{O}_{1.275}$	1.7×10^{-8} wt%

Table 4-3 Chemical components of test steels

	Cr	Mo	W	Si	others
SCM420	1.2	0.2	-	0.2	
F82H	7.7	1.94	1.94	0.1	0.01Ti-0.01Cu
NF616	9	0.5	1.8	0.3	
STBA26	9	1	-	0.2	
SUH3	11	1	-	2	0.4C
ODS	11.7	-	1.9	-	0.29Ti-0.23Y ₂ O ₃ -0.18Y
HCM12A	12	0.3	1.9	0.3	0.9Cu
HCM12	12.1	1.1	1.0	0.3	
SUS405	12	-	-	1	0.1Al
SUS316	18	2-3	-	0.1	10-14Ni
SUS430	18	-	-	0.75	

Table 4-4 Size of specimens

	Length	Width
HCM12A	30	15
HCM12	10	15
SUH3	30	15
STBA26	55	15
NF616	10	15
SUS430	55	15
SUS405	10	15
SUS316	10	15
F82H	10	15
ODS	10	15
SCM420	(Spacer)	15

Table 4-5 Thickness of oxide layers and Pb-Bi penetration obtained from SEM analysis

	Thickness (μm)			Pb-Bi penetration
	Outer layer	Middle layer	Inner layer	
SCM420	-	-	17	-
F82H	-	8.3	4	8.3
STBA26	-	10	2	-
NF616	3	5	2	-
SUH3	-	6.6	1	-
ODS	-	7	11	-
HCM12A	4	4	4	-
HCM12	3	8.2	5	-
SUS405	-	6.7	3.3	-
SUS316	-	-	4.1	8
SUS430	-	6.7	4	-

Table 4-6 Pilling-Bedworth ratio of oxide layer formed on steel in liquid Pb-Bi

Metal oxide / metal	PB ratio	Metal oxide / metal or oxide	PB ratio
FeO / Fe	1.77	Cr ₂ O ₃ / 21Cr Steel	2.06
Fe ₃ O ₄ / Fe	2.1	Cr ₂ O ₃ / 18Cr-8Ni Steel	2.09
Cr ₂ O ₃ / Cr	1.99	Al ₂ O ₃ / 12Cr-4Al Steel	1.81
Al ₂ O ₃ / Al	1.28	Fe(FeCr ₂) ₂ O ₄ / 9Cr Steel	2.1
SiO ₂ / Si	2.15	FeCr ₂ O ₄ / 18Cr-8Ni Steel	2.1
FeO / Carbon steel	1.79	Fe ₃ O ₄ / FeO	~ 1.2
FeO / 1Cr-1Mo steel	1.79	Fe ₂ O ₃ / Fe ₃ O ₄	1.02

Table 4-7 Self-diffusion coefficient of metal in metal oxide layer

(1000 °C) (cm ² /s)	
Metal oxide	Self-diffusion coefficient
FeO	9x10 ⁻⁸
Fe ₃ O ₄	2x10 ⁻⁹
Cr ₂ O ₃	3x10 ⁻¹⁴
Al ₂ O ₃	3x10 ⁻¹⁷
SiO ₂	Self-diffusion coefficient of metal in SiO ₂ is less than that of oxygen (1.3x10 ⁻¹⁸ cm ² /s)

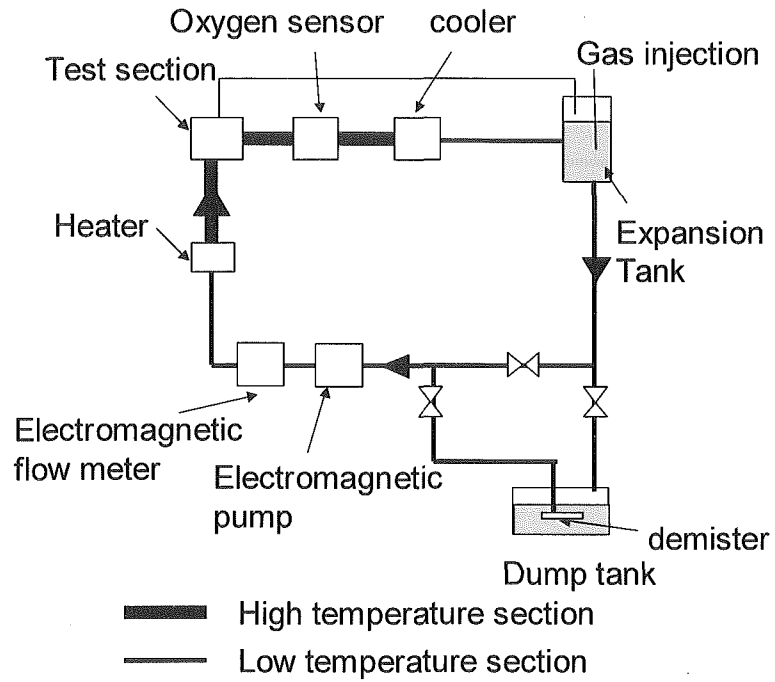


Fig. 4-1 Schematic diagram of corrosion test loop

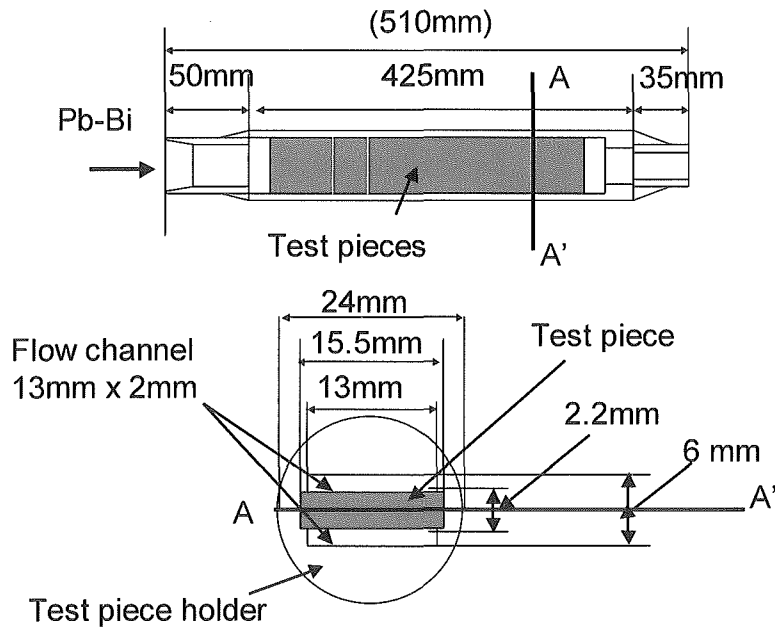


Fig. 4-2 Specimen holder

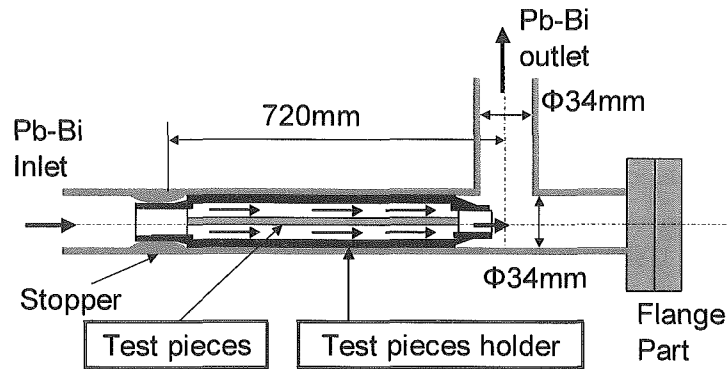


Fig. 4-3 Test section

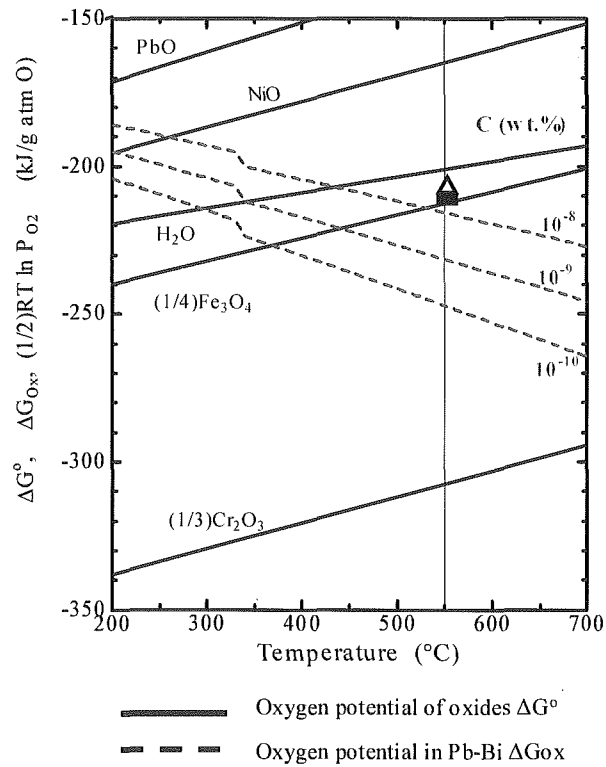


Fig. 4-4 Diagram of oxygen potential; symbol of black triangle: ΔG^0 in is estimated from oxygen potential of $\text{Pb}_{0.45}\text{Bi}_{0.55}\text{O}_{1.275}$, symbol of black square: that is estimated from oxygen potential of PbO

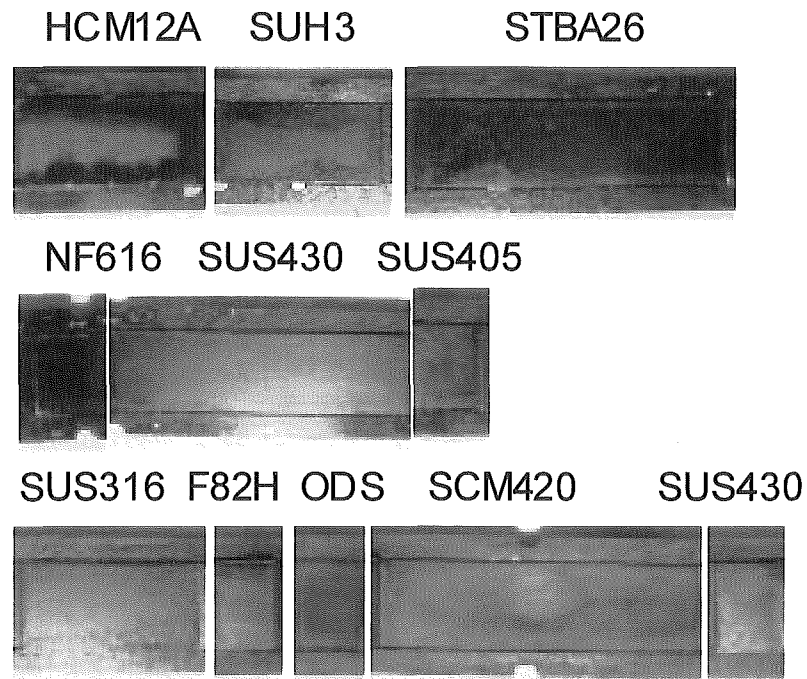


Fig. 4-5 Appearance of specimen surfaces in the Mo holder after 1,000 hr-exposure to the Pb-Bi flow

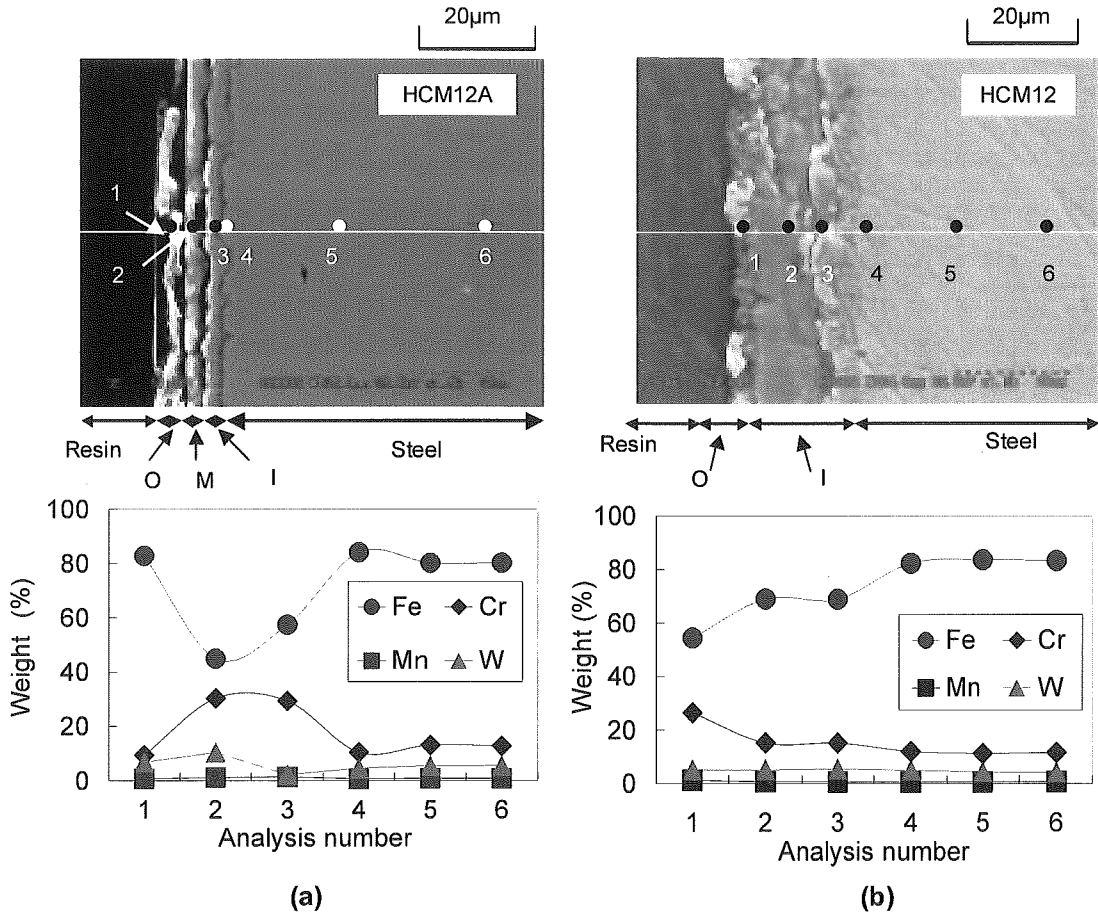


Fig.4-6 Oxide layers and metal elements in (a) HCM12A and (b) HCM12 after 1,000-hr exposure to the Pb-Bi flow

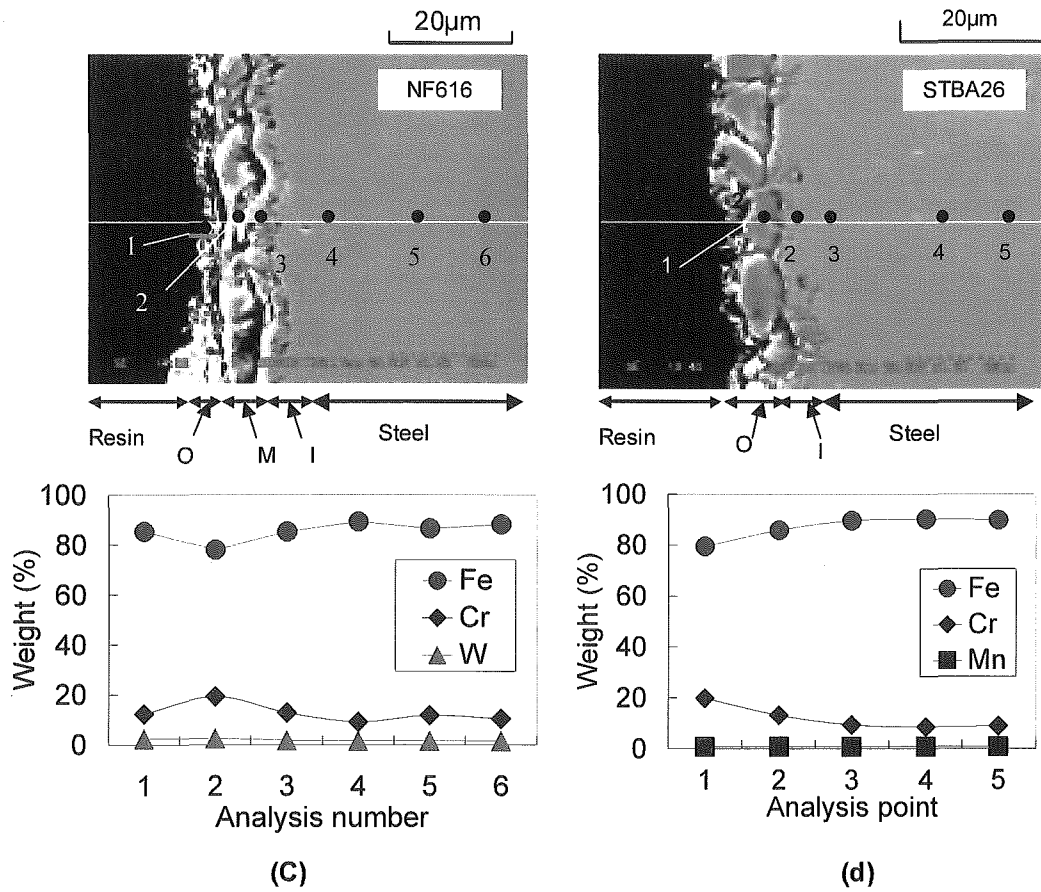


Fig.4-6 Oxide layers and metal elements in (c) NF616 and (d) STBA26 after 1,000 hr-exposure to the Pb-Bi flow

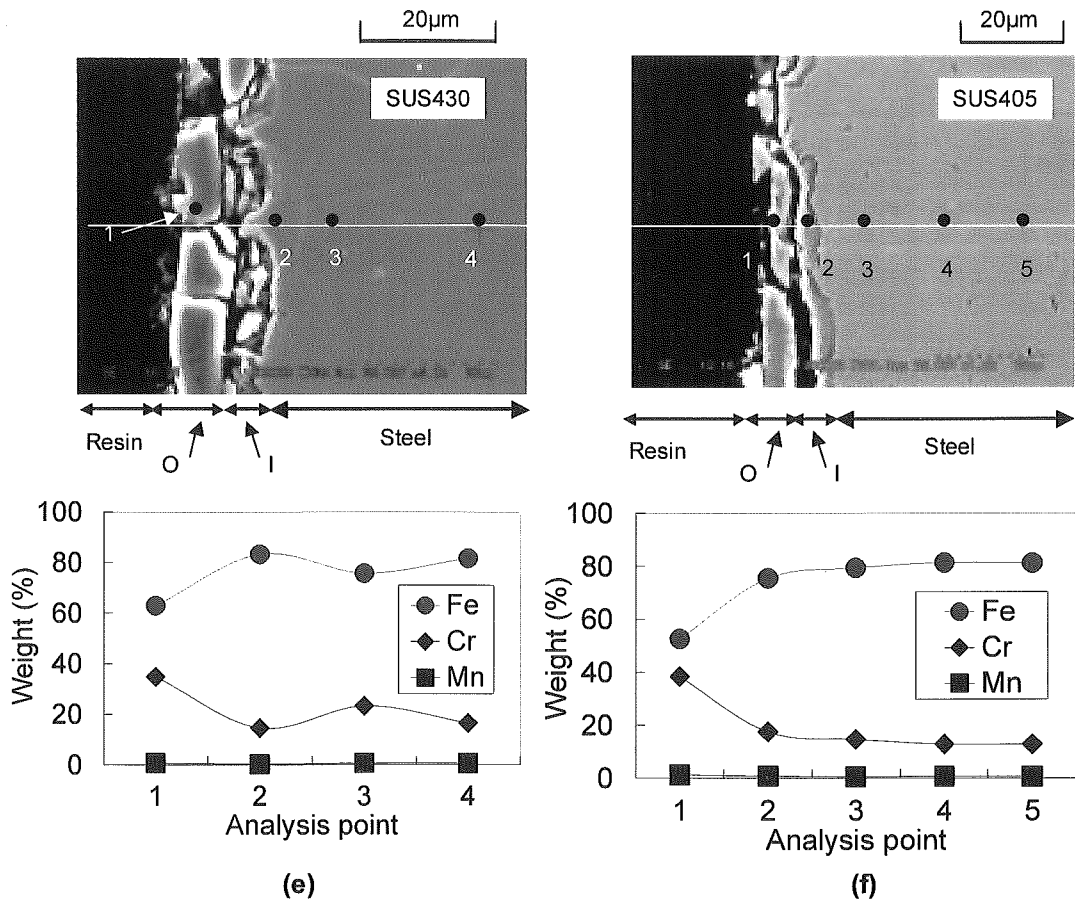


Fig.4-6 Oxide layers and metal elements in (e) SUS430 and (f) SUS405 after 1,000 hr-exposure to the Pb-Bi flow

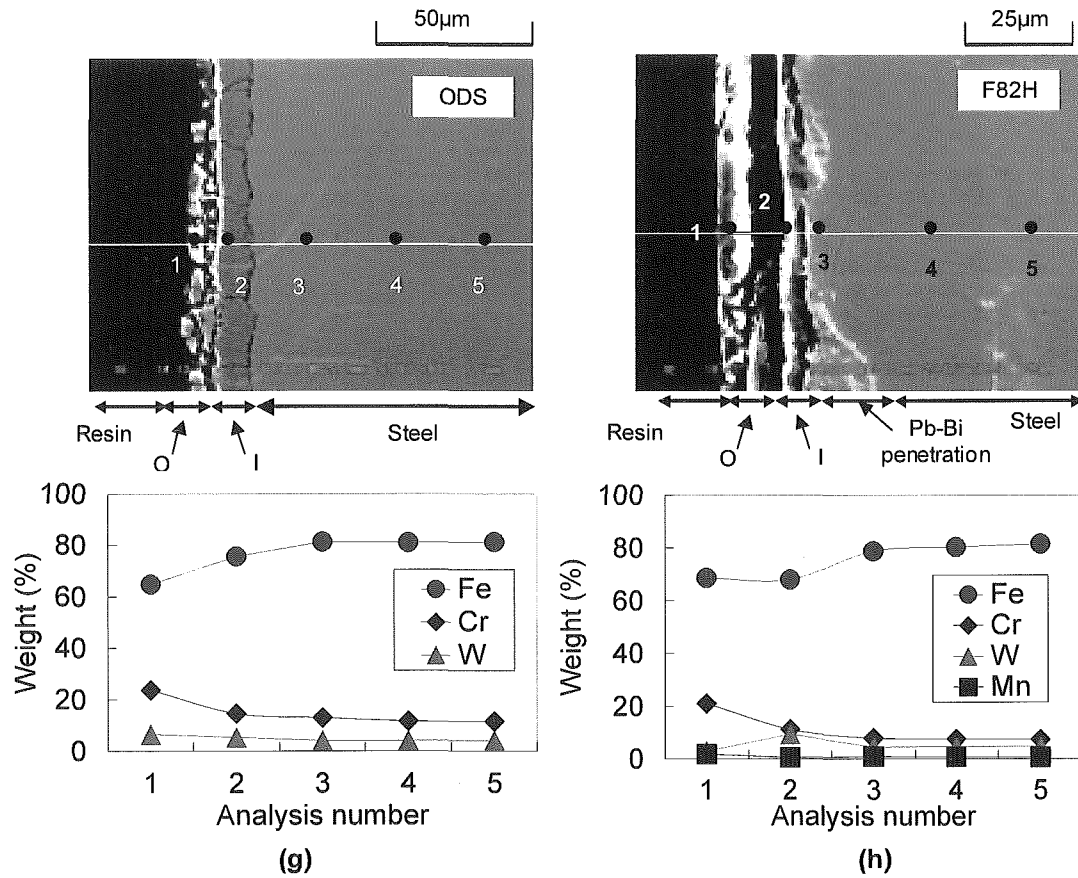


Fig.4-6 Oxide layers and metal elements in (g) ODS and (h) F82H after 1,000 hr-exposure to the Pb-Bi flow

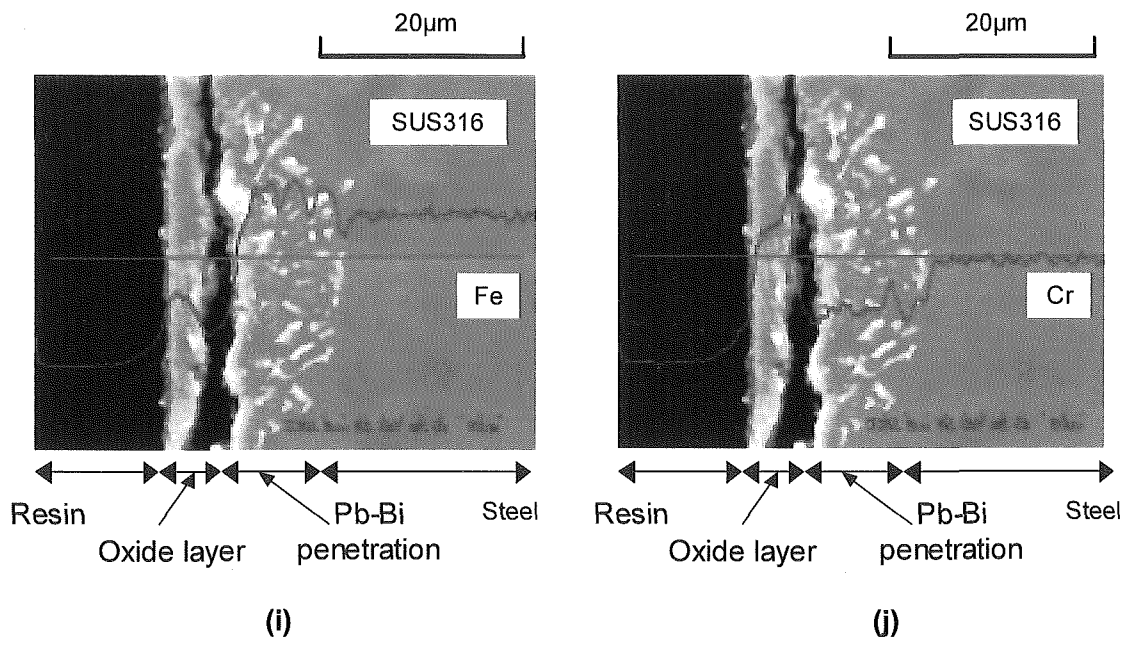


Fig. 4-6 Oxide layers and content of (i) Cr and (j) Fe in SUS316 after 1,000 hr-exposure to the Pb-Bi flow

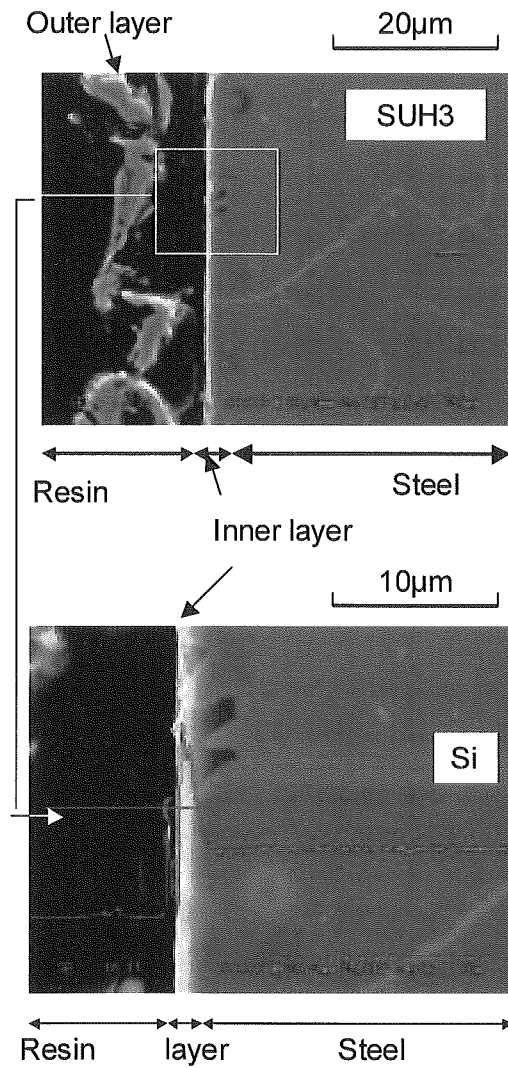


Fig. 4-6 (k) Oxide layers in cross section of SUH3 after 1,000 hr-exposure to the Pb-Bi flow

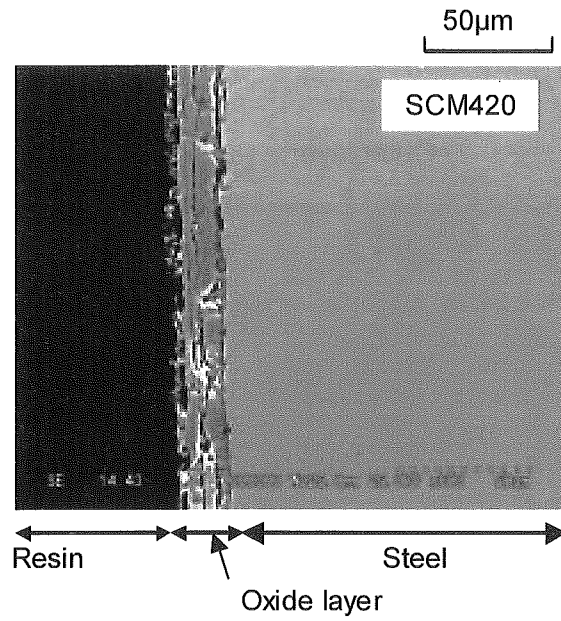


Fig. 4-6 (I) Oxide layers in cross section of SCM420 after 1,000 hr-exposure to the Pb-Bi flow

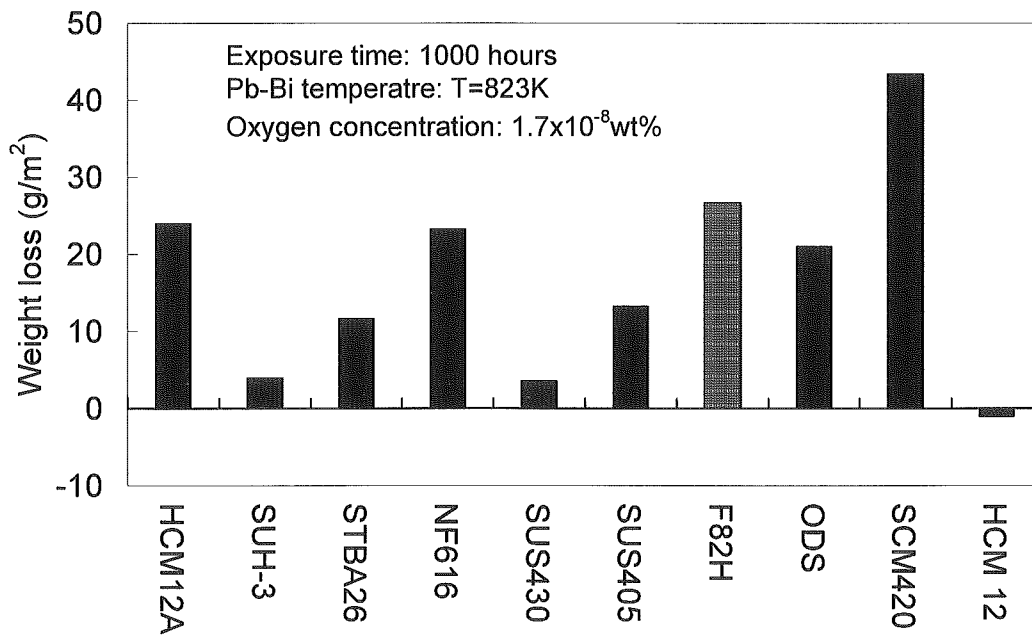


Fig. 4-7 Weight loss of steels in flowing Pb-Bi

Various type of corrosion on steel

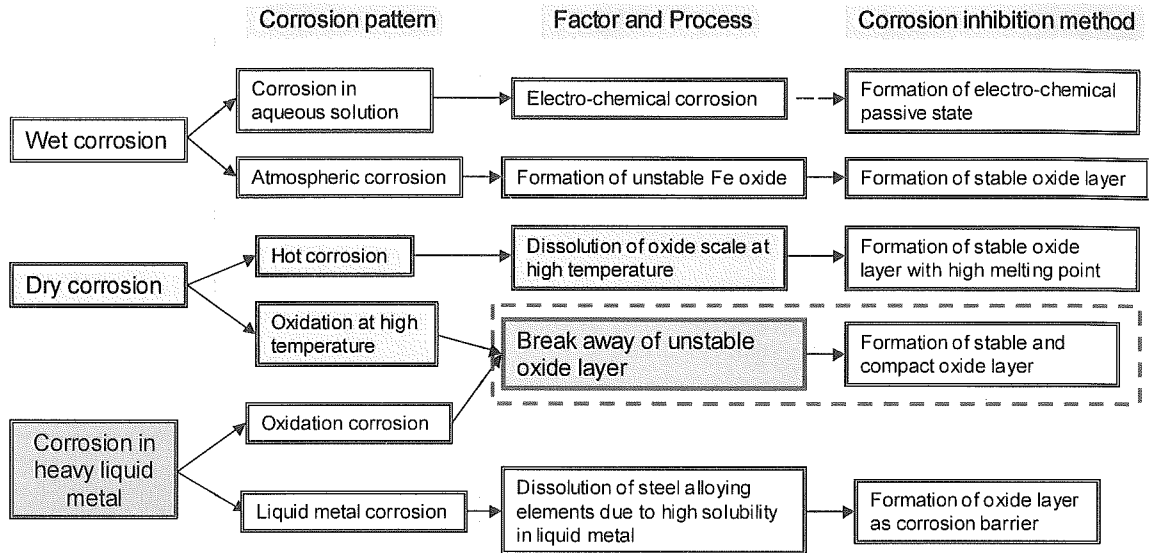


Fig. 4-8 Place of oxidation corrosion of steels in liquid Pb-Bi in general corrosion pattern

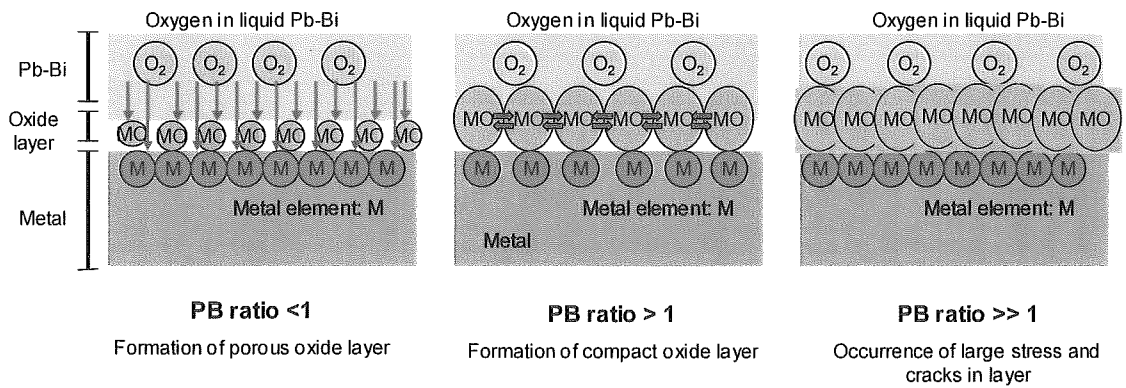


Fig. 4-9 PB ratio on oxidation process in liquid Pb-Bi

Chapter 5

Effect of Surface Treatment of Steels on Corrosion Resistance in Flowing Lead-Bismuth

5.1 Effect of Pre-oxidation of Steels on Corrosion Resistance of Steels in Flowing Lead-Bismuth

5.1.1 Introduction

As described in the *Chapter 4*, the self-healed oxide layers formed on steels are expected to suppress liquid metal corrosion (LMC) as barrier of a metal elements dissolution into the flowing lead-Bismuth (Pb-Bi). Although the detachment of the unstable oxide layer causes oxide corrosion [1], the corrosion rate may be lower than that of the LMC (*Chapter 3.5 and Chapter 4.5*).

However, the LMC can occur in an initial stage since the steels are bare without being protected by the oxide layers. Pre-oxidation of the steels may be effective for suppression of the LMC in the first stage due to the barriers of pre-formed oxide layers.

The corrosion characteristics of pre-oxidized steels in a short-term static immersion was investigated by L. Soler et al. [2]. In 500-hour immersion in static Pb-Bi at the temperature of 400°C-600°C, pre-oxidized specimens showed a better corrosion resistance than the as-received ones. The weight loss of the pre-oxidized specimens were much lower than the as-received specimen at 600°C. This implied that the pre-oxidation layers were effective as barriers for the dissolution corrosion in the first stage. However, as the authors concerned in the paper, the corrosion resistance of the pre-oxidized steels should be tested in the dynamic conditions, since the layer destruction or detachment may be caused by heavy density Pb-Bi flow in the dynamic conditions.

The purpose of the present study is to investigate the effect of the pre-oxidation of the steels on the corrosion resistance in the Pb-Bi flow in the initial stage, and to find effective condition of pre-oxidation. Several existing steels are oxidized in moist air, and were exposed to the flowing Pb-Bi in a short-term corrosion test.

5.1.2 Experimental Apparatus and Procedure

Experimental apparatus

Figure 5-1 shows the Pb-Bi forced convection type corrosion test apparatus used in the present study. The apparatus consists of the electromagnetic pump, the electromagnetic flow meter, the electrical heater, the steel corrosion section, the air cooler, the expansion tank, and the dump tank. The circulation loop has an inventory of 0.022 m³, and consists of a high temperature region (550 °C) from the heater to the cooler and a low temperature region (400°C). The high temperature region is made of STBA26 to avoid the corrosion, and the low temperature region is made of SS316. Thermocouples inserted into the flow at several points of the loop were used for monitor and control of the temperature in the Pb-Bi.

The Pb-Bi flow loop was heated up for removal of volatile contaminants on the inner surfaces of the loop, evacuated and filled with high purity argon of 99.999%. Pb-Bi was melted in the dump tank at 250°C for several days, and the circulation loop was heated up to the temperature of 250°C. Then, Pb-Bi was supplied to the circulation loop at a flow rate of approximately 0.5 L/min by the pressurizing the dump tank at 0.18 MPa with the loop pressure of 0.02 MPa. The Pb-Bi was circulated by the electro-magnetic pump at the rated operating flow rate, and heated up to 400°C uniformly in the loop. Then, the high temperature region was heated up to 550°C by the electrical heater, keeping the low temperature at 400°C by the air cooler.

Experimental conditions

The corrosion test was performed at the conditions shown in Table 2. The oxygen concentration of 1.7×10^{-8} wt% in the Pb-Bi was determined from the measured EMF of a solid electrolyte oxygen sensor (see *Chapter 2-1*) and the Nernst equation, where the correlation of oxygen solubility in the Pb-Bi provided by Gromov et.al [2] was employed. The oxygen concentration was higher than the concentration required for the formation of Fe₃O₄, which suggests that the pre-formed oxide layer can be maintained and grown in the melt.

After the immersion, the specimens were taken out of the holder. In order to keep the oxide layer on the surfaces, glycerin was used for the removal of adhered Pb-Bi instead of nitric acid (see *Chapter 3-2*).

The surfaces of the specimens were observed before and after the exposure to see if erosion occurred or not. For the estimate of corrosion rates, the weights of the specimens were measured before and after the exposure using the electro-reading balance. The specimens were cut at the span-wise center and the cross sections were polished, and then observed by scanning electron microscope and energy-dispersive spectrometer (SEM/EDX).

5.1.3 Test Materials

The specimens with the width of 15 mm, the length of 10 mm and the thickness of 2.3 mm were mounted in the specimen holder, and the holder was inserted into the test section. Steels tested in this study are presented in **Table 5-1**. The corrosion test was performed for normal specimens and specimens with roughened surfaces simultaneously, and the results are reported in *Chapter 5.2*.

The surfaces of the as-received specimens were polished using a mechanical polisher with 9 μ m, 3 μ m and 1 μ m polycrystalline diamonds. The specimens had the smooth surface of arithmetical mean surface roughness, $Ra=1\mu$ m, and the oxide layers were removed from the surfaces before the pre-oxidation treatment.

5.1.4 Pre-Oxidation Process

The specimens were pre-oxidized in moist air at 500°C and the partial pressure of the water vapor of 92.5 Torr for 12, 24 or 72 hours. The surface colors of the pre-oxidized specimens were light black or brown as shown in **Fig. 5-2 (a)**.

To investigate the effect of the layer conditions on corrosion resistances, the pre-formed layer was observed and analyzed before the exposure of the specimens to the Pb-Bi flow. The pre-oxidized specimens were cut at the span-wise center, and the cross section near the surfaces was observed by a scanning electron microscope (SEM) and analyzed by an energy-dispersive X-ray spectrometer (EDX).

The result is summarized in **Fig. 5-3**. Thin oxide layers were formed on high Cr steels, SS405, SS430 and SS316, and Cr was enriched in the layers. Very thin and compact oxide layer was formed on Si rich steel, SUH3, and the Cr was enriched in the layer. Multi-layers were formed on SCM420 and STBA26, where the outer layers were peeled from the substrate. The detached layer or broken layer may not be effective for the protection of steel from corrosion as a barrier.

Figure 5-4 shows the weight gains due to the formation of the oxide layers, that were measured using an electric leading balance with a measuring limit of 0.1 mg. The weight changes of SS316 and SUH3 were negligibly small. The weight gains of high Cr steels, SS430 and SS405 were low, which suggested the oxidation resistance in moist air as indicated by the results of SEM observation in **Fig. 5-3**.

The specimens for corrosion test were pre-oxidized with oxidation time that was determined based on the data, and then mounted in the holder in the following order from upstream to downstream: (1) SS430, (Pre-oxidized for 24 hours and 72 hours) (2) SUH3 (12 hours and 24 hours), (3) STBA26 (12 hours and 24 hours), (4) SS316 (24 hours and 72 hours), (5) SCM420 (12 hours and 24 hours) and (6) SS405 (24 hours and 72 hours) as shown in **Fig. 2**. The bared specimens were mounted upstream with the other normal specimens in the holder.

5.1.5 Corrosion Characteristics of Pre-Oxidized Steels

Surface state of specimens after exposure

After the exposure to the Pb-Bi flow, the surface color of the specimens changed from the light black or brown to black color as shown in **Fig. 5-2 (b)**. This indicated that the corrosion products or oxide layers remained or formed on the surfaces. The erosion did not occur on the surfaces of the specimens.

Corrosion Rate of Pre-Oxidized Steels in flowing lead bismuth

The mechanism of the weight loss of the pre-oxidized specimens may be different from that of the bared specimens. The weight of the bared specimens may be lost in the material dissolution, whereas the weight of the pre-oxidized specimens may be lost in

detachment of the pre-formed oxide layers and dissolution of metal elements. The weight loss of SS316 could not be determined since the Pb-Bi penetrated in the matrix. And, the weight loss of SS405 that was pre-oxidized for 24 hours could not be estimated since adherent Pb-Bi was observed on the surface of SS405. after the Pb-Bi removal process.

Figure 5-5 shows the result for the weight changes of the specimens in Pb-Bi flow.

The weight loss of SS430 was the lowest among those of the steels. It is found that there was no appreciable influence of the pre-oxidation on the weight loss.

The weight loss of the pre-oxidized specimen of SUH3 was lower than that of the bared one. The weight loss of the specimens pre-oxidized for 24 hours was lower than that of the one pre-oxidized for 12 hours.

The specimen of STBA26 pre-oxidized for 12 hours shows higher weight loss than the naked one, possibly because the oxide layer that suppressed initial corrosion was not pre-formed well as shown in **Fig. 5-3**, or the layer detached from the surface and metal dissolution occurred. The weight loss of the specimen pre-oxidized for 24 hours was lower than that in the bared one. This suggests that corrosion was suppressed by a compact inner layer stuck to the surface shown in **Fig. 5-3**.

The SCM420 pre-oxidized specimen shows better compatibility with Pb-Bi than the bared one. The specimen pre-oxidized for 12 hours shows lower weight loss than the specimens treated for 24 hours. That is possibly because the former one had the inner layer stuck to the substrate, and the layer inhibited the dissolution type corrosion initially.

In SS405, bared one increased the weight during the exposure. The specimen pre-oxidized for 72 hours loss the weight possibly due to the detachment of the unstable oxide layer shown in **Fig. 5-3**.

Analysis of Corrosion Using SEM/EDX

Figure 5-6 shows the surface cross section of SS430 after exposure, and the change of Cr content. On the surfaces of bared specimen and specimen pre-oxidized for 72 hours, no oxide layer or oxide scale was observed. Only the specimen pre-oxidized for 24 hours had the Fe rich layer which contributed to the slight weight gain (**Fig. 5-4**).

Figure 5-7 depicts the surface cross section of SUH3 specimens and contents of Si and Cr. In the bared one, thin oxide layer was formed, and Si and Cr were enriched in the layer. Double oxide layers were formed on the specimen pre-oxidized for 12 hours. While the outer layer was Fe rich oxide layer, the inner one was Cr and Si rich layer. The property of the inner layer was similar to the layer formed on the bared one. The specimen pre-oxidized for 24 hours formed single layer which was also similar to the layer on the bared one. The compact Si and Cr rich layer may suppress corrosion. The decrease in the weight loss with pre-oxidation is shown in **Fig. 5-5**, which implied that the pre-oxidized layer worked as a barrier for protection from corrosion.

A Cr rich layer was observed on pre-oxidized specimen of STBA26, while the bared one did not have the layer as shown in **Fig. 5-8**. However, the layer was broken to some pieces with cracks. After the exposure, there were no compact layers which were observed before the exposure. The layer was probably lost by the Pb-Bi flow.

In the SCM420, the layer did not exist on the surfaces. However, the results of weight measurement indicated that the layer was effective initially for inhibiting the Fe dissolution into the Pb-Bi.

In the SS405 specimen pre-oxidized for 72 hours (**Fig. 5-9**), the pre-formed layer could not be detected, which might be the cause of the large weight loss. Although the pre-formed layer was lost, the new layer was formed. In the specimens pre-oxidized for 24 hours, the layer was not detected.

In the bared sample of SS316, a Cr-rich layer was detected on the smooth surfaces (**Fig. 5-10**). Pb-Bi penetration into the steel matrix was observed for the pre-oxidized SS316 specimens. The Pb-Bi penetrated into the grain boundaries. In the specimen of SS316 pre-oxidized for 24 hours, the grains were surrounded by the Pb-Bi, and the loss of the grain led to a rough surface and erosion. In the sample pre-oxidized for 72 hours, a Cr-rich layer was detected on the penetrated surfaces. The pre-oxidation of SS316 seemed to promote the corrosion. This is possibly because their surface lost the element of Cr by the detachment of the pre-formed Cr-rich layer, and the Cr-less surface caused the Pb-Bi penetration without the formation of the layer.

5.1.6. Summary

The short-term corrosion test with the pre-oxidized steel was performed to investigate the effect of pre-oxidation on corrosion resistance in the initial stage. The results are summed up as follows:

- (1) High Cr steels had higher resistance for oxidation in moist air than low Cr steels. Although they can be pre-oxidized with long-term treatment, the formed oxide layers were unstable, and the pre-oxidation for high Cr steels was not effective for the corrosion resistance in the flowing Pb-Bi.
- (2) In the low Cr steel, SCM420, and 9Cr steel, STBA26, the pre-oxidation was effective for the corrosion resistance if the pre-formed oxide layer was compact and not detached from the substrate.
- (3) The Si-rich steel, SUH3, shows the oxidation resistance in the moist air. The results of the weight change measurements after the exposure show that the pre-oxidized SUH3 had good compatibility with Pb-Bi flow due to the barrier of a stable pre-oxidized layer in the initial stage of the corrosion.

5.2. Effect of Surface Roughness of Steels on Corrosion Resistance of Steels in Flowing Lead Bismuth

5.2.1 Introduction

In the previous studies, steel corrosion tests were carried out with the parameter of the oxygen content in the flowing Pb-Bi, where the oxygen content was controlled by the injection of gas mixture (*Chapter 3.*) or the use of mass exchanger with lead oxide (PbO) particles (*Chapter 2-2.*). The results showed that the steels were protected by a formed oxide layer from a liquid metal corrosion (LMC) in the Pb-Bi with adequate oxygen content (*Chapter 4.*). However, it was also found that the steels caused a so-called oxidation corrosion via the oxide layer destruction and detachment in the Pb-Bi.

It is well known that the characteristics of the oxidation corrosion is well influenced by the circumstances [1]. In case of the flowing Pb-Bi, high density of the flowing Pb-Bi causes large frictional and shear stress that act on the surface of the formed oxide layer. Then, the surface roughness of the steels may influence on the above-mentioned hydrodynamic circumstance in the flowing Pb-Bi. This is because the large frictional and shear stress made by the high density Pb-Bi flow can be concentrated in the layer at irregular parts of the substrate.

High Cr steels formed multiple oxide layers in liquid Pb-Bi, and each layer has different chemical components as reported in *Chapter 4* and ref. [4-6]. In this case, an interfacial stress causes between an inner oxide layer and an outer one due to unequal growth rates of them [1]. These stress work as the factor for the destruction of the oxide layer. These stress can be concentrated in the layer at irregular part of the substrate.

Thus, the surface roughness of steels may promote the destruction of the protective oxide in the flowing Pb-Bi. However, the effect of the surface roughness of the steels on the oxidation corrosion in the flowing Pb-Bi was not made clear so far.

In the present study, a series of corrosion tests was performed to determine the effect of surface roughness of the steels on oxidation corrosion in the flowing Pb-Bi. The specimens of 12Cr and 9Cr steels, which had the surface of smooth, rough and their middle roughness, were exposed into the Pb-Bi flow at the temperature of 550°C, the temperature difference of 150°C, the flow velocity of 1m/s and the oxygen concentration of 1×10^{-8} and 10^{-6} wt% for 500, 1000 and 2000 hours.

5.2.2 Experimental Apparatus and Procedure

Pb-Bi forced convection loop

Figure 5-11 shows the schematic of Pb-Bi forced convection-type corrosion test loop used in the present study. The loop has an inventory of 0.022 m³, and consists of a hot loop region (550 °C) from the heater to the cooler and a cold loop region (400°C). The hot loop region is made of STBA26 to avoid corrosion, and the cold loop region is made of SS-316.

Liquid Pb-Bi was circulated by the electromagnetic pump, and the flow rates were measured by the electromagnetic flow meters (see Chapter 8-2). The Pb-Bi temperature at several points of the loop were monitored using sheathed thermocouples inserted into the flow.

The specimens were mounted in a cylindrical holder made of Mo, and the holder was inserted in the test section of the loop.

Experimental conditions

Corrosion tests were carried out at the conditions summarized in Table 5-3 without interruption during the test period.

The oxygen content in the Pb-Bi was determined by the measurement of the Electro motive force (EMF) using solid electrolyte oxygen sensor at 550 °C and theoretical calculation using the Nernst equation (See Chapter 2-1). The oxygen concentrations in the 500-hour test and 1000-hour test were controlled as 1.7x10⁻⁸wt%, and plotted with the symbol of inverse triangle in Fig. 5-12. In the 2000-hour test, the oxygen content was controlled at 1x10⁻⁶wt% by the use of the mass exchanger with PbO particles. This condition was plotted with the symbol of black triangle.

Examination of corrosion

After the test, the specimens were demounted from the loop. In order to keep the oxide layers formed on the specimen surfaces, glycerin was used for the removal of adhered Pb-Bi without removal of the formed oxide layers [6].

To investigate the change of surface roughness on the steels exposed in the flowing Pb-Bi, the surface roughness were analyzed using color laser 3D profile microscope before and after the exposure. The distributions of local surface height of test steels, $y=f(x)$, were measure over the length of L as shown in Fig. 5-13, and the arithmetical mean surface roughness, Ra , was calculated by

$$Ra = \frac{1}{L} \int_0^L |f(x)| dx \quad (5-1)$$

Hydrodynamic environment around the specimens in the holder was summarized in **Table 5-4**. The Reynolds number in the specimen holder was nearly 22,600, and the flow is turbulent. The corrosion products or oxide scales formed on the steel surface may be influenced by turbulent flow, if the height of them is higher than the thickness of buffer-layer of 0.9 μ m as shown in **Fig. 5-14**.

After the measurement of surface roughness, the specimens were cut at span wise center, and their cross sections were observed and analyzed by the scanning electron microscope (SEM) and energy-dispersive X-ray spectrometer (EDX).

5.2.3 Test materials

Chemical components of test materials are presented in **Table 5-5**. 9Cr steels, STBA26 and STBA28, are for high temperature boilers. 12 Cr steels, HCM12A and HCM12, were developed for the structural material of supercritical pressure boilers. These steels were machined into the specimen of 15 x 10 x 2.3 mm dimension for the corrosion tests.

5.2.4 Surface Polishing Process

In the 500-hour test, the specimen surfaces of STBA26 and HCM12A were made smooth, middle and rough using a mechanical polisher with polycrystalline diamonds and ethanol (polishing lubricant). The as-received specimen was used for the rough surface one without polishing. The middle one was made by polishing with 9 μ m cloth. The smooth one was made by polishing with 9 μ m, 3 μ m and 1 μ m polycrystalline diamonds.

In the 1000-hour test, STBA28 and HCM12 with smooth, middle and rough surfaces were exposed into the Pb-Bi flow. The rough surfaces were obtained by polishing with 9 μ m polishing cloth. Middle one was made by polishing with 9 μ m and 6 μ m. Smooth surfaces was prepared in the same way as that of the 500-hour test.

In the 2000-hour test, the steels of HCM12A, STBA26 with smooth and rough surfaces were exposed to Pb-Bi flow. The surface polishing of them were done as the same as the smooth and rough surface of the specimens in 1000-hour test.

These specimens were arranged in the specimen holder as shown in **Fig. 5-15** and exposed to the Pb-Bi flow.

5.2.5 Effect of Surface Roughness of Steels on Corrosion Resistance of Steels

Surface Observation

Microscope images of the specimen surfaces in 12Cr steel (HCM12A, HCM12) and

9Cr steel (STBA26 and STBA28) after 500-, 1,000- and 2000-hour exposure were summarized in **Fig. 5-16**. The specimen showed no sign of severe LMC and erosion.

In 500-hour exposure to the Pb-Bi flow, the colors of the specimen surfaces changed from initial metallic luster before the exposure to black or brown after the exposure. This indicated that the corrosion products or oxide layers formed on the surfaces. In the surface-roughened specimens, traces made by the surface polishing before the exposure were clearly detected.

In 1,000-hour exposure to the Pb-Bi flow, the colors of all the specimens changed to mat black. Although the traces made by polishing before the exposure are detected in the surface-roughened specimens, that could not be clearly observed. This is because the oxide layers or scales were formed and grown on the surfaces in the Pb-Bi flow.

The specimen surfaces observed after 2000-hour exposure to the Pb-Bi flow was similar to that after 1000 hour exposure. The traces made by polishing before the exposure are rarely detected in the surface-roughened specimens.

Change of Surface Roughness

Surface roughness of the specimens after the exposure in the Pb-Bi flow for 500, 1000 and 2000 hours is plotted in **Fig. 5-17**. A dotted line indicates the initial surface roughness before the exposure.

In 500-hour test, smoothness remained on the initial smooth surfaces. The initially roughened surfaces were little smoothed during the exposure. This is possibly because some parts of convex surfaces were shaved by the Pb-Bi flow.

In 1000-hour test, the surfaces of HCM12 and STBA28 became rougher than that before the exposure. This indicated that the specimens formed the oxide layers on the surfaces in the Pb-Bi flow, and this increased the surface roughness.

In 2000-hour test, the surface smoothed and roughened specimens of STBA26 and HCM12A had rough surface after the exposure.

From these results, the rough surfaces of steels were initially smoothed by the erosion shortly after the exposure into the Pb-Bi. The surface roughness of the steels increased with exposure time, due to the formation of the oxide layers.

Oxide Layer formed on smooth and rough surface

9Cr steels (STBA26 and STBA28)

In the 500-hour exposure, STBA26 steels did not form the oxide layer on the surfaces no matter what the surface roughness. This contributed the no change of the surface roughness in surface smoothed specimens (**Fig. 5-17**). **Figure 5-18** shows the surface cross section of the surface-smoothed specimen after 500-hour exposure. No layer was detected on the surface.

In the 1000-hour test, the effect of surface roughness on the oxide layer property could be found. The double oxide layers with different characteristics were formed on the specimen surfaces (**Figs. 5-19 (a) through (c)**). The double oxide layer: A and B formed on the surface-roughened STBA28 specimen was detached from the substrate (**Fig. 5-19 (a)**). While, the surface-smoothed specimen also formed double oxide

layer (**Fig. 5-19 (c)**). However, these layers did not detached from the substrate, although some cracks existed in the layer. The inner layer B did not develop enough. The specimen, which had middle surface roughness before the exposure, formed the layer which had intermediate characteristics between above two cases (**Fig. 5-19 (b)**).

In the 2000-hour exposure in the Pb-Bi, the cracked oxide layers were formed on the surfaces (**Figs. 5-20 (a) and (b)**). On the surface-roughened specimen, the cracked layer was detached from the substrate (**Fig. 5-20 (a)**). Under the layer, initial development of the inner layer was detected. As for the surface-smoothened specimen, double oxide layer was detected on the surface. Although the cracks were existed with regular intervals in the layer, the layer well stuck to the steel surface (**Fig. 5-20 (b)**). The thickness of the layer formed on the smooth surface was thinner than that on rough one.

The oxide layer was not detected on the steel surface in 500 hour-exposure to the Pb-Bi, while a developed oxide layer appeared after 1,000 hour-exposure. This means that the oxide layer on 9Cr steel grew mainly during the exposure time from 500 to 1,000 hours.

In the surface roughened specimens, the layer detachment occurred to relief the stress, which concentrated between the layer and the substrate. The layer detachment could be caused more easily than the cracking since the shear strength between the layer and the steel is weaker than the shear strength of the layer itself [1]. Once the layer detached from the substrate, the layer did not growing and cause the cracking after the layer detached from the substrate, since the metal element was not provided from the steel surface. In the detached layer, the cracks did not exist as shown in Fig.9 (a) and Fig.10 (a).

12Cr steels (HCM12 and HCM12A)

In the 500-hour exposure, a single oxide layer formed only on the HCM12A specimen which had smooth surface (**Fig. 5-21**). The layer was very thin and well stuck to the substrate. In the layer, Cr was enriched.

In the 1000 hour exposure, thick oxide layer of 10-20 μ m was formed on the specimen surfaces (**Figs. 5-22 (a) through (c)**). On the surface-roughened specimen, unstable double layer was remained (**Fig. 5-22 (a)**). Transverse cracks existed in the outer layer, particularly on the convex part of the substrate. On the surface smoothened specimen, double oxide layer were formed in stable (**Fig. 5-22 (c)**). An outer layer A was compact with few cracks. Beneath the outer layer A, the inner layer began to develop. The specimen with middle surface roughness formed the layer which had intermediate state between above two specimens (**Fig. 5-22 (b)**).

In the 2000-hour test, well-grown oxide layers were detected. Figs. 5-23 (a) and (b) shows the single and multiple oxide layers were formed on the surface of HCM12A specimens. In the surface roughened case, the single layer was detected on the surface (**Fig. 5-23 (a)**). In the layer, transverse cracks were existed. Partly on the surface, bared place without the layer protection can be found. As for surface-smoothened case, double oxide layer was detected (**Fig. 5-23 (b)**). Although the transverse cracks existed in the outer layer, inner layer was compact with few cracks. In the inner layer, Cr was enriched.

In the layers formed on the surface-roughened specimen, the transverse cracks were

existed. The cracks existence concentrated particularly at convex part of the steel surface. This indicated the crack behavior in the layer as shown in **Fig. 5-24**. Due to the shear stress of the flowing Pb-Bi and the growing of oxide layer, the stress might concentrate in the layer at the convex part of the substrate. Then, the cracks were caused in the layer at the convex part. In case of multiple layer as shown in **Fig. 5-23 (b)**, the cracks were caused in the outer layer possibly due to the interfacial stress.

5.2.6 Summary

The results are summed up as follows:

- (1) The rough surfaces of steels were initially smoothed by the erosion in the flowing lead-bismuth.
- (2) The steels increased surface roughness due to the formation of the oxide layers in the flowing Pb-Bi.
- (3) In 9Cr steels, cracked layers were formed on the surface. Then, the rough surface promoted the layer detachment due to the concentration of the around the irregular part of the substrate.
- (4) In 12 Cr steels, the transverse cracks were existed in the layers on the surface-roughened specimen. The crack existence concentrated particularly at convex part of the surface. Few cracks appeared in the oxide layer formed on the smooth surface.

5.3 Conclusions

The pre-oxidized steel specimens showed better corrosion resistance than the normal specimens in the initial stage of the corrosion in the flowing Pb-Bi. By the pre-oxidation of the steels, initial dissolution may be inhibited by the existence of the pre-formed oxide layers on the steels.

The effect of surface roughness influences on the corrosion resistance for the long term in the flowing Pb-Bi. This is because the surface roughened steels form unstable oxide layers, which have cracks at the convex part of the substrate. For the formation of the stable oxide layer, the steel surface should be polished as smooth as RA (arithmetical mean surface roughness) of 1.5 μm .

References

- [1] High temperature oxidation of metal, Japan Society of Corrosion Engineering, (1882). (in Japanese)
- [2] L. Soler Crespo, F. J. Martin Munoz, D. Gomez Briceno, "Short term static corrosion tests in lead-bismuth", *J. Nucl. Mater.*, **296**, 273-281 (2001).
- [3] B. F. Gromov, Y. I. Orlov, P. N. Martynov, V. Agulevsky, "The problem of technology of the heavy liquid metal coolant (Lead-bismuth, Lead)", *Proc. of HLMC1999*, 87-100, Obninsk, Russia (1999).
- [4] C. Fazio, G. Benamati, C. Martini, G. Palombarini, "Compatibility tests on steels in molten lead and lead-bismuth", *J. Nucl. Mater.*, **296** (2001).
- [5] G. Benamati, C. Fazio, H. Pinakova, A. Rusanov, "Temperature effect on the corrosion mechanism of austenitic and martensitic steels in lead-bismuth", *J. Nucl. Mater.*, **301**, 23 (2002).
- [6] F. Barbier, A. Rusanov, "Corrosion behavior of steels in flowing lead-bismuth", *J. Nucl. Mater.*, **296**, 231 (2001).

Table 5-1 Chemical components of test steels

	Cr	Mo	W	Si	Others
SCM420	1.2	0.2	-	0.2	-
STBA26	9	1	-	0.4	-
SS405	12	-	-	1	0.1Al
SS430	18	-	-	0.75	-
SS316	18	2-3	-	0.1	-
SUH3	11	-	1	2	0.4C

Table 5-2 Corrosion test conditions

Duration time (hour)	500
Test temperature (°C)	550
Temperature in cold region (°C)	400
Flow velocity (m/s)	1
Oxygen concentration (wt%)	1.7×10^{-8}

Table 5-3 Corrosion test conditions

Duration time (hour)	500	1,000	2000
Test temperature (°C)	550	550	550
Temperature in cold region (°C)	400	400	400
Flow velocity (m/s)	1	1	1
Oxygen concentration (wt%)	1.7×10^{-8}	1.7×10^{-8}	1×10^{-6}
Test steels	STBA26 HCM12A	STBA28 HCM12	STBA26 HCM12A

Table 5-4 Hydrodynamic conditions of test piece

Flow velocity (m/s)	1
Reynolds number	22,600
Thickness of buffer-layer (μm)	0.9
Wall frictional stress (Pa)	32

Table 5-5 Chemical components of test materials

	Cr	Mo	W	Si	Others
STBA28	8.8	1	-	0.4	
STBA26	9	1	-	0.2	
HCM12A	12	0.3	1.9	0.3	0.9Cu
HCM12	12.1	1.1	1.0	0.3	

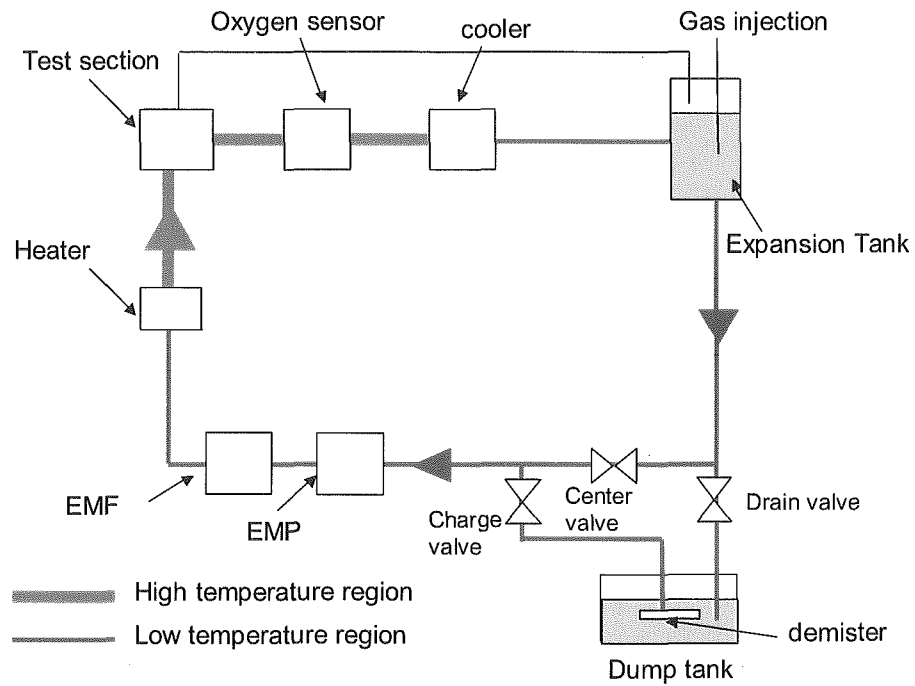


Fig. 5-1 Pb-Bi forced convection loop

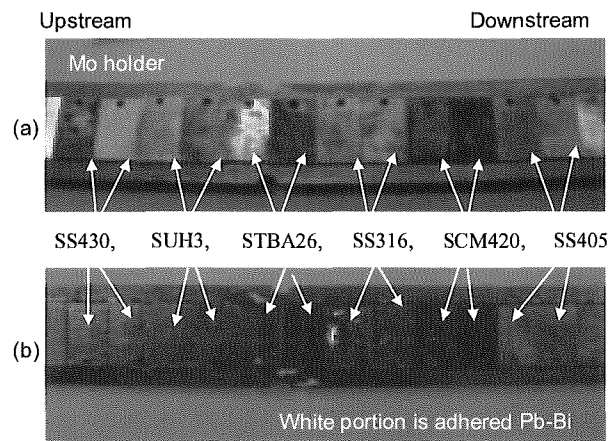


Fig. 5-2 Surface conditions of pre-oxidized specimens (a) before exposure to Pb-Bi flow, (b) after exposure to Pb-Bi flow

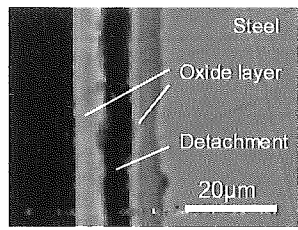
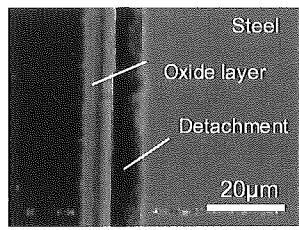
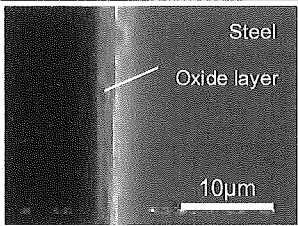
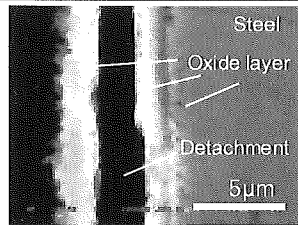
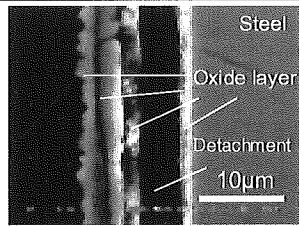
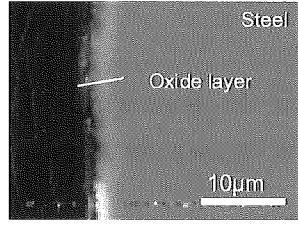
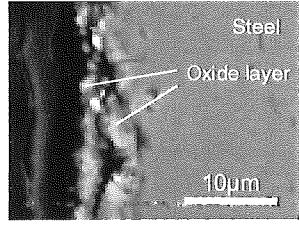
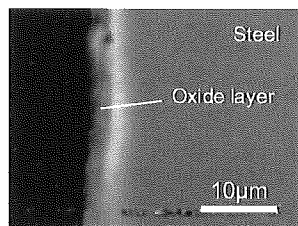
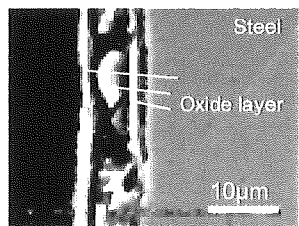
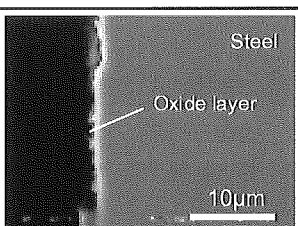
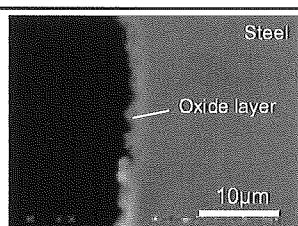
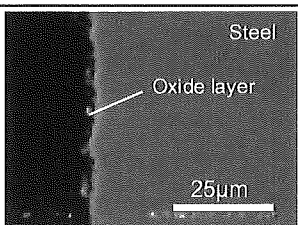
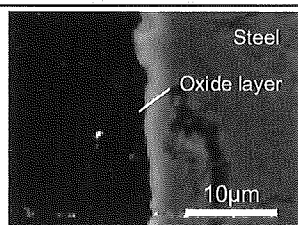
	12 hr- pre-oxidation	24 hr- pre-oxidation	72 hr- pre-oxidation
SCM 420	-		
STBA 26			
SS405	-		
SS430	-		
SS316			-
SUH3			-

Fig. 5-3 Pre-formed oxide layers on test steels

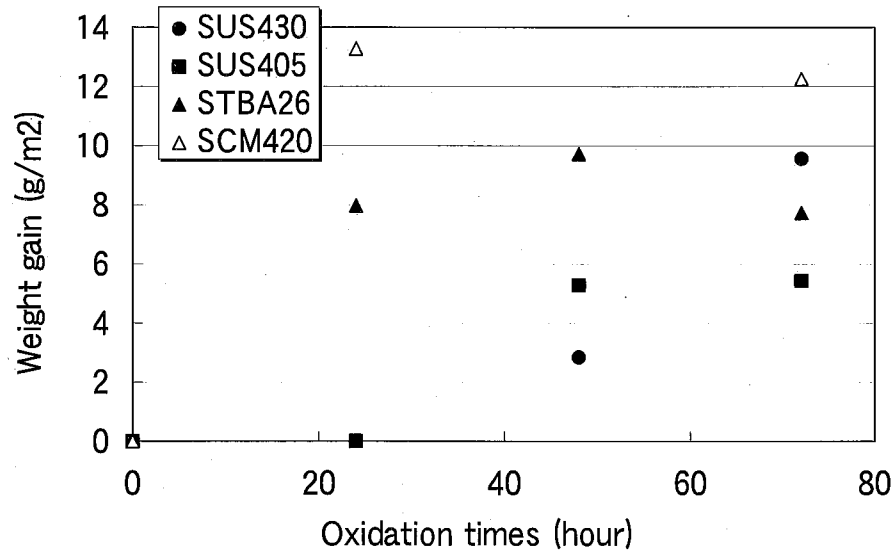


Fig. 5-4 Weight gains of test steels in pre-oxidation process

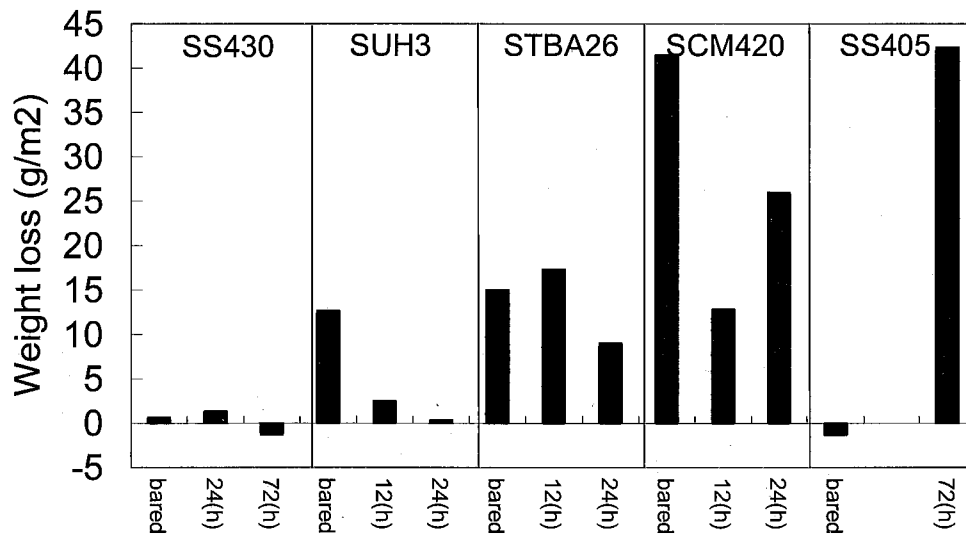


Fig. 5-5 Weight loss of pre-oxidized specimens and bared specimens

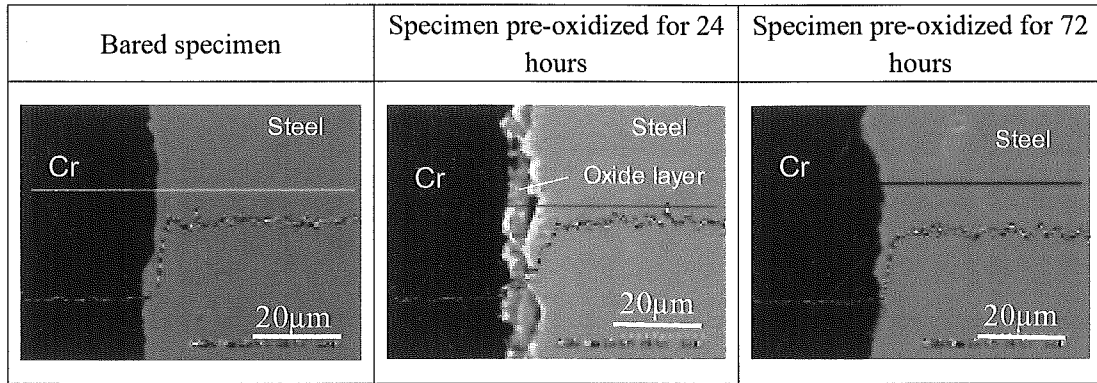


Fig. 5-6 Surface cross section of SS430 with Cr content after exposure into Pb-Bi for 500 hours

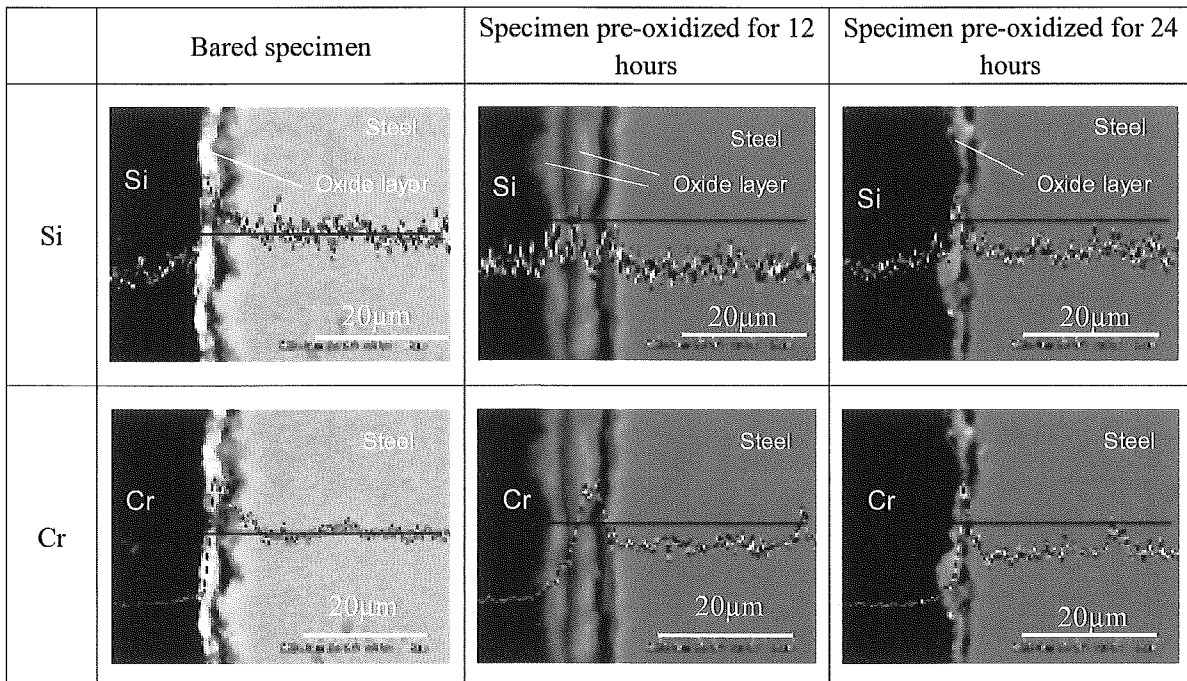


Fig. 5-7 Surface cross section of SUH3 with Cr and Si contents after exposure into Pb-Bi for 500 hours

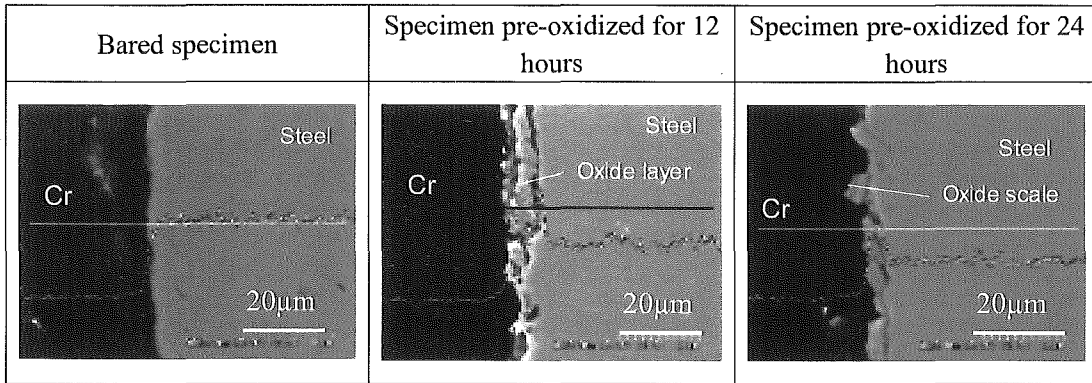


Fig. 5-8 Surface cross section of STBA26 with Cr content after exposure into Pb-Bi for 500 hours.

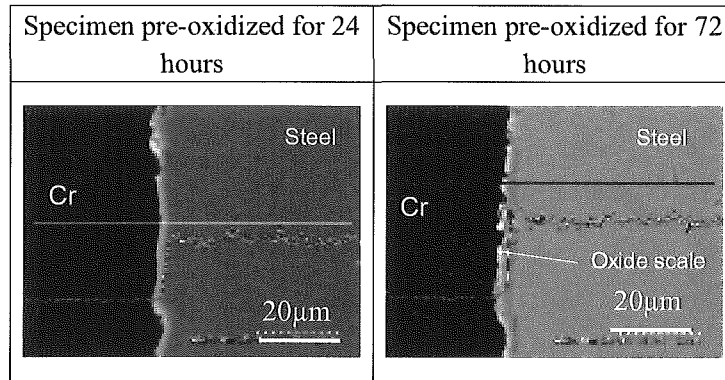


Fig. 5-9 Surface cross section of pre-oxidized SS405 with Cr content after exposure into Pb-Bi for 500 hours.

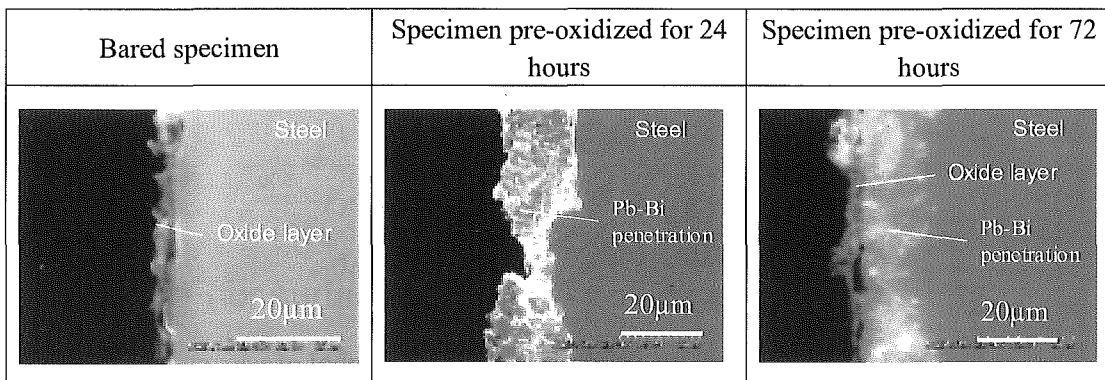


Fig. 5-10 Surface cross section of SS316 after exposure into Pb-Bi for 500 hours

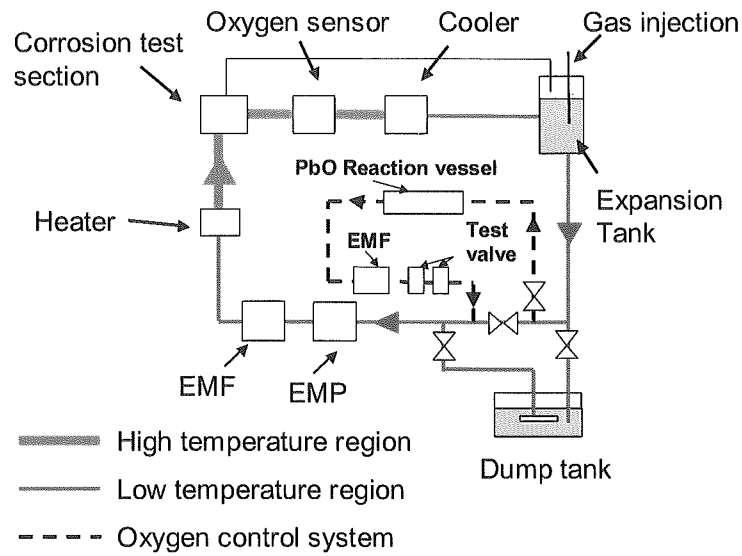


Fig. 5-11 Pb-Bi forced convection test loop

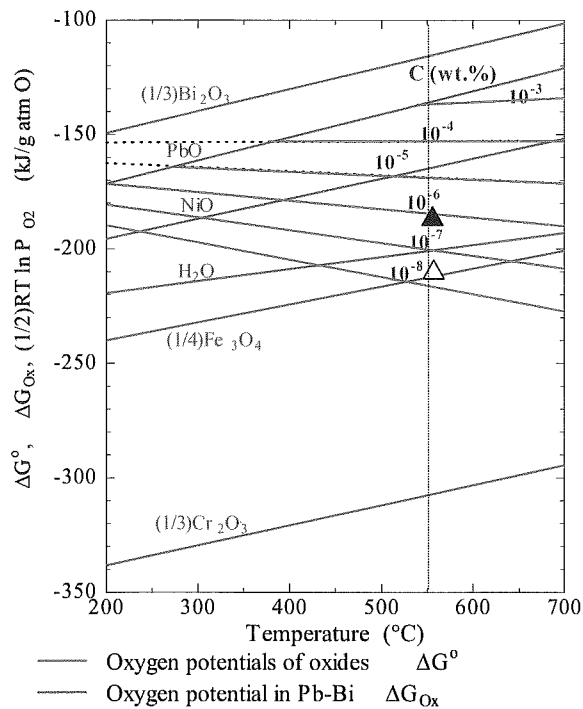


Fig.5-12 Diagram of oxygen potential; symbol of vacant triangle indicates oxygen concentration in the 500-hour and 1000-hour corrosion tests. symbol of black triangle indicate oxygen concentration in 2000-hour corrosion test.

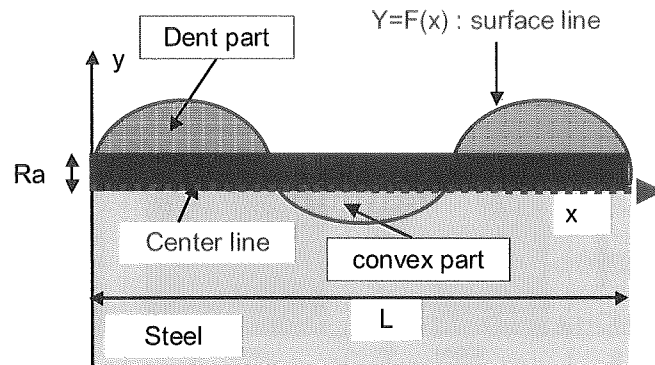


Fig. 5-13 Analysis way of arithmetical mean surface roughness (R_a)

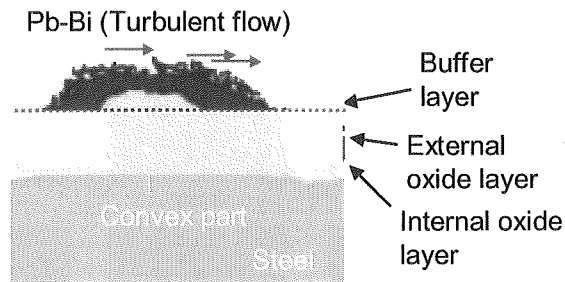


Fig. 5-14 Schematic of oxidized surface and laminar sub layer

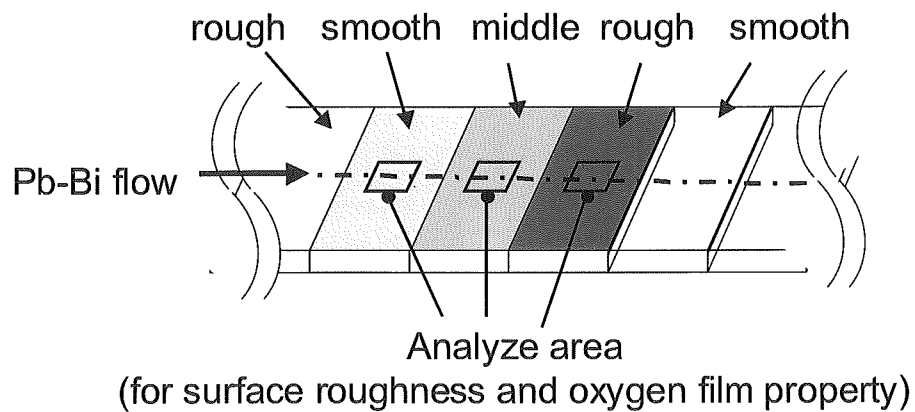


Fig. 5-15 Test pieces with smooth, middle and rough surfaces

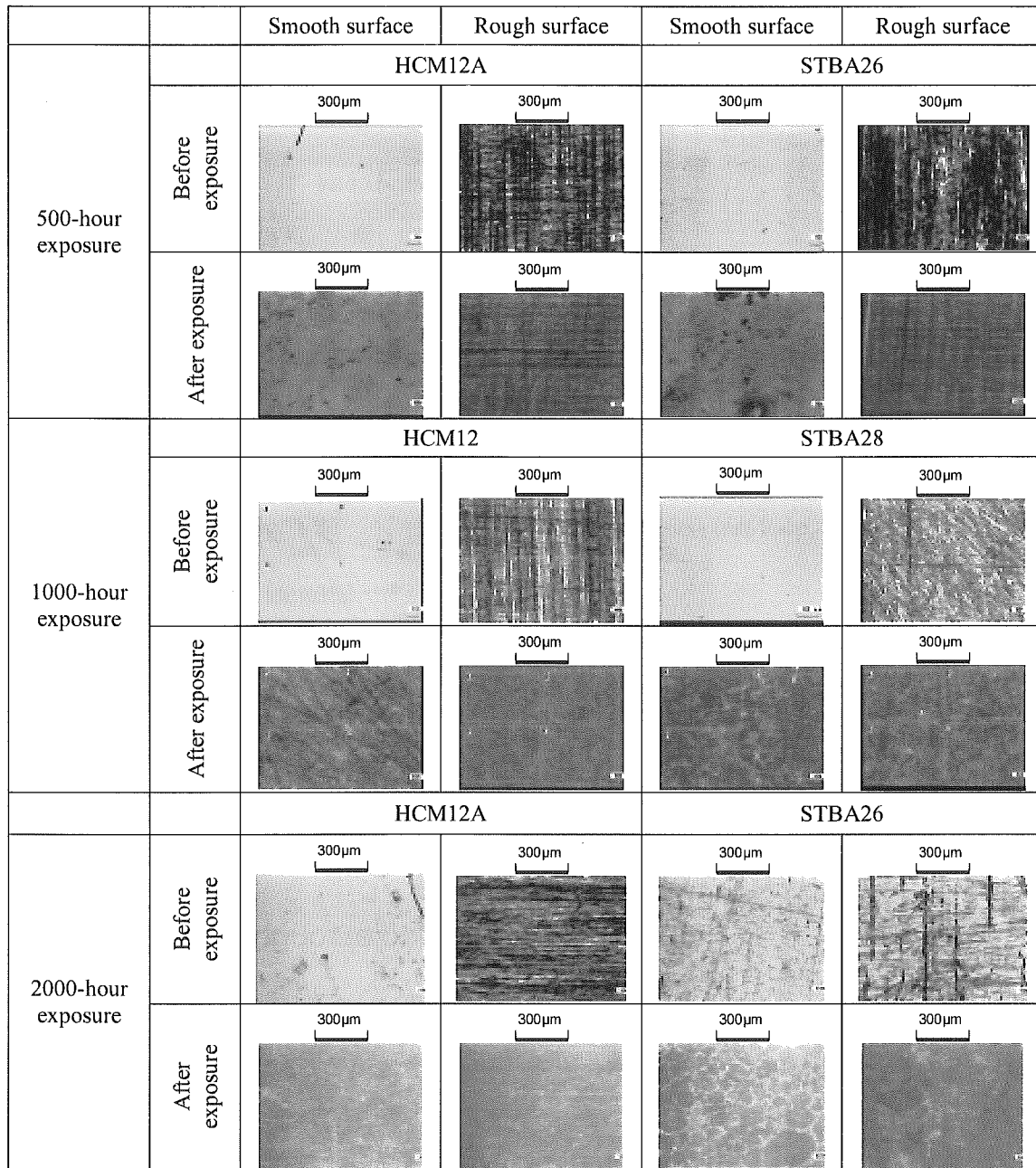


Fig. 5-16 Microscope images for specimen surfaces in HCM12A, HCM12, STBA28 and STBA26 after exposure to Pb-Bi flow for 500, 1000 and 2000 hours.

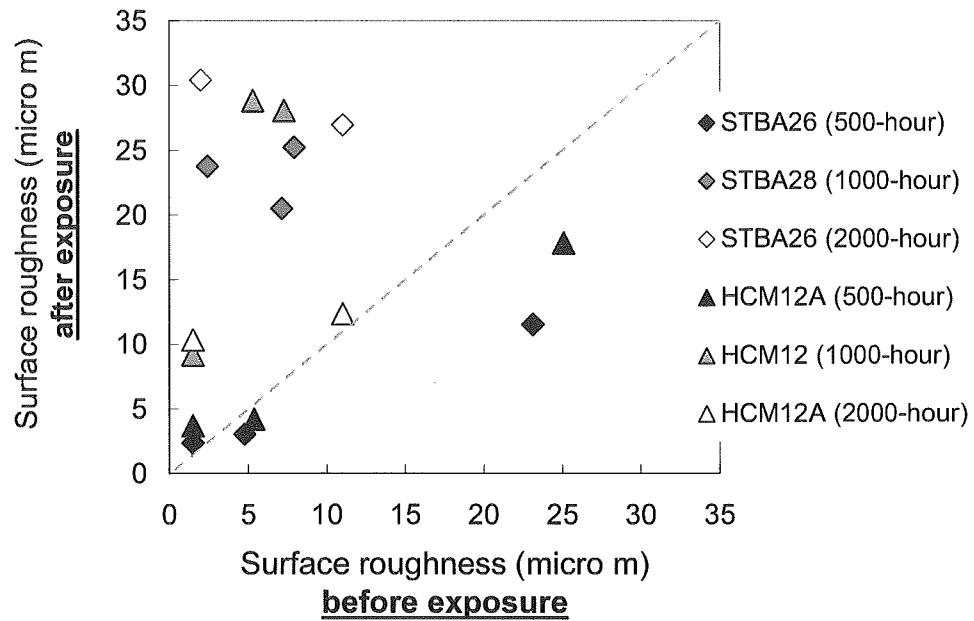


Fig. 5-17 Change of surface roughness during 500-, 1000- and 2000-hour exposure to Pb-Bi flow

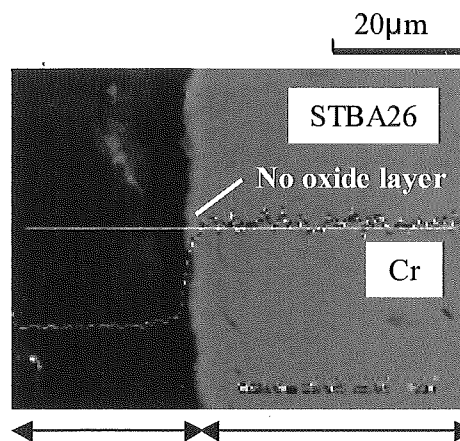


Fig. 5-18 Surface cross section and Cr content profile of surface-smoothened STBA26 after exposure into Pb-Bi for 500 hours

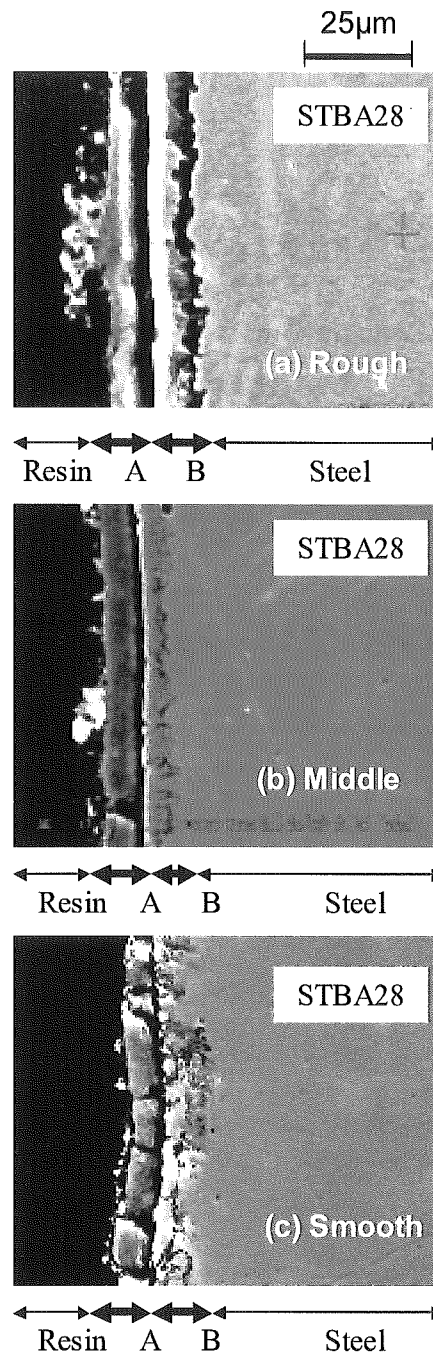


Fig. 5-19 Oxide layers on the roughened, smoothed and medium rough surfaces of STBA28 exposed to Pb-Bi flow for 1,000 hours

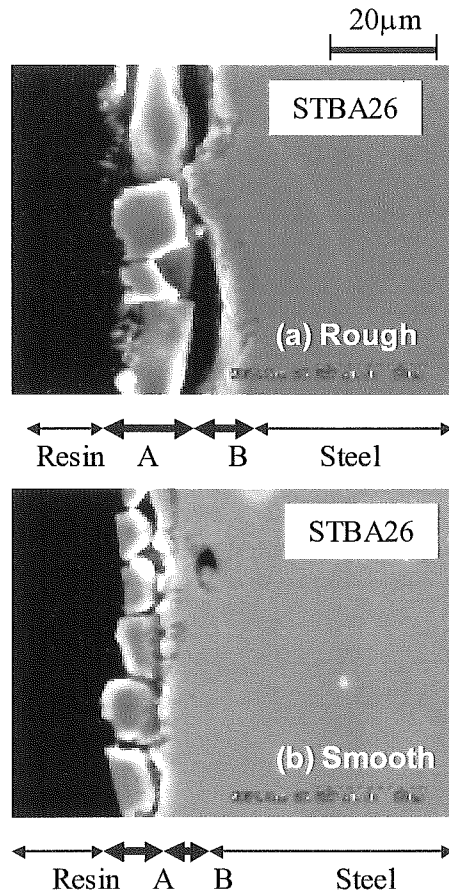


Fig. 5-20 Oxide layers on the roughened and smoothed surfaces of STBA26 exposed to Pb-Bi flow for 2,000 hours

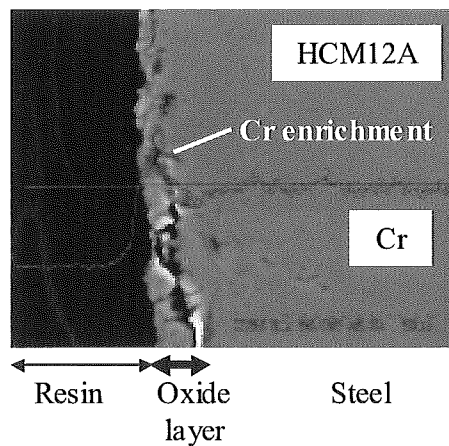


Fig. 5-21 Surface cross section and Cr content profile of surface-smoothened HCM12A after exposure into Pb-Bi for 500 hours

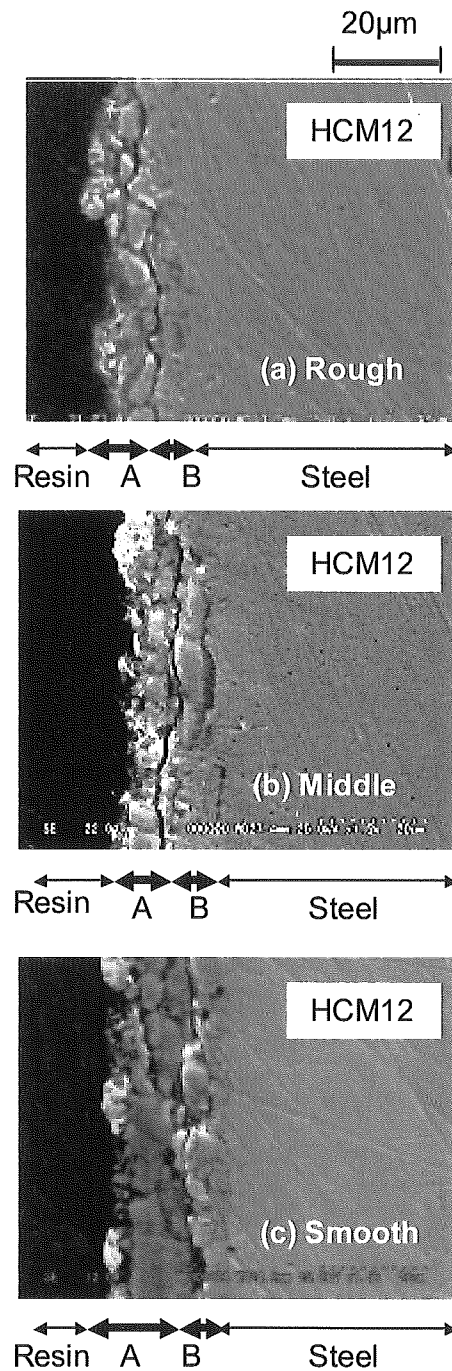


Fig. 5-22 Oxide layers formed on the roughened, smoothed and middle rough surfaces of HCM12 exposed to Pb-Bi flow for 1,000 hours

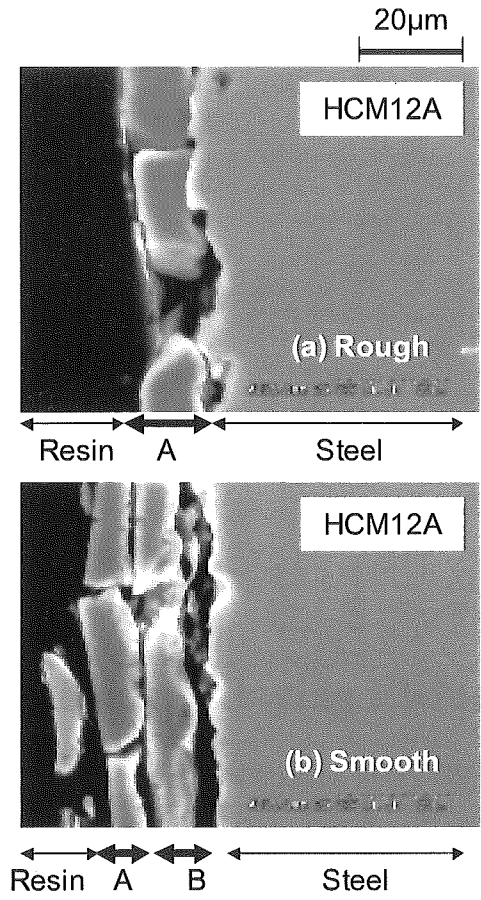


Fig. 5-23 Oxide layers on the roughened and smoothed surfaces of STBA26 exposed to Pb-Bi flow for 2,000 hours

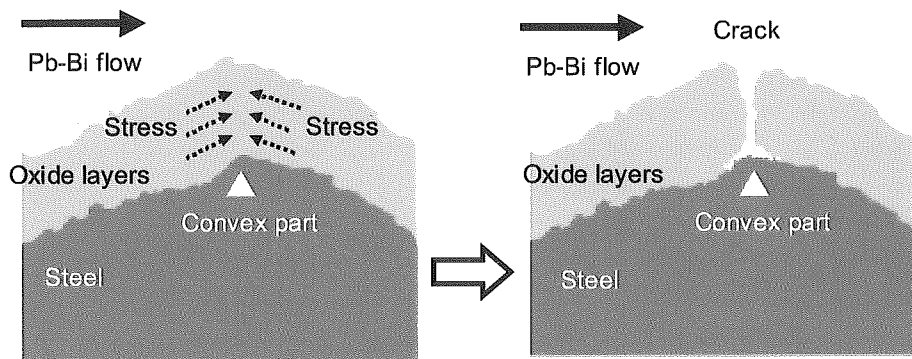


Fig. 5-24 Crack behavior of oxide layer at convex part

Chapter 6

Effect of Alloying Elements in Steels on Corrosion Resistance in Flowing Lead-Bismuth

6.1 Effect of Cr Contents in Steels on Corrosion Resistance in Flowing Lead-Bismuth

6.1.1 Introduction

The development of corrosion resistant-cladding and structural materials is one of the critical issues for the development of lead-bismuth (Pb-Bi) cooled fast reactors (LFR). Then, a series of corrosion study has been carried out using the Pb-Bi forced convection loop by the authors.

In the first stage of the corrosion study, corrosion test was performed at low oxygen concentration in the liquid Pb-Bi. The mechanism of erosion in the liquid Pb-Bi was investigated by means of metallurgical analysis of the eroded part of the specimens. From the results, it was found that the erosion of steels in the flowing Pb-Bi was promoted by the corrosion. The steel surfaces were weakened by the so-called liquid metal corrosion (LMC), and eroded by the flow of the heavy density fluid, Pb-Bi. The oxide layers, which could be corrosion barrier, were not formed on the steel surfaces because of the low oxygen concentration in the Pb-Bi (*Chapter 3*).

In the second stage, oxygen control system (OCS) was developed in order to keep an adequate oxygen concentration in the Pb-Bi, where the oxide layers were formed and self-healed on the steel surfaces. The oxygen in the flowing Pb-Bi was measured by an oxygen sensor (*Chapter 2-1*). The sensor cell was immersed in the flow at high temperature. A sensor with small cell (solid electrolyte conductor: MgO-ZrO₂, Y₂O₃-ZrO₂) was used to avoid the destruction of the sensor cell by thermal shock. The oxygen concentration was controlled by the temperature control of lead oxide particles (PbO) (*Chapter 2-2*). Using these OCS techniques, corrosion tests have been carried out in the liquid Pb-Bi with high oxygen concentration to avoid the occurrence of severe LMC.

As explained in *Chapter 4*, the formation and detachment of the unstable layer caused the oxidation corrosion. It was also indicated that the characteristics of the oxide layers formed on the steel surfaces depended on the chemical components of the steels. The effect of chromium (Cr) on the corrosion behaviors should be made clear, since Cr is one of the major alloying elements in the steels.

In this chapter, the effect of Cr contents in the steels on corrosion resistance in the flowing Pb-Bi was investigated. The corrosion tests with the steels, which contained various contents of Cr, were carried out in the flowing Pb-Bi up to 2000 hours.

6.1.2 Experimental Apparatus and Procedure

Experimental Apparatus

The present corrosion study was performed in the Pb-Bi forced convection corrosion test loop. The schematic of the loop was shown in **Fig. 6-1**. The liquid Pb-Bi was circulated by an electro magnetic pump, and the flow rate was measured by an electro magnetic flow meter. And, an ultrasonic flow meter was installed in the low temperature region [1].

The oxygen sensor was installed in the high temperature region of the loop. The sensor cell was made of solid electrolyte conductor of Y_2O_3 -MgO with the reference fluid of oxygen-saturated Bi (*Chapter 2-1*). A by-pass line that has the electromagnetic flow meter, the bellow valves and the PbO reaction vessel was installed in the low temperature region. The temperature of solid PbO particles in the PbO reaction vessel was controlled to have a desired oxygen concentration in the Pb-Bi loop (*Chapter 2-2*).

Experimental Condition

The corrosion test conditions are shown in **Table 6-1**. These corrosion tests were performed without any interruption in the operations.

The corrosion test for 500, 1,000 and 2,000 hours at high oxygen concentration was performed. The results of the former study in *Chapter 4* were reflected in this works. The specimens of the steels, which were corrosion resistant in the former test, were mounted in the upstream in the specimen folder in the latter tests. This was done to remove the influence of the dissolved alloying elements in the upstream region on the corrosion of specimens in the downstream region in the corrosion test section.

Corrosion Analysis

After exposed in the Pb-Bi flow, the specimen holder was demounted from the test loop. Then, the holder with the specimens was immersed in a glycerin pool at the temperature of 180°C to remove adherent Pb-Bi from the outside and inside of the holder. Then, the holder was opened and the specimens were taken out of the holder, and rinsed again in glycerin pool at the temperature of 180°C to melt and remove adherent Pb-Bi from the specimen surfaces without removal of oxide layers [2]. Finally, glycerin on the specimen surface was removed in warm water at the temperature of 70°C.

The surfaces of the specimens were observed before and after the exposure to inspect the occurrence of erosion. In order to determine the corrosion rate, weight losses of the specimens were measured using an electro reading balance with an accuracy of 0.1mg. The specimens were cut at the span wise center and the cross sections were polished, and then observed by a scanning electron microscope (SEM) and analyzed by an energy-dispersive X-ray spectrometer (EDX).

6.1.3 Test Materials

The chemical components of test materials were presented in **Table 6-2**. In the present study, steels with the high content of Cr were chosen as the test materials.

The surfaces of the steel specimens were mechanically polished smoothly to eliminate the effect of surface roughness and oxide layer preliminary formed on the corrosion in the flowing Pb-Bi (see *Chapters 5-1 and 5-2*). The surface roughness of the specimens was measured by 3D laser microscope. The arithmetical mean surface roughness (Ra) was 1.5 μ m.

6.1.4 Effect of Cr Content in Steels on Corrosion Characteristics

Surface Observation

Figure 6-2 shows the results of the surface observation in the 500, 1,000 and 2,000 hour-tests.

After the 500 hour-exposure, the specimens showed smooth surface without erosion. The surface color changed to brown or black from initial metallic luster, which suggested the formation of corrosion products or oxide layers on the surfaces.

Even after the 1000 and 2,000 hour-exposure, the specimens showed smooth surfaces. It can be seen that no appreciable traces of erosion existed on all of the steel surfaces. The surface state was similar to each other in all the specimens. The colors of the steel surfaces changed from the initial metallic luster before the exposure into black after the exposure as the same as that in the 500 hour-exposure.

Effect of Cr Contents in Steels on Corrosion Rate

The results of the weight loss measurement in the 500-, 1000- and 2,000- hour test are presented in **Figs. 6-3 – 6-5**.

In the 500- hour test (**Fig. 6-3**), the dependence of the weight loss of specimens on Cr content in the steels showed that the weight loss was lower as the Cr content was higher in the order of SCM420, STBA26, HCM12 and SUS430. There were slight weight increases in SS405, which could be also attributed to the formation of thick oxide layers or penetration and/or adherence of Pb-Bi. Although SS316 increased the weight, this was due to the penetration of the Pb-Bi into the steel matrix and/or adherence of the Pb-Bi promoted by the corrosion reaction.

In the 1000- hour test (**Fig. 6-4**), the weight loss of the steels was lower as the Cr content was higher as the same as the results of 500- hour test. The weight loss of SUH3 was remarkably lower than those of the other steels possibly due to the influence of the formation of stable and thin Si-rich oxide layer (See *Chapter 6-2*). The weight loss of SUS316 was not able to evaluate in the present experiment. That was because Pb-Bi

penetrated into the porous layer formed by the dissolution of Ni and Cr into Pb-Bi was not completely removed in the glycerin. The weight loss of F82H might be larger than the measured one since Pb-Bi that rarely penetrated into steel matrix could not be completely removed by glycerol.

In the 2000- hour test, it seemed not to have certain relation between Cr contents in steels and the weight loss. However, the weight change of SS430 (18-Cr) was smallest in the steels. The weight loss of the STBA26 was nearly the same as that of NF616 which had similar components. The weight loss of 12-Cr steel, HCM12A and SS405 was larger than that of the 9-Cr steels. The weight loss of 316FR was the largest among the tested materials. This is because the Ni in 316FR had high solubility in the liquid Pb-Bi at 550C [3], and dissolved into the liquid Pb-Bi.

The weight loss of SS430 in the liquid Pb-Bi was compared with those of STBA26 (9-Cr) and HCM12A (12-Cr) in the tests for 500-2000 hours as shown in **Fig. 6-6**. The less weight loss of SS430 was less than those of STBA26 and HCM12A. The weight loss of STBA26 and HCM12A specimens in 2000 hour-test was much higher than the curve expected from the results of 500 and 1000 hour-tests. This is because the oxygen concentration in the Pb-Bi in 2000 hour-test was higher than those in the 500 and 1000 hour-tests.

Effect of Cr Content in Steels on Oxide layer characteristics

The results of the SEM-EDX analysis for SS430, HCM12A and STBA26 were described here as the typical of 18-, 12- and 9-Cr steels (**Fig. 6-7**).

9-Cr Steels

9-Cr steel, STBA26, did not form the oxide layer on the surface in the 500- hour test. It is reasonable to think as the weight loss detected in the 500- hour test (**Fig. 6-3**) was not caused by the oxidation corrosion. Then, the weight loss of STBA26 specimens possibly showed the dissolved ratio of the alloying elements from the steel surface into the flowing Pb-Bi. However, the liquid metal penetration was not detected on the specimen surface. This indicated that the liquid metal penetration may be caused after the dissolved corrosion.

The STBA26 formed single oxide layers in the Pb-Bi flow in 1000- and 2000- hour immersion. The layers had cracks and were broken into some pieces. However, the LMC did not occur beneath the layers. This indicated that these layers were effective as the LMC barrier even the layers had some cracks.

The weight loss in 2,000 hour-test was higher than the curve extrapolated from the results of 500 and 1,000 hour-tests (**Fig. 6-6**). This is because the specimens caused so-called oxidation corrosion at high oxygen concentration due to the detachment of the cracked layers.

12-Cr Steels

The 12-Cr steel, HCM12A, formed oxide layer in the 500- hour immersion, although the 9Cr steel did not form the oxide layer. This indicates that the 12Cr steel forms the oxide layer earlier than the 9Cr steels in the flowing Pb-Bi. This characteristics beneficially influenced that the weight loss of the HCM12A was lower than that of 9Cr

steel in 500 hour test.

In the 1000- and 2000- hour tests, HCM12A formed that the multiple oxide layers. The outer one was broken to some fragments, and the layer was not seemed to be protective barrier for the corrosion. The inner layer was Cr-rich compact layer and stuck well to the substrate surface. Beneath the layers, the sign of the LMC occurrence was not detected. Thus, the Cr-rich inner layer might inhibit the LMC.

The weight loss of specimens during 2,000 hour-exposure was larger than the curve extrapolated from the results of 500 and 1,000 hour-tests (**Fig. 6-6**). It is possible to interpret that these steels caused the oxidation corrosion via the detachment of the unstable outer oxide layers. The SEM-EDX analysis for the HCM12A after 1,000 and 2,000 hour-exposure indicated that the outer layers were broken and detached from the substrate. In the multiple layers which has different composition, shear stress in the boundary must be caused due to the growth of the outer and inner layers with different growth rates [5].

18-Cr Steels

The 18-Cr steel, SS430 kept the smooth surfaces without the occurrence of the corrosion. On the surface, the oxide layer or scale was formed, where Cr was enriched. In SS430, well-developed oxide layer was not detected nevertheless the other steels formed the thick oxide layers in the Pb-Bi at high oxygen concentration. This indicated that 18Cr steel had good oxidation resistance in the flowing Pb-Bi. The sign of the LMC occurrence was not detected. The scale or the layer worked as the corrosion barrier. This contributed the small weight loss in the 2,000 hour-exposure.

The weight loss of the specimen in the Pb-Bi flow can be negligible no matter of the exposure time and/or oxygen concentration in the Pb-Bi (**Fig. 6-6**), even though the 12-Cr or 9-Cr steel lost the weight due to the oxidation corrosion.

The corrosion resistance of the SS430 steel in the liquid Pb-Bi at high oxygen concentration is due to the large amount of Cr in the steel matrix. The Cr on the steel surfaces was consumed by the formation of Fe-Cr oxide layer on the steel surface (**Fig. 6-8**). When the layer was broken away, the inner layer already formed beneath the outer layer started to work as outer layer. Then, the inner layer started to form in the matrix by inner diffusion of the oxygen from the Pb-bi through the outer layer. If the Cr is not condensed on the surface, a Fe-rich layer, which is more unstable than the Fe-Cr layer, may be formed. Then, the corrosion rates of the steels are increased, since the stability of the formed oxide layers were decreased gradually. However, the reformation of Cr-rich Fe layer can be kept if the Cr is condensed quickly as the large amount of the Cr was contained in the matrix as the SS430 steel.

6.1.5 Summary

The effect of Cr contents on corrosion resistance was investigated by means of corrosion tests in the flowing Pb-Bi. The results are summed up as follows;

- (1) The 12Cr steel and 9Cr steels caused the oxidation corrosion in the flowing Pb-Bi. The oxidation corrosion might be caused by the detachment of unstable oxide layers, where Cr was not enriched.
- (2) The 18-Cr steel, SS430, showed good corrosion resistance in the flowing Pb-Bi at 550°C up to 2,000 hours. The specimens of SS430 did not form thick oxide layers due to the good oxidation resistance in the flowing Pb-Bi. The weight loss of the SS430 specimens in the Pb-Bi flow was the lowest among the tested steels.

6.2 Effect of Alloying Elements in Steels on Corrosion Resistance in Flowing Lead-Bismuth

6.2.1 Introduction

The author have investigated corrosion characteristics of steels in the flowing Pb-Bi to grasp the influence of major alloying elements on their corrosion characteristics for the development of corrosion-resistant materials. In the *Chapter 4*, it was found that severe liquid metal corrosion (LMC) could be inhibited if an oxide layer was formed and kept stably on the surface in the flowing Pb-Bi. Furthermore, it was found that high content of Cr in steels and smooth steel surface promoted the formation of a compact oxide layer, and consequently improved the corrosion resistance in the flowing Pb-Bi [Chapters 5-2 and 6-2].

Recently, Kurata *et al.* [5] reported that 5wt% of Si in SX steel (17.6Cr-19Ni-4.8Si) beneficially influenced the corrosion resistance due to the formation of Si-oxide layer. And, this layer inhibit corrosion in the static Pb-Bi. Barbier *et al.*[9] reported that 1.8wt% of Si in EP823 steel (12Cr-1.2W-1.8Si) improved oxidation corrosion-resistance in the Pb-Bi flow.

In addition to Si, Al in steels may also enhance oxidation corrosion-resistance due to formation of stable Al-enriched oxide layers in the flowing Pb-Bi [4]. The corrosion characteristics of Si- and Al-rich steels in the flowing Pb-Bi should be investigated under various conditions extensively for further material development.

The purpose of the present study is to investigate the corrosion resistance of Si- and Al-rich steels in the flowing Pb-Bi experimentally.

6.2.2 Experimental apparatus and Procedure

Experimental Procedure

The corrosion tests were carried out using the Pb-Bi forced convection loop. **Figure 6-8** shows schematic of the loop. The loop consists of a cold region made of 9Cr-1Mo steel and a hot region made of SS-316, where Pb-Bi flows from the electro-magnetic pump, through the electro-magnetic flow meter, and the air cooler in the cold region and then flows through the heater, the test section, the oxygen sensor and the expansion tank in a hot region. For the corrosion test, cylindrical test piece holder made of molybdenum (Mo) was used. The volume of the liquid Pb-Bi in the loop was 22L.

In the present corrosion tests, oxygen concentration in the flowing Pb-Bi was measured by oxygen sensor, which was made of solid electrolyte conductor of ZrO_2 -MgO with the reference fluid of oxygen-saturated Bi (see *Chapter 2-2*). The Pb-Bi flows through the bypass loop in the cold region where the mass exchanger filled with solid lead oxide particles was installed for the

oxygen control in the liquid Pb-Bi. The controllability was reported in *Chapter 2-2*.

The electromotive, that was monitored using the oxygen sensor. The oxygen concentration was kept at 1.7×10^{-8} wt% in the 500-hour test and 1,000-hour test, and it was 1×10^{-6} wt% in 2,000 hour tests. The oxygen concentration in the latter test was made higher than the former tests by oxygen control using the mass exchanger. The conditions of oxygen potential are plotted in **Fig. 6-9** for comparison with on Gibbs free energy of oxides. It is found that the oxygen potentials were higher than the curve of Al_2O_3 , SiO_2 and Fe_3O_4 formation potential [6].

Corrosion examination

After exposed in the Pb-Bi flow, the specimen holder was demounted from the test loop. Then, the holder with the specimens immersed in a glycerin pool at the temperature of 180°C to remove adherent Pb-Bi from the outside and inside of the holder. Then, the holder was opened and the specimens were taken out of the holder, and rinsed again in glycerin pool at the temperature of 180°C to melt and remove adherent Pb-Bi from the specimen surfaces without removal of the oxide layers [7]. Finally, glycerin on the specimen surface was removed in warm water at the temperature of 70°C .

The surfaces of the specimens were observed before and after the exposure to inspect the occurrence of erosion. In order to determine the corrosion rate, weight losses of the specimens were measured using an electro reading balance with an accuracy of 0.1mg. The specimens were cut at the span wise center and the cross sections were polished, and then observed by a scanning electron microscope (SEM) and analyzed by an energy-dispersive X-ray spectrometer (EDX).

6.2.3 Test Materials

A series of corrosion tests was performed for SUH3 steel (10Cr-1Mo-2Si), Recloy10 steel (18Cr-1Al-1Si) and NTK04L steel (18Cr-3Al) in Pb-Bi flows.

The chemical components of the SUH3 steel, the NTK04L steel and the Recloy10 steel are shown in **Table 6-3**. As-received material was machined to specimen plates and the surfaces of the specimen were mechanically polished smoothly as arithmetical mean surface of $1\mu\text{m}$ to remove the effect of surface roughness of steels on corrosion resistance (see *Chapter 5-2*). Then, they were mounted in the specimen holder to be immersed in the flowing Pb-Bi at the conditions shown in Table 6-4. The specimens made of the other high Cr steels and ceramics were also mounted with SUH3, NTK04L and Recloy10 steels in the specimen holder.

6.2.4 Effect of Si and Al Contents in Steels on Corrosion Characteristics

SUH 3.

After the 500 hour-exposure to the flowing Pb-Bi, the surface of the Si-rich steel SUH3 was smooth without appreciable traces of erosion as shown in **Fig. 6-10 (a)**. The surface color changed from metallic luster before the exposure to black. This indicates that the oxide layer or corrosion products were formed on the surface. The surface color of the SUH3 after the 1,000-hour and 2,000 hour-exposure (**Fig. 6-10 (b) and (c)**) was similar to that after 500 hour-exposure (**Fig.6-10 (a)**).

The weight of SUH3 specimen decreased due to the corrosion in the flowing Pb-Bi as shown in **Fig. 6-11**. Weight loss in 2,000 hour-exposure was much larger than the extrapolated curve from weight loss data in 500-hour and 1,000 hour-exposure.

The results of SEM/EDX analysis show the existing of the single oxide layer on the surface of SUH3 specimen exposed to the Pb-Bi flow for 500 hours as shown in **Fig.6-12**. No penetration of the Pb-Bi was detected beneath the layer. The thickness of the layer can be estimated as 2-4 μm , and this is much thinner than the layer formed on the other Fe-Cr steels as reported in *Chapters 4 and 6-1*. In the layer, Si and Cr were enriched while Fe content was decreased. Also, bared place without the oxide layer can be detected.

After the 1,000 hour-exposure, double layers were formed on the SUH3 steel as shown in **Fig. 6-13**. The double layers consisted of outer layer (**Fig. 6-13** layer [O]) and inner layer (**Fig. 6-13** layer [I]). The outer layer detached from the substrate, and the thickness was 5-7 μm . The inner layer was compact, and the thickness was 1-2 μm . Si was enriched in the inner layer, and the layer was stuck to the steel matrix stably. This means that the outer layer was unstable, and could be easily taken out by high density fluid flow after the layer detached from the substrate. In the other words, the inner layer may protect the steel matrix from the LMC, while oxidation corrosion is caused by the detachment of the outer layer in the flowing Pb-Bi.

In the 2,000 hour-exposure, oxidation corrosion occurred in the SUH3 steel. From the results of the weight loss measurement for the SUH3 steel (**Fig. 6-11**), it was found that weight loss in the 2,000 hour test was larger than that expected from the results of 500-hour and 1,000-hour tests. That is because oxidation corrosion occurred due to the detachment of cracked layer as shown in **Fig. 6-14**. The cracked layer was single layer and the thickness was 5-7 μm . Although Si and Cr was enriched in the layer, the layer was cracked and detached from the substrate in some places. The oxidation corrosion occurred in the 2,000-hour test due to higher oxygen concentration than that in the 500- and 1,000-hour tests.

NTK04L

Initial metallic luster was kept on the surface of the NTK04L steel in the 500 hour-exposure to the Pb-Bi flow (**Fig. 6-10 (a)**). The weight loss of NTK04L was very

small and single Al-enriched oxide layer $1\mu\text{m}$ in thickness was formed on the surface in 500 hour-test (**Fig. 6-15**). The oxide layer on NTK04L was thinner than that formed on the SUH3 steel (**Fig. 6-12**).

Also in the 2,000 hour-exposure, corrosion did not occur in the NTK04L specimen. Weight loss was low. Metallic luster was kept on the surface (**Fig. 6-10 (c)**), and the color on the surface was the same as that after 500 hour-exposure (**Fig. 6-10 (a)**). Single oxide layer was formed on the surface (**Fig. 6-16**). The thickness and property of the layer was similar to those of the layer formed in 500 hour-exposure. The layer had no cracks.

Therefore, it is concluded that the Al-enriched oxide layer is formed on the surface of Al-rich NTK04L, and it inhibited the LMC. Since the formed layer was very thin and stable, neither cracks nor detachment occurred in spite of strong stress of high density Pb-Bi flow. The Al-enriched layer inhibited development of the oxide layer and consequently suppressed the oxidation corrosion.

Recloy10

In the Al- and Si-rich steel, Recloy10, shiny surface condition before the exposure was kept in 500-hour-exposure (**Fig. 6-10 (a)**). This was similar to that observed in the Al-rich NTK04L. The weight loss in the flowing Pb-Bi was negligibly small (**Fig. 6-11**). Most of the Recloy10 steel surface was covered with very thin Al- and Si-enriched layer of $1\mu\text{m}$ in thickness (**Fig. 6-17**). Pb-Bi did not penetrate into the steel beneath the oxide layer.

Also in the 2,000 hour-exposure, initial metallic luster was kept on the surface as shown in **Fig. 6-10 (c)**. The weight loss in the 2,000 hour test was nearly equal to zero. A $1\mu\text{m}$ -thick Al-enriched layer was formed on the surface (**Fig. 6-18**), which was similar to that in the 500 hour-exposure. The layer was well stuck to the steel surface.

Therefore, it is found that the Recloy10 steel has as good corrosion resistance for the high temperature Pb-Bi flow as the NTK04L steel. The thin Al-enriched layer inhibited not only the liquid metal corrosion but also oxidation corrosion.

Al content in steel promoted the formation of the stable oxide layer. The influence of the Al radiation may not be critical problem, although it has not been made clear, since the amount of Al in steel is small enough and the half time of irradiated Al is short.

6.2.5 Formation of Si- and Al- Rich Oxide Layer on Steels in Flowing Pb-Bi

The formation process of the Al- and Si- rich oxide layers on the steels in the flowing Pb-Bi is possibly explained as shown in **Fig. 6-19**. The Fe-Cr oxide layers were formed on the steel surfaces due to the elements of Fe and Cr on the steel surfaces selectively reacted with the oxygen in the liquid Pb-Bi. Then, the Al or Si on the surfaces were condensed. The oxygen diffused through the Fe-Cr oxide layer reacted in the Al- and/or Si- condensed region. Then, the Al and/or Si rich oxide layers were formed on the steel surfaces without the dissolution of the Al and/or Si due to the direct contact with corrosive liquid Pb-Bi.

6.2.6 Summary

For the development of corrosion-resistant materials for Pb-Bi-cooled fast reactor and Pb-Bi target type accelerator driven system, corrosion resistance of Si- and Al-rich steels in flowing Pb-Bi was investigated by means of the exposure of the SUH3 steel (10Cr-2Si), the NTK04L steel (18Cr-3Al) and the Recloy10 steel (18Cr-1Si-1Al) to the Pb-Bi flow at the temperature of 550°C for 500, 1,000 and 2,000 hours. Summaries are as follows:

- 1) Si- and Cr-enriched 1 μ m thick oxide layer was formed on the surface of the SUH3 steel that had 2wt% of Si in the Pb-Bi flow. No LMC occurred beneath the layer. The SUH3 steel exhibited excellent corrosion resistance in the Pb-Bi flow at low oxygen concentration. Oxidation corrosion occurred at high oxygen concentration due to the growth, destruction and detachment of Si-enriched layer.
- 2) An initial metallic luster was kept on the surface of the Al-rich steel, NTK04L in the Pb-Bi flow. Al-enriched single layer stuck to the matrix was formed on the surface. This layer protected the matrix from not only the liquid metal corrosion but also the oxidation corrosion since this layer had oxidation resistant in the Pb-Bi flow at high oxygen concentration. The weight of the NTK04L steel decreased only a little due to corrosion with exposure time.
- 3) Initial surface state was kept on the surface of the Al- and Si-rich Recloy10 steel in the exposure to the Pb-Bi flow. A single Al- and Si-enriched layer was formed on the surface. The property of the layer was similar to that in the NTK04L steel. By the exposure to the Pb-Bi flow for 2,000 hours, the weight of the Recloy10 steel did not decrease due to no corrosion.

6.3 Corrosion Rate of Corrosion Resistant Steels in Flowing Pb-Bi

The corrosion rates of the steels were estimated from their weight changes in the liquid alloy (**Table 6-5**). In the present study, the corrosion characteristics of the steels in the liquid alloy at the oxygen concentration of 1×10^{-6} , 1.7×10^{-8} and 2×10^{-9} wt%. Then, the relation between the corrosion rates of the steels and the oxygen concentration in the liquid Pb-Bi is shown in **Fig. 6-20**.

It was found that the corrosion transition point in the flowing liquid Pb-Bi place at the oxygen concentration, which corresponded to the Fe_3O_4 formation potential in the liquid Pb-Bi. This is since This is since the corrosion behavior of the steels depended on the that of the Fe, which occupied app. 80% in the steel matrix.

The corrosion rates of the Al-rich steel NTK04L and the 18Cr steels were lower than the allowable corrosion rates estimated from the corrosion margin of the Joyo type fast reactor (See *Chapter 1* and Eqs. (1-1) and (1-2)).

6.4 Conclusion

By using oxygen control system explained in *Chapter 2*, the corrosion tests were carried out in the flowing Pb-Bi at high oxygen concentration. The 18-Cr steel, SS430, formed Cr rich single oxide layer. The Cr-rich layer inhibited not only the dissolution type corrosion (*Chapter 3*) but also the oxidation corrosion, while the low-Cr steels which formed Fe- rich oxide layers caused the corrosion. This is because the Cr rich oxide layers were stable more than Fe-oxide layers in the flowing Pb-Bi.

In case of Al and Si rich steels, the stable oxide layers were formed on their surface in the flowing Pb-Bi. The Al-rich oxide layer was thinner than that formed on the Si rich steel and Cr-rich SS430 steel. The formation of the thinner oxide layer implies less oxidation-corrosion risk, since the oxidation corrosion is caused by the detachment of thick and unstable oxide layer. Thus, Al is the most foreseen element of the steels for the corrosion inhibition in the flowing Pb-Bi, even though the elements of Si and Cr increase the oxidation corrosion resistance.

Reference

- [1] M. Hirabayashi, M. Kondo, K. Ara and M. Takahashi, "Development of Ultrasonic Flow Meter for Liquid Lead-Bismuth", Proc.of 13th Int. Conf. On Nucl. Eng. (ICONE-13), ICONE13-50001, May 16-20, Beijing, China (2005).
- [2] F. Barbier and A. Rusanov, "Corrosion Behavior of Steels in Flowing Lead-Bismuth", J. Nucl. Mater., **296**, 231-236 (2001).
- [3] B. F. Gromov, Y. I. Orlov, P. N. Martynov and V. A. Gulevsky, "The Problems of Technology of The Heavy Liquid Metal Coolants (Lead-bismuth, Lead)", Proc. of HLMC1999, 87-100 (1998).
- [4] High temperature oxidation of metal, Japan Society of Corrosion Engineering, (1882) (in Japanese)
- [5] Y. Kurata and M. Futakawa, "Excellent Corrosion Resistance of 18Cr-20Ni-5Si Steel in Liquid Pb-Bi", J. Nucl. Mater., **325**, 217-222 (2004).
- [6] The Oxide Hand Book, second edition, edited by G. V. Samsonov, IFI/PLENUM

Table 6-1 Corrosion test conditions

Exposure time (h)	500	1000	2000
Pb-Bi temperature in test section (°C)	550		
Pb-Bi temperature in low temperature region (°C)	400		
Pb-Bi charge temperature (°C)	250		
Flow rate (L/min)	3		
Flow velocity (m/s)	1		
Oxygen concentration in Pb-Bi (wt%)	1×10^{-8}	1×10^{-8}	1×10^{-6}
Test material	STBA26, NF616, HCM12A, SS316, SS405, SS430	SCM420, F82H, NF616, STBA26, ODS HCM12A, HCM12 SS316, SS405, SS430	STBA26, NF616, HCM12A, SS405, SS430 316FR

Table 6-2 Chemical components of specimens (wt%)

	Cr	Mo	W	Si	others
SCM420	1.2	0.2	-	0.2	
F82H	7.7	1.94	1.94	0.1	0.01Ti-0.01Cu
NF616	9	0.5	1.8	0.3	
STBA26	9	1	-	0.2	
ODS	11.7	-	1.9	-	0.29Ti-0.23Y ₂ O ₃ -0.18Y
HCM12A	12	0.3	1.9	0.3	0.9Cu
HCM12	12.1	1.1	1.0	0.3	
SUS405	12	-	-	1	0.1Al
SUS316	18	2-3	-	0.1	10-14Ni
SUS430	18	-	-	0.75	

Table 6-3 Chemical components of test steels (wt%)

	Cr	Si	Al	Mo	C
SUH3	10.39	1.90	-	0.72	0.42
Recloy10	17.69	0.99	0.89	-	0.01
NTL04L	17.84	0.41	3.34	0.14	0.002

Table 6-4 Test conditions

Exposure time (hour)	500	1,000	2,000
Flow velocity (m/s)	1	1	1
Temperature of Pb-Bi (°C)	550	550	550
Oxygen concentration (wt%)	1.7×10^{-8}	1.7×10^{-8}	1×10^{-6}
Test steel	SUH3	SUH3	SUH3
	NTK04L		NTK04L
	Recloy10		Recloy10

Table 6-5 Corrosion rates of steels in flowing Pb-Bi

Steels	Density (g/m ³)	Experimental conditions			Results		Corrosion rate per year (mm/year)
		Test temperature (°C)	Oxygen concentration (wt%)	Exposure time (hour)	Weight changes (g/m ²)	Estimated weight changes per year (g/m ² year)	
NTK04L	7700000	550	1×10^{-6}	2000	8.5	37.3	4.8×10^{-3}
SS430	7700000	550	1×10^{-6}	2000	0.15	1.3	1.7×10^{-4}
316FR	798000	550	1×10^{-6}	2000	476.5	2087.2	2.6×10^{-1}
STBA26	7850000	550	2×10^{-9}	1000	197.1	1726.6	2.2×10^{-1}
	7850000	550	1.7×10^{-8}	1000	21.5	188.3	2.4×10^{-2}
	7850000	550	1×10^{-6}	2000	125.4	549.3	7.0×10^{-2}
HCM12A	7750000	550	2×10^{-9}	1000	68	595.7	7.7×10^{-2}
	7750000	550	1.7×10^{-8}	1000	24	210.2	2.7×10^{-2}
	7750000	550	1×10^{-6}	2000	248	1086.2	1.4×10^{-1}
ODS	7750000	550	2×10^{-9}	1000	584.1	5117.3	6.6×10^{-1}
	7750000	550	1.7×10^{-8}	1000	21.1	184.9	2.4×10^{-2}
	7750000	550	1×10^{-6}	2000	-87.4	-383.0	-4.9×10^{-2}
F82H	7850000	550	2×10^{-9}	1000	1614.8	14145	1.8
	7850000	550	1.7×10^{-8}	1000	233	233.6	3.0×10^{-2}
	7850000	550	1×10^{-6}	2000	-278	-278.86	-3.5×10^{-2}
Corrosion allowable rate in Joyo type reactor		550	-	-	-	-	1×10^{-2}

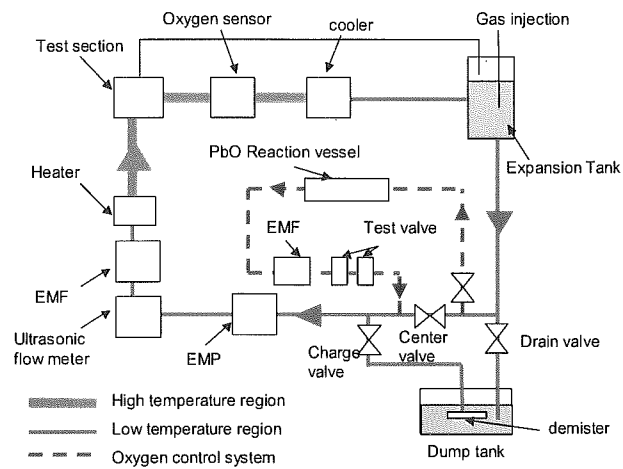


Fig. 6-1 Schematic of Pb-Bi forced convection loop

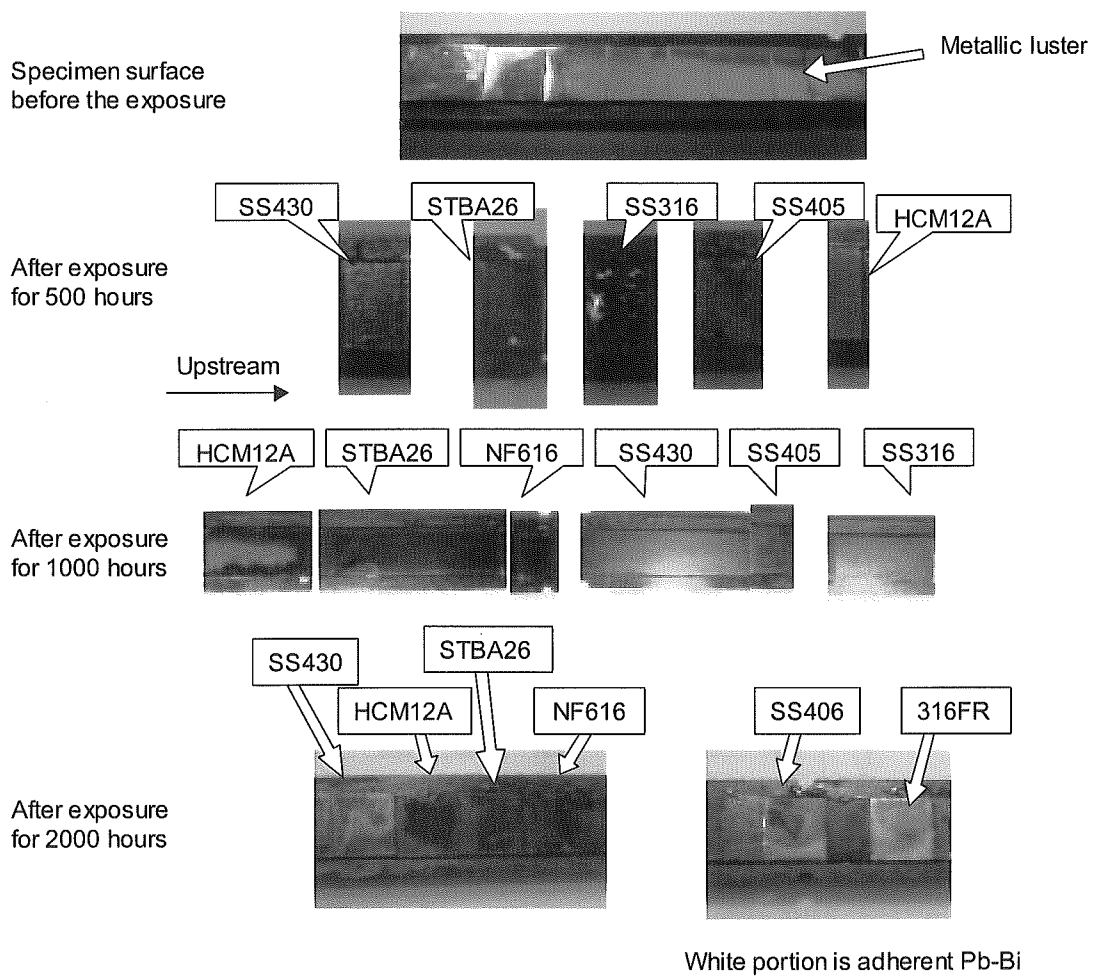


Fig. 6-2 Surface observation of specimens after corrosion test

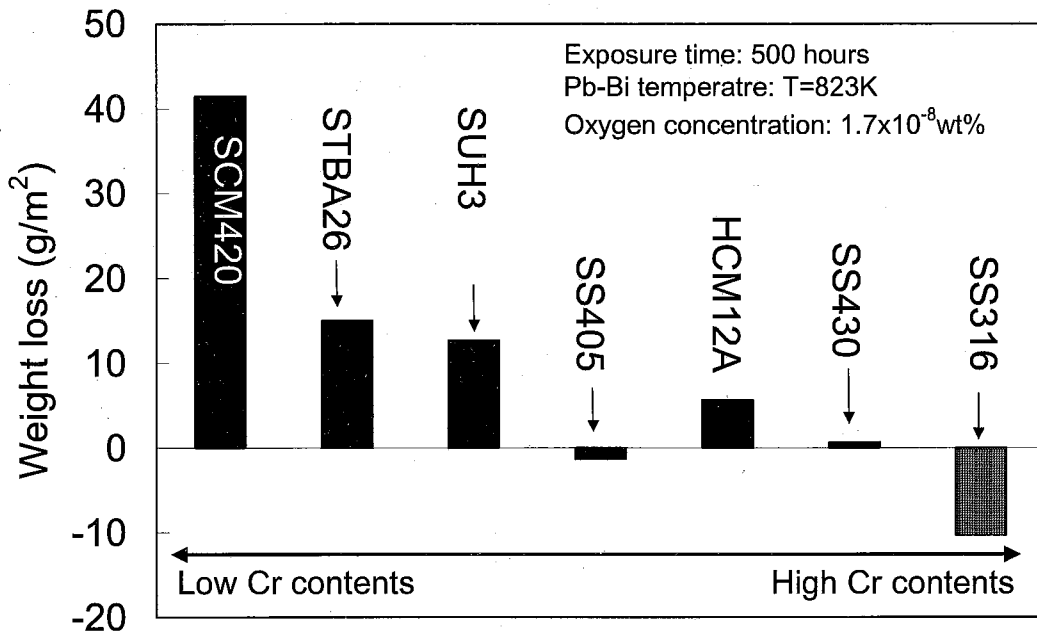


Fig. 6-3 Weight loss of steels and ceramic materials in 500 hour-test

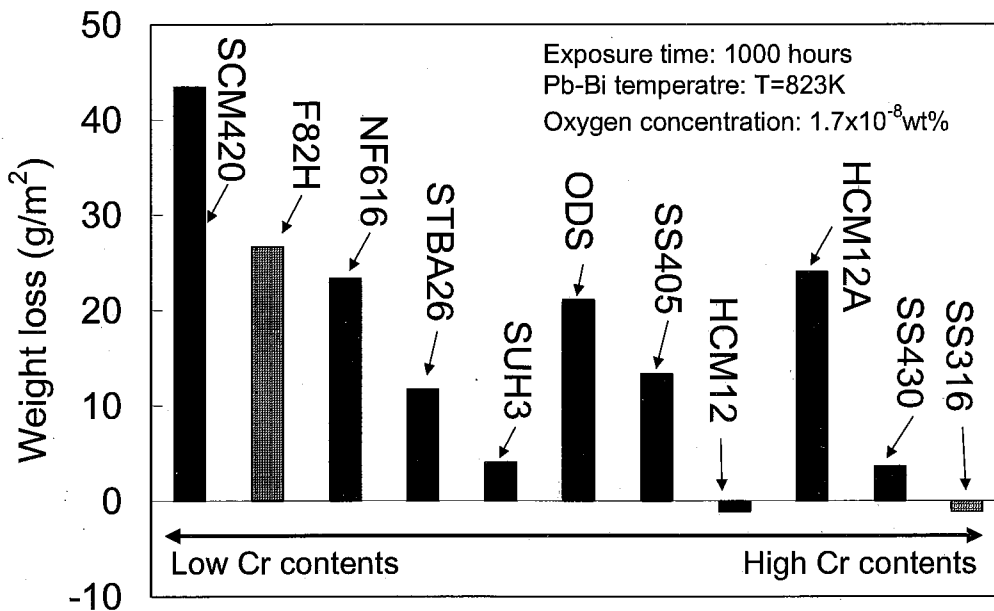


Fig. 6-4 Weight loss of steels and ceramic materials in 1000 hour-test

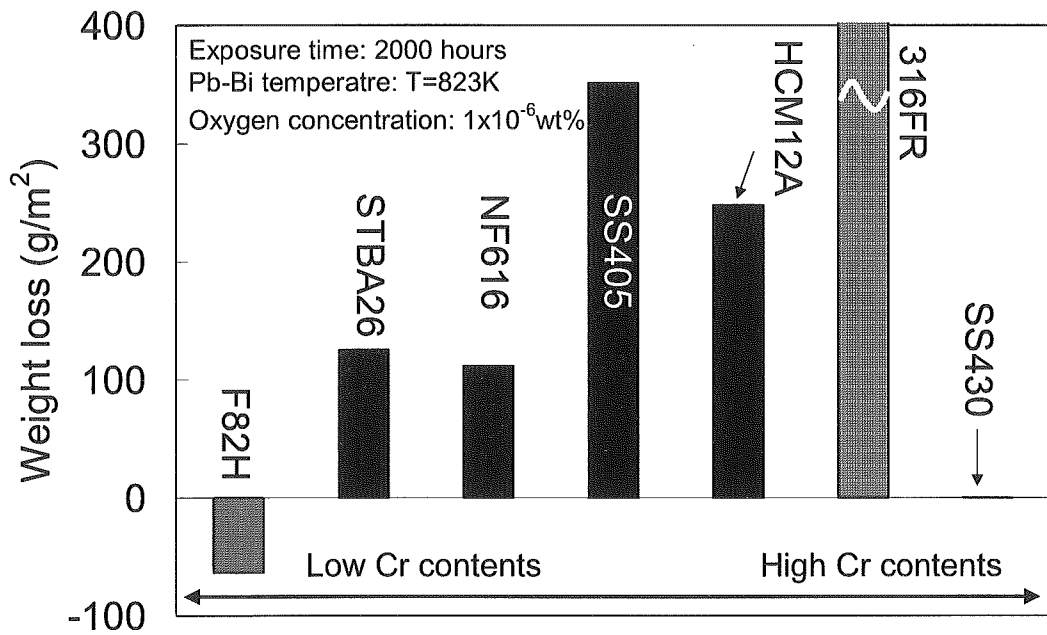


Fig. 6-5 Weight loss of steels and ceramic materials in 2,000 hour-test

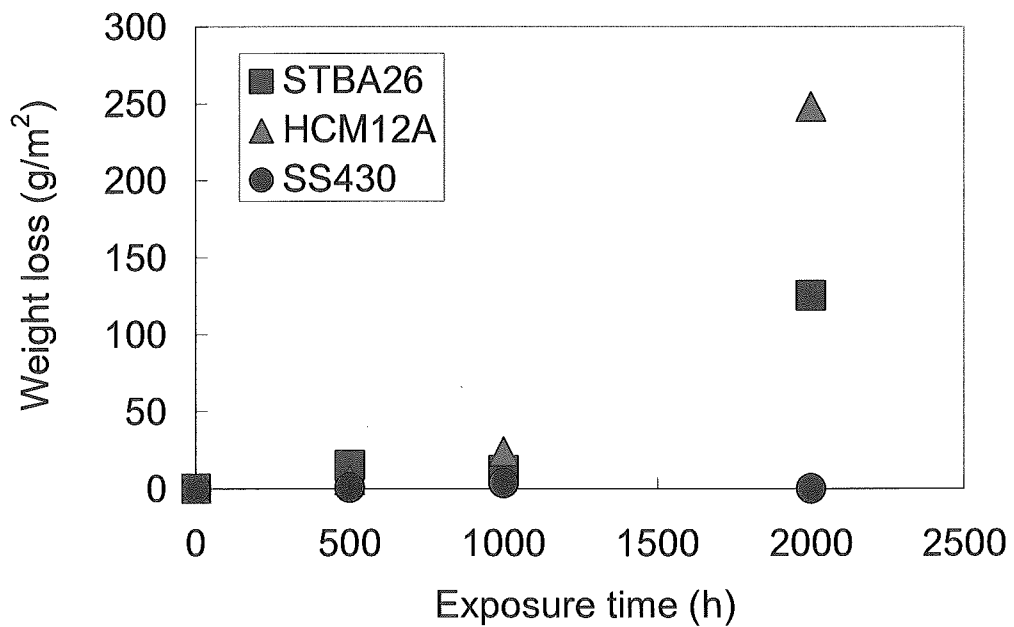


Fig. 6-6 Weight loss of SS430 (18-Cr), HCM12A (12-Cr) and STBA26 (9-Cr) specimens in Pb-Bi flow

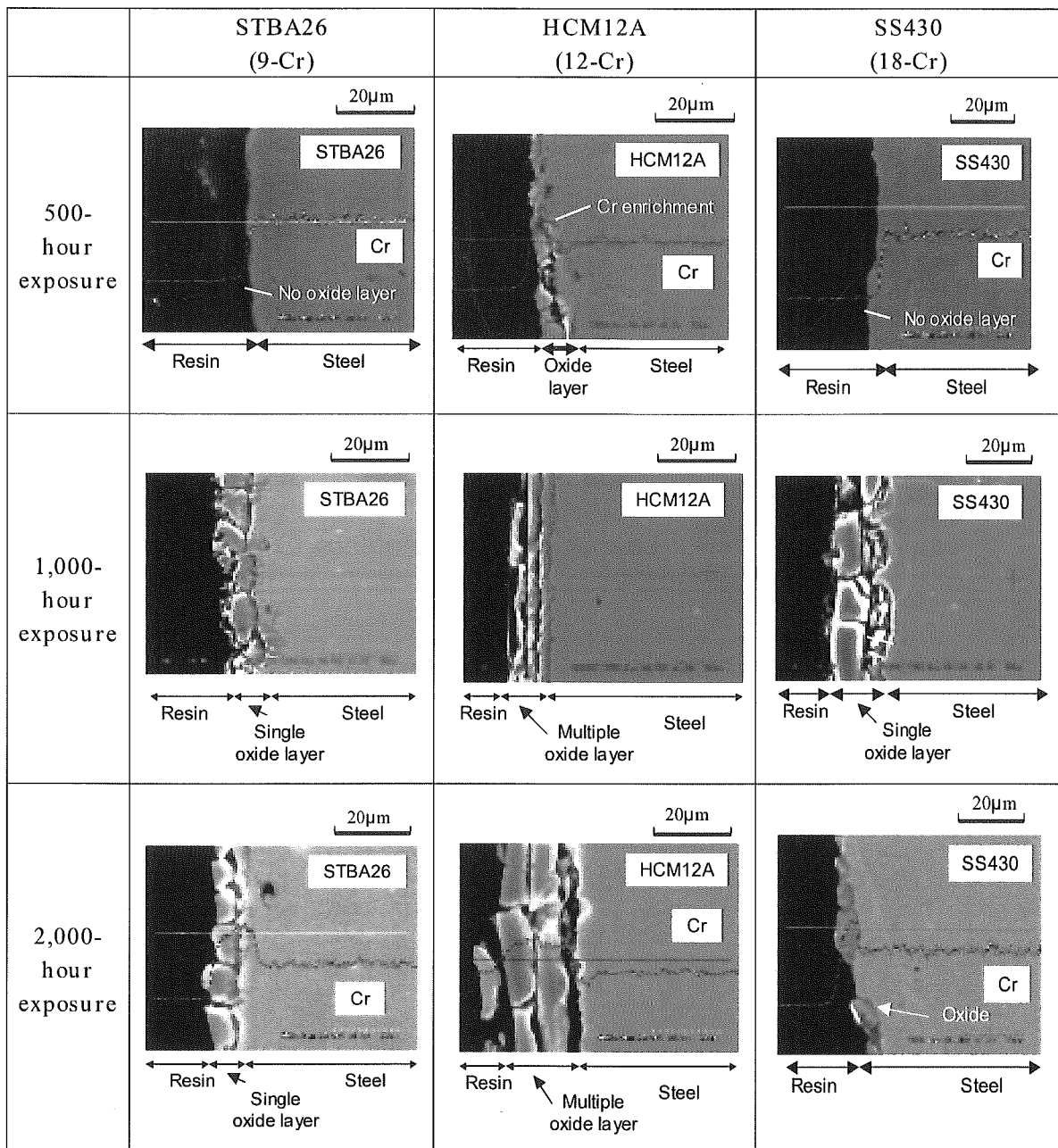


Fig. 6-7 Surface cross section of SS430, HCM12A, STBA26 after 500, 1,000, 2,000 hour-tests

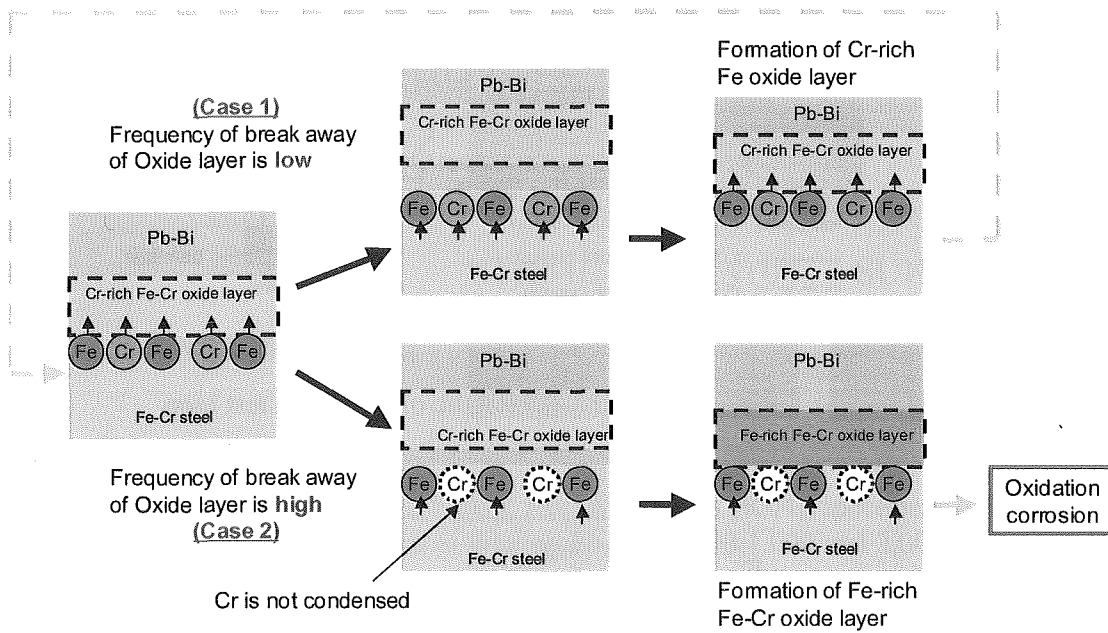


Fig. 6-8 Decrease of influence of Cr in steels on formation of Fe-Cr oxide layer in liquid Pb-Bi.

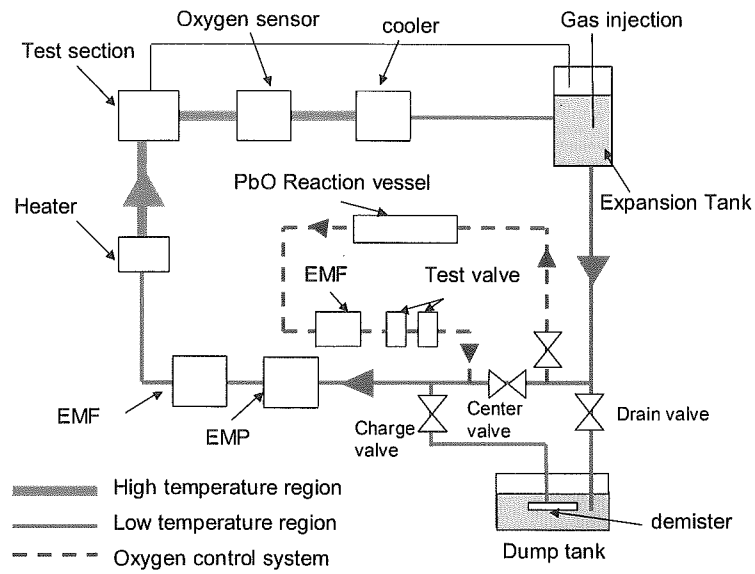
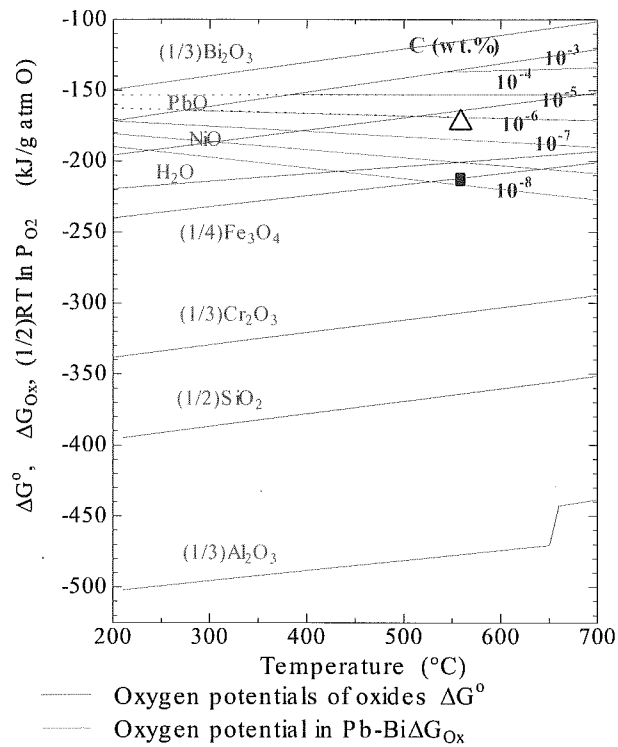


Fig. 6-9 Schematic of corrosion test loop



5

Fig. 6-10 Diagram of oxygen potential; oxygen condition in 500-hour and 1,000-hour test was shown in black square; oxygen condition in 2000-hour test was

shown in vacant triangle

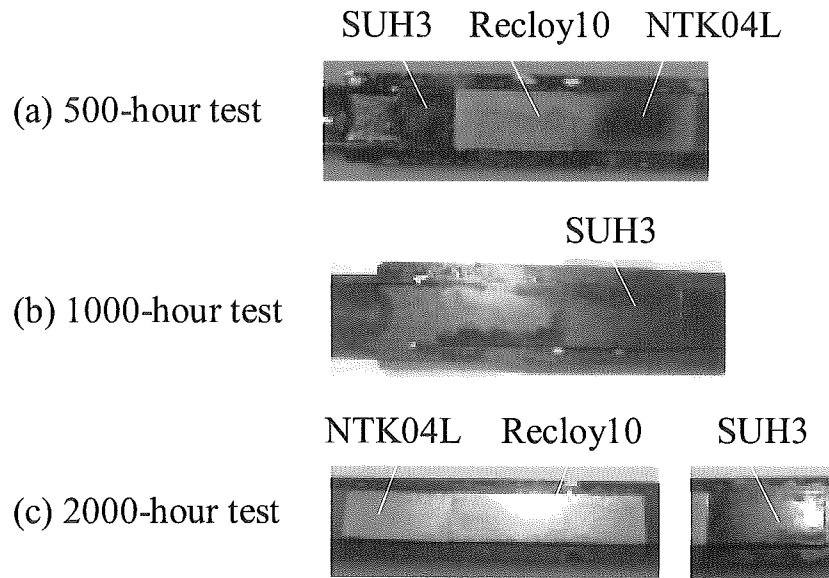


Fig. 6-11 Appearance of SUH3, Recloy10 and NTK04L specimens in Mo-test piece holder after exposure to flowing Pb-Bi for 500,1,000 and 2,000 hours

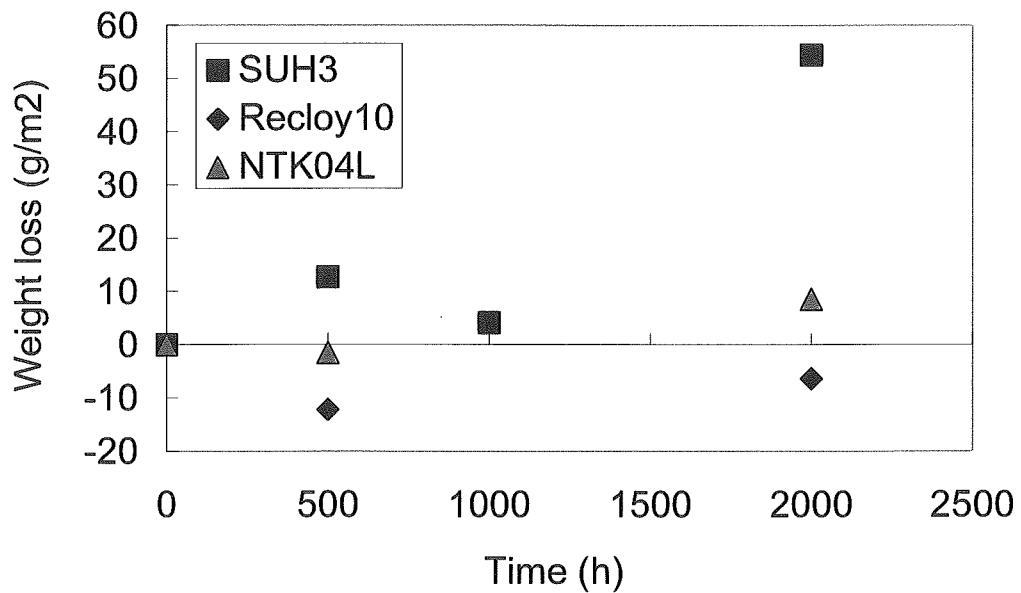


Fig. 6-12 Weight loss of SUH3, Recloy10 and NTK04L steels in flowing Pb-Bi

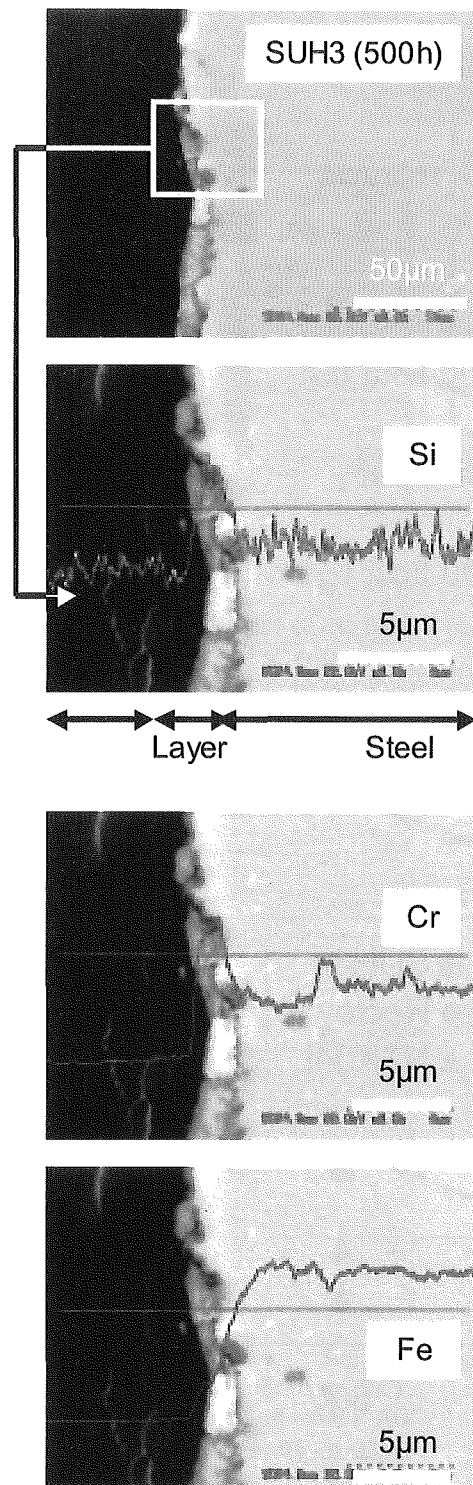


Fig. 6-13 Si-enriched single oxide layer formed on SUH3 surface in 500 hour-exposure to flowing Pb-Bi

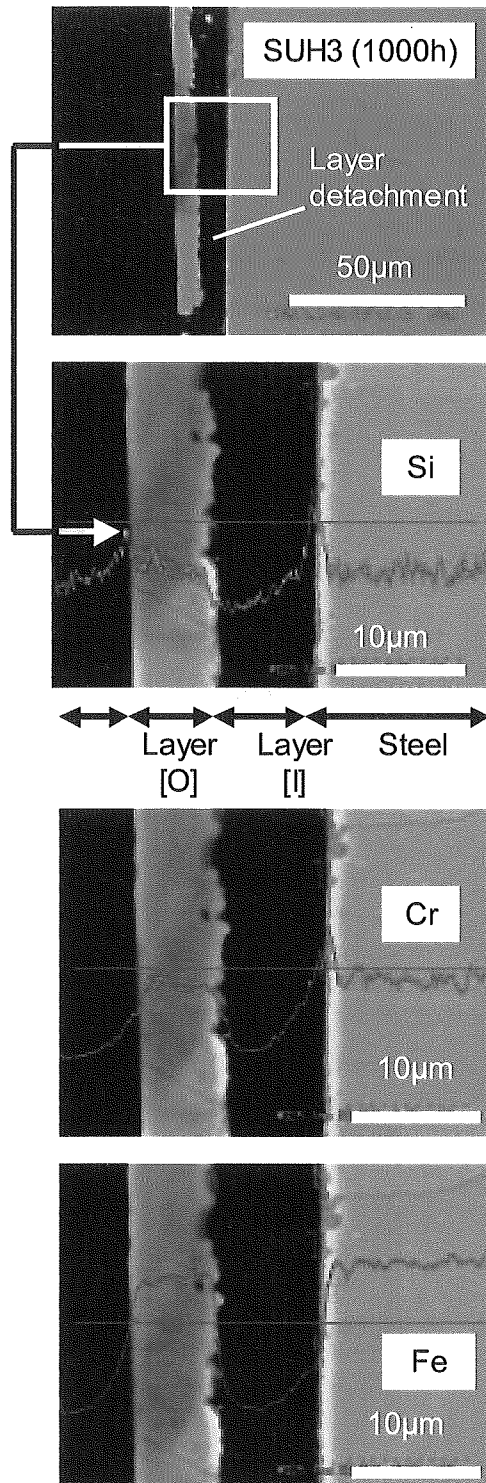


Fig. 6-14 Double oxide layer consists of outer [O] layer and inner [I] layer formed on SUH3 surface in 1,000 hour-exposure to flowing Pb-Bi

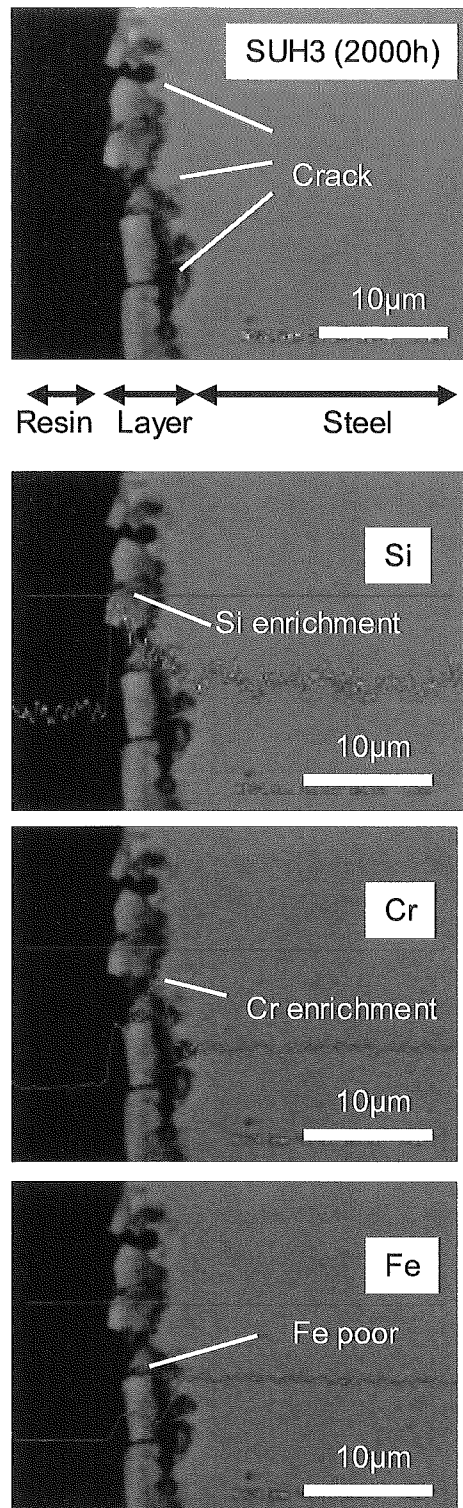


Fig. 6-15 Cracked oxide layer formed on SUH3 surface in 2,000 hour-exposure to flowing Pb-Bi

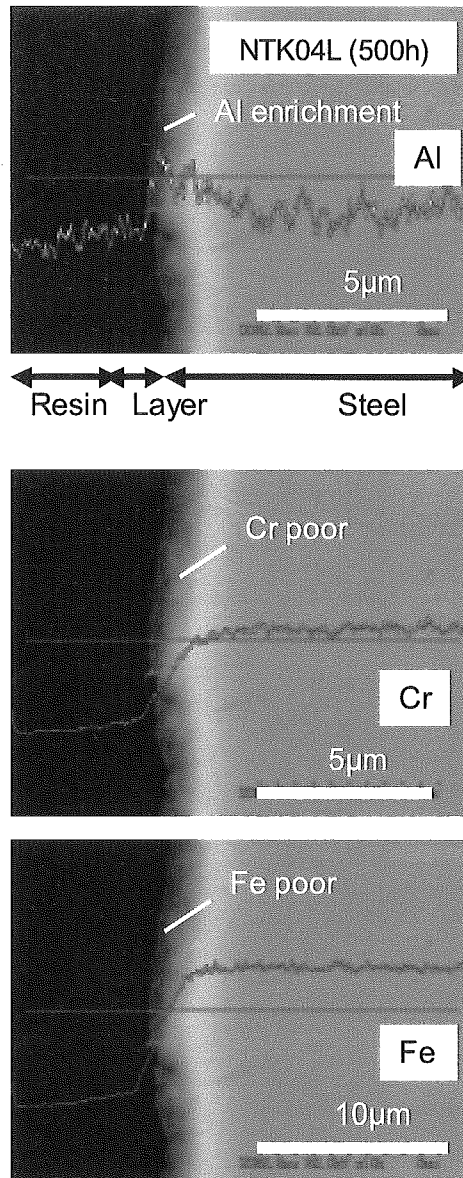


Fig. 6-16 Ai-enriched oxide layer formed on NTK04L steel in 500-hour test

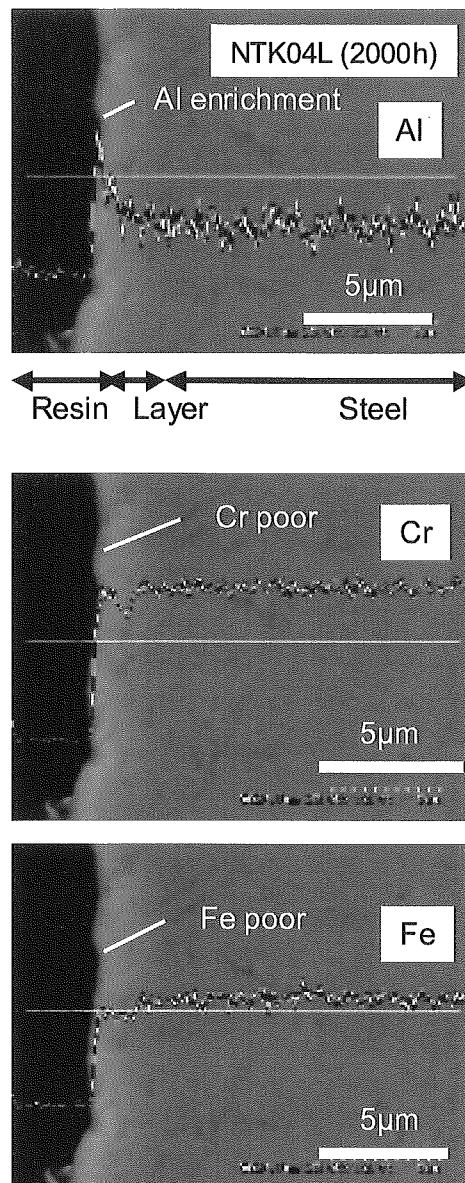


Fig. 6-17 Al-enriched layer formed on NTK04L steel in 2,000-hour test

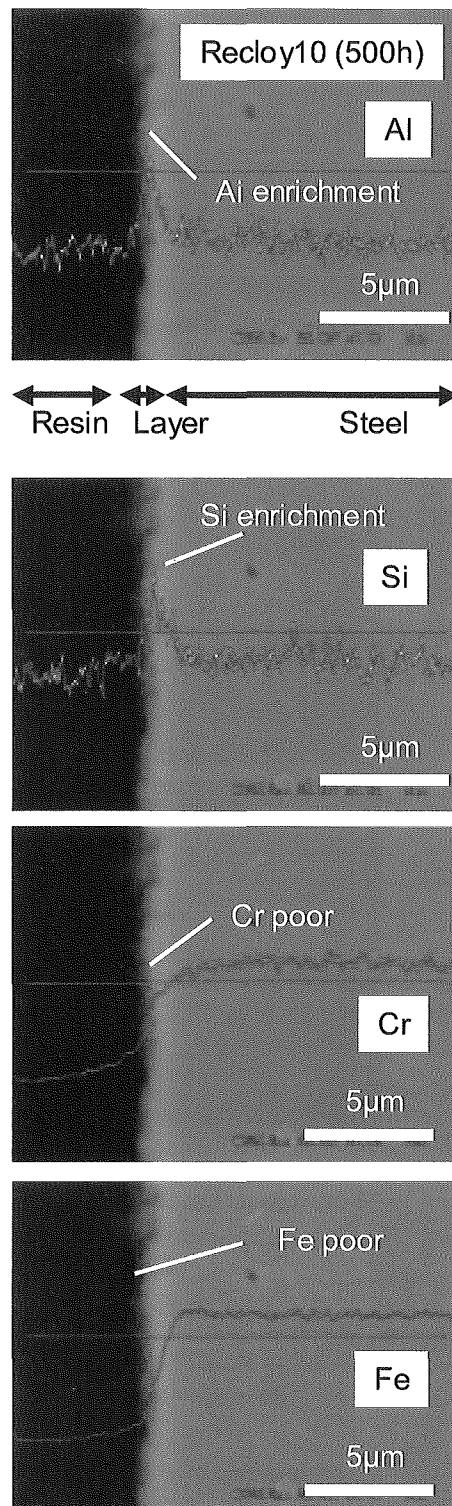


Fig. 6-18 Al-enriched thin layer formed on Recloy10 steel in 500 hour-exposure to flowing Pb-Bi

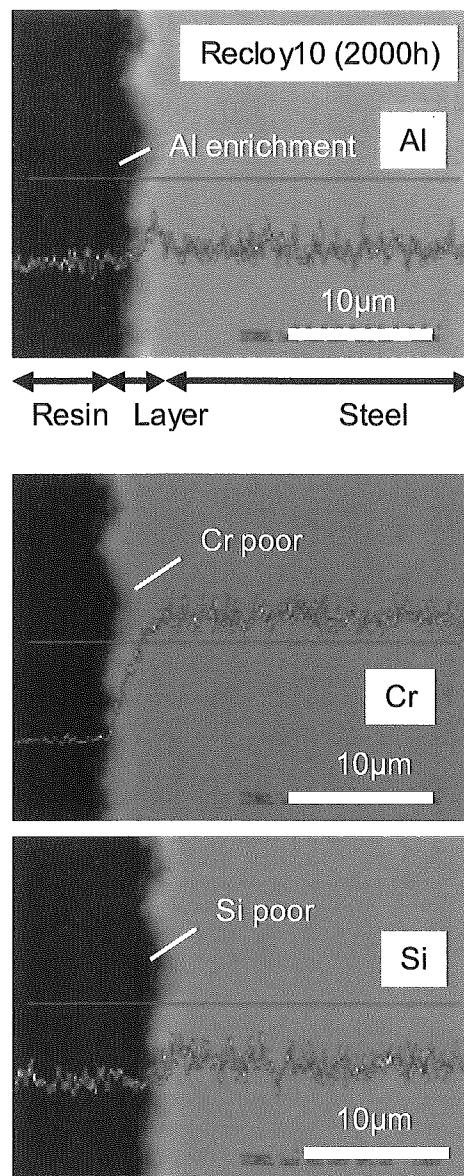


Fig. 6-19 Al-enriched thin layer formed on Recloy10 steel in 2,000 hour-exposure to flowing Pb-Bi

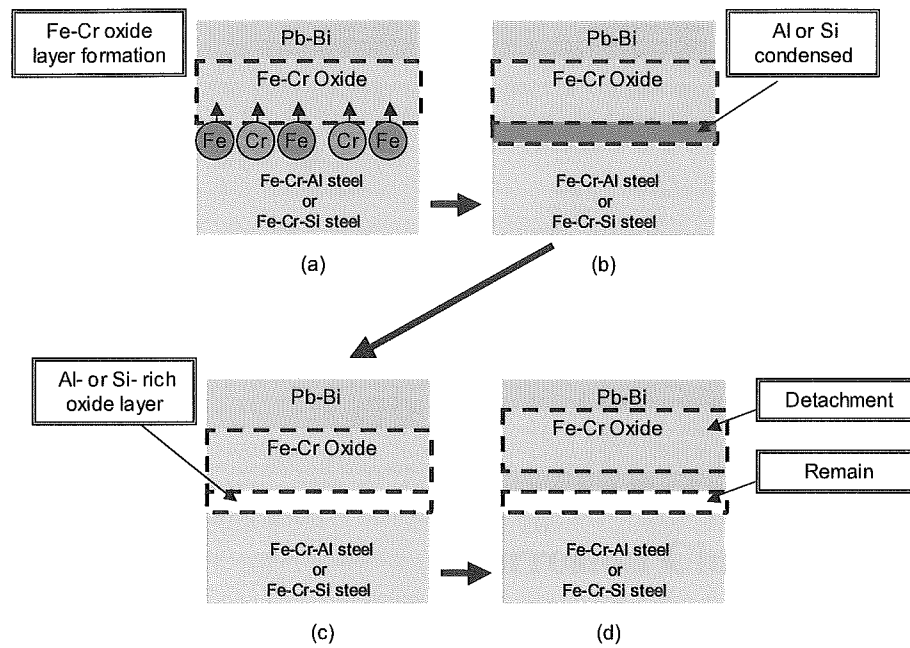
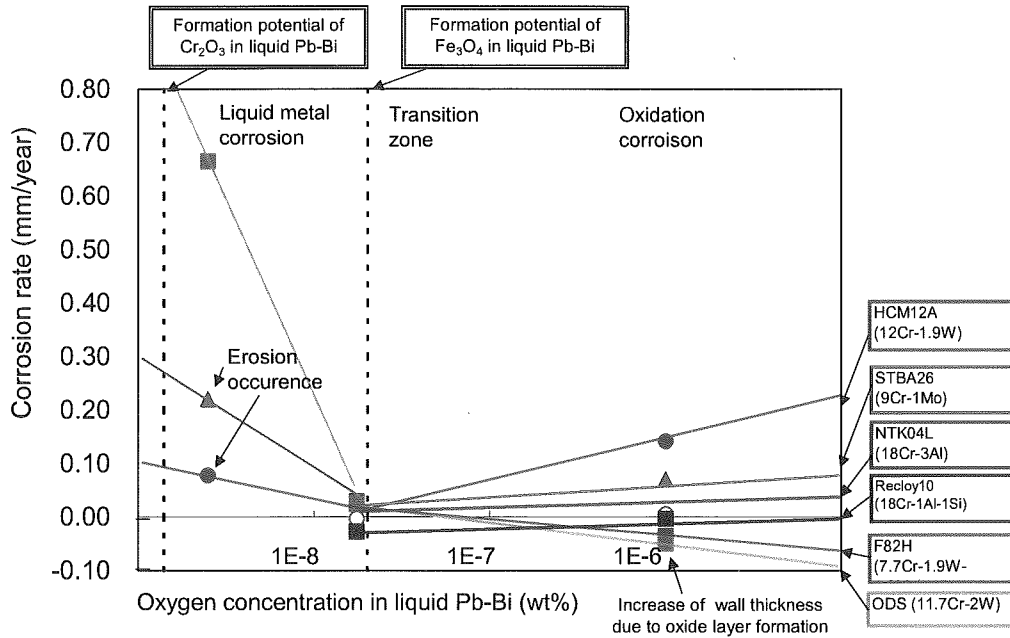


Fig. 6-20 Formation of Al- and Si- rich oxide layers on steels in flowing Pb-Bi



Corrosion rate at 2×10^{-9} wt% was estimated from corrosion test results done with Pb-Bi flow velocity of 2m/s, while the corrosion rate at the other oxygen conditions were estimated from the test done with flow velocity of 1m/s

Fig. 6-21 Corrosion rates of corrosion resistance steels in flowing Pb-Bi

Chapter 7

Corrosion Characteristics of Ceramic Materials, SiC and Si₃N₄, in Flowing Lead-Bismuth

7.1 Introduction

The self-healing oxide layers formed on the steels are expected to work as corrosion barriers in the flowing Pb-Bi (*Chapters 4*). However, Martin et al. indicated that an unstable oxide layers could be disappeared in the long-term immersion even in the static Pb-Bi [1]. Then, it has been challenged to inhibit the corrosion using surface treatment technique, e.g. Kurata et al. investigated the corrosion resistance of the Al- surface treated steels in static Pb-Bi [2] and L. Soler et al. did the pre-oxidation for the formation of stable oxide layers preliminary for the corrosion protection [3]. Authors also challenged to inhibit the corrosion by using surface treatment technique and Si Al-rich steels, which expect to form a stable Al₂O₃ oxide layer in the flowing Pb-Bi (*Chapter 5* and *Chapter 6*).

The ceramic materials of SiC and Si₃N₄ and their composite are considered as promising thermal structural materials due to their high thermal shock resistance, high thermal conductivity, low thermal expansion and creep resistance at high temperature. Also, these ceramic materials have excellent oxidation resistance, although the resistance depends on the environments.

In this chapter, the results of corrosion test for the SiC and Si₃N₄ ceramic materials were reported. The oxygen concentration in the flowing Pb-Bi was controlled at the potential higher than that required for the formation of SiO₂ by using mass exchanger type oxygen control system (*Chapter 2-2*). The purpose of the present study is to investigate the corrosion characteristics of SiC and Si₃N₄ in the flowing Pb-Bi at high oxygen concentration.

7.2 Experimental Apparatus and Procedure

In the work, Pb-Bi forced convection test loop was used for the corrosion test. The schematic of the loop is shown in **Fig. 7-1**. After the specimens were mounted in the loop, the Pb-Bi was charged into the loop from the dump tank at 250°C. The charge of the melt was done by using the pressure difference between the dump tank and the loop. Then, the Ar gas of 99.999% purity was used to pressurize the dump tank. The Ar gas was used as cover gas in the loop. The temperature of the Pb-Bi was increased up to 550°C in the hot region and 400°C in the cold region.

The corrosion test was conducted at the conditions presented in **Table 7-1**. The oxygen concentration in the flowing Pb-Bi was monitored by a solid electrolyte type oxygen sensor at 550°C. The concentration was estimated as 1x10⁻⁶wt% from the obtained sensor output using the Nernst equation and equations for oxygen solubility in the Pb-Bi (*Chapter 2-1*). This oxygen concentration was higher than that required for the formation of SiO₂. In the present test, some steel specimens were immersed in the same time.

After the corrosion test, the specimens were extracted from the loop. An adhered Pb-Bi on the specimens was removed in the glycerol pool at 180°C. Then, an adhered

glycerol on the specimens was removed with the hot water at 70C. This technique is also used in Los Alamos National Laboratory in USA [4] and CEA-CEREM/SCECF in France [5].

The surface conditions of specimens after the exposure were analyzed using field emission- scanning electron microscope (FE-SEM) with energy dispersion X ray (EDX). The surface roughness of the specimens before and after the exposure was measured using 3D Lazar micro scope.

The weight of the specimens before and after the corrosion test was measured using an electro reading balance with an accuracy of 0.1mg in order to estimate the weight changes of the specimens. The weight changes of the ceramic materials were compared with that of the other steel specimens exposed in the same time.

After the weight measurement, the specimens were cut at span wise center and embedded in the resin, in order to analyze the surface cross section using FE-SEM/EDX. In the analysis, the Pt/Pd coating was done on the specimens to keep the good electrical conductivity.

7.3 Test Materials

The chemical components of SiC and Si₃N₄ used in the present work was 98 SiC-0.2SiO₂-0.1Si-1.2C and 90Si₃N₄-9(Al₂O₃-Y₂O₃)-CaO, respectively. These materials were machined into the specimens, which have the size of 15mm x 30mm x 2mm. The surface of the specimens was not polished. The surface roughness of these specimens measured by using Lazar 3D microscope was 5μm in arithmetical mean surface roughness (Ra). These ceramic materials were supplied from NIKKATO corporation.

7.4 Corrosion Characteristics of Ceramic Materials, SiC and Si₃N₄ in flowing Pb-Bi

Corrosion Rate of SiC and Si₃N₄

The specimens of SiC and Si₃N₄ slightly lost their weight (**Fig. 7-2**) in the flowing Pb-Bi. The weight loss of the SiC was 13.2g/m² and this is briefly larger than that of Si₃N₄ of 5.48 g/m². This is because the SiC top region was eroded in the small part.

The weight changes of SiC and Si₃N₄ specimens were compared with the steels explained in *Chapters 4 and 6*. The weight loss of the ceramic materials were much lower than that of the 9Cr, 12Cr and austenitic steels. However, the weight loss of the ceramic materials was slightly higher than those of the SS430, Recloy10 and NTK04L steels which were specially characterized by the alloying elements of Cr, Al and Si in *Chapter 6*. These indicated that the ceramic materials had good resistance not only for dissolution type corrosion but also oxidation corrosion in the flowing Pb-Bi.

The corrosion rates of these ceramic materials were estimated as shown in **Table 7-2**. It was found that the corrosion rate of Si₃N₄ was lower than allowable corrosion rate of the structural material in Joyo type reactor (See *Chapter 1*).

SiC and Si₃N₄ Surface After Exposure

Fig. 7-3 shows the surface of SiC and SiN specimens before and after the corrosion test. The specimens were kept the initial surface color of silky in the flowing Pb-Bi. In the top region of the SiC specimen, brief erosion was detected. This erosion was caused by the collision with high density Pb-Bi flow, since the SiC was arranged in the uppermost stream in the corrosion test section. Such a phenomenon was reported in case of steel in *Chapter 3*. From the measurement results of surface roughness, the surface kept the initial surface roughness.

The surface conditions of the exposed specimens were analyzed using FE-SEM/EDX (**Figs. 7-4 and 7-5**). In the initial surface of SiC specimen (**Fig. 7-4 (a)**), the trace of the mechanical processing was observed. Then, some cracks were also detected. After the exposure, the trace was rarely detected (**Fig. 7-4 (b)**). The most part of the surface seems to be cracked. The segregation of the material components and the Pb-Bi were not detected in the EDX analysis.

In the SiN specimen (**Figs. 7-5 (a) and (b)**), the surface condition did not change in the flowing Pb-Bi. In both specimens, adhered Pb-Bi was not detected.

Metallurgical analysis for surface cross sections

In the surface of SiC specimen (**Fig. 7-6**), oxide layer was not detected. Several cracks were detected locally. The crack depth can be measured as 25μm in maximum. In the cracked region, the diffusion of the Pb and/or Bi was not detected. Also, the

segregation of the Si and/or C was not detected. These facts indicated that the cracks were caused by the mechanical factor such as shear and/or normal stress by the heavy density Pb-Bi flow, not by the chemical reaction such as the corrosion.

Also in the Si₃N₄ (Fig. 7-7), oxide layer was not detected. The dent surface was detected, and the depth could be measured as 25μm in maximum. In this part, few cracks were detected (Fig.7-8). The Pb-Bi was not diffused and adhered on this part. This dent part might be formed by the influence of shear and/or normal stress of heavy density fluid Pb-Bi flow.

Some of the detected cracks and dent parts in the SiC and Si₃N₄ was possibly due to the initial conditions which was well influenced by the machining process. Thus, it should take into account that the weight loss of these specimens was caused by the erosion of the unstable surface region which was made by the initial specimen machining process.

In the chemical corrosion point of view, the SiC and Si₃N₄ had good corrosion resistance for the Pb-Bi.

7.5 Conclusions

The corrosion test was performed to investigate the corrosion characteristics of the ceramic materials of SiC and Si₃N₄. Major conclusions are as follows;

- (1) Specimens of SiC and Si₃N₄ kept smooth surface without corrosion in the flowing Pb-Bi for 2000 hours. On these surfaces, oxide layers and adherence of Pb-Bi were not detected.
- (2) The SiC and Si₃N₄ lost their weight briefly in the flowing Pb-Bi. The weight loss of these ceramic specimens in the flowing Pb-Bi was smaller than those of 9Cr steels and 12Cr steels, and slightly higher than those of 18Cr steel, SS430, Al rich steel, NTK04L, and Al and Si rich steel, Recloy 10.
- (3) The surfaces of the SiC and Si₃N₄ specimens showed several cracks after the immersion in the flowing Pb-Bi. In the cracks, Pb-Bi was not diffused.

Reference

- [1] F. J. Martin, L. Soler, F. Hernandez, D. Gomez-Briceno, "Oxide layer stability in lead- bismuth at high temperature", *J. Nucl. Mater.*, **335**, 194-198 (2004).
- [2] Y. Kurata, M. Futakawa, S. Saito, "Corrosion behavior of Al-surface-treated steels in liquid Pb-Bi in a pot", *J. Nucl. Mater.*, **335**, 501-507 (2004).
- [3] L. Soler Crespo, F. J. Martin Munoz, D. Gomez Briceno, "Short-term static corrosion tests in lead-bismuth", *J. Nucl. Mater.*, **296**, 273-281 (2001).
- [4] J. Zhang, N. Li, Y. Chen, A. E. Rusanov, "Corrosion behaviors of US steels in flowing lead-bismuth eutectic (LBE)", *J. Nucl. Mater.*, **336**, 1-10 (2005)
- [5] F. Barbier, A. Rusanov, "Corrosion behavior of steels in flowing lead-bismuth", *J. Nucl. Mater.*, **296**, 231 (2001).

Table 7-1 Corrosion test conditions

Exposure time (h)	2000
Pb-Bi temperature in test section (°C)	550
Pb-Bi temperature in low temperature region (°C)	400
Pb-Bi charge temperature (°C)	250
Flow rate (L/min)	3
Flow velocity (m/s)	1
Oxygen concentration (wt%)	1x10 ⁻⁶

Table 7-2 Corrosion rates of SiC and Si₃N₄ in flowing Pb-Bi

Steels	Density (g/m ³)	Experimental conditions			Results	Estimated weight changes per year (g/m ² year)	Corrosion rate per year (mm/year)
		Test temperature (°C)	Oxygen concentration (wt%)	Exposure time (hour)	Weight changes (g/m ²)		
SiC	3100000	550	1x10 ⁻⁶	2000	13.2	57.8	1.9 x 10 ²
Si ₃ N ₄	3200000	550	1x10 ⁻⁶	2000	5.5	24.0	7.5 x 10 ³
Corrosion allowable rate of materials in Joyo type reactor		550	-	-	-	-	1x10 ⁻²

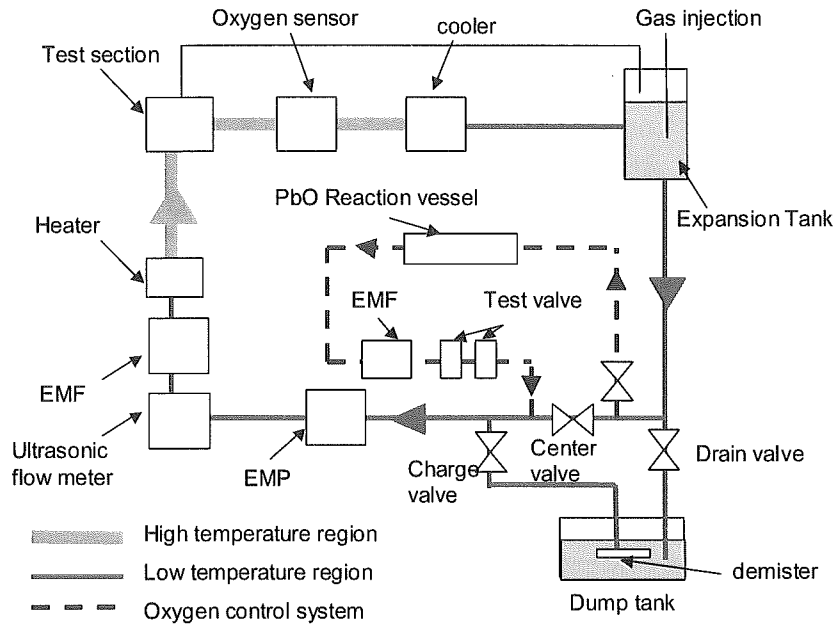


Fig. 7-1 Schematic of Pb-Bi forced convection loop

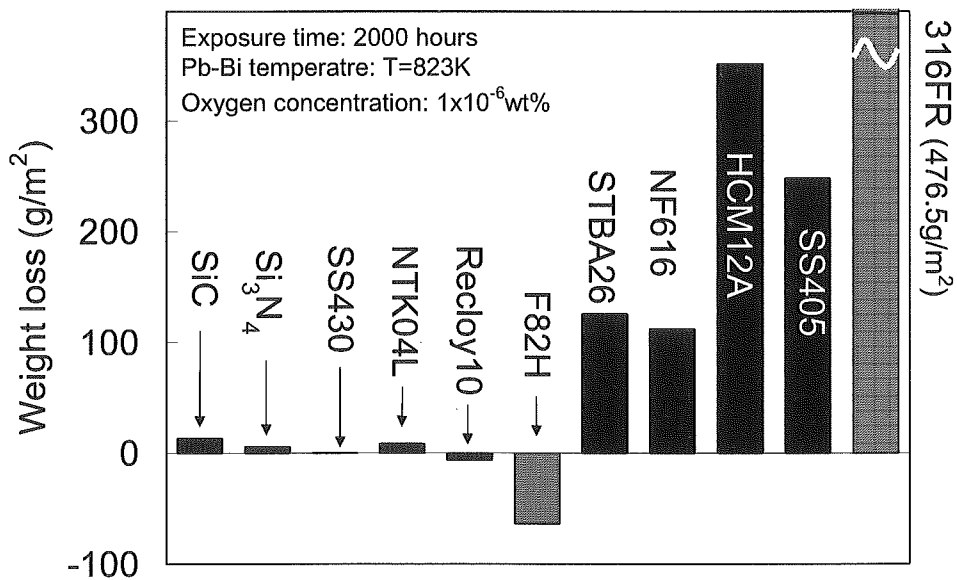


Fig. 7-2 Weight change of SiC and Si₃N₄ specimens compared with other steel specimen

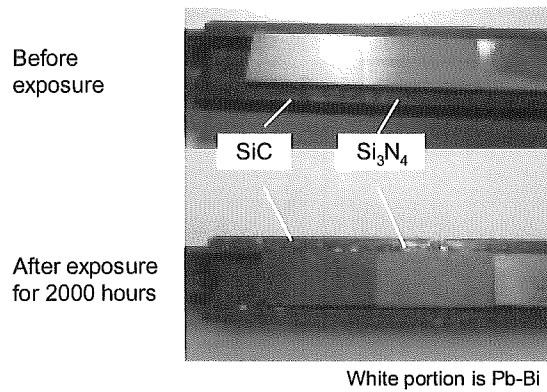


Fig.7-3 SiC and Si₃N₄ surfaces before and after corrosion test

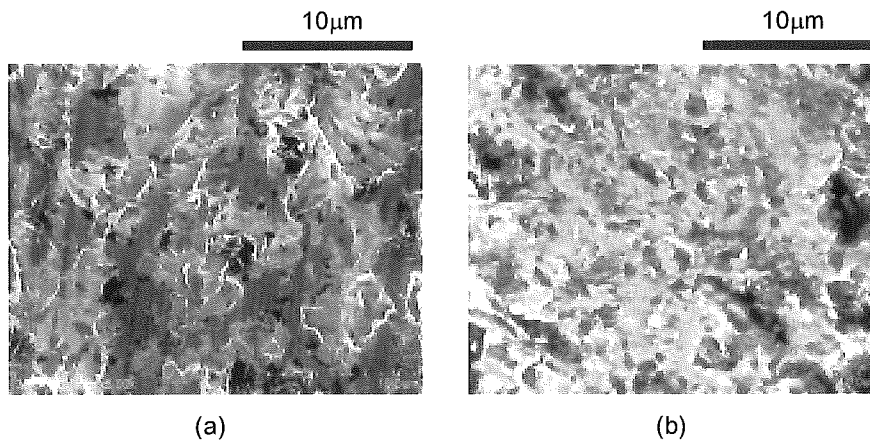


Fig.7-4 FE-SEM image of SiC specimen;
(a) initial SiC surface; (b) after immersion in Pb-Bi for 2000 hours

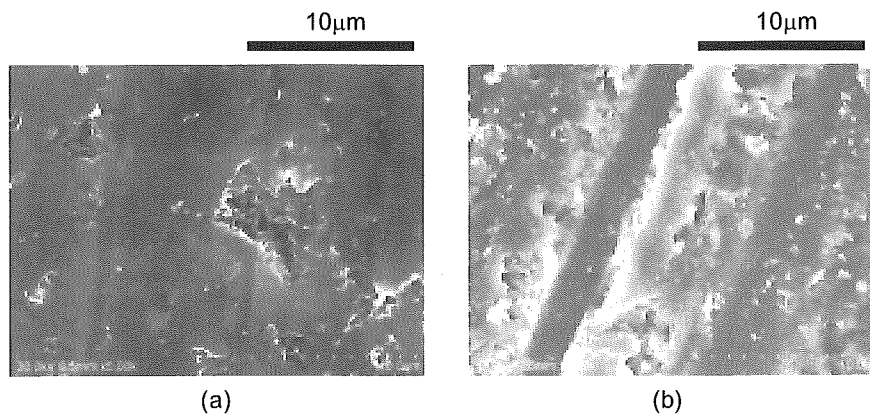


Fig.7-5 FE-SEM image of Si₃N₄ specimen;
(a) initial SiN surface; (b) SiN surface after immersion in Pb-Bi for 2000 hours

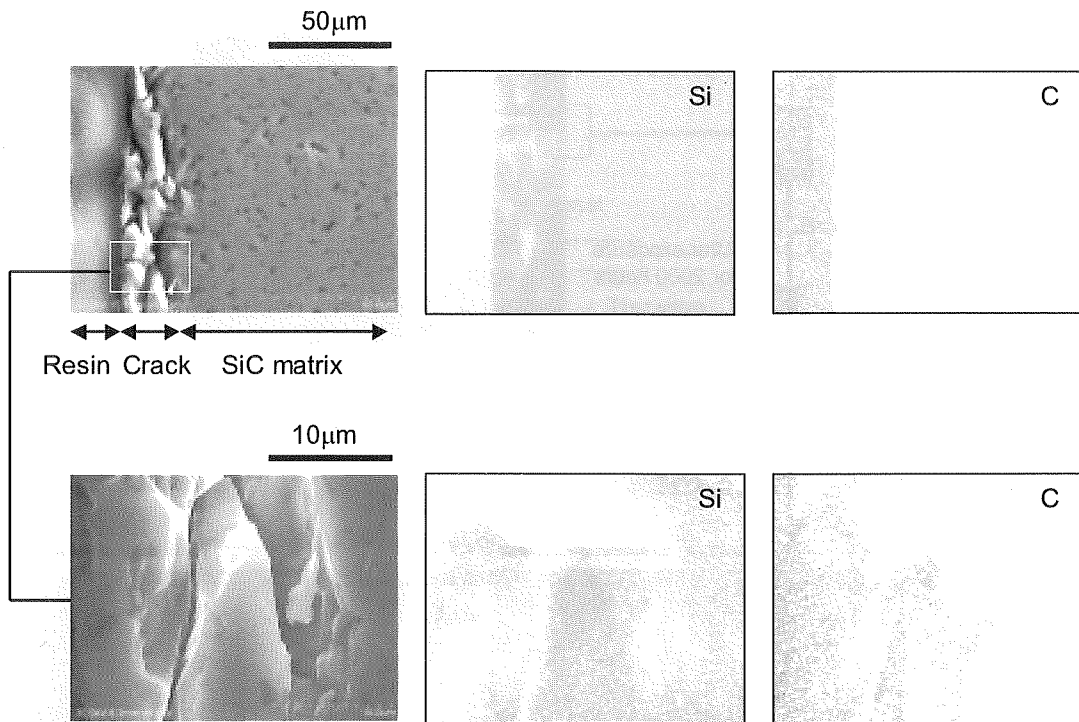


Fig.7-6 Fe-SEM image and EDX analysis for surface cross section of SiC

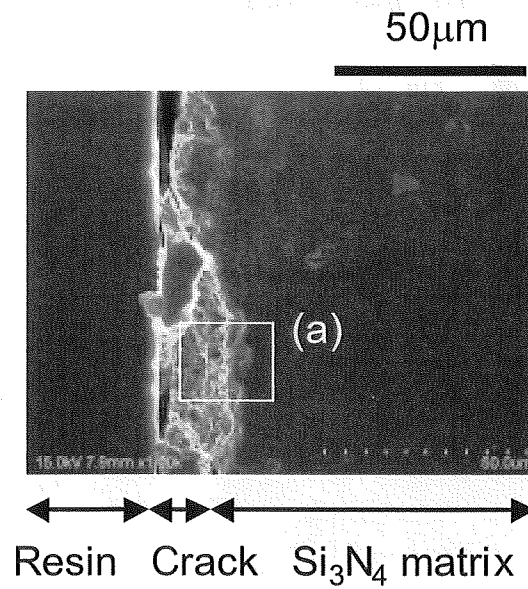


Fig. 7-7 Fe-SEM image for surface cross section of Si₃N₄

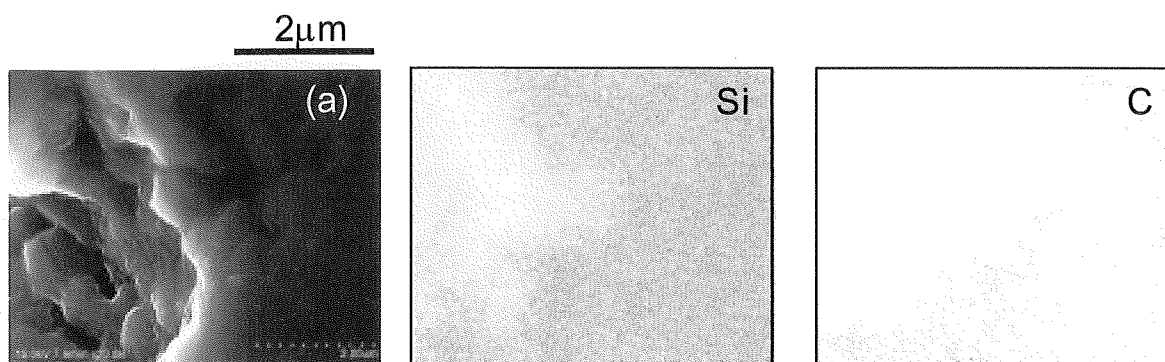


Fig. 7-8 Fe-SEM image and EDX analysis for dent part (a) in Si₃N₄

Chapter 8

Effect of Corrosion on Tube Rupture Behavior and Liquid Contamination

8.1 Effect of Corrosion on Tube Rupture Behavior in Liquid lead-bismuth

8.1.1 Introduction

Liquid metal corrosion (LMC) and liquid metal embrittlement (LME) are critical issues for the development of fuel rod cladding material for use in lead-bismuth (Pb-Bi) cooled fast reactors [1] and turbine blade material in direct-contact type Pb-Bi-cooled fast reactors [2].

A Pb-Bi forced convection test loop has been used to carry out a series of steel corrosion and flow technology tests for the feasibility study of a Pb-Bi-cooled small fast reactor. Previous studies have shown that LMC or oxidation corrosion occurs in steels in Pb-Bi at high temperature depending on the oxygen concentration in the liquid Pb-Bi [3, 4], although Pb-Bi is not so corrosive at low temperature no matter what the oxygen concentration is [5, 6]. However, liquid Pb-Bi at low temperature may cause LME [7, 8], *i.e.* the ductility may decrease in steels in contact with liquid Pb-Bi and they may become stressed. Reports of actual cases of tube or pipe rupture in the Pb-Bi due to the LMC and/or LME are rare.

Accidental tube rupture occurred in the Pb-Bi sampling line of the Pb-Bi forced convection test loop while the loop temperature was being increased. Metallurgical analysis and fractography studies of the ruptured tube were carried out. This reports focused on investigating the major factor causing tube rupture in the liquid Pb-Bi.

8.1.2 Experimental Procedure

Material

The Pb-Bi sampling line was installed in the low temperature region of the Pb-Bi forced convection test loop as shown in **Fig. 8-1**. The Pb-Bi sampling line is shown schematically in **Fig. 8-2**. The tube was made of 316SS (18Cr-2Mo-12Ni), which had an outer diameter of 12.7mm and wall thickness of 1mm. A sheathed heater of 1600mm length and 2.3mm in diameter was wound around the tube with a pitch of 30mm. A thermocouple was placed at the center of the tube in order to monitor the temperature. The ends of the sampling line were connected to the main loop via bellow valves. After Pb-Bi was charged in the line, one of the valves was closed to keep a static condition.

The sampling line was heated up and cooled down in the same way as for the temperature control of the low temperature region of the main loop. In the heat up process, all parts of the loop were heated from room temperature (RT) to 250°C for 1 hour. Then, the liquid Pb-Bi was charged into the sampling line at 250°C from the dump tank. Next the sampling line was heated from 250°C up to 400°C at the rate of 25°C per

30 min. The sampling line was cooled down in the same way as in the heat up process. For corrosion tests, the temperature of the sampling line was increased and decreased cyclically as presented in **Table 8-1**. The sampling line had experienced 3,440 hour-exposure in the liquid Pb-Bi at 400°C until the rupture occurred (**Table 8-2**).

The liquid Pb-Bi initially charged in the sampling line contained oxygen at several ppm. The oxygen content was kept high enough to get formation of Fe oxide at 400°C even if the Pb-Bi in the sampling line mixed with Pb-Bi in the main loop during the periods of the corrosion tests.

Analysis

After rupture, the sampling line was removed for inspection and metallurgical analysis. The deformation around the ruptured part was investigated. The ruptured area of the tube was partially cut open, and the fractured face was rinsed using the nitric acid to remove adhering Pb-Bi. Then, the face was observed with a scanning electron microscope (SEM).

After the SEM observation of the fractured face, the tube was cut as a cross section for metallurgical analysis. Then, the inner surface of part (a) distant from the fracture crack and part (b) near the crack were analyzed using SEM and an energy dispersive X-ray analyzer (EDX); these were done without removing adhering Pb-Bi (**Fig. 8-2**).

8.1.3 Effect of Corrosion on Tube rupture Behavior

Appearance and size change of the ruptured tube

The accidental rupture of the tube occurred in the Pb-Bi sampling line during the heat up process of the main loop of Pb-Bi forced convection test loop from room temperature to 250°C. At that time, the liquid Pb-Bi leaked from the tube to the heat insulator. **Figure 8-3** shows a photo of the ruptured tube. The fracture crack appeared at span wise center of the tube. **Figure 8-4** shows the size of the fracture crack and the deformation of the tube around the crack. The crack length was 8.3mm. The crack width was not uniform, and had a maximum width of 1.1mm around the middle of the crack. Secondary cracks could not be observed by visual inspection. There was local expansion of the tube around the fractured part and deformation there was not uniform. The outer diameter and the thickness of the tube were initially 12.7mm and 1mm, and after the rupture they were 16 mm in maximum and 0.75mm in minimum at the fracture part, respectively (**Fig.4**). There, the sheathed heater cut into the expanded tube.

Fractography study

As shown in SEM image (**Fig. 8-5**), the fracture face could be separated into two regions, *i.e.* the region near the outer tube wall and that near the inner tube wall. Although the former had visible dimple marks characteristics of a ductile fracture (**Fig.**

8-6), the inner region did not have the dimple marks. No dimpling was seen 200 μm from the inner surface.

Metallurgical examination

Figure 8-7 (a) shows the SEM images and component profiles for a cross section of the inner tube wall surface in area (a) which is distant from the fracture crack. The Cr and Ni contents were lower than those in the steel matrix (Fig. 8-7 (a) Nos.4 and 6). This means that Cr and Ni were dissolved into the Pb-Bi. In the corroded region, the Pb-Bi penetrated into the steel matrix to the depth of 8 μm on average. Dissolved matrix elements were not detected in the adhering Pb-Bi. This was possibly because the total amount of the elements dissolved from the steel into the liquid Pb-Bi was small, and the dissolved elements penetrated uniformly in the liquid Pb-Bi.

Near the ruptured part (Fig. 8-7 (b)), a region with dissolved Cr and Ni was detected (Fig. 8-7 (b), Nos. 3-6), and the Pb-Bi penetrated into the steel matrix as in area (a). However, penetration was more significant there than in area (a). The depth of the penetrated region was 100 μm on average, and this was 12 times deeper than that of area (a). The steel matrix of the inner tube surface was partially damaged. This was because the corroded surface was damaged due to the increased inner pressure in the tube, when thermal expansion of the Pb-Bi occurred in the heat up process. At the same time, the Pb-Bi penetration was promoted because the Pb-Bi was pushed into the steel matrix by the increased inner pressure. Fe dissolved from the inner tube surface was detected in the adhering Pb-Bi. This indicated that the amount of dissolved Fe from the steel surface was much larger than that in area (a).

8.1.4 Phenomena of Liquid Metal Embrittlement

Around the fractured part of the tube, local deformation was observed. This implied that the tube rupture was caused by the increased internal pressure due to thermal expansion of the Pb-Bi in the tube, since the Pb-Bi melted in the center part of the tube earlier than in other parts in the same tube. Around the valve, the pitch of the heater wound outside could be larger than that around the center of the tube. However, it was hard to consider that the tube rupture was caused by the thermal expansion of the Pb-Bi in one temperature increase cycle. That is because the volume change of the Pb-Bi in each process of freezing, cooling, melting, and heating was less than 1% as reported in ref. [9]. Therefore, it is more probable that the thermal expansion of the Pb-Bi occurred repeatedly in heat-up processes.

On the inner tube surface that made contact with Pb-Bi, the steel matrix was corroded by the liquid Pb-Bi during long exposure (3500 hours) at 400°C. This corrosion was dominated by so-called LMC (Chapter 3). Ni and Cr dissolved from the surface into the Pb-Bi due to their high solubility for the Pb-Bi [4]. Then, the corroded inner tube surface became porous, and the Pb-Bi could penetrate into the porous area. The depth of the penetration around the ruptured part was much deeper than elsewhere.

This was because the Pb-Bi was repeatedly pushed into the corroded matrix of the inner tube wall by the repeated increase of the inner pressure, which was due to the repeated thermal expansion of Pb-Bi in the heat up process. In the Pb-Bi penetrated region, the grains were surrounded by Pb-Bi, and the grain-grain bond was weakened. The material strength must be weakened. This possibly influenced tube rupture occurrence.

Another possible explanation was that tube rupture in the liquid Pb-Bi was promoted by LME in addition to the corrosion. In the liquid Pb-Bi, the LME can occur simultaneously with loss of the mechanical strength by corrosion. According to the report of Nicholas and Old [10], there are two requirements for the occurrence of the LME, *i.e.* a sufficiently high applied stress to produce plastic deformation and a direct contact between the stressed solid and the embrittler, in this case Pb-Bi. The both of them were satisfied in the present case, although the stress would be difficult to determine accurately in the present case since the tube ruptured in a complex stress system. The direct contact was promoted by the severe penetration of Pb-Bi into the steel matrix or along the grain boundary. Also in ref. [10], the dependence of the reaction temperature on the strain rate of steel in a liquid metal-steel system was described, and the minimum ductility by LME was obtained around the melting point of the embrittler: Pb-Bi. This also agreed with the present case since the melting point of the embrittler, Pb-Bi, was 125°C, and the rupture occurred when increasing from room temperature to 250°C.

In the present case, tube rupture occurred in the low temperature region of the main loop. Corrosion of the inner tube wall exposed to Pb-Bi at low temperature was not so severe. However, the thermal expansion of the Pb-Bi which remained in the tube may promote the corrosion of the inner tube wall, and finally cause the tube rupture. Thus, the Pb-Bi in the low temperature region of the loop must be drained completely into the dump tank after test use, and the Pb-Bi has to be melted and heated in the dump tank not in the main loop.

The Pb-Bi may remain in the tube, if a plugging accident is caused by the freezing of the Pb-Bi in part of the low temperature region of the loop. A possible cause might be a temperature control problem, *e.g.* the malfunction of the heater and/or the thermocouple. As a countermeasure, a spare Pb-Bi drain line should be included in the low temperature region of the loop. Also, a level meter should be installed in the dump tank in order to check the amount of drained Pb-Bi.

8.1.5 Summary

Metallurgical analysis and fractography studies were carried out for a ruptured tube that had been installed in the sampling line of the Pb-Bi forced convection test loop to investigate the major factor of tube rupture in liquid Pb-Bi. The results are summed up as follows:

- (1) The tube rupture was caused by the increase of inner pressure due to the thermal expansion of Pb-Bi in the heat up process of the loop from room temperature to 250°C after a series of corrosion tests. The ruptured tube was deformed locally, and the thickness of the tube wall was reduced around the ruptured part. Particularly at the ruptured part, the outer diameter and the tube thickness were changed from initial 12.7 mm and 1 mm to 16 mm and 0.75 mm, respectively.
- (2) Liquid metal corrosion occurred on the inner tube wall surface was in contact with the liquid Pb-Bi. In the corroded region, the steel alloying elements of Ni and Cr were dissolved into the liquid Pb-Bi, and the liquid Pb-Bi penetrated into the steel matrix. The corrosion around the ruptured part was more severe than elsewhere in the same tube. Around the ruptured part, the thermal expansion of the Pb-Bi in the tube during the temperature increasing process of the sampling line promoted the corrosion.
- (3) The fracture face exhibited a mixed fracture surface with ductile and brittle areas. The area near the outer tube wall had visible dimple marks characteristics of a ductile fracture. The area near the inner tube wall, which was in contact with liquid Pb-Bi, did not have the dimple marks.

8-2 Effect of Corrosion on Performance of pump and flow meter in flowing Pb-Bi

8.2.1 Introduction

Lead bismuth eutectic (Pb-Bi) is one of the candidates for a coolant of fast breeder reactors. The development of an electro-magnetic pump (EMP) which can be used as main circulation pump of the FBRs with Pb-Bi coolant is foreseen to simplify the design. However, key problem is that a corrosion/erosion of the pump core material by liquid Pb-Bi flow and a precipitation of corrosion products in narrow pump channel worsen the performance.

The coolant loop of the Pb-Bi cooled FBR may be divided into a high temperature region around fuel assembly and a low temperature region which is equipped with the EMP and flow meter. Corrosion products from steels in the high temperature region, must contaminate the Pb-Bi. And, it may precipitated in the low temperature region by solubility difference at different temperature [4]. The performance of the EMP and the flow meter may be influenced by the precipitated materials on their surfaces.

In the case of an electro-magnetic flow meter (EM-flow meter), the precipitation of corrosion products on the electrode surface seemed to have little of influence on the wettability. Therefore, the flow meter kept the stable performance during the operation even if a little precipitation occurred. However, in the case of the EMP, precipitation of the corrosion products in narrow pump channel might worsen the performance possibly due to the plugging.

The purpose of the work in this chapter is to investigate the effect of Contamination of liquid Pb-Bi on the performance of Electro Magnetic flow meter and pump.

8.2.2 Experimental Apparatus and Procedure

Pb-Bi forced convective test apparatus

Figure 8-8 (a) shows the schematic of the forced convective Pb-Bi circulation loop which has been used for steel corrosion test. The loop consists of a high temperature region made of 9Cr-1Mo steel and a low temperature region made of SS316 (18Cr-12Ni-2Mo) steel. The heater, the corrosion test section, the oxygen sensor are installed in the high temperature region, and the air cooler, the EMP and the EM-flow meter are in the low temperature region. Pb-Bi is circulated by the EMP at the rated operation flow rate, and the flow rate is measured by the electromagnetic flow meter.

Figure 8-8 (b) shows the geometries of the electrode of the EM-flow meter used in the present study. This type has simple geometry, but the wettability of not only electrode surface but also channel-wall surface has influence on the electro motive force

(EMF) because of no electrical insulation between the electrode and the channel wall. The electrode was made of SS316. The tips of the electrodes were plated with Au and Rh with 1 μm and 10 μm in thickness, respectively, to avoid initially the formation of the oxide layer which caused contact resistance and worsened the wettability.

The EMP is a linear induction type with an annular gap between a cylindrical core and a circular duct. The main specification of the EMP are as follows: flow rate 0-6.0 L/min, annular channel gap 1.35 mm, frequency 50 kHz, inner duct diameter 34.0 mm, outer duct diameter 42.7 mm, duct thickness 3.0 mm, phase voltage 200 V. The geometry of the pump core was schematically shown in **Fig. 8-8 (c)**. Pb-Bi enters the pump from the horizontal pipe and flows through the annular channel. The pump core and the outer duct are made of SS316. The core is welded and fixed at upstream part and that at downstream part is axially free without welded to relieve axial thermal expansion of the core. The EMP system is ungrounded, which could reduce the disturbance in the magnetic fields. Electrodes and electro-magnetic flow meter, (c) Circular duct and core of electro-magnetic pump

Test condition

The Pb-Bi forced convection loop was operated for steel corrosion tests in the corrosion test section at the temperature of 550°C. The performance of the EMP was evaluated after a series of the operations listed in **Table 8-3**. The oxygen concentration that was varied might not influence the corrosion behavior of the pump core since all the oxygen potentials were higher than that required for the formation of Fe_3O_4 at the temperature of 400°C.

Metallurgical analysis

After the operation for the third corrosion test, the electrode of the flow meter was taken out of the test loop, and the cross section of the electrode was observed by scanning electron microscope (SEM) and the energy dispersive X-ray analyzer (EDX). After the fourth corrosion test, the pump core was removed from the EMP duct. The core was cut into test pieces without removal of adhered Pb-Bi, and the test pieces were analyzed by the SEM/EDX.

8.2.3 Effect of Corrosion on Performance of Electro-Magnetic Flow Meter

The EMF of the electro-magnetic flow meter was stable during the operations for the third and fourth corrosion tests. **Fig. 8-9 (a)** shows the calibration curves obtained before and after the 1000 hour-operation for the third corrosion test. It is found that the calibration curves agree well with each other.

The cross section of the electrode observed by SEM/EDX after the operation for the third corrosion test is shown in **Fig. 8-9 (b)**. The plated Rh and Au on the surface were not observed. Rh and Au might be dissolved and flow out during 1000 hour-exposure. Some lumps, which was round in shape and approximately 20 μm in diameter, shown in **Fig. 8-9 (c)** might be a corrosion product precipitated on the electrode surface. The results of EDX analysis indicated that the composition of the metal elements in the lump were Fe-96.85wt%, Cr-0.46wt%, Ni-0.02wt%, Mo-0.92wt%, Si-0.2wt%, Pb-0wt% and Bi-0wt%, which means that the lumps are made of Fe. These facts indicated that the precipitation of corrosion products on the electrode surface during 1000 hour-operation did not influence the performance of the electro-magnetic flow meter.

8.2.4 Effect of Corrosion and Precipitation on Performance of Electro Magnetic Pump

During the third and the fourth corrosion test, the flow rate which was monitored by the electro-magnetic flow meter (chapter 8.2.3) decreased as shown in **Figs. 8-10 (a) and (b)**.

Figure 8-10 (a) shows that the flow rate decreased in 200 hour-intervals in the third corrosion test in spite that an applied voltage in EMP was increased repeatedly to keep the flow rate constant. Although the voltage of 50 V was applied in the EMP to keep the flow rate of 3 L/min within the operation for initial 300 hours, voltage of 65 V was required to keep the constant flow rate, finally.

Figure 8-10 (b) shows that the flow rate decreased in short-time intervals in the operation for the fourth corrosion test. Around the time of 400 hours, the drop of the flow rate was relatively large. The voltage applied to the EMP was increased in the same manner of the third corrosion test.

These facts suggest that the performance of the EMP became worse during the operations for the corrosion tests. It might be caused by the plugging of the flow channel by precipitation of corrosion products produced by corrosion in the high temperature region and transported into the low temperature region.

8.2.5 Precipitation of corrosion products

Figures 8-11 (a) to (c) show the appearance of the pump core after the series of operations for the corrosion tests. The surface color of the pump core changed from initial metallic luster to black as shown in Fig. 8-11 (a), which means that oxide layer was formed or corrosion products were precipitated on the surfaces.

In the part A, there was no corrosion and erosion on the pipe wall. Fig. 8-11 (b) shows the front view of the core head upstream (Part B) and downstream (Part D). Severe erosion was observed on the surface of the EMP core head upstream (Part B). However, the other part of the EMP core was not eroded as shown in Figs. 8-11 (b) and (c).

These facts imply that the corrosion behavior on the surface of the EMP core head (Part B) was exceptional compared with those on the other part. That is because Pb-Bi flowed into the pump core, and then the flow collided with only front part of the core head. Pb-Bi penetrated into the steel matrix, which might weaken the surface. Then, the erosion was caused in the way that the weakened area was destroyed by normal and shear stresses of the flow in the complex shape of the inlet part.

Figures 8-12 (a) to (f) show the results of SEM/EDX analysis for the core head upstream (part B). In top region (Fig. 8-12 (a)), the steel matrix was locally eroded to the depth of approximately 100 μm , and Pb-Bi adhered to the eroded region. Pb-Bi penetration in the steel matrix, the condition of which was similar to that reported in Chapter 3 was observed in the eroded part.

Fig. 8-12 (b) shows that the surface was eroded at the bottom of the spacer, and Pb-Bi adhered to the eroded region. In the adherent Pb-Bi, the lump of Fe with the diameter of approximately 10 μm were observed. The lump might be a precipitation product since the shape and the components were similar to that reported in ref [11]. As the same as area (a), Pb-Bi penetration into the steel matrix was observed in the eroded part. Fig. 8-12 (c) shows that Pb-Bi selectively penetrated along the welded part between the ring spacer and the spacer. This means that the area sensitized by the welding process was weaker for Pb-Bi corrosion than the other part. In the adherent Pb-Bi, the some lump of Fe was observed. Fig. 8-12 (d) shows the magnified view of the corrosion products. The size and component were similar to those of the area shown in Fig. 8-12 (b). Fig. 8-12 (e) shows that the corrosion product, which consisted of small Fe lumps with the diameter of approximately 10 μm , adhered to the surface of the ring spacer. The lump contained Pb-Bi inside. The size of the corrosion products is 100 μm in width and 50 μm in height. Fig. 5 (f) indicated that the corrosion products adhered to the surface of core part (e). The size of the corrosion products was 50 μm in width and 50 μm in height.

Figures 8-13 (a) and (b) show the results of SEM/EDX analysis for the core head downstream (part D). The surface was smooth without any corrosion.

Figure 8-13 (a) shows that the corrosion products with the diameter of 40 μm had double layer structure. The component of the outer layer was Fe of 90wt% and Pb-Bi of 10wt%. That of inner layer (diameter range of 0-20 μm) was 99wt% Fe. Pb and Bi were enriched in the interface between the inner layer and the outer layer. The outer layers of

corrosion products were merged with adherent Pb-Bi as if the interface was not clear. **Fig. 8-13 (b)** shows that corrosion products which has double layer structure adhered to the surface.

The corrosion products, which were mainly composed of Fe, might be precipitated on the surface of the pump core due to the difference in solubility with the temperature difference of 150°C in the loop. The size of 20 µm in diameter and the components of the precipitation material in the present study were similar to those in the precipitation material in liquid Pb-Bi reported by Kikuchi et al. [11]. More precipitation materials were observed in the outlet part than in the inlet part. The precipitation products which were combined with each other were also observed. The precipitation products could be the cause of channel plugging that worsened the performance during the operation. Then, the strong magnetic fields in EMP may have influence on trap of Fe in the channel and promote the plugging.

The precipitated material had the double layer structure. The inner layer should contain Pb-Bi, if the precipitation is not finished completely in Pb-Bi. However, the analysis results indicated that the inner layer did not contained Pb-Bi. Therefore, the precipitation must be finished in the inner layer. On the contrary, the outer layer contained Pb-Bi. It indicated that the precipitation did not finish in the outer layer. Then, the precipitation mechanism can be summarized as that the precipitation occurs step by step from the inner layer to the outer one. The double layer structure might be caused by difference of the precipitation period.

Erosion occurred at the inlet of the pump core. In the eroded part, Pb-Bi was penetrated into the steel matrix. Thus, the erosion mechanism may be explained as follows: Pb-Bi penetration into the steel matrix weakened the surface, and the weakened area was destroyed by dynamic normal and shear stresses. However, Fe in the steels might not dissolve since the Fe concentration in Pb-Bi was saturated in the low temperature region as the precipitation of the Fe in adhered Pb-Bi was observed. Therefore, dissolution of Ni or Cr into Pb-Bi from the steel matrix might be the cause of erosion.

8.2.6 Summary

The corrosion and precipitation behaviors were investigated on the electrode surface of an electro-magnetic flow meter and the surface of an electro-magnetic pump (EMP) core to clarify the effect of the corrosion of precipitation on the performance of the EMP. The results are summed up as follows:

- (1) Some round lumps approximately 20 μm in diameter were precipitated on the electrode surface. The main metal elements in the lump were Fe.
- (2) The erosion was observed only at the entrance of EMP flow channel. In the eroded part, Pb-Bi penetrated into the steel matrix, which might weakened the surface and caused the erosion in the way that the weakened area was destroyed by normal and shear stresses of the flow in the complex shape of the inlet part.
- (3) The precipitation products were made of a double-layer structure. The inner layer (diameter range of 0-20 μm) contained Fe in the fraction of 99wt%, and the outer layer (diameter range of 20-40 μm) contained Pb-Bi in the fraction of 10wt%. The double layer structure might be caused by difference of precipitation period. These precipitation products could be the cause of channel plugging.

8.3 Conclusions

The phenomena of tube rupture and precipitation of corrosion products in the liquid Pb-Bi were metallurgically investigated.

In *Chapter 8.1*, it was found that the Pb-Bi penetrated tube had weaker mechanical strength than the normal tube. The use of corrosion resistant materials (explained in *Chapter 6 and 7*) as the tube material must inhibit the penetration type corrosion in the liquid Pb-Bi. Then, the tube can keep the mechanical strength in the liquid Pb-Bi, and avoid the occurrence of the tube rupture.

In *Chapter 8.2*, it was found that the precipitated material was Fe, which was dissolved from the steels in the liquid Pb-Bi in the high temperature region of the loop. Therefore, the use of corrosion resistant material (explained in *Chapter 6 and 7*) as the structural material in the high temperature region of the loop may inhibit the dissolution of their alloying elements from the materials into the flowing Pb-Bi, and this can stop the occurrence of the precipitation, consequently.

Reference

- 1) M. Takahashi, M. Igashira, T. Obara, H. Sekimoto, K. Kikuchi, K. Aoto and T. Kitano, "Studies on Materials for Heavy-Liquid-Metal-Cooled Reactors in Japan", *Proc. of 10th Int. Conf. Nuc. Eng.*, Arlington, VA, Apr. 14-18, 2002, ICONE10-22166 (2002).
- 2) S. Uchida, H. Osada, Y. Kasahara, M. Takahashi and K. Hata, "A Feasibility Study on the Lead-bismuth Cooled Direct Contact Boiling Water Fast Reactor", *Proc. of 11th Int. Conf. Nuc. Eng.*, Tokyo, Japan, Apr. 20-23, 2003, ICONE11-36320 (2003).
- 3) B.F. Gromov, Yu.S. Belomitcev, E.I. Yefimov, M.P. Leonchuk, Yu.I. Orlov, Yu.I. Pankratov, Yu.G. Pashkin, G.I. Toshinski, V.V. Chekunov, B.A. Shmatko, V.S. Stepanov, "Use of lead-bismuth coolant in nuclear reactors and accelerator-driven systems", *Nuc. Eng. Design*, **173**, 207 (1997).
- 4) B.F. Gromov, Y.I. Orlov, P.N. Martynov, V.A. Gulevsky, "The problems of technology of the heavy liquid metal coolants (Lead-bismuth, Lead)", *Proc. of HLMC1998*, Obninsk, Russia, Oct. 5-9, 87 (1998).
- 5) C. Fazio, G. Benamati, C. Martini, G. Palombarini, "Compatibility tests on steels in molten lead and lead-bismuth", *J. Nucl. Mater.*, **296**, 243 (2001).
- 6) G. Benamati, C. Fazio, H. Pinakova, A. Rusanov, "Temperature effect on the corrosion mechanism of austenitic and martensitic steels in lead-bismuth", *J. Nucl. Mater.*, **301**, 23 (2002).
- 7) A. Legis, G. Nicaise, J.-B. Vogt, J. Foct, "Liquid metal embrittlement of the martensitic steel 91: influence of the chemical composition of the liquid metal experiments and electronic structure calculations", *J. Nucl. Mater.*, **301**, 70 (2002).
- 8) H. Glasbrenner, D. Viol, "Tensile testing of MANET II in flowing Pb-Bi alloy at elevated temperature", *Fusion Eng. and Design*, **61**, 691 (2002).
- 9) E.H. Pylchenkov, "The Issue of Freezing-Defreezing Lead-Bismuth Liquid Metal Coolant In Reactor Facilities Circuit", *Proc. of HLMC1998*, Obninsk, Russia, Oct. 5-9, 110 (1998).
- 10) A.G. Nicholas and C.F. Old, "Review of Liquid metal embrittlement", *Journal of material science*, **14**, 1 (1979).
- 11) K. Kikuchi, T. Sasa, S. Ishikura, K. Mukugi, T. Kai, N. Ouchi, I. Ioka, "Current status of JAERI spallation target material program", *J. Nucl. Mater* **296** (2001) 34-42

Table 8-1 Temperature change of Pb-Bi sampling line

Process	Heating		Cooling	
	RT-250	250-400	400-250	250-RT
Temperature change (°C)				
Total number of temperature change cycles	23	23	23	23

Table 8-2 Total exposure time of Pb-Bi sampling line

Temperature (°C)	250	300	350	400
Total exposure time (hour)	622	50	4	3440

Table 8-3 EMP operating conditions

	1st corrosion test	2nd corrosion test	3rd corrosion test	4th corrosion test
Temperature of pump core (°C)	400	400	400	400
Temperature of hot region (°C)	550	550	550	550
Flow rate (L/min)	2	2	1	1
Test time (hour)	959	1000	1000	500
Oxygen concentration (wt%)	5×10^{-7}	1×10^{-9}	1.7×10^{-8}	1.7×10^{-8}

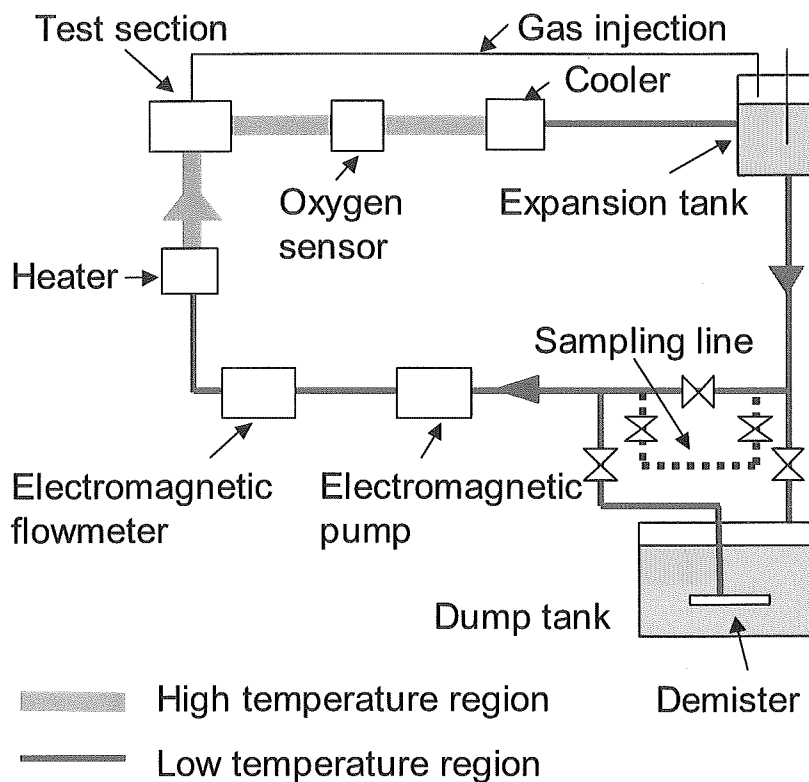


Fig. 8-1 Pb-Bi forced convection test loop

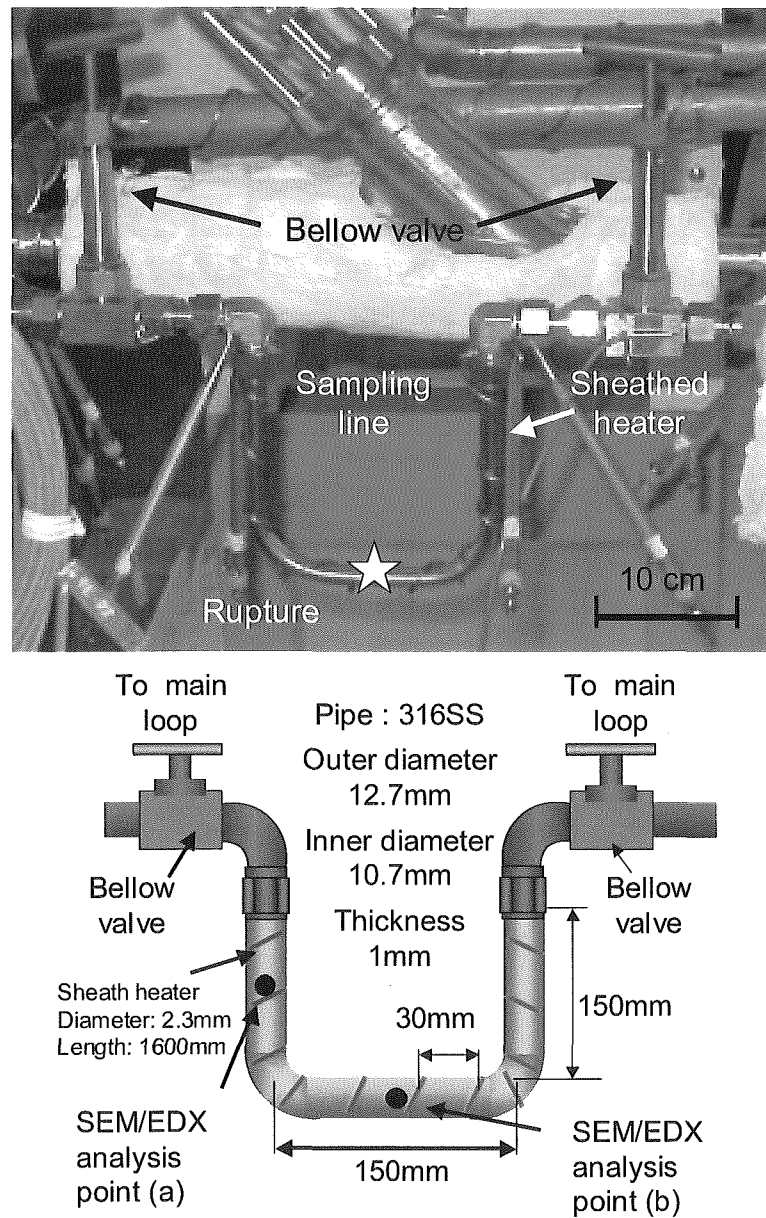


Fig. 8-2 Schematic and photo of Pb-Bi sampling line in Pb-Bi forced convection test loop

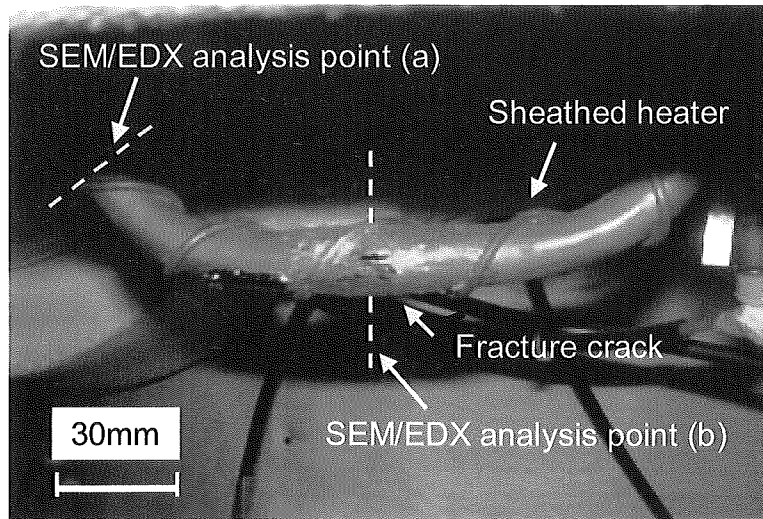


Fig. 8-3 View of ruptured tube

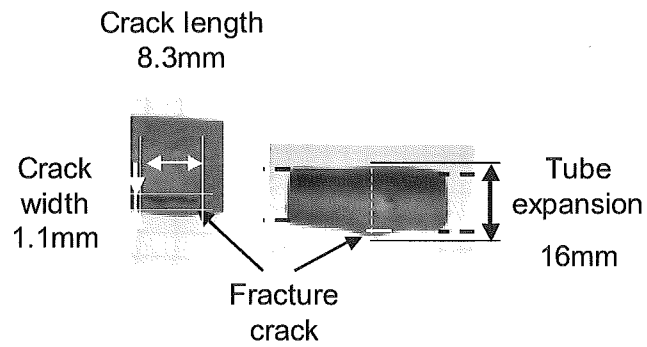


Fig. 8-4 Size of fracture crack and deformation of ruptured tube

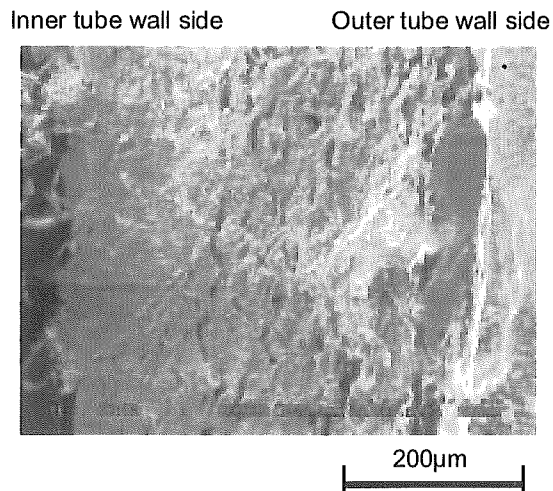


Fig. 8-5 SEM image of fractured face

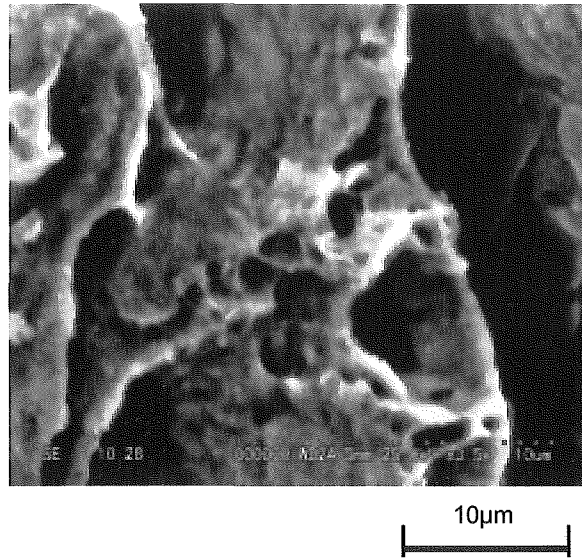


Fig. 8-6 Dimple marks observed on the outer side of fractured face

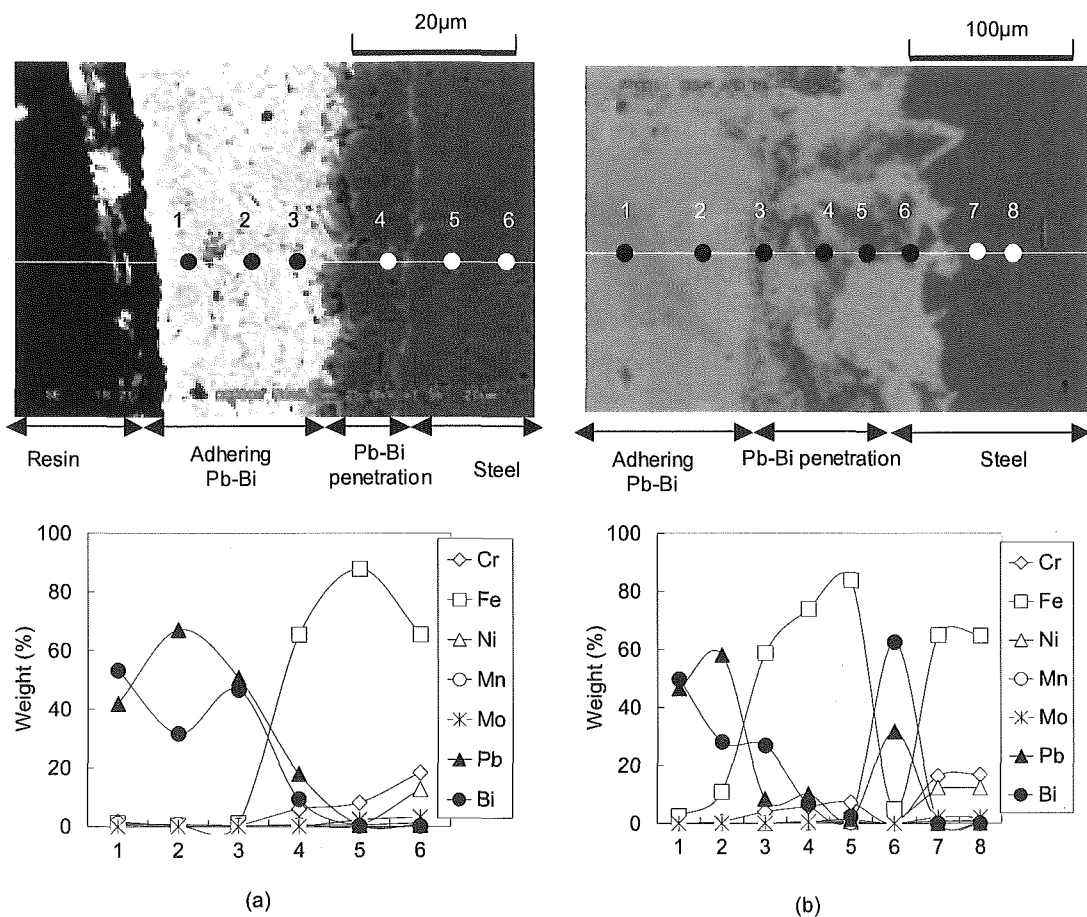


Fig. 8-7 SEM images and component profiles: analysis point (a) distant from ruptured part; analysis point (b): near ruptured part

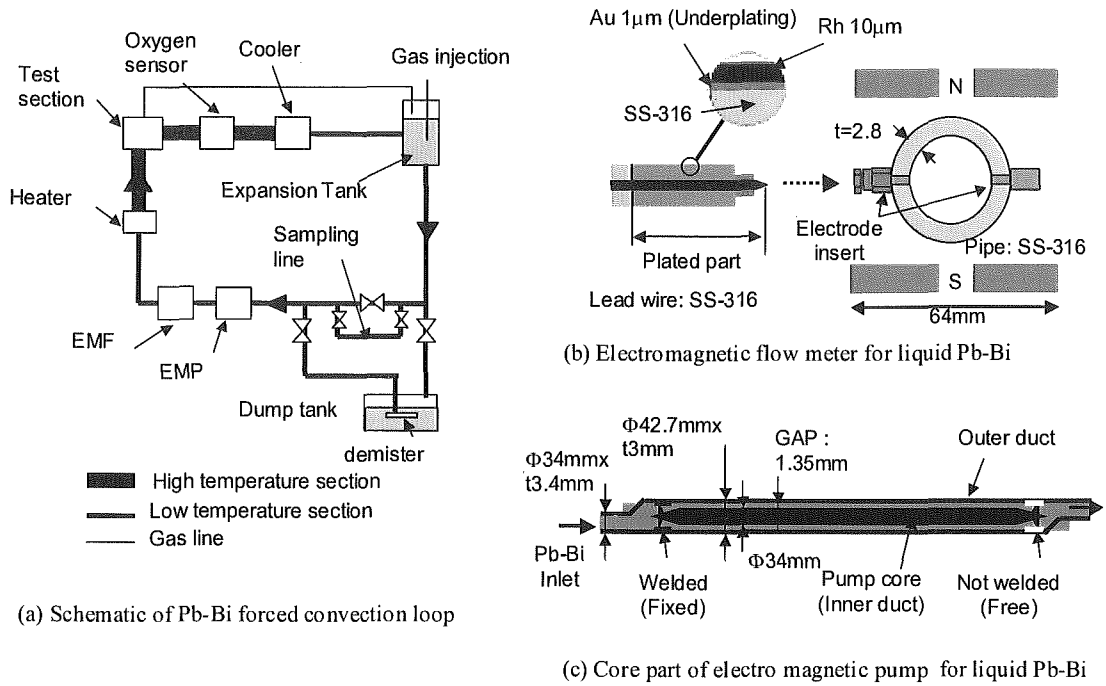


Fig. 8-8 Schematic of experimental apparatus, (a) Pb-Bi forced convective loop, (b) Electrodes and electromagnetic flow meter, (c) Circular duct and core of electromagnetic pump

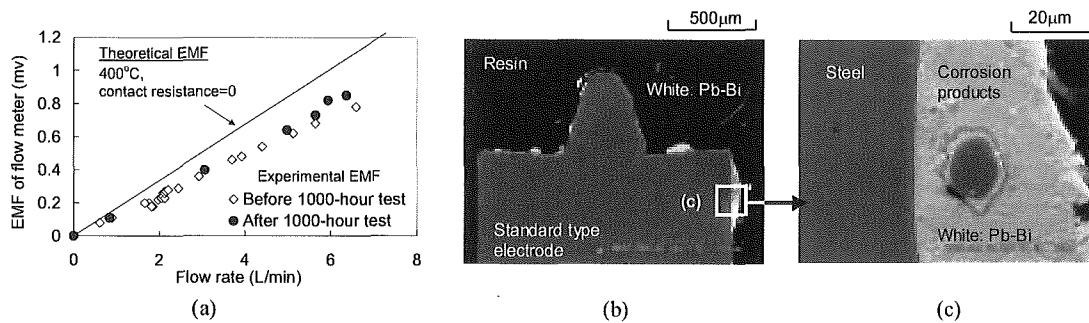


Fig. 8-9 (a) EMF calibration curves before and after the operation for the third corrosion test and after test; (b) and (c) Corrosion and precipitation on the surface of electrode of electro-magnetic flow meter after the operation for the third corrosion test

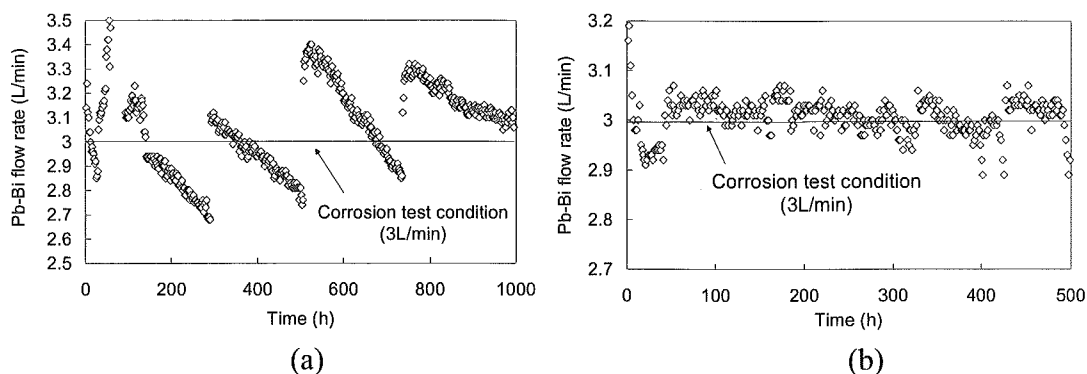


Fig. 8-10 Decreases in Pb-Bi flow rate during operations for
(a) third corrosion test and (b) fourth corrosion test

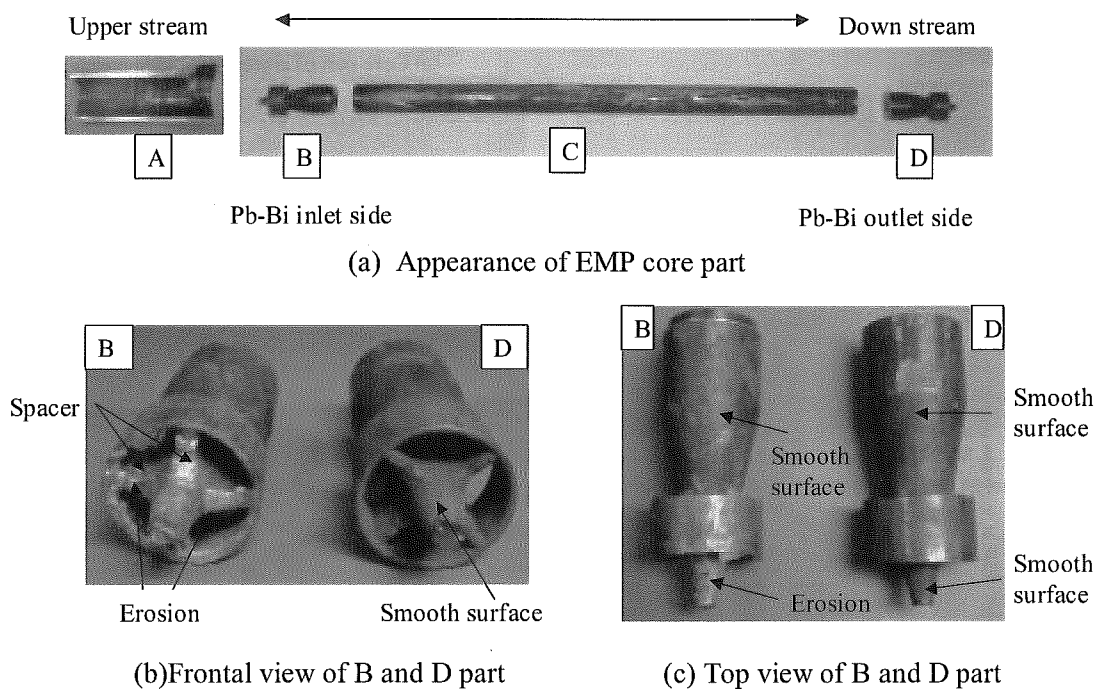


Fig. 8-11 Appearance of EMP core after fourth corrosion test,
(a) EMP core part, (b) frontal view of EMP core head, (c) top view of EMP core head

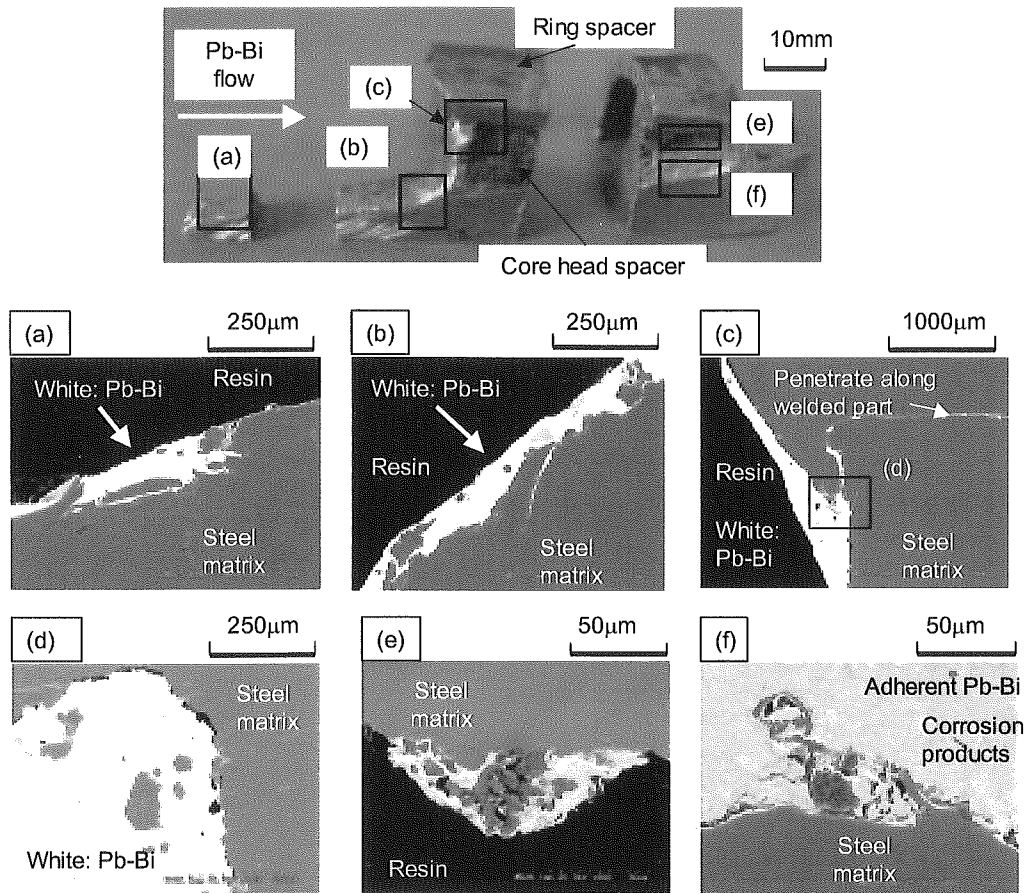


Fig. 8-12 Corrosion and precipitation of EMP core head, (a) erosion at top of core head, (b) erosion at the bottom of spacer, (c) Pb-Bi penetration along welded part, (d) enlarged view of (c), (e) lump of corrosion products adhered on surface of ring spacer, (f) lump of corrosion products adhered on surface of EMP core

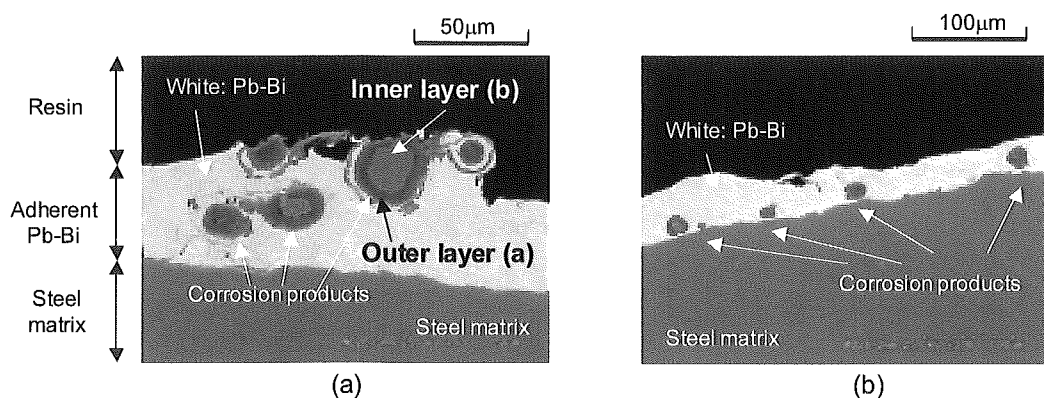


Fig. 8-13 Corrosion products on surface of EMP core down stream, (a) double layer corrosion products in adhered Pb-Bi, (b) corrosion products adhered on surface of EMP core downstream.

Chapter 9

Conclusions

Conclusions

In order to outline the corrosion control by using corrosion resistant materials and chemical control technique in the flowing Pb-Bi, the corrosion characteristics of various materials were investigated and oxygen control system was developed. The following conclusions are drawn from the study above.

In the *Chapter 2*, it was found that the solid electrolyte type oxygen sensor had reliability in the long-term use in the flowing Pb-Bi. The performances of the sensor cells made of yttria stabilized zirconia and magnesia stabilized zirconia were the same, even though the former one caused the erosion. With this oxygen sensor, the performance of the mass exchanger type oxygen control system was investigated. The oxygen exchange between the flowing Pb-Bi and PbO was depended on the solubility of the oxygen in Pb-Bi, that is, the oxygen concentration depended on the reaction temperature of the PbO sinter with Pb-Bi. According to a calculation applying the Nernst equation to the EMF signals, the oxygen concentration was controlled between 1×10^{-5} wt% (temperature of PbO sinter: 315°C) and 3×10^{-6} wt% (temperature of PbO sinter: 280°C). This indicated that the oxygen concentration in the Pb-Bi flow controlled in the corrosion-inhibited region.

In the *Chapter 3*, the mechanism of erosion and corrosion of steels in the flowing Pb-Bi was investigated. It was found that the liquid metal corrosion (LMC), or Pb-Bi penetration into steels occurred in all the steels, and severe erosion took place in some of the steels under low oxygen concentration of 1.57×10^{-10} wt% in the flowing Pb-Bi. It was confirmed that the erosion was caused by hydrodynamic carrying away of weakened surface materials due to Pb-Bi penetration. The large-scale erosion could be caused by the detachment of lumps of corroded materials that had defects formed by dissolution of alloying elements.

In the *Chapter 4*, the corrosion test was performed at the oxygen potential higher than that for the formation of Fe oxide in order to inhibit severe LMC, which was explained in the *Chapter 3*, by the formation of oxide layer on the steels. In the work, the oxygen measurement technique explained in the *Chapter 2* was used. Consequently, the LMC was inhibited by single or multiple oxide layers formed on the steel surfaces. The oxide layers can be classified to an inner layer and an outer one. The existence of the inner oxide layer might be more important for the corrosion resistance since the inner one was compact and stuck to the steel surface while the outer one was easily broken into small pieces with cracks and peeled from the substrate. It was found that an oxidation corrosion was caused by the detachment of the unstable oxide layers in the flowing Pb-Bi.

In the *Chapter 5*, the effects of surface roughness of steels and pre-oxidation of steels on oxidation corrosion in the flowing Pb-Bi, which was partly explained in the *Chapter 4*, were studied experimentally.

The corrosion characteristics of pre-oxidized steels were investigated by means of short term corrosion test with the specimens of SS430 SS405, SUH3, STBA26, SS316 and SCM420, which were pre-oxidized in moist air at the temperature of 500°C, partial pressure of water vapor of 92.5mmHg and oxidation time of 12, 24 and 72 hours. The weight losses of the pre-oxidized steels were lower than those of the test pieces without pre-oxidation, which means that the initial corrosion was inhibited by the existence of the preformed layers. However, the pre-formed oxide layer could not be observed possibly because they were flowed out by the heavy density fluid flow. The layer different from the preformed one was observed. Then, it can be concluded that the preformed oxide layer was effective only for initially. And, the self-healed oxide layer was formed and the layer inhibited the corrosion after the flowed out of the preformed oxide layers.

The effect of surface roughness of the steels on the corrosion behaviors was investigated by the expose of the specimens, which had the surface of smooth, rough and their middle roughness, in the flowing Pb-Bi at the temperature of 550°C. As the test steels, 12Cr- and 9Cr- steels were selected. In the surface-smoothened specimens, compact oxide layers were formed on the surfaces. In the surface-roughened specimens, oxide layers with cracks were detected on their surfaces, and the cracks mainly existed around the convex part of the substrate. This implies that frictional and shear stress by the heavy density Pb-Bi flow concentrated in the layer at the convex part of the substrate. The rough surface of the steels promoted the oxidation corrosion in the flowing Pb-Bi.

In the *Chapter 6*, the effect of alloying elements, Cr, Si, and Al in steels on corrosion resistance was investigated. First, the corrosion characteristics of high Cr steels were investigated by means of corrosion tests with the specimens of steels, which have various contents of Cr, in the flowing Pb-Bi. SS430 (18-Cr steel) showed excellent corrosion resistance after the exposure in the flowing Pb-Bi at 550°C up to 2,000 hours. The weight loss of the SS430 specimen in the Pb-Bi flow was lower than those of the other steels. This is because the SS430 steel formed the Cr rich single layer, and the Cr-rich layer had resistance not only for the LMC but also for the oxidation corrosion in the flowing Pb-Bi.

Then, the corrosion resistance of Si- and Al-rich steels in the flowing Pb-Bi was studied experimentally. The specimens of SUH3 (10Cr-1Mo-2Si), NTK04L (18Cr-3Al) and Recloy10 (18Cr-1Al-1Si) were exposed to the Pb-Bi flow at the temperature of 550°C up to 2,000 hours. The oxygen concentration in the flowing Pb-Bi was higher than that for the formation of the oxide of Al, Si, Cr and Fe. After the exposure, the surface of the Si-rich steel, SUH3, was kept smooth with no liquid metal corrosion (LMC). On the surface, thin oxide layer was formed. The layer had a double layer structure that consisted of an unstable outer layer and a compact inner one. The inner layer worked as barrier for the LMC, while detachment of the outer layer could cause oxidation corrosion. As for the Al-rich steel, NTK04L, an Al-rich single layer was formed and stuck on the surface. This layer protected the matrix from the LMC. Oxidation corrosion did not occur on the steel, since this layer was oxidation resistant even in the condition of high oxygen potential. The weight losses of the NTK04L steel

in 500-hour and 2000 hour-exposure were negligibly small. As for Al- and Si-rich steel, Recloy10, an Al- and Si-enriched single layer was formed on the surfaces. The property of the layer was similar to that in the NTK04L steel. The weight loss of the Recloy10 steel was also negligibly small.

From these results, it was found that high Cr steel, such as SUS430 (18Cr) steel, had corrosion resistant in the flowing Pb-Bi even at high oxygen concentration. Al and Si around 1-3wt% in steels drastically improved the oxidation corrosion resistance in the flowing Pb-Bi. Thus, the corrosion of the steels in the flowing Pb-Bi in the oxygen concentration higher than that for the formation of Fe-oxide can be inhibited by the use of Cr-, Si- and/or Al- rich steels.

In the *Chapter 7*, corrosion characteristics of SiC and Si₃N₄ ceramic materials in the flowing Pb-Bi were investigated. It was found that the specimens of SiC and Si₃N₄ kept smooth surface without a corrosion and an oxidation in the Pb-Bi. Although the surface showed several cracks, the Pb-Bi was not diffused in the cracks. These cracks might be caused by a shear and/or normal stress of the heavy density Pb-Bi flow. The weight loss of the SiC and Si₃N₄ specimens in the flowing Pb-Bi was negligibly small. Thus, the ceramic materials, such as SiC and Si₃N₄, can be used in the flowing Pb-Bi, even though the improvement of mechanical properties is necessary to avoid the occurrence of the cracks on the surfaces.

In the *Chapter 8*, metallurgical analysis for the ruptured tube and precipitated material in the flowing Pb-Bi was carried out. The tube rupture occurred while the loop temperature was being increased from room temperature to 250°C. The rupture occurred for a tube which had been used with Pb-Bi at 400°C for 3,500 hours and 23 increasing temperature cycles. The tube expanded locally around the ruptured part, which indicated that the rupture was caused by the thermal expansion of the Pb-Bi in the tube. More severe liquid metal corrosion was observed at the inner tube surface around the ruptured part than elsewhere in the tube. The fracture mechanism in the rupture face could be classified into two types, *i.e.* brittle fracture without any sign of dimple marks in the inner region of the tube wall and ductile fracture in the outer region of the tube wall. By the analysis of the precipitated materials on the immersion part of the electro magnetic pump, it was found that the Fe precipitated in the flowing Pb-Bi in the low temperature region of the loop by the temperature drop. By using corrosion resistant structural material such as explained in *Chapters 6 and 7* in the loop, the penetration of the Pb-Bi into the steels is inhibited, and the tube will keep the regular mechanical properties in the flowing Pb-Bi. Also, the dissolution of the alloying elements of the steels into the flowing Pb-Bi in the high temperature region must be drastically decreased. Then, The amount of the Fe precipitate will be decreased.

List of Publications

List of Publications

Refereed Journals

- (1) M. Kondo, M. Takahashi, T. Suzuki, K. Ishikawa, K. Hata, S. Qiu and H. Sekimoto, "Metallurgical study on erosion and corrosion behaviors of steels exposed to liquid lead-bismuth flow", J. Nucl. Mater., **343**, 349-359 (2005) **(Relevant to Chapter 3)**.
- (2) M. Kondo, M. Takahashi, N. Sawada and K. Hata, "Corrosion of Steels in Lead-Bismuth Flow", J. Nucl. Sci. and Technol., **Vol.43**, No.2 107-116(2005) **(Relevant to Chapter 4)**.
- (3) M. Kondo and M. Takahashi, "Metallurgical Analysis for Ruptured Tube in Lead Bismuth Corrosion Test Facility", J. Nucl. Sci. and Technol., **Vol.43**, No.2 174-178 (2005) **(Relevant to Chapter 8-1)**.
- (4) M. Kondo and M. Takahashi, "Metallurgical study on electro-magnetic flow meter and pump for liquid lead-bismuth flow", Progress in Nuclear Energy, **47/1-4**, pp. 639-647 (2005) **(Relevant to Chapter 8-2)**.
- (5) M. Kondo and M. Takahashi, "Corrosion Resistance of Al- and Si- Rich Steels in Lead Bismuth Flow", J. Nucl. Mater., *under review* **(Relevant to Chapter 6-2)**.
- (6) M. Kondo and M. Takahashi, "Study on Control of Oxygen Concentration in Lead Bismuth Flow Using Lead Oxide Particles", J. Nucl. Mater., *under review* **(Relevant to Chapter 2-2)**.
- (7) A. Heinzl, M. Kondo and M. Takahashi, "Corrosion Investigations of Steels with Surface treatment and Al-Alloying by GESA Exposed in Lead-Bismuth", J. Nucl. Mater., *in press* (2006).
- (8) M. Kondo and M. Takahashi, "Corrosion Resistance of Ceramic Materials, SiC and Si₃N₄ in Flowing Lead-Bismuth", *to be submitted* **(Relevant to Chapter 7)**.
- (9) M. Kondo and M. Takahashi, "The use of solid electrolyte type oxygen sensor in flowing Pb-Bi and corrosion of sensor materials", *to be submitted* **(Relevant to Chapter 2-1)**.
- (10) M. Kondo and M. Takahashi, "Effect of Surface Roughness of Steels on Corrosion in a Liquid Lead-Bismuth Flow", *to be submitted* **(Relevant to Chapter 6-1)**.

International Congress/ Seminar/ Symposium

- (11) M. Kondo, K. Hata and M. Takahashi, "Design of Material Strength Test in Lead Bismuth Flow", Proc. of 10th Int. Conf. On Nucl. Eng. (ICONE-10), ICONE10-22736, April 14-18, Arlington, VA, (2002).
- (12) M. Takahashi, M. Kondo, N. Sawada and K. Hata, "Corrosion of Steels in Lead Bismuth FLOW", Proc. of Int. Conf. of Global 2003, New Orleans, USA, 2104-2112, (2003). **(Relevant to Chapter 4)**
- (13) M. Kondo and M. Takahashi, "Experimental Study on Erosion/corrosion Behavior of Stainless Steel in a Liquid Lead Bismuth Flow" 6th International Workshop on Spallation Materials Technology (IWSMT6), Nov. 30-Dec. 5, Hayama, Kanagawa, Japan (2003). **(Relevant to Chapter 3)**
- (14) M. Takahashi, M. Kondo, N. Sawada, S. Yoshida and K. Hata, "Experimental Study on Steel Corrosion in a Pb-Bi", Proc. of Conf. of Heavy Liquid Metal Coolants in Nuclear Technology 2003, Obninsk, Russia (2003). **(Relevant to Chapters 3 and 4)**
- (15) M. Takahashi, T. Iguchi, A. Otsubo, M. Kondo, A. Yamada, S. Yoshida, N. Sawada, Y. Hoshi, Y. Qi, H. Nei, T. Obara, H. Sekimoto, K. Hata, K. Hara, S. Uchida, H. Osada, Y. Kasahara, K. Matsuzawa, N. Sawa, Y. Yamada, K. Kurome, K. Koyama, Y. Okubo, O. Watanabe and K. Ara, "Research Study for Development of Pb-Bi Cooled Direct Contact Boiling Water Small Fast Reactor", 2003 Annual physics Seminar proc., Oct.2, 2003, Bandung, Indonesia (2003). **(Relevant to Chapter 1)**
- (16) M. Takahashi, T. Obara, T. Iguchi, A. Otsubo, M. Kondo, Y. Qi, M. Matsumoto, E. Yusiabni, T. Akashi, A. Yamada, H. Nei, K. Hata, K. Hara, S. Uchida, H. Osada, Y. Kasahara, K. Matsuzawa, N. Sawa, Y. Yamada, K. Kurome and Y. Okubo, "Design and Experimental Study for Development of Pb-Bi Cooled Direct Contact Boiling Water Small Fast Reactor (PBWFR)" Proc. of Int. Cong. on Advanced Power Plant 2004 (ICAPP'04), Paper 4058, Pittsburgh, PA, USA, June 13-17, (2004). **(Relevant to Chapter 1)**
- (17) M. Kondo, M. Takahashi, S. Yoshida, N. Sawada, A. Yamada and K. Hata, "Experimental Studies on Pb-Bi Flow Technology and Steel Compatibility with Pb-Bi", Proc. of 12th Int. Conf. On Nucl. Eng. (ICONE-12), ICONE12-49285, April 14-18, Arlington, VA (2004). **(Relevant to Chapter 4)**
- (18) M. Kondo, M. Takahashi, A. Yamada, K. Ishikawa, N. Sawada and T. Suzuki, "Metallurgical Study on Performance of Electro magnetic Flow Meter For

- Liquid Lead-Bismuth”, Proc.of 12th Int. Conf. On Nucl. Eng. (ICONE-12), ICONE12-49218, April 14-18, Arlington, VA (2004). **(Relevant to Chapter 8-2)**
- (19) M. Kondo, M. Takahashi, S. Yoshida and N. Sawada, “Effect of Surface Roughness of Steels on Oxide Layer Formation in a Liquid Lead-Bismuth Flow”, Proc. of Int. Cong. on Advanced Power Plant 2004 (ICAPP’04), June 13-17, Paper 4044, Pittsburgh, PA (2004). **(Relevant to Chapter 5-2)**
- (20) M. Kondo and M. Takahashi, *Corrosion of steels in Lead-Bismuth Flow*, COE-INES International Workshop on Design and R&D of Pb-Bi Cooled Reactors, Nov.8 and 9, Tokyo Institute of Technology, Tokyo, Japan (2004). **(Relevant to Chapter 6)**
- (21) M. Kondo and M. Takahashi, “Corrosion characteristics of Pre-Oxidized Stainless Steels in Pb-Bi”, Proc. of Int. Cong. on Advanced Power Plant 2005 (ICAPP’05), May 15-19, Paper 5187, Seoul, Korea (2005). **(Relevant to Chapter 5-1)**
- (22) M. Kondo and M. Takahashi, “Control of Oxygen Concentration in Lead-Bismuth Flow by Temperature Control of Solid Lead Oxide”, Proc. of Int. Cong. on Advanced Power Plant 2005 (ICAPP’05), Paper 5190, May 15-19, Seoul, Korea (2005). **(Relevant to Chapter 2-2)**
- (23) M. Hirabayashi, M. Kondo, K. Ara and M. Takahashi, “Development of Ultrasonic Flow Meter for Liquid Lead-Bismuth”, Proc.of 13th Int. Conf. On Nucl. Eng. (ICONE-13), ICONE13-50001, May 16-20, Beijing, China, 2005. **(Relevant to Chapter 1)**
- (24) M. Kondo and M. Takahashi, “Control of Oxygen Concentration in Lead-Bismuth Flow”, The 7th International Workshop on Spallation Materials Technology (IWSMT-7), May 29-June 3, Thun, Switzerland. (2005) **(Relevant to Chapter 2-2)**
- (25) M. Kondo and M. Takahashi, “Corrosion Resistance of Si- and Al-Rich Steels in Flowing Lead Bismuth”, The 7th International Workshop on Spallation Materials Technology (IWSMT-7), May 29-June 3, Thun, Switzerland (2005) **(Relevant to Chapter 6-2)**
- (26) M. Takahashi and M. Kondo, “Corrosion Resistance of High Cr Steels and Ceramic Materials in Lead Bismuth Flow”, Proc. of Int. Conf. of Global 2005, Paper No.425, Tsukuba, Japan (2005). **(Relevant to Chapter 6-1)**
- (27) M. Kondo and M. Takahashi, “Performance of Solid Electrolyte Type Oxygen Sensor in Flowing Lead Bismuth”, Proc. of Int. Conf. of Global 2005, Paper No.503, Tsukuba, Japan (2005). **(Relevant to Chapter 2-1)**
- (28) M. Kondo and M. Takahashi, “Corrosion of Steels and Ceramics in Flowing

Lead-Bismuth”, MIT-Tokyo Tech. Symposium on Innovative Nuclear Energy Systems (MIT-INES), Nov. 2-4, Royal Sonesta Hotel, Boston, MA (2005)
(Relevant to Chapters 4, 6 and 7)

Congress/ Seminar/ Symposium

- (29) M. Takahashi, M. Kondo, S. Yoshida, N. Sawada and J. Matuzaki, “Development of Advanced Oxygen Sensor for Liquid Pb-Bi”, AESJ annual meeting, L68, Mar. 27-29, Nagasaki, Japan (2003). **(Relevant to Chapter 2-1)**
- (30) N. Sawada, M. Takahashi and M. Kondo, “Development of Pumps and Flow meters of Lead-Bismuth”, AESJ annual meeting, K25, Mar. 27-29, Nagasaki, Japan (2003). **(Relevant to Chapter 8-2)**
- (31) M. Kondo, N. Sawada, M. Takahashi, K. Hata and S. Yoshida, “Corrosion Characteristics of Steels and Control Technique of Oxygen Potential in Flowing Lead-Bismuth Eutectic”, JSME Mechanical Engineering Congress 2003, Aug. 5-8, Tokushima, Japan, (2003) **(Relevant to Chapter 4)**
- (32) M. Kondo and M. Takahashi, “Effect of Surface Roughness of Steels on Corrosion in Liquid Lead Bismuth”, Nov. 11, Ryukyuu, Japan (2003) **(Relevant to Chapter 5-2)**
- (33) M. Kondo, M. Takahashi and K. Hata, “Observation of Pipe Rupture Surface in Lead Bismuth Circumstance”, AESJ fall meeting, H41, Sep. 24-26, Shizuoka, Japan (2003). **(Relevant to Chapter 8-1)**
- (34) K. Hata, H. Hara and N. Sawada, M. Kondo and M. Takahashi, “Development of Oxygen sensor for Lead-Bismuth Eutectic”, AESJ fall meeting, H41, Sep. 24-26, Shizuoka Japan, (2003). **(Relevant to Chapter 2-1)**
- (35) M. Kondo, M. Takahashi, N. Sawada and K. Hata, “Development of Pb-Bi Cooled Direct Contact Boiling Water Fast Reactor (I) –(7) Corrosion Behavior of Cr, Si and Al Rich Steels in Pb-Bi flow -”, AESJ annual meeting, O7, Mar. 29-31, Okayama, Japan (2004). **(Relevant to Chapter 6)**
- (36) M. Takahashi and M. Kondo, “Development of Pb-Bi Cooled Direct Contact Boiling Water Fast Reactor (III) –(1) Active Control of Oxygen Concentration Using Granular Sinter of Lead Oxide”, AESJ annual meeting, F30, Mar. 29-31, Okayama, Japan (2004). **(Relevant to Chapter 2-2)**
- (37) M. Kondo, M. Takahashi K. Ara and M. Hirabayashi, “Development of Pb-Bi Cooled Direct Contact Boiling Water Fast Reactor (III) –(3) Corrosion Characteristics of Immersed Material of Ultrasonic Flow Meter for Liquid Lead Bismuth”, AESJ annual meeting, F31, Mar. 29-31, Okayama, Japan (2004). **(Relevant to Chapter 1)**

Acknowledgments

Acknowledgments

I gratefully acknowledge to

- My supervisor, Prof. Minoru Takahashi for his immense support, kind advice, and sincere guidance in the every process of research work and school life,
- Prof. H. Sekimoto, Prof. T. Yano, Prof. K. Kato and Prof. T. Obara for their fruitful advise and critic,
- Dr. T. Suzuki and Mr. K. Ishikawa for their experimental guidance in the erosion test, Dr. S. Yoshida, Mr. N. Sawada and Mr. K. Hata for their experimental support in the corrosion test,
- Mr. Imai and Mr. Tobituka for their technical support in metallurgical analysis using SEM/EDX and FE-SEM/EDX,
- Mr. A. Yamada for their active support in the performance tests for the oxygen sensor and the electro-magnetic flow meter in Pb-Bi,
- Mr. T. Iguchi and Dr. A. Otusbo, Dr. Y. Qi and Dr. S. Qiu for their valuable discussion,
- Mr. Miura and Mr. Onituka in R&D Sect., SUKEGAWA Electric Co., LTD. for their technical support on the development of the electrodes of the electro-magnetic flow meter and PbO direct immersion type mass exchanger and improvement of core part of the electro-magnetic pump for the liquid Pb-Bi,
- Dr. Dostal, Ms. Elin, Ms. Matsumoto, Ms. Y. Yamada, Mr. Novitrian, Mr. Abu, Mr. Akashi and Mr. Kumagai for their kind cooperation and encouragement,
- My family and friends for their continuous encouragement during the four years in master and doctor courses of Tokyo Institute of Technology.